STUDIES ON FABRICATION, MORPHOLOGY AND PERFORMANCES OF BI-LAYER ELECTROSPUN NANOFIBRE MEMBRANES

A thesis submitted in fulfilment of the requirements for the degree of Doctor of Philosophy

Nor Dalila Nor Affandi

B.Sc. (HONS) Textile Technology, Universiti Teknologi MARA, Malaysia 2005

Textile Technology

School of Fashion and Textiles

Design and Social Context

RMIT University

September 2010

DECLARATION

I, Nor Dalila Nor Affandi certify that:

a. except where due acknowledgement has been made, the work is that of the candidate alone;

b. the work has not been submitted previously, in whole or in part, to qualify for any other academic award;

c. the content of the thesis is the result of work which has been carried out in the School of Fashion and Textiles, RMIT University between February 2007 and 2010.

d. any editorial work, paid or unpaid, carried out by a third party is acknowledged.

e. ethics procedures and guidelines have been followed.

Nor Dalila Nor Affandi

September 2010

ACKNOWLEDGEMENTS

DEDICATION

This work is dedicated to my parents and family

members.

TABLE OF CONTENTS

LIST OF FIGURES

deviations were neglected due to low values.

LIST OF TABLES

LIST OF ABBREVIATIONS

ASTM	American Society for Testing and Materials
BET	Brunauer, Emmet, Teller gas adsorption
CA	Cellulose acetate
COD	Chemical oxygen demand
cPs	Centipoises
DC	Direct current
DH	Degree of hydrolysis
DMAc	*N,N*-dimethyl acetamide
DMEM	Dulbecco's Modified Eagle Medium
DMF	*N,N*-dimethylformamide
DMFC	Direct methanol fuel cell
DMT	Derjaguin, Muller and Toporov theory
DSC	Differential scanning calorimetry
ECM	Extra cellular matrix
ES	Ethylene-styrene copolymers
EST-SWNTs-PU	Esther-single wall nanotubes-polyurethane
FESEM	Field Emission Scanning Electron Microscope
FTIR	Fourier transform infrared spectroscopy
HEPA	High efficiency particulate air
HFIP	1,1,1,3,3,3 hexafluoro-2-propanol
HMW	High molecular weight
JKR	Johnson, Kendall and Roberts theory
LDPE	Low density polyethylene
LiCl	Lithium chloride
LMW	Low molecular weight
MF	Microfiltration
MMW	Medium molecular weight
MPC	2-methacryloyloxyethyl phosphorycholine
MSCs	Marrow-derived mesenchymal stem cells
MWNTs	Multi-walled carbon nanotubes
N_2	Nitrogen gas
NF	Nanofiltration
P(LLA-CL)	Poly(L-lactid-caprolactone)

PAA	Polyacrylic acid
PAN	Polyacrylonitrile
PBI	Polybenzimidazole
PCL	Poly (caprolactone)
PDLLA	Poly(D,L-lactide)
PEO	Polyethylene Oxide
pH	pH values
PLGA	Poly(D,L-lactide-*co*-glycolide)
PLLA	Poly(L-lactide)
POM	Polyoxymethylene
PMMA	Poly(methyl methacrylate)
PP	Polypropylene
PS	Polystyrene
PS	Polysulfone
PS-PDMS	Poly(styrene-*b*-dimethylsiloxane)
PTFE	Poly(tetrafluoroethylene)
PU	Polyurethane
PVA	Polyvinyl Alcohol
PVDF	Poly(vinylidene fluoride)
RH	Relative humidity
SE	Secondary electrons
SEM	Scanning electron microscopy
SF	Separation factor
SPU	Segmented polyurethane
TFE	2,2,2-trifluoroethanol
THF	Tetrahydrofuran
UF	Ultrafiltration
ULPA	Ultra low penetration air
WAXD	Wide angle X-ray diffraction
XRD	X-ray diffraction

SYMBOL NOMENCLATURE

Symbol	Definition	Unit
A	Area	m^2, cm^2, nm^2
a	Areas of contact between two surfaces	mm^2, nm^2
N	Avagadro number (6.022×10^{23})	
2θ	Bragg's angle	°
C_{feed}	Concentrations of feed	%
$C_{permeate}$	Concentrations of permeate	%
θ	Contact angle	°
V_c	Critical voltage	kV
α	Cross sectional area of the absorbed gas molecule	cm^2
Q_c	Current filter flow	%
d_c	Current maximum pore diameter	µm
ρ	Density	g/cm^3
ΔP	Differential pressure	psi
Q_d	Dry flow rate	l/min
E^*	Elastic modulus for the contacts	MPa
p_0	Equilibrium of vapour pressure	Pa
p_v	Gas vapour pressure	Pa
l	Gauge length at given load	mm
Q	Incremental of filter flow	%
k	Instrument constant	
L	Length of needle	mm
P	Load	N
m	Mass	g
E	Modulus	MPa
H	Needle tip-to-collector distance	mm
n	Number of wavelengths	
l_0	Original length at zero stress	mm

$v_1{}^2$	Poisson's ratio of material 1	
$v_2{}^2$	Poisson's ratio of material 2	
D	Pore diameter (pore size)	µm
ε	Porosity	%
Q_p	Previous filter flow	%
d_p	Previous maximum pore diameter	µm
R	Radius	m, mm, nm
$\left[\dfrac{ds}{dt}\right]$	Rate of shear	1/sec
f	Shear stress	D/cm^2
d	d -spacing	nm
S	Surface area	m^2/g
γ	Surface tension	dynes/cm
σ	Tensile stress	MPa
η	Viscosity	centipoises
λ	Wavelength of the X-ray	nm
Q_w	Wet flow rate	l/min
W	Width	m, cm, m
G	Fracture energy	J/m^2
J	Volume of flux	$l.hr^{-1}.m^{-2}$, $g.\ hr^{-1}.m^{-2}$
ΔP	Pressure different	N/m^2

ABSTRACT

Homogeneous and heterogeneous bi-layer membranes were fabricated using electrospinning technique and their physical properties were characterized. The membranes were fabricated from two of the following four polymers: hydrophilic polymers such as polyamide 6 (Nylon 6) and polyvinyl Alcohol (PVA) and hydrophobic polymers such as polyacrylonitrile (PAN) and copolymer poly(vinylidene fluoride)-Hexafluoropropylene (copolymer PVDF)) polymers.

A preliminary study was carried out to determine the optimal conditions of electrospinning for each of the above polymers prior to the fabrication of bi-layer membranes. The optimal conditions for each polymer were different and were determined based upon uniform cylindrical fibres, large coverage area and uniform membrane structures.

The study demonstrated that the resultant average fibre diameters for electrospun Nylon 6, PVA, PAN and copolymer PVDF were 109 ± 16, 259 ± 39, 677 ± 205 and 570 ± 105 nm, respectively. The differences in the resultant average fibre diameters for the electrospun polymers were found to affect membrane surface roughness (µm), surface area (m^2/g) and pore sizes.

From the FTIR analysis, it was found that the electrospinning was able to transform crystal phases of polymers such as Nylon 6 and PVDF. Changes in the crystal phases were confirmed by the wide angle X-ray diffraction (WAXD) diffraction peaks.

The optimal conditions for each polymer were then used to fabricate bi-layer membranes. The bi-layer membranes were fabricated as: homogeneous bi-layer membranes (membrane composed of two identical polymers) and heterogeneous bi-layers membranes (membrane composed of two different polymers, hydrophobic and hydrophilic)

The use of a non-contact method to measure the thickness of electrospun membranes has been developed in the study. The non-contact white light profilometry has successfully measured the thickness of electrospun membranes without any compression. From the results, the thickness of single layer electrospun Nylon 6, PVA, PAN and copolymer PVDF was in a range of 40 to 51 µm, whereas the thickness for homogeneous and heterogeneous bi-layer membranes was in a range of 82 to 99 µm.

The surface wettabilities (water contact angles) of homogeneous bi-layer membranes were affected by the functional groups of polymers and surface roughness of the membranes. The hydrophilic polymers such as homogeneous bi-layer Nylon 6/Nylon 6 and PVA/PVA exhibited water contact angles lower than 90°. For hydrophobic polymers, the homogeneous bi-layer PAN/PAN and copolymer PVDF/PVDF showed water contact angles more than 90°. For heterogeneous bi-layer membranes, the water contact angles were influenced by a combination of polymers used in the membrane. For example, the heterogeneous bi-layer Nylon 6/PAN exhibits water contact angles more than 90° due to the presence of electrospun PAN as a base membrane, which prevents further downward movement of the water droplet.

The tensile properties (such as tensile strength, strain and modulus) of homogenous and heterogeneous bi-layer membranes were investigated. The tensile properties for homogeneous bi-layer could be affected by the membranes pore sizes and bonding between fibres in the membrane. The bi-layer Nylon 6/Nylon 6 exhibited the highest tensile strength and modulus at approximately 6.1 MPa and 23.2 MPa compared to other homogeneous bi-layer membranes. The bi-layer copolymer PVDF/PVDF exhibited the highest tensile strain at about 197% compared to other homogeneous bi-layer membranes. For heterogeneous bi-layer membranes, the tensile properties were different depending on the combination of polymers used.

A modified 180° peel test was developed to evaluate adhesion strengths between the top and bottom layers of the bi-layer membranes. A support system (glass slide) was introduced in order to prevent unnecessarily movement of the sample during the test. The bi-layer PVA/PVA showed far higher adhesion highest adhesion strength at about 78 mN/mm^2 compared to others. It was expected that the residual water solvent from the PVA top layer affected the high adhesion for the bi-layer PVA/PVA. For other membranes, the adhesion strengths were lower than 7 mN/mm^2. The low adhesion of these membranes could be due to the physical bonding between the top and bottom layer, where these layers are attached due to surface contact between fibres.

The application of homogenous and heterogeneous bi-layer electrospun membranes for the removal of contaminants in textile effluent was investigated. It was found that the membrane pore sizes affect the clarity of permeate. The fine

pore sizes of homogenous bi-layer Nylon 6/Nylon 6 exhibited the best performance with the highest effluent removal of 99%. The large pore sizes of commercial membrane gave a much lower performance of improving 33 to 35% of the effluent turbidity. Poor quality of permeate was also observed for the large pore sizes of homogenous bi-layer PAN/PAN and homogenous copolymer PVDF/PVDF membranes. However, the accumulation of suspended solid particles over the homogenous bi-layer Nylon 6/Nylon 6 surface exhibited the lowest flux for the membrane as compared to the commercial membrane and homogeneous bi-layer membranes. For heterogeneous bi-layer membranes, the membranes were found to give a lower flux due to the presence of electrospun Nylon 6. However, the presence of electrospun Nylon 6 in the membranes was found to give an excellent removal of suspended solids from liquid.

CHAPTER 1 INTRODUCTION

To date, electrospun nanofibre membranes have been considered as a 'new class of nonwoven' (*1*) as the fibres are accumulated in the form of fibrous web structures. The electrospun nanofibre membranes are fabricated using a technique known as electrospinning. Given that the fibres generally have diameter less than a micron, the electrospun nanofibre membranes are characterized by higher surface-to-volume ratio (*2-7*) compared to bulk fibres and film, light weight (*4*), and small pore sizes (*2-3*). Due to these combinations of properties, electrospun membranes are finding favour in a variety of applications such as biomedical applications (*2-3, 6, 8*), protective clothing (*2, 6, 8*), filtration media (*1-3, 6, 9*) and electronic applications (*2, 6*).

1.1 Aim and objectives

The versatility of the electrospinning process and the unique combination of properties of the resultant electrospun membranes has encouraged the author to investigate this field as a research study. For this doctoral study, the author fabricates, characterizes as well as measures the performance of homogeneous and heterogeneous bi-layer electrospun nanofibre membranes comprised of a combination of hydrophilic and hydrophobic polymers. Thus, the aim of this research is to develop methodology of fabricating bi-layer electrospun membranes and to correlate membrane performances to electrospun nanofibre properties. Although the ultimate focus of this work is on the bi-layer membranes, a pre-requisite study on single layer electrospun polymer will be carried out prior to the fabrication of the bi-layer. Thus, the objectives related to the experimental aspects of this work are as follows:

1. Identify conditions of optimal fibre formation by studying the effect of electrospinning conditions for each hydrophilic and hydrophobic polymer such as solution concentration, applied voltage and needle tip-to-collector distance.

2. Characterize each optimal electrospun membrane according to fibre morphology, pore sizes, surface wettability (water contact angle) and chemical structures.

3. Develop fabrication methodology for bi-layer electrospun membranes based on the above identified conditions.

4. Develop a test methodology for the investigation of the adhesion strength between layers of the bi-layer electrospun membrane.

5. Measure the mechanical properties such as tensile and adhesion strength of the bi-layer electrospun membranes.

6. Study liquid filtration properties of the bi-layer electrospun membranes.

1.2 Contribution of this study

The body of the work presented in this thesis encompasses fundamental studies mainly on homogeneous and heterogeneous bi-layer fabrication, characterization (morphological structures), membrane properties (surface wettability, chemical structures, adhesion of the bi-layers and tensile strength,) and performances particularly for liquid filtration. By undertaking the research work, promising properties of the bi-layer membranes will be identified and potential applications with respect to those properties will be proposed. Multilayer membranes are common in other fields, but it is novel in electrospinning.

Normally, electrospun membranes are collected over very small spot areas with the diameter of 7 cm (*10*). In this research work, a large coverage area of electrospun membrane will be developed, where the distribution of fibre diameter and membrane thickness are evenly formed throughout the membrane. In addition, the electrospinning process used in the study is scalable, thus the coverage area of the membrane could be increased to cover an A4 or larger area.

Another contribution of this study is to introduce newly developed test methods to measure the adhesion strengths between two electrospun materials. The adhesion test method would not only be of benefit to electrospun membranes but also to other thin porous materials or films. In the electrospinning, for instance, it is very common for researchers to coat or deposit a layer of electrospun membrane onto a supporting substrate. Recent studies (*11-14*) proved that layering of electrospun nanofibre membrane onto other substrates can improve substrate performance. As reported by Grafe *et al.* (*11*), the deposition of electrospun webs onto a cellulose substrate could increase the filtration efficiency for submicron particles by holding 2.5 times more dust mass than the pure cellulose filtration media. Research done at Natick (*12, 15*) discovered that a thin

layer of electrospun membrane deposited onto a meltblown fabric can enhance the filtration efficiency mainly in aerosol filtration. In protective clothing, a fabric laminated with electrospun polypropylene membrane enhanced barrier performance against liquid penetration (*14*). The enhanced properties of electrospun/substrate systems are already recognized, however the adhesion strengths between the electrospun membrane and the substrate is also paramount in their final performance. Therefore, an adhesion test method will be developed to measure adhesion forces between ultra thin membranes particularly for bi-layer electrospun membranes.

At the end of the study, more knowledge will be gained particularly concerning bi-layer fabrication, membrane properties and potential application of the membranes for liquid filtration.

CHAPTER 2 LITERATURE REVIEW

2.1   Introduction to Electrospinning

Electrospinning is a versatile technique for the fabrication of polymeric fibres in the nanometer diameter range (*16-19*). The accumulation of the ultra-fine fibres forms a nonwoven membrane, known as electrospun nanofibre membrane. The fundamental idea of electrospinning system was patented by Anton Formhals (*20*) in 1934. In his patents, cellulose acetate from an acetone solution was electrospun to form an artificial thread. Figure 2-1 illustrates the electrospinning system invented by Formhals (*20*). It consists of a wheel, two electrodes (not shown in Figure 2-1), vessel and rotating collector. The cellulose acetate solution was sprayed from the vessel due to the high electric field produced by two electrodes. With the aid of the rotating wheel, the charged solution was collected onto a rotating collector as threads. The threads were then passed through a thread washing device and were further stretched and dried in the stretching and drying compartments.
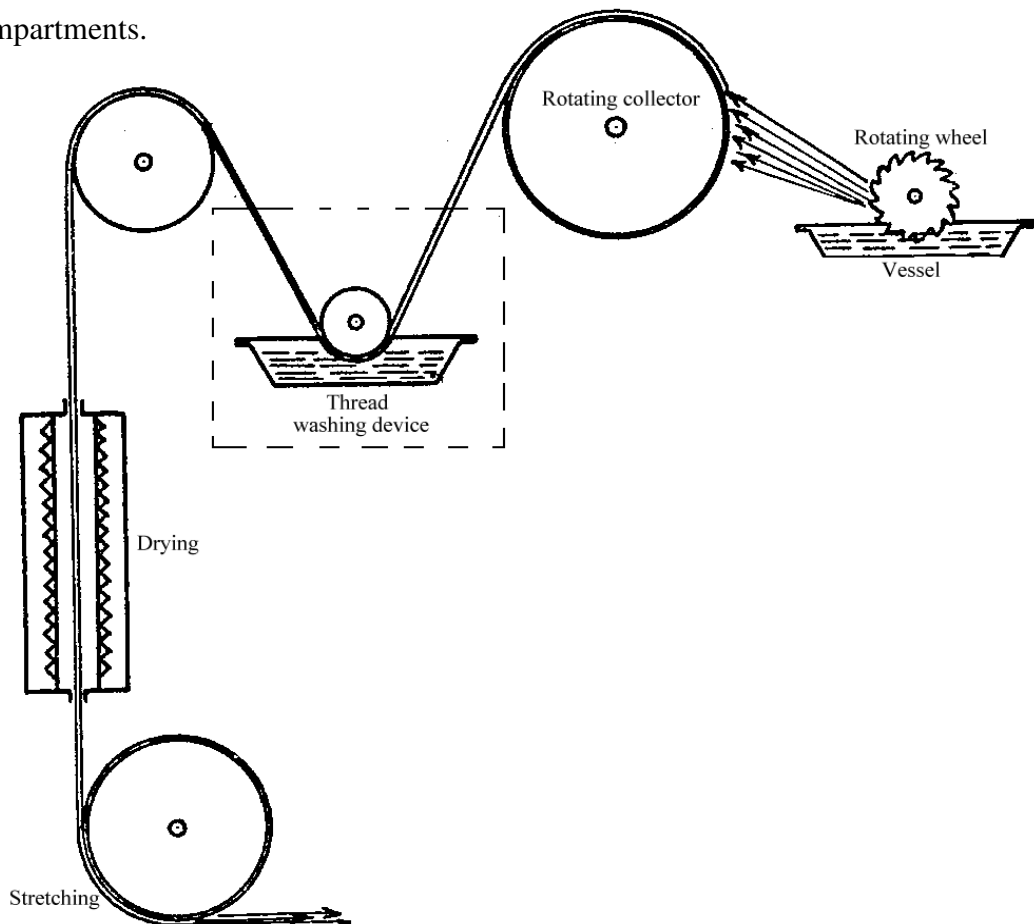
Figure 2-1: Schematic diagram of electrospinning system invented by Formhals (*20*).

Originally, the electrospinning technique remained more of a curiosity. In the late 1990's, interest in the technique has increased. To date, a number of electrospinning systems have been further developed in order to produce electrospun materials for study as well as to increase the production rate of the electrospun membrane. Figures 2-2 (a-f) show different types of electrospinning systems that have been used by researchers and manufacturers. The systems include:

1. Single nozzle electrospinning

Figures 2-2 (a-b) are two examples of lab scale electrospinning systems. Both systems consist of a reservoir, a grounded collector and an applied voltage. Prior to the fabrication of electrospun membranes, polymers are dissolved in appropriate solvents in order to form polymer solutions. The polymer solution is pumped constantly by a metering pump (Figure 2-2 (a)) or is forced by gravity into a capillary (Figure 2-2 (b)). In a typical electrospinning process, an electrically charged jet of the polymer solution is accelerated and stretched in the presence of an electric field. Solvent from the jets is usually evaporated before depositing on the grounded collector plate. The deposition of the dried jets forms an electrospun nanofibre membrane. Recent studies reported that a single nozzle electrospinning system (as shown in Figure 2-2 (a-b)) gave lowest production rate compared to other methods (*21-23*). As reported by Wang *et al.* (*24*), the production rate of single nozzle was approximately 300 mg per hour per needle. Hence, the single nozzle electrospinning system is mainly suitable for lab scale study (*24)* or the fabrication of small samples.

2. Multi-nozzle electrospinning

Another alternative method to scaling up single nozzle electrospinning is by using a number of single nozzles in parallel known as multi-nozzle electrospinning. Figure 2-2 (c) shows a typical multi-nozzle electrospinning system invented by Theron *et al.* (*22*). In this system, the authors used nine syringes organized in a 3 x 3 array to electrospin polyethylene oxide (PEO) solutions. They reported that the production rate of multi-nozzle electrospinning was in the range of 22.5 $L.cm^{-2}.min^{-1}$ to 22.5 $mL.cm^{-2}.min^{-1}$ (*22*).

3. Needle-less electrospinning

Although the multi-nozzle electrospinning was reported to increase the production rate of electrospun nanofibre membranes (*22*), several problems were encountered using this system such as the complexity of the process and the repulsion between charged jets from adjacent needles, which inhibit the formation of electrospun nanofibres. The system also requires larger operating space (*21, 23-24*). The invention of needle-less electrospinning, was reported to give a better electrospinning process compared to multi-nozzle electrospinning (*21, 23-25*). Jirsak *et al.* (*26*) described the formation of multi-jets from a polymer solution uploaded on a rotating horizontal cylinder (Figure 2-2 (d)). This system was patented and was commercialized by Elmarco under the brand name of Nanospider™. Other needle-less electrospinning includes bubble electrospinning (*25*) and coil wire electrospinning (*24, 27*).

4. Co-axial electrospinning

A bi-component electrospun nanofibre (fibre with two different polymers) can also be fabricated using the electrospinning technique. The technique is also known as co-axial electrospinning. In a typical co-axial electrospinning process, two concentrically aligned nozzles are used to electrospin two polymer solutions, simultaneously (Figure 2-2 (e)) (*8, 28*). Both nozzles have the same applied voltage in order to form a compound droplet. When jets are generated from the droplet, a core–sheath nanofibre is created (*8, 28*).

5. Melt-electrospinning

Melt-electrospinning is another alternative method to fabricate electrospun fibres. Basic mechanisms of melt-electrospinning are illustrated in Figure 2-2 (f). A thermoplastic polymer is melted in heating zones at particular temperature (*29*). As a polymer droplet is held by its surface tension at the needle tip, an electrically charged jet of molten polymer is drawn out and accelerated to form electrospun fibres on the collector. The fibres are solidified due to cooling from the surrounding air (*29*).
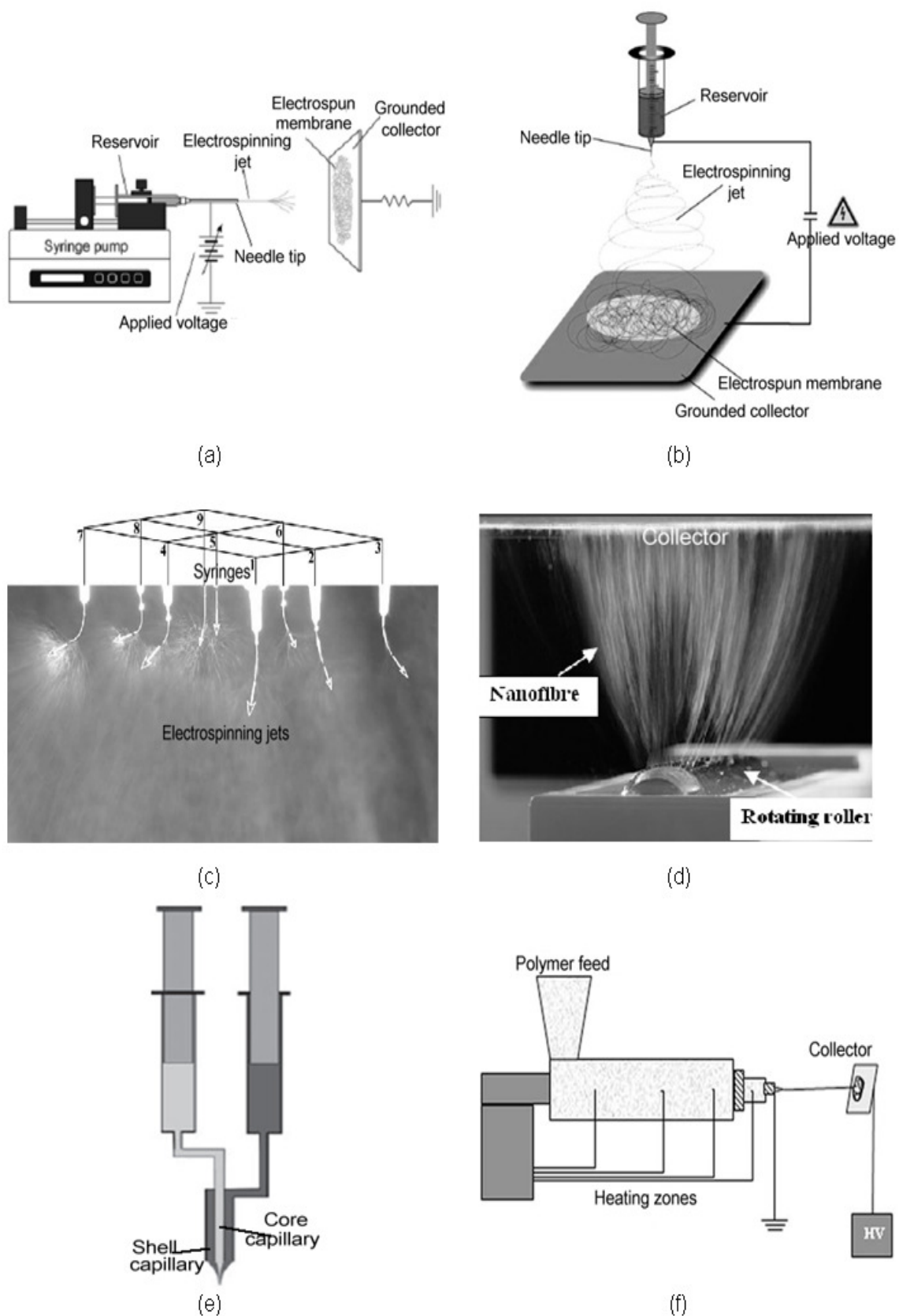
Figure 2-2: Schematic diagrams and photographs of various electrospinning systems. Single nozzle electrospinning: a) with pump (*30*), b) without pump (*8*), c) multi-nozzle electrospinning (*21*), d) needle-less electrospinning (*26*), e) co-axial electrospinning (*8*) and f) melt-electrospinning (*29*).

2.2 Materials For Electrospinning

2.2.1 Polymers

Chemically, a polymer has a long chain molecule made up of hundreds or thousands of smaller repeating units called monomers (*31*). Polymers are classified into natural and synthetic depending on their sources. Examples of natural polymers include protein, starch, wool and cotton. In the nineteenth century, some synthetic polymers were discovered. However, the synthetic polymers were not commercially used until the late 1930s, when they were used to replace some natural materials due to the shortage during the inter-war years (*32*).

Polymers can be classified in many ways such as by source (natural or synthetic), structural shape (linear, branched or network), method of synthesis or polymerization mechanisms and end uses (fibre, plastic) (*32-33*). Thermal processing is another methods of the polymer classification, which can be divided into two groups: 1) thermoset and 2) thermoplastic (*32, 34*). Thermoset refers to polymers having internal cross-linking to form an interconnected network of polymers. These polymers are normally rigid and cannot be dissolved or heated at high temperatures due to the resulting continuous chemical deformation, for example epoxy (*32*). Thermoplastic polymers can be melted by the application of heat and they solidify upon cooling (*32*).

In the molten state, polymers consist of a tangled mass of molecules. Upon cooling, the molten polymer may solidify as a fully crystallized polymer structure (Figure 2-3 (a)), partially crystallized structure (Figure 2-3 (b)) or even as a non-crystallized structure (amorphous) as shown in Figure 2-3 (c) (*32-35*).

(a)   (b)   (c)
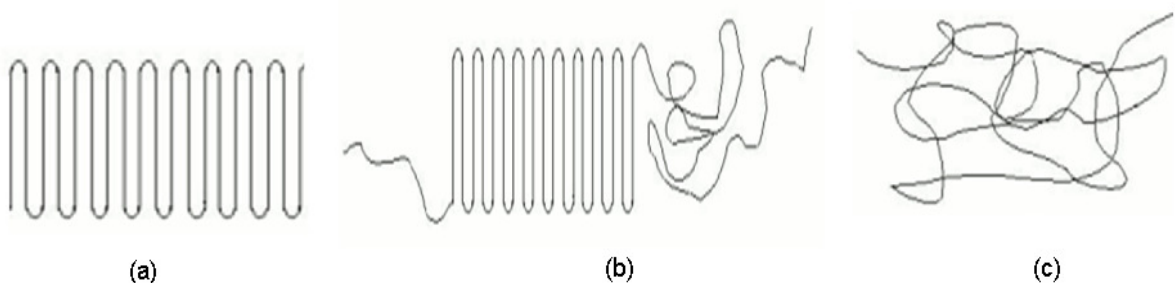
Figure 2-3: Schematic diagrams of : a) crystalline structures, b) semi-crystalline structures and c) non-crystalline structures (amorphous) (*32-35*).
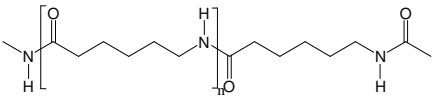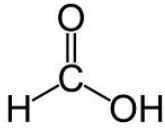
Polymer surfaces are inherently different in terms of hydrophilicity or hydrophobicity. The term hydrophilic is defined as "water loving" (*36*). A material with hydrophilic surfaces interacts with polar solvents (particularly water or other polar groups), which gives contact angles lower than 90° on the material surface. The examples of hydrophilic polymers are Nylon 6 and polyvinyl alcohol.

Hydrophobic materials have poor affinity to water molecules. The minimization of Lifshitz-van der Waals forces and poor interactions between the water-polymer surfaces lead to a high water contact angle (more than 90°) on a hydrophobic surface (*31, 37*). Fluorocarbon polymers such as poly(tetrafluoroethylene) (PTFE) and polyvinylidene fluoride (PVDF) are two examples of hydrophobic polymers.

A lot of work has been done on the use of both hydrophilic and hydrophobic polymers to fabricate electrospun nanofibre membranes. The polymers are usually dissolved in appropriate solvents to form polymer solutions. Some examples of the hydrophilic and hydrophobic polymers, as well as solvents used for electrospinning are summarized in Tables 2-1 and 2-2.

Most of the polymers described in Tables 2-1 and 2-2 are synthetic. Recent studies have also demonstrated the electrospinning of biopolymer fibres. Biopolymers are polymers derived from the renewable sources such as polysaccharides, proteins, lipids and polyphenols (*38*). Similar to the synthetic polymers, these biopolymers are dissolved in solvents before electrospinning the polymer solutions. Summaries on the electrospun biopolymers are tabulated in Table 2-3.

Table 2-1: Summary of the hydrophilic polymers used in electrospinning

Polymer	Molecular weight	Parameters studied	Solvent	Electrospinning parameters	Observation	References
Polyamide 6 (Nylon 6)	• Low molecular weight (LMW): 43659, 79689 and 1.825 • High molecular weight (HMW): 85078, 197951 and 2.327	Study the effect of electrospinning parameters on the average fibre diameters, fibre distribution and the production rate of electrospun Nylon 6	Formic acid	• Multi-nozzle electrospinning (10 nozzles) • Viscosity: 500, 1000 and 1500 cPs • Voltage: 30 to 50 kV • Needle-to-collector distance: 10 to 20 cm • Nozzle size: 0.3 to 0.5 mm • Salt content (potassium formate): 1 to 2 % • Feeding pressure: 0 and 0.4 bar • Electric field: 1.5 to 2.0, 2.5 to 3 and 3.3 to 5 kV/cm.	• Solution viscosity, needle tip-to-collector distance, nozzle size and feeding pressure were the main parameters affecting fibre diameter. Other parameters did not affect the resultant fibre diameter. • The effect of molecular weight on fibre diameter was insignificant. • The strength of the electric field affected the production rate of electrospun Nylon 6.	Heikkila and Harlin (39) Other studies: Zhang *et al.* (40), Supaphol *et al.* (41-42), Stephen *et al.* (43), Shan *et al.* (44), Ojha *et al.* (45).

Polyvinyl Alcohol (PVA)	74.8 kDa	Study the effects of electrospinning parameters such as applied voltage, needle tip–to-collector distance, concentration and degree of hydrolysis (DH) on morphological structures of electrospun PVA fibres.	Distilled water	• Single nozzle electrospinning • Blunt needle: Gauge 9 and nozzle diameter 0.9 mm • Applied voltage: 5 to 15 kV • Needle tip-to-collector distance: 8 to15 cm • Solution concentration: 6 to 8 %wt. • Degree of hydrolysis: 80 to 99%	• Applied voltage and solution concentration affected the resultant average fibre diameter. • Solution concentration and degree of hydrolysis (DH) of PVA influenced the formation of beaded, cylindrical and flat ribbon fibres. • Needle tip-to-collector distance did not affect the fibre diameter.	Zhang *et al.* (*46*). Other studies: Yang *et al.* (*47*), Stanger *et al.* (*48*), Liu *et al.*(*49*), Lee et al. (*50*)
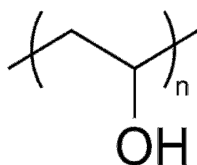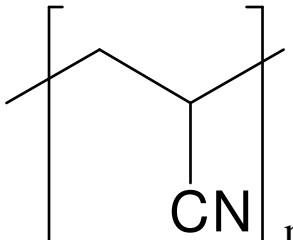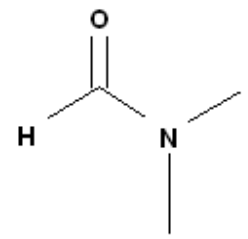
Polyethylene Oxide (PEO) $-\left[CH_2 - CH_2 - O\right]_n-$	400,000 g/mol	Study the effects of applied voltage and solution concentration on the structures and morphologies of electrospun PEO.	Deionised water	• Single nozzle electrospinning • Blunt needle: Gauge 23 and nozzle diameter 0.35 mm • Applied voltage: 5.5 to 15 kV • Needle tip-to-collector distance: 16.5 cm • Solution concentration: 4 to 10 wt%.	• Applied voltage influenced the formation of beads in the fibre. • Solution concentration affected the average fibre diameter. The increase of the average fibre diameter was corresponded to a power law relationship.	Deitzel *et al.* (*10, 51*) Other studies: Fong et *al.* (*52*), Theron (*53*), Tan et al. (*54*)

Other hydrophilic polymers that can be used in electrospinning: Nylon 6,6 (*55*), Nylon 12 (*43*) and polyacrylic acid (PAA) (*56-57*).

Table 2-2: Summary of the hydrophobic polymers used in electrospinning.

Polymer	Molecular weight	Parameters studied	Solvent	Electrospinning parameters	Observation	References
Polyacrylonitrile (PAN)	• 100,000 g/mol	Study the effects of operating parameters such as electric voltage, solution feed rate and needle tip-to-collector distance on the morphologies of electrospun PAN nanofibres	*N,N*-dimethylformamide (DMF)	• Single nozzle electrospinning • Applied voltage: 10 to 20 kV • Feed rate: 1, 2 and 4 mL/h • Needle diameter: 0.7 mm outer diameter	• Average diameters of nanofibres decreased with increasing applied voltage from 10 to 20 kV, but broader distribution in diameters was observed particularly above 15 kV. • At shorter needle tip-to-collector distance particularly below 7.5 cm, wet fibres was deposited on the collector. • At 1 mL/h and 4 mL/h feed rates, beaded nanofibres were collected, but at 2 mL/h uniform nanofibres were obtained.	Jalili *et al*. (*58*). Other studies: Jalili *et al*. (*59*), Liu and Hsieh (*60*), Qin *et al*. (*61*), Fennessey *et al*. (*62*).

| Polyvinylidene fluoride (PVDF) | 427, 000 g/mol | Study the effects of concentration, feed rate and needle tip-to-collector distance on fibre diameter, morphology and crystalline structure of electrospun PVDF nanofibre | *N,N*-dimethylformamide (DMF) | • Single nozzle electrospinning
• Needle diameter: 1 mm
• Concentration: 10 to 26 wt%
• Applied voltage: 7.5 to 15 kV
• Needle tip-to-collector distance: 8 to 15 cm
• Feed rate: 0 to 12 µL/min
• Wide angle X-ray diffraction (WAXD): $2\theta=$ 10 to 34° | • Polymer concentration was found to affect the fibre diameter of electrospun PVDF and the formation of beaded fibres.
• The resultant average fibre diameter was 80 to 700 nm.
• The fibre diameter increased with increasing applied voltage.
• The increase of needle tip-to-collector distance did not affect the PVDF fibre diameter.
• The average fibre diameter was observed to decrease when the feed rate increased from 0 to 12 µL/min.
• Electrospinning process affected the formation of oriented β-phase crystalline structure of PVDF fibres. | Nasir *et al.* (*63*)

Other studies: Choi *et al.* (*64*), Gao *et al.* (*65*), Kim *et al.* (*66*) |

| Poly(vinylidene fluoride)-hexafluoropropylene | Not mentioned | Investigate the physical and electrochemical properties of electrospun copolymer PVDF for the application of lithium polymer batteries | A mixture of Acetone and *N,N*-dimethyl acetamide (DMAc)

Ratio of Acetone:DMAc (7:3) by weight | • Single nozzle electrospinning
• Solution concentration: 12 to 18 %wt.
• Other electrospinning conditions were not mentioned in the literature | • The average fibre diameter of electrospun copolymer PVDF increased from 0.5 to 2.5 µm when the concentration increased from 12 to 18 %wt | Kim *et al.* (*66*)
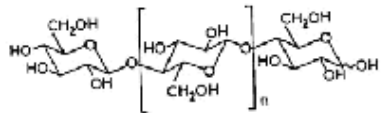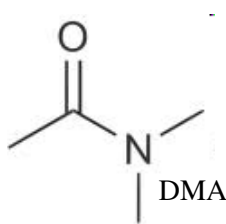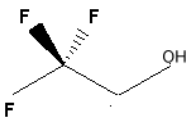
Other studies: Li *et al.* (*30*) and Yao *et al.* (*67*) |

Other hydrophobic polymers that can be used in electrospinning: Poly[bis(2,2,2-trifluoroethoxy)phosphazene] (*68*), polypropylene (*14*) and Poly(Styrene-*block*-dimethylsiloxane) Block Copolymer (*69*).

Table 2-3: Summary of the biopolymers used in electrospinning.

Polymer	Molecular weight	Parameters studied	Solvent	Electrospinning parameters	Observation	References
Cellulose (Cellulose was obtained by grinding cotton linter paper and surgical cotton batting)	Not mentioned	• Fabricate electrospun cellulose on the cellulose filter media • Investigate the application of heated collector on the electrospun cellulose/ cellulose filter media. • Introduce the use of post-spinning treatment (coagulation) in electrospinning process	• The cellulose was pre-treated in water at room temperature (20°C) for 8 hours. • The cellulose solution was then mixed with *N,N*-dimethyl acetamide (DMAc) and Lithium chloride (LiCl) DMAc	• Concentration for cellulose/water: 1 to 3 wt%. • Concentration for DMAc/LiCl: 8 wt% • Single nozzle electrospinning with heated collector in coagulant bath. • Temperature of collector: room temperature and 100 to 105°C. • Water coagulation • Electric field: 1 to 4 kV/cm • Flow rate: 0.1 mL/min	• The increase of temperature on heated collector has successfully removed the solvent (DMAc) from the electrospun cellulose. • A post-spinning coagulation was found to remove salt (LiCl) from the electrospun cellulose fibres. • The removal of DMAc and LiCl prevented the aggregation of cellulose fibres and subsequently produced uniform and dry fibres	Kim *et al.* (*70*) Other studies: Liu and Hsieh (*71*), Kim *et al.* (*72*)

Gelatine (porcin) and a mixture of gelatine and poly (caprolactone) (PCL) PCL	Gelatine :Not mentioned PCL : 80,000 g/mol	Study the physical, mechanical, and biological performances of electrospun gelatine and a mixture of gelatine and poly (caprolactone) (PCL)	2,2,2-trifluoro-ethanol (TFE) 	• Single nozzle electrospinning • Blunt needle with needle diameter of 1.2 mm. • Electric fields: 0.3, 0.5 and 0.8 kV/cm • Tensile test: 10N load cell with 10 mm/min crosshead speed • Water contact angle: 0.25 µL of deionised water	• At 2.5 to 12.5 % w/v concentrations, the electrospun gelatine fibres can only be obtained at 10 %w/v. Thus, the 10 %w/v was selected and mixed with PCL at ratio of 50:50. • The electrospun gelatine/PCL was observed to improve surface wettability and tensile properties as compared to electrospun pure gelatine and PCL membranes.	Zhang *et al.* (*73*) Other studies: Huang *et al.* (*74*), Li *et al.* (*75*)

Collagen (collagen Type I)	Not mentioned	Investigate the fabrication of electrospun collagen using electrospinning	1,1,1,3,3,3 hexafluoro-2-propanol (HFIP)	• Single nozzle electrospinning • 18 gauge blunt needle • Feed rate : 0 to 25 mL/h • Applied voltage: 15 to 30 kV. • Rotating drum collector: 500 rpm (speed) • Solution concentration: 0.08 to 0.083 g/mL	• For type I collagen (calfskin), there was no fibres were obtained at concentration of 0.008 g/mL. • When the concentration increased up to 0.083 g/mL, fibres were deposited. • At different applied voltages, fibres can only be obtained at 25 kV. • An optimal electrospinning feed rate was observed at 5 mL/h, respectively. • Smooth muscle cells were observed to grow into the fibrillar network of collagen.	Mathews *et al.* (*76*). Other studies: Mathews *et al.* (*77*), Buttafoco *et al.* (*78*)

Other biopolymers that can be used in electrospinning: fibrinogen (*79-80*), chitosan (*81-82*), etc

2.2.2   Composites

Functional materials such as nanoparticles, nanotubes and nanowires can also be added directly in a polymer solution prior to electrospinning in order to diversify the functionalities of electrospun nanofibre membranes. Son *et al.* (*83*) demonstrated the incorporation of silver nanoparticles in cellulose acetate (CA) solution in order to form anti-microbial electrospun CA fibres. They observed that the fibres inhibited the growth of bacteria such as S. aureus, E. coli, K. pneumoniae, and P. aeruginosa (*83*).

Carbon nanotubes have been extensively used in electrospinning. The incorporation of carbon nanotubes in electrospun nanofibres was reported to improve mechanical strength and electronic conductivity of electrospun fibres (*84-88*). Sen *et al*. (*85*) fabricated a composite electrospun EST-SWNTs-PU (ester-single wall nanotubes-polyurethane) membranes by mixing polyurethane (PU) solution with the EST-SWNTs (ester-single wall nanotubes). The authors observed that the tensile strength of the composite membrane was enhanced by 104% as compared to pure electrospun PU membrane (*85*). The unique properties of carbon nanotube in electrospun fibres were also reported by Ge *et a.l* (*84*). They fabricated highly oriented surface-oxidized multi-walled carbon nanotubes (MWNTs) along the axis of electrospun polyacrylonitrile (PAN) fibre (Figure 2-4). The highly orientation of the PAN/MWNT composite nanofibres enhanced mechanical properties, thermal deformation temperature, thermal stability and dimensional stability as compared to the pure electrospun PAN membrane (*84*).
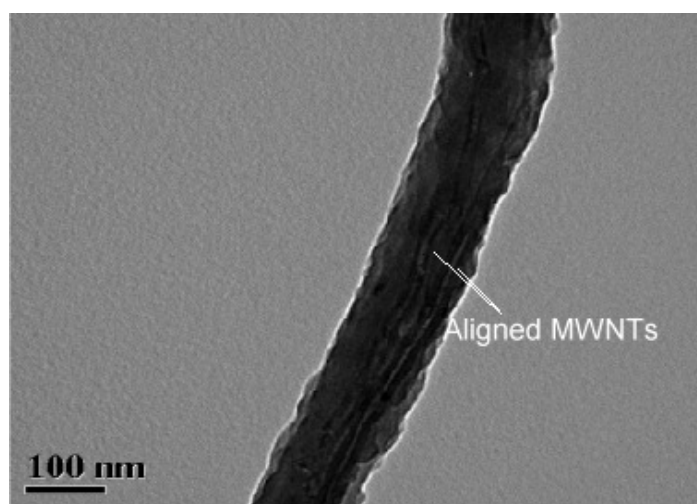
Figure 2-4: TEM image of electrospun PAN/ MWNT composite nanofibres (*84*).

2.2.3 Ceramics

Ceramic nanofibres can also be made using electrospinning. In contrast to conventional electrospinning processes, the fabrication of ceramic nanofibers requires the use of spinnable precursor (*89*). A typical procedure to fabricate ceramic nanofibers through electrospinning consists of three major steps: (i) preparation of polymer solution containing an alkoxide, salt, or polymer precursor, (ii) electrospin the solution to produce composite nanofibers consisting of the polymer and the precursor, (iii) calcination, sintering or chemical conversion of the precursor into ceramic (*2, 89*).

Recent studies demonstrated that the ceramic nanofibres using electrospinning have potential to be used as electrodes in energy conversion and storage devices such as batteries, dye-sensitized solar cells, gas sensing and photovoltaic devices (*90-93*).

2.3 Formation of Nanofibres using Electrospinning

In a typical electrospinning process, a polymer solution is pumped at constant flow by a metering pump or is forced by gravity into a capillary. At the capillary tip, a polymer droplet is formed and held together by its surface tension. In the presence of an electric field, the charged polymer jets are ejected from the droplet and formed whipping instabilities. During the whipping instabilities, the polymer jets are elongated and travelled to the collector plate to form electrospun fibres. The formation of electrospun fibres and the quality of fibres are generally affected by a number of conditions, which are illustrated in Figure 2-5.
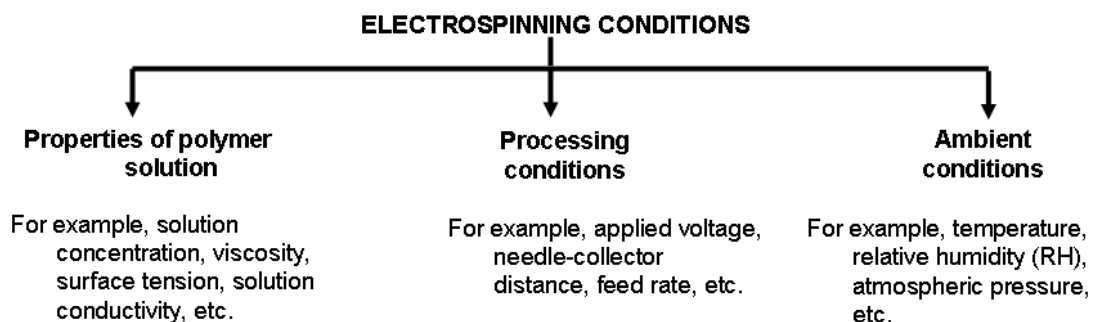
Figure 2-5: Electrospinning conditions

These conditions were also reported to affect the formation of Taylor cone and whipping instabilities in electrospinning (*94-95*). The descriptions of some electrospinning conditions, Taylor cone and whipping instability are outlined below.

2.3.1 Polymer solution properties

2.3.1.1 Effect of solution concentration

Solution concentrations were reported to be dominant parameters in electrospinning since they affect the fibre formation and the electrospinning process (*46*). In electrospinning, solution concentration refers to the amount of polymer in solvent (*2*) and it is related to the viscosity of polymer solution. In liquid states, the viscosity is measured by the shear stress of the liquid flow, which can be measured using equation 2.1.

$$f = \eta \left[\frac{ds}{dt} \right]$$
equation 2.1

where f is shear stress (D/cm^2), η is viscosity (centipoises, cPs) and $\left[\dfrac{ds}{dt} \right]$ is the rate of shear (1/sec).

The effect of solution concentration in electrospinning has been studied extensively by a number of researchers (*18, 39, 46, 51-52, 54, 63, 96-100*). Deitzel *et al.* (*51*) discovered that the polyethylene oxide (PEO) fibre diameters increased with an increase of solution concentration. The correlation between the PEO average fibre diameter and solution concentration was through a power-law relationship with an exponent of 0.5. This correlation was confirmed by other studies (*39, 46, 52, 54, 63, 96-98*). They observed that higher concentrations yielded bigger fibre diameters for electrospun polyvinyl alcohol (PVA), Nylon 6, polyvinylidene fluoride (PVDF) and sulphonated polyetherimide/ polyetherimide blends (*39, 46, 52, 54, 63, 96-98*). Solution concentration also influenced the formation of beaded fibres and droplets. A number of studies reported that the formation of beaded fibres was correlated to low solution viscosity (*52, 99*). Fong *et al.* (*52*) observed that the low concentration of polyethylene oxide (PEO)

solution gave lower viscosity for the solution. At lower viscosity (approximately 74 cPs), chain entanglement of polymer in the solution was insufficient to overcome the solution surface tension and high culombic repulsion forces, which resulted in the formation of beaded electrospun polyethylene oxide (PEO) fibres (Figure 2-6 (a)). When the viscosity increased up to 1250 cPs, the beaded PEO fibres were gradually reduced, forming cylindrical and smooth electrospun fibres (Figure 2-8 (b)) (*52*).

(a)   (b)
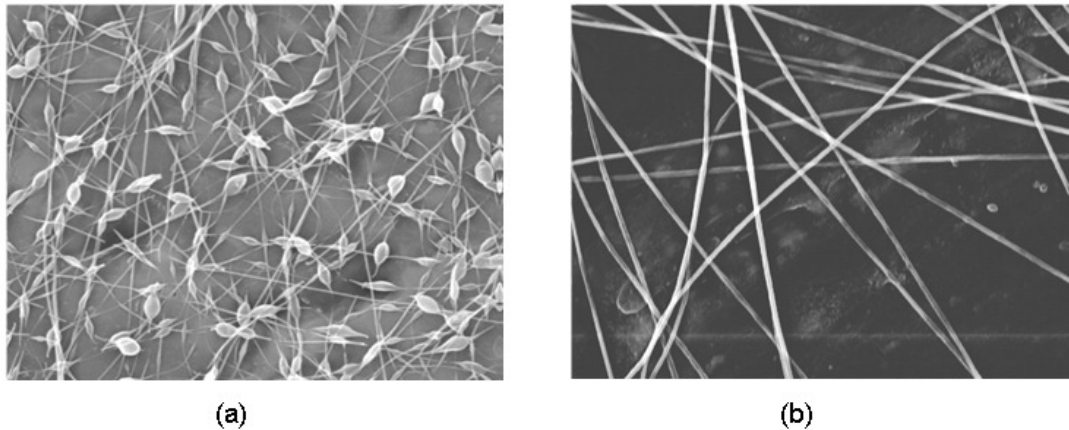
Figure 2-6: SEM images of electrospun PEO nanofibres: a) beaded fibres and a) uniform cylindrical fibres (*52*).

The solution concentration was also reported to influence the formation of coverage area for electrospun membranes (*99*). Mit-uppatham *et. al* (*99*) observed that the coverage area of electrospun Nylon 6 decreased with increasing solution concentration from 30 to 46% w/v. At higher concentration, the Nylon 6 jets had greater resistance towards thinning its fibre diameter. This caused the jets to travel linearly before forming bending instability. As a result, a small area of electrospun Nylon 6 was observed at higher concentration (*99*).

2.3.1.2 Effect of surface tension

Surface tension (γ) can be defined as the energy required to increase the surface area of a liquid by a unit amount (J/m^2) (*31*). For example for a water droplet, the surface tension tends to hold a drop of water in a spherical shape because a sphere has a smallest surface area for a given volume. In electrospinning, the surface tension was reported to affect the bending instability of electrospinning jets (*101*) and the formation of electrospun fibres (*52*).

Fong *et al.* (*52*) reported that the increase of ethanol in polyethylene oxide (PEO)/water solution exhibited higher viscosity and lower surface tension. Both conditions were found to form smooth electrospun PEO fibres (*52*). Koski *et al.* (*102*) suggested that a polymer solution of low surface tension was desirable in electrospinning because it reduced the critical voltage (V_c) needed for the ejection of jets from the Taylor cone, which can be measured in equation 2.2 (*102*) .

$$V_c = \frac{4H^2}{L^2}\left(In\,\frac{2L}{R}-\frac{3}{2}\right)0.117\pi\gamma R \qquad\qquad \text{equation 2.2}$$

where V_c critical voltage (kV), H is needle tip-to-collector distance (mm), L length of needle (capillary) (mm), R is radius of the needle (capillary) (mm) and γ is surface tension of the solution (dynes/cm).

However, other studies also reported that a solution with lower surface tension was not always suitable for electrospinning (*71, 98, 103*). Liu and Hsieh (*71*) used a number of solvents such as acetone, dimethylacetamide (DMAc) and a mixture of both solvents to dissolve cellulose acetate (CA). The surface tensions of the polymer in acetone, DMAc and Acetone/DMAc (2:1) were 23.7, 32.4 and 26.5 dynes/cm, respectively. The lowest surface tension of acetone gave beaded fibres similar to DMAc. For a mixture of acetone:DMAc (2:1), the solution exhibited unpredictable viscosities. Surprisingly, this mixture formed a smooth surfaced fibre with a uniform fibre diameter around 700 nm.

2.3.1.3 Effect of conductivity

In general, solvents (except organic solvents) have free-ions, forming a weak conductivity of polymer solution. Addition of salt, acid or bases in a polymer solution was reported to increase the solution conductivity (*2, 26, 39, 54, 61*) and therefore jet elongation (*2, 54*). For instance, the resultant fibre diameter of electrospun poly(L-lactide-caprolactone) (P(LLA-CL)) was observed to reduce from 300 to 100 nm when the P(LLA-CL) solution conductivity increased from 0 to 13 μS/cm. According to Tan *et al.* (*54*), when the solution conductivity increased, the P(LLA-CL) jets was expected to have higher elongation along its

axis, which could result in a finer fibre diameter. These results were also in agreement with Zhang *et al.* (*46*), who reported that the resultant average fibre diameter of electrospun polyvinyl alcohol (PVA) reduced from 214 to 159 nm with the addition of sodium chloride from 0.05% to 0.2%.

2.3.2 Processing conditions

2.3.2.1 Effect of applied voltage

Recent studies have offered different opinions on the effect of applied voltage on the resultant fibre diameter of electrospun nanofibres. A number of studies reported that an increase in applied voltage reduced the resultant fibre diameter of electrospun nanofibres (*39, 51, 58, 104-105*). Jalili *et al.* (*58*) and Megelski *et al.* (*104*) reported that an increase in applied voltage gave higher elongation to the polymer jet because of the increase in culombic forces. Those results were contrasted to other literature reports, where it was reported that an increase in applied voltage produced larger fibre diameter (*41, 46, 63, 106-109*). Nasir *et al.* (*63*) observed that at higher voltage, the mass throughput of polyvinylidene fluoride (PVDF) solution increased, which resulted in bigger fibre diameter of the electrospun PVDF. Other studies have reported that an increase in applied voltage resulted in insignificant difference in fibre diameters (*54, 110-111*). Tan *et al.* (*54*) also reported that the effect of applied voltage on the poly(L-lactide acid) P(LLA) fibre diameter was insignificant. This could be due to a high voltage creates multiple jets, which forms fibres with similar diameter.

The formation of beaded fibres is also influenced by the applied voltage. Deitzel *et al.* (*51*) described the formation of beads at higher voltages. At lower voltage (5.5 kV), an electrospinning jet was ejected from the Taylor cone (Figure 2-7 (a)), forming uniform cylindrical nanofibres (Figure 2-7 (b)). As the voltage increased up to 9 kV, the Taylor cone was no longer suspended at the needle tip (Figure 2-8 (a)) and the jet extruded directly from the tip. The jet hits the internal needle wall, forming beaded fibres as shown in Figure 2-8 (b) (*51*). However, the result can be debatable because it is based on the physical observation. Therefore, the current study will investigate the effect of applied voltage on the morphological structures of electrospun fibres. Other researcher also reported the formation of beaded fibres at higher voltage (*112*). The formation of beaded fibres could be due to the increase of mass flow at higher voltage (*112*).
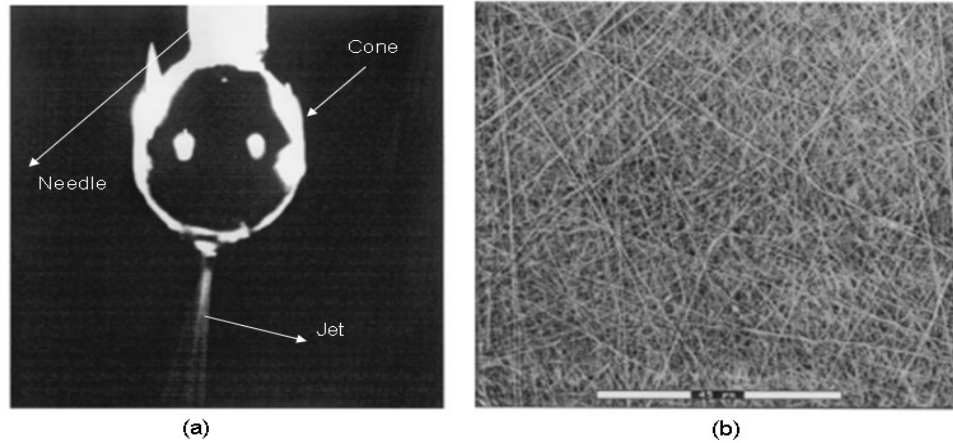
Figure 2-7: a) Photographs of electrospinning jets at 5.5kV. b) A typical SEM image of fibre morphology after spinning at 5.5kV (*51*).
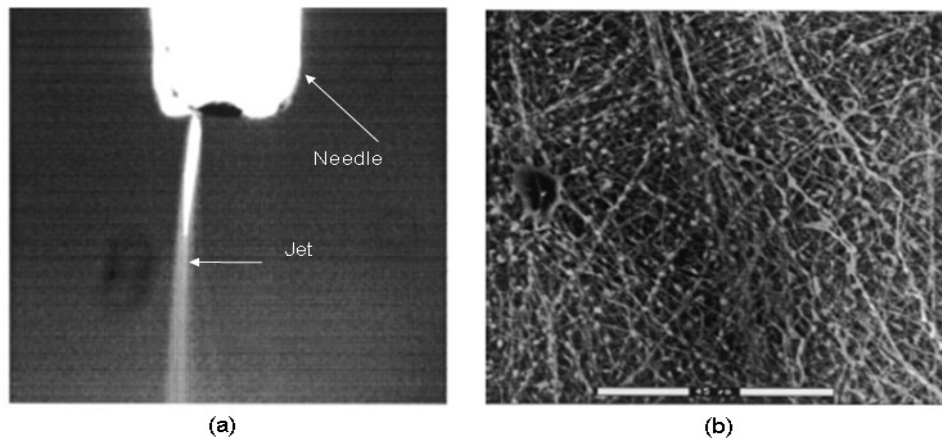
Figure 2-8: a) Photographs of electrospinning jets at 9kV. b) A typical SEM image of fibre morphology after spinning at 9kV (*51*).

Applied voltages were also reported to affect the formation of coverage area of electrospun membranes (*41*). Supaphol *et al.* (*41*) reported that the increase of applied voltage increased the electrostatic field strength. As the electrostatic field increased, the bending instability of Nylon 6 jets was assumed to decrease, which resulted in a small coverage area for the electrospun Nylon 6 membrane (*41*).

2.3.2.2 Effect of needle tip-to-collector distance

Changing the needle tip-to-collector distance was found to influence the formation of beads, interconnected flat fibres and uniform cylindrical fibres. Megelski *et al.* (*104*) observed that when a high voltage was applied at shorter

needle tip-to-collector distances, it can increase the field strength in electrospinning process. This resulted in the formation of beaded polystyrene (PS) fibres. From this experiment, it also shows that the operating distance, voltage and field strength are linearly dependent.
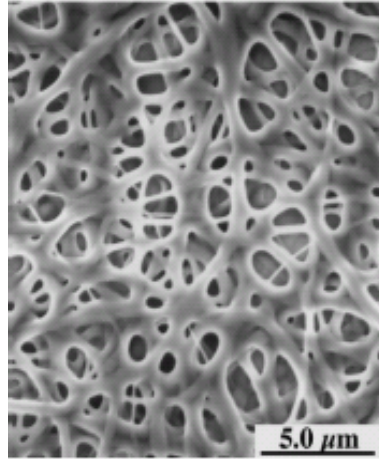
Figure 2-9: SEM image of electrospun Nylon 6,6 membrane deposited at 0.5 cm (*55*).

Buchko *et al.* (*55*) found that at shorter electrospinning distances (0.5 cm), the Nylon 6,6/ formic acid did not provide sufficient time for the formic acid solvent to evaporate, producing a series of interconnected flat fibres, as shown in Figure 2-9. However, the authors do not consider the effect of other parameters such as field strength and feed rate on the formation of interconnected flat fibres. Thus, further investigation on the electrospinning distance will be carried out in the current study.

2.3.2.3 Effect of feed rate

Feed rate indicates the amount of solution dispensed per unit time. The effect of feed rate on morphological structures of electrospun fibres was different depending on polymer solution (*2, 54, 63, 112-113*). Kidoki *et al.* (*113*) reported that the average fibre diameter of electrospun segmented polyurethane (SPU) increased (from 3 to 12 µm) with an increase in feed rate (ranging from 1 to 10 mL/hr). An increase in the fibre diameter was due to the increase in volume of the solution that was drawn from the needle tip (*113*).

However, the effect of feed rate on electrospun morphology was negligible for some of electrospun nanofibre membranes. Tan *et al.* (*54*) reported that the

effect of feed rate on the resultant average fibre diameter of electrospun Poly(L-lactide acid) P(LLA) was insignificant in concentration range of 1.25 to 4 %wt.

2.3.3 Effect of ambient parameters

The formation of electrospun nanofibre membranes can be influenced by environmental conditions such as relative humidity (RH) and atmospheric pressure. Tripatanasuwan *et al.* (*114*) demonstrated that the increase of relative humidity (RH) from 5.1% to 48.7% reduced the average fibre diameter of polyethylene oxide (PEO) from 253 nm to 144 nm. The reduction in fibre diameter was due to longer elongation of the PEO jet at higher RH. RH was also reported to affect the solvent evaporation from the electrospun nanofibres (*105*). Baumgarten (*105*) found that solvent (dimethyl formamide (DMF) evaporated faster at lower RH (less than 5%). This resulted in fibre clogging at the needle tip, that blocked the acrylic/DMF solution (*105*).

2.3.4 Other parameters

Other parameters that could influence the electrospinning process are polymer's molecular weight (*45, 54, 102, 115*) and needle diameter (*108, 116-118*). Ojha *et al.* (*45*) reported that the effect of molecular weight on fibre diameter was insignificant. The fibre diameter of electrospun Nylon 6 remain unchanged (approximately 41 nm) when the molecular weight increased from 30,000 to 63,000 g/mol. The effect of needle diameter on electrospun fibre diameter has been reported by Macossay *et al.* (*116*). They found that there was no correlation between the needle diameter and the average fibre diameter of electrospun poly(methyl methacrylate) (PMMA) (*116*).

2.3.5 Taylor cone

The formation of the Taylor cone is due to an equilibrium between solution surface tension and electrostatic forces (*112*). As mentioned earlier, the electrospinning jet is ejected from Taylor cone in order to form electrospun fibres (Figure 2-10). Taylor (*119*) reported that the electrospinning jet can be obtained if the Taylor cone angle reaches 49.3°. However, this angle can be different whether it is a polymer solution or melt. For instance, Rangkupan and Reneker (*120*)

reported that the cone angle of molten polypropylene (PP) in melt-electrospinning was approximately 37.5°.
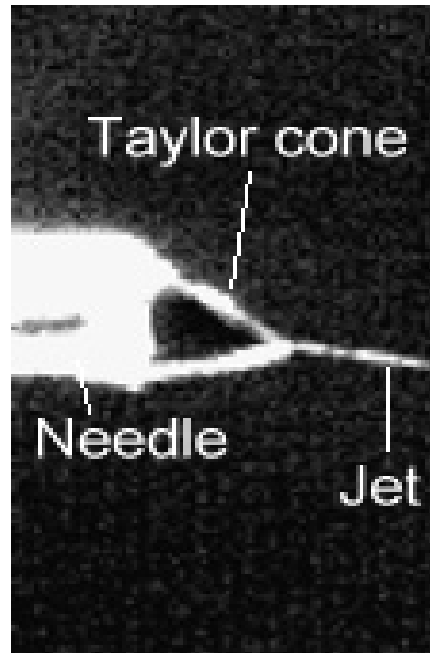
Figure 2-10: Photograph of a typical Taylor cone in electrospinning (*30*).

2.3.6 Bending (whipping) instability

Reneker *et. al* (*121*) observed that when the jet is initiated from the Taylor cone, it travels for a few centimetres in a straight line and then forms a rapid bending and whipping process in which the jet is continuously stretched and elongated by electrostatic repulsive forces (Figure 2-11). This process resulted in long, thin, and uniform electrospun fibres.
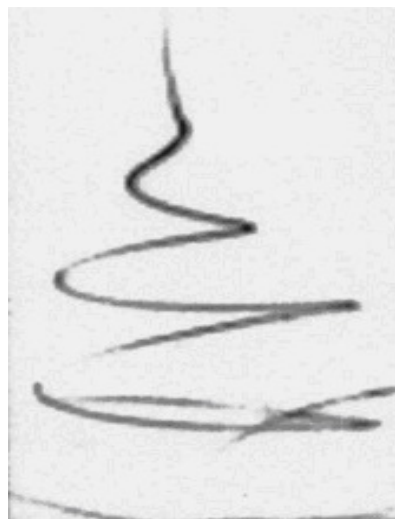
Figure 2-11: Stereographic image of a typical bending instability for electrospun nanofibres (*121*).

The formation of this bending instability (Figure 2-11) was divided into three steps (*121*);

1) the electrospinning jet was initially straight or slightly curved and then suddenly formed a series of bends

2) the elongated jet formed a series of spiral loops with a growing loop diameter

3) as the loop diameter was increased, the cross sectional diameter of the jet became smaller.

The bending instability of the electrospinning jets varies depending upon a number of factors such as the initial charge density, solution surface tension, viscoelastic properties of polymer solution, as well as the evaporation rate and dielectric constant of solvent (*30*).

A variety of jet instabilities has been reported by Eda *et al.* (*30*). They observed that the electrospinning jets of polystyrene vary for different solvents (tetrahydrofuran (THF), and *N,N*-dimethylformamide (DMF)). In Figure 2-12 (a), the polystyrene/THF solution formed several mini-jets emerging from capillary tip. For polystyrene/DMF solution, a cloud of jets was formed a few millimetres away from the Taylor cone (Figure 2-12 (b)). This cloud consists of jets undergoing whipping at a high frequency. The authors explained this observation as being due to relatively high dielectric constant and the polyelectrolyte behaviour of polystyrene/DMF solution, which produced higher charge density of jets than the polystyrene/THF solution. However, the authors did not report the evaporation of solvents and viscosities of polystyrene/DMF and polystyrene/THF solutions, which could also affect the bending instabilities of jets (*30*).

(a)　　　　　　　　　　　　　　　　　　　　(b)
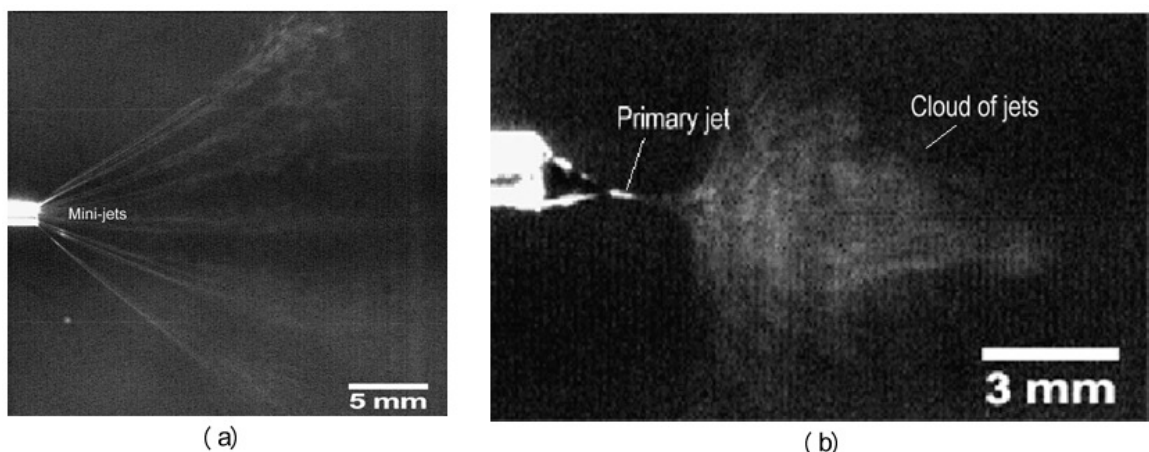
Figure 2-12: Photographs of bending instabilities of electrospun polystrene using a) THF and b) DMF (*30*).

2.4 Characterization of Electrospun Nanofibre Membranes

2.4.1 Surface roughness and wettability

Electrospun membranes are known to be materials with higher surface roughness and porous structure as compared to flat films. It was reported that the fibrous architecture of electrospun polysulfone (PSU) exhibited higher water contact angle at approximately 140° compared to the PSU cast film. The water contact angle for PSU cast film was in range of 70° to 90° (*2*).

The surface wettability of electrospun membranes can be controlled by a number of methods: 1) varying the fibre diameter (*122-124*) and 2) beaded fibres (*123*). Cui *et al.* (*122*) observed that the increase of electrospun poly(D,L-lactide) (PDLLA) fibre diameter from 0.6 to 2.4 µm reduced its water contact angle from 143 to 103°. From these results, it shows that the topography of electrospun nanofibres could influence the liquid-solid interface (*122*).

Ma *et al.* (*123*) reported that beaded electrospun poly(caprolactone) (PCL) fibres provided higher water contact angle as compared to bead-free fibres (Figure 2-13). They showed that the beaded PCL fibres formed superhydrophobic surfaces with water contact angle ranging from 133 to 139°, whereas the bead-free fibres exhibited water contact angles below 130°. The beaded fibres can be controlled by changing the operational parameters of electrospinning such as applied voltage, solution viscosity, surface tension, etc (*52, 97, 99, 122-123*).
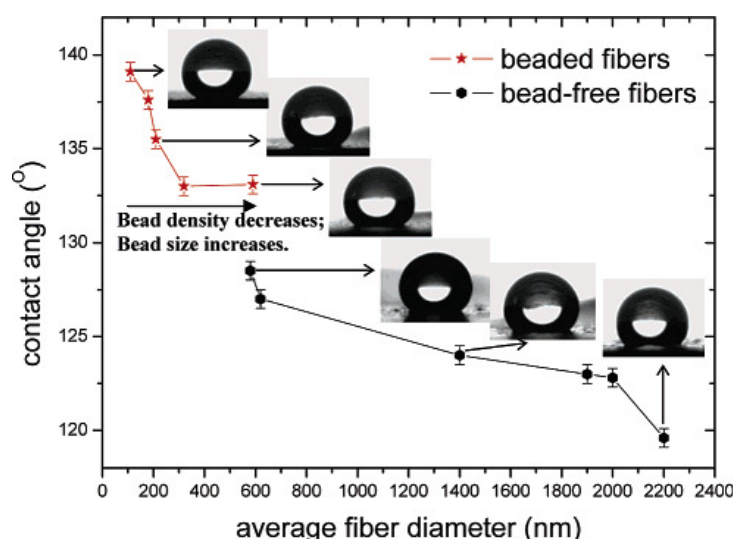
Figure 2-13: Water contact angle of beaded fibres and bead-free fibres of electrospun poly(caprolactone) (*123*).

From these experiments, it shows that the surface roughness of electrospun membrane can enhance the water contact angle of polymer. The surface roughness of electrospun membrane is usually measured using an atomic force microscopy (AFM) (*115, 125-126*). From the AFM test, Chen *et. al* (*126*) found that the deposition of electrospun poly(caprolactone) (PCL) on top of PCL substrate increased the surface roughness of the substrate. Although the AFM has been widely used to measure the membrane surface roughness, the current study will introduce the use of non-contact equipment, which is known as the white light profilometry. Details on the white light profilometry can be found in Chapter 3, Section 3.2.

2.4.2   Pore size

Particle sizes are dependent on the pore sizes of filter medium (*127*). For electrospun nanofibres membranes, the pore sizes are extremely small ranging from 4 to 100 times smaller than those of typical meltblown nonwovens (*98*). The pore sizes of electrospun membranes can be measured using a number of methods such as bubble point (*9*), liquid intrusion porosimetry (*128*) and capillary flow porometry (*129*).

Gopal *et al.* (*9*) showed that electrospun polyvinylidene fluoride (PVDF) membranes have potential to be used as microfiltration membranes because of their fine pore sizes ranging from 10.6 to 4.0 µm (*9*).

Gibson *et al.* (*12*) reported that the small pore sizes of electrospun polybenzimidazole (PBI), polyacrylonitrile (PAN) membranes and electrospun Nylon 6,6 on a carbon-loaded foam provided good resistance to the penetration of chemicals and aerosols, while allowing water vapour transport for comfort (*12*).

2.4.3   Membrane thickness

One of the advantages of the electrospinning technique is the ability to form very thin porous membrane. For example, a thin layer electrospun membrane produces a light weight air filter (*40, 130*). However, the ability to measure very thin membrane is crucial. There are two methods to measure electrospun membrane thickness: 1) direct methods such as scanning electron microscopy (SEM) (*130*) and digital micrometer (*65, 131-132*) and 2) indirect method such as equivalent thickness (*133*).

SEM has been widely used to measure a material's thickness because of its accuracy and its ability to gain detailed information of sample surfaces or cross section. Barhate *et al.* (*130*) reported that the thickness of their electrospun polyacrylonitrile was relatively easy to measure using SEM in a range of 100 to 240 µm. However, several problems were encountered mainly in SEM sample preparation. SEM requires cutting the membranes, which could distort the membrane structure. It is a time consuming method and is a complex piece of instrumentation.

A micrometer is fast and simple technique to measure sample thicknesses of any materials. Gopal *et al.* (*131*) used a micrometer to measure the thickness of an electrospun polysulfone (PS) membrane of approximately 135 µm. A micrometer requires direct contact with the sample which involving the application of a force. This is particularly an issue for spongy or compressible materials such as electrospun membranes. The compression of electropun membrane has been reported by Nisbet *et. al* (*5*). Due to its open and highly porous structure, the electrospun membrane is likely to be compressed and distorted during testing (*5*).

McKee *et al.* (*133*) proposed the equation of equivalent thickness (equation 2.3) to estimate the thickness of electrospun membrane.

$$\text{Equivalent thickness} \ = \frac{m}{A.\rho} \qquad\qquad \text{equation 2.3}$$

m indicates mass of electrospun membrane, *A* is area of the membrane and ρ is density of polymer used.

From equation 2.3, the authors were able to estimate the thickness of electrospun poly (urethane urea) membranes for tensile test.

Apart from these techniques, the current study will introduce the use of non contact equipment to measure the thickness of electrospun membrane.

2.4.4 Chemical characterisation of electrospun membranes

Fourier Transform Infrared spectroscopy (FTIR) has been used to monitor the chemical integrity of polymer before and after electrospinning. Li *et al.* (*134*) used the FTIR to monitor the chemical structures of cast film and the electrospun Nylon 6,66,1010 terpolymer. It was found that the IR spectra for electrospun Nylon 6,66,1010 terpolymer and cast film were comparable, indicating that the high voltage of electrospinning did not change the molecular structures of polymer (Figure 2-14).

In another study, Zhang and Hsieh (*135*) observed that a mixture of PAN and PEO exhibited two peaks, indicating the existence of the $-C \equiv N$ bond for PAN and $-CH_2-CH_2-O$, C-C/C-O bonds for PEO.

The IR spectra can also provide an indication of the crystal phases of electrospun fibres. According to Nasir *et al.* (*63*), the peaks at 613 and 766 cm^{-1} were associated with the α-phase of PVDF and the peaks at 840, 510 and 420-472 cm^{-1} were associated with the β-phase.
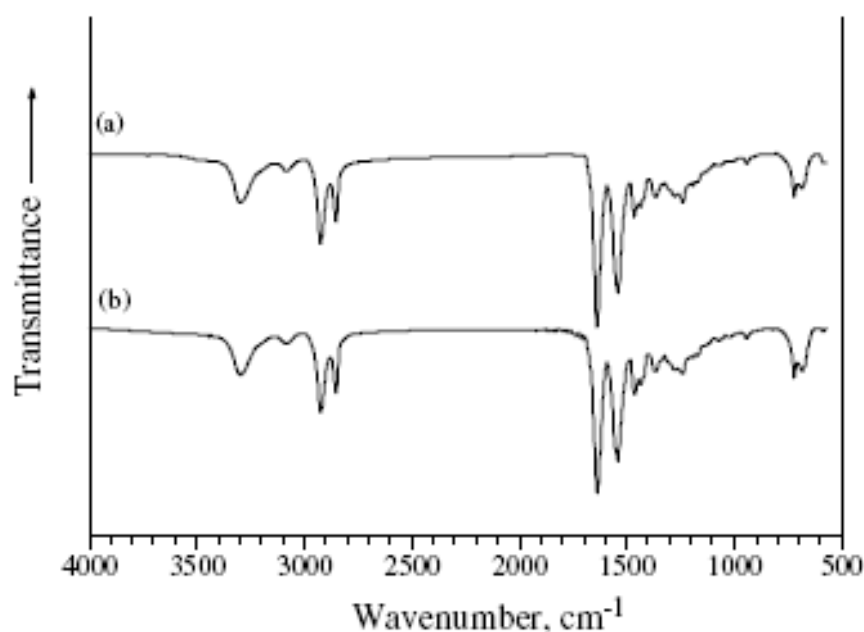
Figure 2-14: Infrared spectra of Nylon 6,66,1010 terpolymer. a) casting films b) electrospun nanofibre membranes(*134*).

2.4.5 Thermal properties of electrospun membranes

The determination of thermal properties such as melting point and enthalpy of electrospun membranes using DSC has been carried out by a number of studies (*65, 134, 136*).

Li *et al.* (*134*) demonstrated that the low melting enthalpy of electrospun Nylon 6,66,1010 terpolymer was the result of a lower percentage of crystallinity compared to the corresponding cast film. They reported that the lower crystallinity of electrospun membrane was due to the rapid solidification of the fibres that limited the development of fibre crystallinity (*134*). The cast film also exhibited a sharp exothermic peak in the DSC thermogram, whereas electrospun Nylon 6,66,1010 terpolymer showed the same transition but at a lower melting temperature (*134*). However, there is no further explanation from the authors regarding the low melting temperature of the electrospun Nylon 6,66,1010 terpolymer.

Similar results were reported by Gao *et al.* (*65*). They found that the electrospun polyvinylidene fluoride (PVDF) membrane gave a lower melting enthalpy compared to the bulk PVDF polymer. The authors expected that the rapid solidification of PVDF molecular chains under high elongation rate during the electrospinning process, retards the development of crystallinity.

Apart from melting enthalpy, electrospun membranes were reported to give lower melting temperature compared to films (*136*). In Figure 2-15, the electrospun membrane exhibited lower melting temperature (approximately 288°C) compared to the cast film (293°C). The difference was due to the molecular re-orientation of the electrospun PAN.
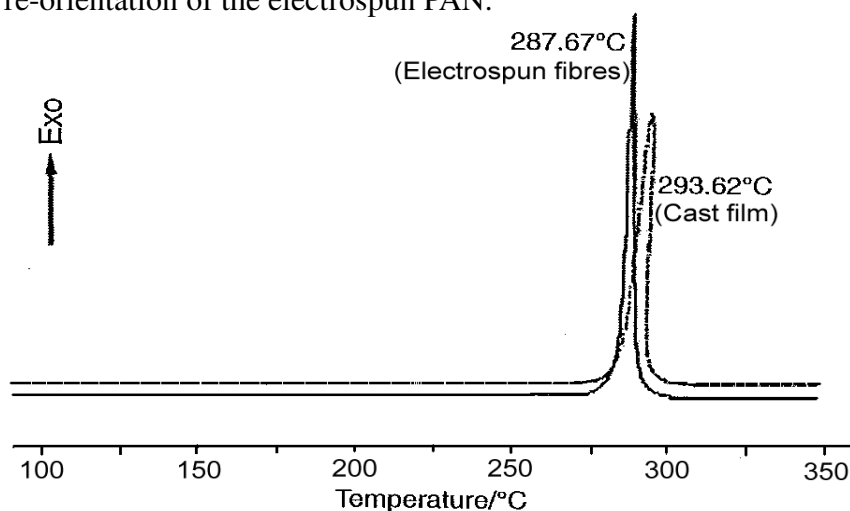
Figure 2-15: DSC thermogram of electrospun PAN and PAN cast film (*136*).

2.4.6   Crystallinity of electrospun membranes

The X-ray diffraction (XRD) is useful to determine the crystallinity of electrospun membranes as well as the chain orientation in the fibres of the membrane. Li. *et al.* (*134*) studied the crystallinity of electrospun Nylon 6,66,1010 terpolymer and corresponding cast films using the wide angle X-ray diffraction (WAXD) analysis. In Figure 2-16, the WAXD patterns of both electrospun Nylon-6,66,1010 terpolymer and the cast film exhibited two peaks. The diffraction peaks at about $2\theta = 20°$ was (100) planes, whereas at $2\theta = 23°$ was (010,110) planes. Both planes showed α-phase crystals of typical triclinic form of nylons. The authors also reported that the diffraction peaks of electrospun Nylon 6,66,1010 terpolymer were relatively low and broad compared to the corresponding cast film which had higher and sharper peaks (Figure 2-16). The broad peak of the membrane can be explained using the Bragg's equation, where the *d* -spacings (distance between adjacent crystalline planes) of electrospun membrane were much broader than those for cast films. This indicates that the macromolecular chains in the electrospun fibres may not be well-arranged due to the rapid evaporation of solvent during electrospinning. However, the authors did not discuss the effect of particle size on the peak broadening in the WAXD.

Other studies also observed that the rapid solidification during electrospinning retarded the development of crystallinity in the fibres (*59, 109, 137-138*).
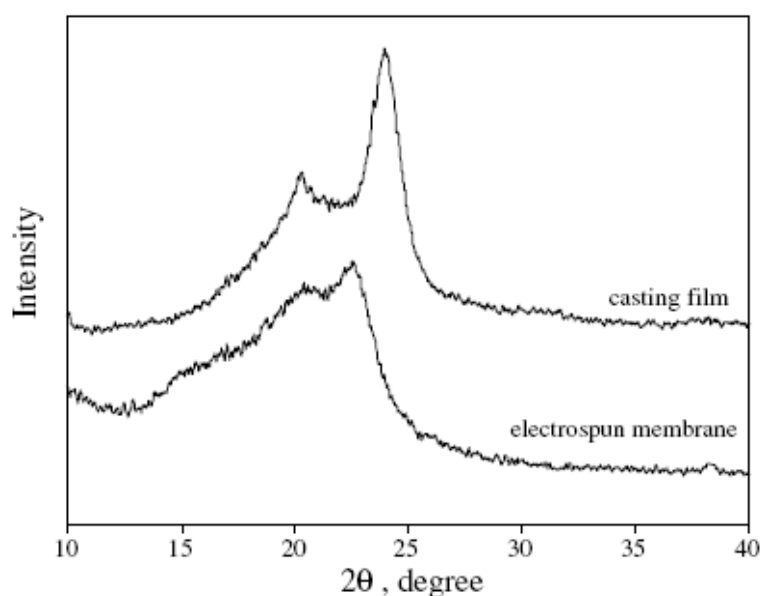
Figure 2-16: WAXD patterns of the electrospun Nylon-6,66,1010 terpolymer and cast film (*134*).

The crystallinity for electrospun fibres can be influenced by applied voltage, annealing and drum rotation (*139-140*). Bhattarai *et al.* (*140*) observed that by annealing the electrospun copolymer poly(*p*-dioxanone) (PPDO)-polyethylene glycol (PEG)- poly (L-lactide) (PLLA) at 50° for two hours provided a narrow crystalline peak at 2θ=16.4° compared to the same electrospun fibres dried at room temperature. The authors concluded that annealing the electrospun fibres can improve the cystallinity of the fibres.

Using a rotating drum as the collector for electrospun fibres was observed to increase the crystallinity of electrospun fibres. Inai *et al.* (*141*) reported that the increase of take up velocity of rotating drum from 63 to 630 m.min^{-1} formed highly ordered molecular orientation of electrospun poly(L-lactide) (PLLA) nanofibres (*141*). The resultant average fibre diameter was also observed to decrease from 890 to 610 nm, when the take up velocity increased.

The use of higher voltages in electrospinning was reported to result in higher degree of crystallinity of electrospun fibres. According to Zhao *et al.* (*108*), the crystallinity of electrospun ethyl-cyanoethyl cellulose fibres increased from 40% to 60% by increasing the applied voltage from 30 to 50 kV. The increase of applied voltage was reported to provide higher electrostatic fields on the polymer molecules, resulting in highly ordered polymer molecules (*108*).

2.5   Physical properties of electrospun fibres and membranes

Tensile test is usually used to identify the tensile properties of electrospun membranes. Details on the tensile properties of electrospun membranes are outlined below.

2.5.1   Tensile properties of random oriented electrospun membranes

The tensile deformation of a random oriented electrospun nanofibres membrane is usually related to the rearrangement or orientation of nanofibres within the membrane. Peng *et al.* (*142*) investigated the tensile behaviour of electrospun polyoxymethylene (POM), polyurethane (TPU) and core/sheath electrospun POM/TPU membranes. The polymers were blended at different mass ratios (9:1, 8:2 and 7:3 for POM:TPU) at a fixed concentration in order to improve the toughness of POM. Figure 2-17 illustrates the stress versus strain graphs of pure POM, TPU and blended POM and TPU. They observed that the pure TPU exhibited higher elongation-at-break and lower modulus than the pure

POM because of the elasticity of TPU. The pure TPU also gave higher tensile strength compared to the pure POM due to the lower porosity of TPU membranes (approximately 49%) compared to the POM membranes (approximately 80%) (*142*).

For core/sheath electrospun POM/TPU, the increase of TPU in the blending ratio was reported to increase the elongation-at-break of the membrane. This was due to the increase in elasticity of the membranes. When the amount of TPU increased from 0 to 30%, the tensile strength was observed to increase due to a reduction in membrane porosity. The membrane tensile strain of core/sheath electrospun POM/TPU was considerably lower than that of the pure POM (approximately 44%) because of the elastomeric behaviour showed by the electrospun POM/TPU membrane (*142*). However, results presented in Figure 2-17 cannot be directly compared because these membranes are made off different polymers.
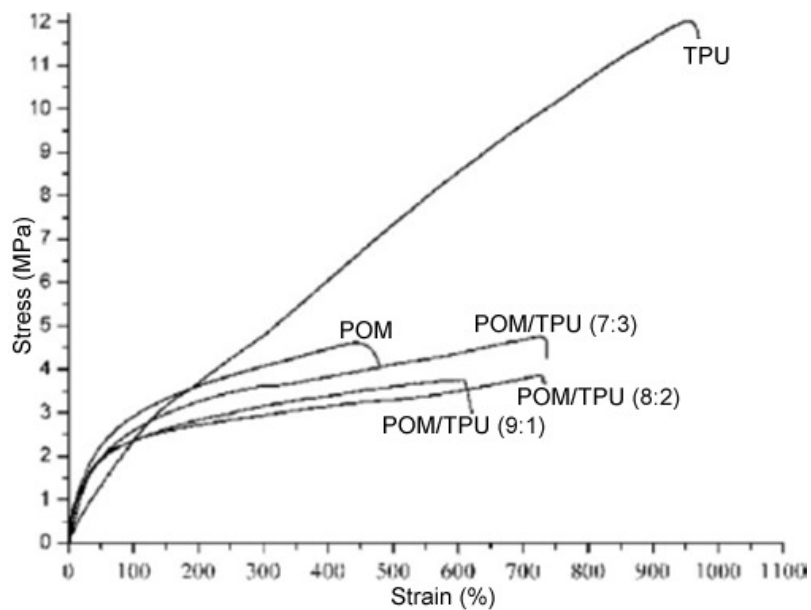
Figure 2-17: A plot of stress-strain behaviour of the pure POM, TPU and blended POM/TPU electrospun fibre mats (*142*).

The tensile properties of mono- and double layered electrospun homopolymer polyvinylidene fluoride (PVDF) membranes have been studied by Na *et al.* (*139*). The mono and double-layered of homopolymer PVDF membranes were hot pressed at 25 to 155°C using a roller hot presser in order to improve fibre

bonding of the membranes. From their experiments, it was found that the moduli and tensile strength of mono- and double- layer PVDF increased, as the temperature increased from room temperature to 155°C. The increase of tensile moduli and strength were attributed to the improvement of fibre bonding in the membrane (*139*).

A study on the tensile properties of electrospun Nylon 6 membranes at different molecular weights (high molecular weight (HMW), medium molecular weight (MMW) and low molecular weight (LMW)) was carried out by Ojha *et al.* (*45*).

Table 2-4: Tensile properties of electrospun Nylon 6 membranes at different molecular weight (MW) (*45*).

Electrospun membranes	MW (g/mol)	Porosity (%)	Tensile strength (MPa)	Elongation at break (%)	Modulus (MPa)
High Molecular Weight (HMW)	63,000	85	52 ± 5	16.6 ± 2.5	333 ± 39
Medium Molecular Weight (MMW)	50,000	87	46 ± 2	18.7 ± 0.8	332 ± 45
Low Molecular Weight (LMW)	30,000	86	21 ± 2	9.3 ± 1.7	231 ± 15

The authors found that doubling the molecular weight (Mw) of Nylon 6, they doubled the tensile strength of the electrospun Nylon 6 (*45*). However, there is no statistical difference in tensile strength, elongation at break and modulus between the HMW and MMW. For LMW, the Young's modulus was found to be lower than the MMW and HMW.

The authors also investigated the effect of fibre-fibre bonding on the tensile properties (such as tensile strength, elongation at break and modulus) of the membranes. They observed that the increase in MW did not significantly affect the strength of fibre-fibre bonding. This could be due to the fact that the porosities for the HMW, MMW and LMW membranes are almost identical (*45*).

2.5.2 Tensile properties of aligned electrospun nanofibre membranes

Huang *et al.* (*28*) investigated that the tensile properties of random and aligned electrospun polyimide (PI) membranes. The random oriented electrospun PI membranes were collected on the collecting cylinder at surface speed of 0.59

m/s, whereas the aligned oriented PI membranes were collected at surface speed of 23.45 m/s. From the experiments, the authors observed that the aligned electrospun PI exhibited higher tensile strength (187 MPa) than the non-aligned electrospun PI (40 MPa). The higher tensile strength and modulus were due to the higher molecular orientation of the aligned PI fibres as compared to random fibres. (*28*).

2.5.3   Tensile properties of single electrospun nanofibre

Inai *et al.* (*143*) reported that when the random oriented electrospun poly(L-lactide-co-ε-caprolactone) copolymers (P(LLA-CL)) membranes were uniaxially strained, the load was not equally applied to all the nanofibres, resulting in a re-aligned along the axis of strain (Figure 2-18). The authors also observed fibre fusion after the tensile test.
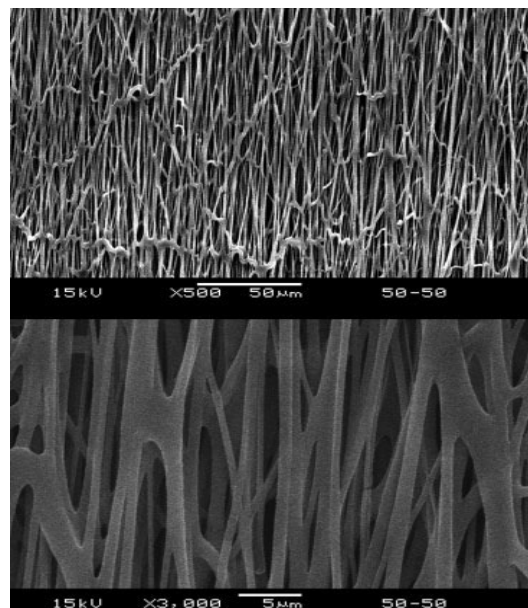
Figure 2-18: SEM image of fibre alignment after tensile test (*143*).

The formation of fibre fusion was left unexplained. The authors modified their sample preparation in order to understand the tensile properties of electrospun P(LLA-CL) fibres. They invented a rotating disk collector with an attachable table (conductive plate and paper tab holder) to collect aligned electrospun nanofibres (Figure 2-19). Several aligned nanofibres were collected onto the paper frame after short period of spinning. A single electrospun nanofibre was removed with the aid of a microscope. From the experiments, they concluded

that the tensile strength of a single electrospun P(LLA-CL) fibre increased with increasing on rotating speed. This high tensile strength could be due to the formation of a highly orientated molecular structure of P(LLA-CL) fibres at the higher rotating speeds. In the wide angle X-ray diffraction (WAXD) pattern, the electrospun P(LLA-CL) fibres collected at 630 m/min exhibited semi-crystalline fibres with a broad peak at $2\theta = 17°$. For non-aligned electrospun P(LLA-CL) fibres, there was no peak observed, indicating that the fibres were amorphous or less crystalline than the aligned fibres. The authors also found that, the highly orientated fibres reduced the strain-at-break of a single electrospun P(LLA-CL) fibre (*141*). This could be due to the fibres have greater crystallinity, which reduce the strain-at-break of the fibres (*141*).
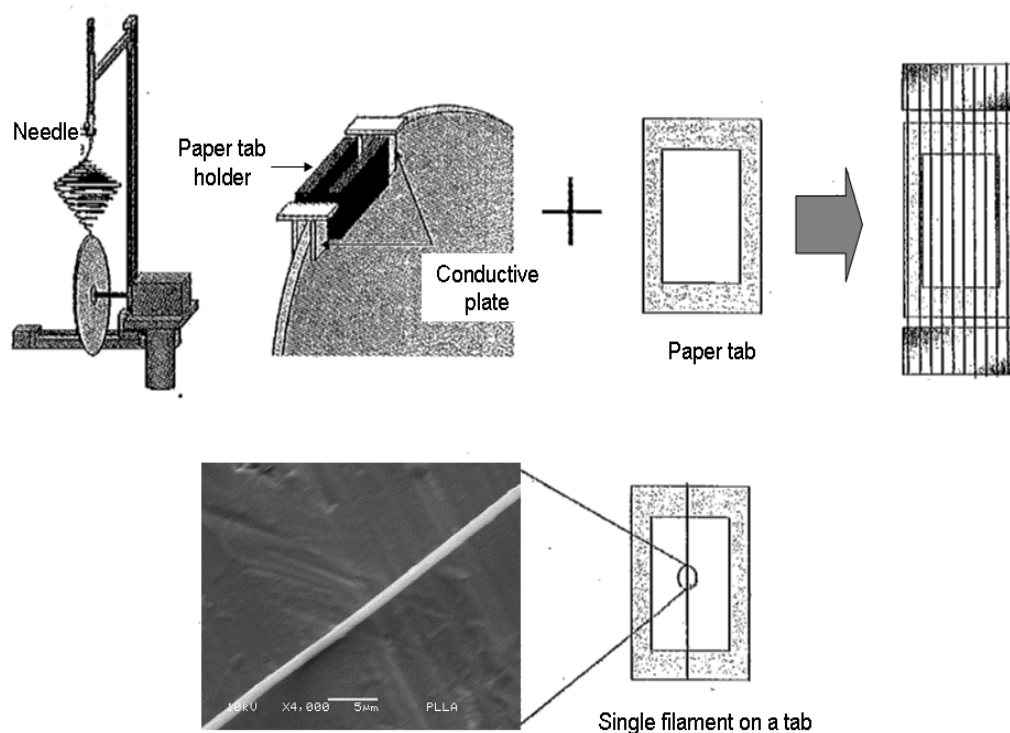
Figure 2-19: Tensile specimen of P(LLA-CL) single nanofibre invented by Inai *et al.* (*2, 141*).

The tensile properties of a single electrospun fibre was also carried out by Wong *et al.* (*144*). The authors emphasized the effect of fibre diameter, molecular orientation and degree of crystallinity on the tensile strength of a single electrospun poly(caprolactone) (PCL) fibre. The sample preparation involved in single fibre tensile testing illustrated in Figures 2-20 (a-b). The electrospun PCL fibres were collected onto aluminium foils. Each foil was placed onto two non-

conductive strips and was connected to the ground as shown in Figure 2-20 (b). The fibres were then mounted on a trimmed cardboard sheet with double sided tape as shown in Figure 2-20 (b). These fibres were trimmed under the microscope in order to leave exactly a single fibre intact on the cardboard sheet. The single PCL fibre was tested using ultra-sensitive testing equipment (MTS NanoBionix®). From the scanning electron microscopy (SEM) analysis, the resultant fibre diameters varied ranging from 300nm to 2500nm. The authors reported that the tensile strength of a single electrospun PCL fibre increased when the fibre diameter was decreased. The reduction of fibre diameter was found to give higher crystallinity and molecular orientation of electrospun PCL fibres (*144*).
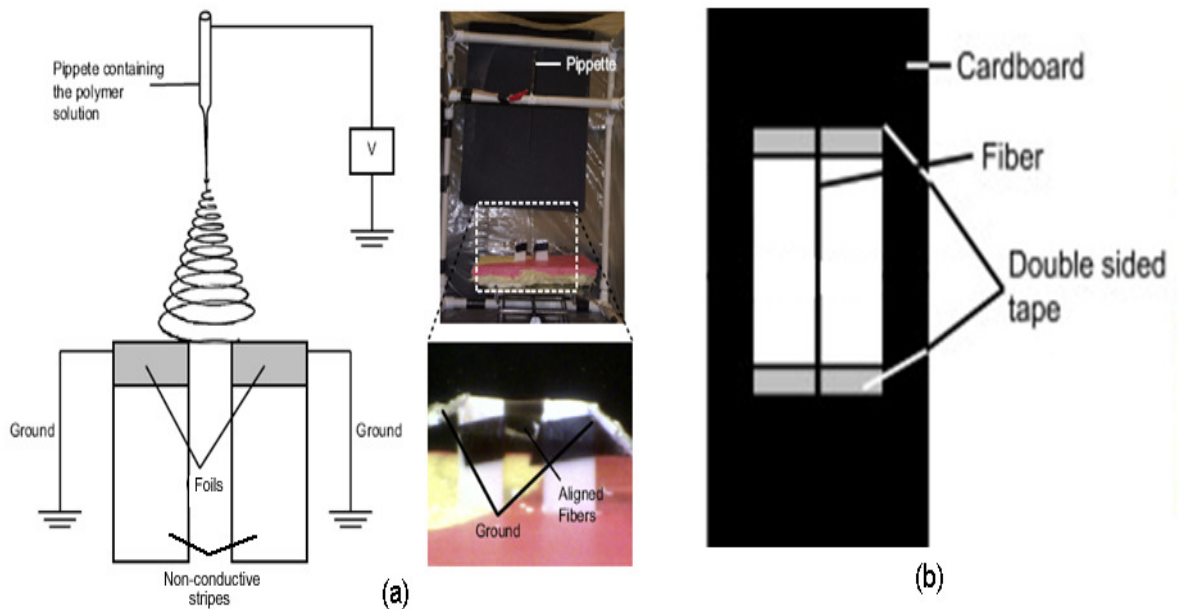
Figure 2-20: Photographs of: a) electrospinning system invented by Wong *et al.* (*144*) and b) sample preparation for single fibre testing (*144*).

2.5.4 Tensile properties of electrospun yarn

Apart from electrospun fibres and membranes, the tensile properties of electrospun yarn have also been investigated. Fennessey and Farris (*62*) studied the tensile properties of electrospun PAN yarn. The electrospun PAN fibres were collected on a rotating drum with a surface speed of 9.8 m/s. The fibres with average diameter of 0.27–0.29 µm were twisted with angles of twist ranging from 1.1 to 17°. The increase of these twist angles was found to change the yarn size in

a range of 326 and 618 denier (denier is mass (g) per 9000 m length of yarn). At 1.1° twisting angle, they found that the tensile strength and modulus of the yarn was 3.8 GPa and 91 MPa, respectively. When the twisting angle increased up to 11°, the tensile strength and modulus increased to 5.8 GPa and 163 MPa, respectively. However, further increase in twisting angle (above 11°) reduced the tensile strength and modulus of the electrospun PAN yarn.

2.6   Adhesion strength

Adhesion strength is an interfacial phenomenon between two or more layered materials (*145*). It is one of the essential physical properties in technical applications particularly in microelectronic packaging (*146*), polymer composites (*147-149*), adhesive tape (*150*), etc. The peel test is one of the common methods to measure the adhesion strength between bonded materials (*151*). (Details on the theory of peel test will be discussed in Chapter 3). There are a number of standard test methods for peel test listed in the American Society for Testing and Materials (ASTM) and International Organization for Standardization (ISO) such as T-peel test panel and test specimen (ASTM D1876), Roller peel test (ASTM D3167), climbing drum peel test (ASTM D1781), 180º peel test (ASTM D903), 90º peel test (ASTM D6862-04), T-peel test for flexible-to-flexible bonded assemblies (ISO 11339:2010), Peel test for a flexible-bonded-to-rigid test specimen assembly Part 2: 180 degree peel (ISO 8510-2:2006) and Determination of adhesion to a rigid substrate: 90 degree peel method (ISO 813:2010).

These test methods can be applied to different types of bonded material. Bundy *et al.* (*152*) used a 90° peel test to measure the adhesion strength of soft tissue on biomaterials such as skin to stainless steel. Three tissue adhesives (cyanoacrylate, fibrin glue and glycerol) were attached to mouse skin and stuck onto a stainless steel substrate, shown in Figure 2-21.
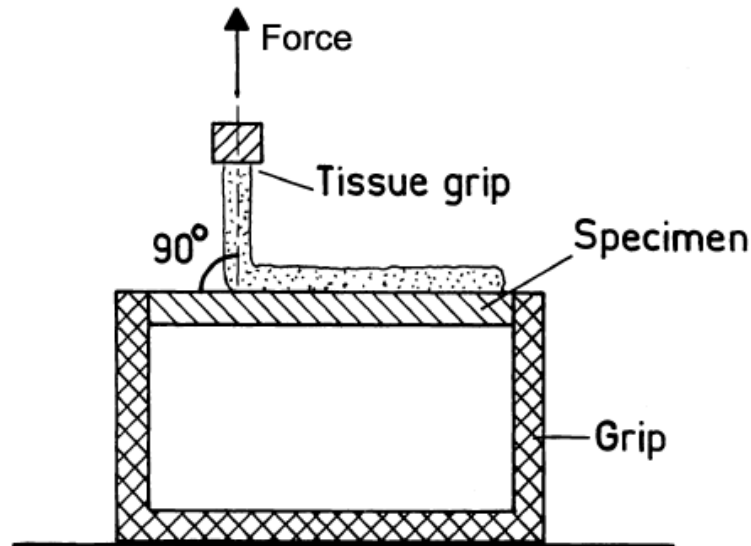
Figure 2-21: Schematic diagram of 90° peel test used to determine adhesion strength for biomaterials (*152*).

The samples were tested using a peel test device designed by the authors. The peel device consisted of a transducer, a pre-amplifier and a chart recorder. In this system, a DC motor controlled the speed and power of the peel-tester. Signals from the force transducer were amplified using a pre-amplifier. During the test, the peel profile was recoded by the chart recorder. The maximum load (N) was recorded and divided by the sample width (mm) in order to determine the bonding strength (N/mm). From these experiments, the authors found that cyanoacrylate gave highest adhesion, followed by fibrin glue and glycerol (*152*).

Mc Cabe *et. al* (*153*), designed an experimental system using a 180° peel test to measure the adhesion strength between the polyvinylsiloxane denture soft liner and denture material, as shown in Figures 2-22 (a-b).
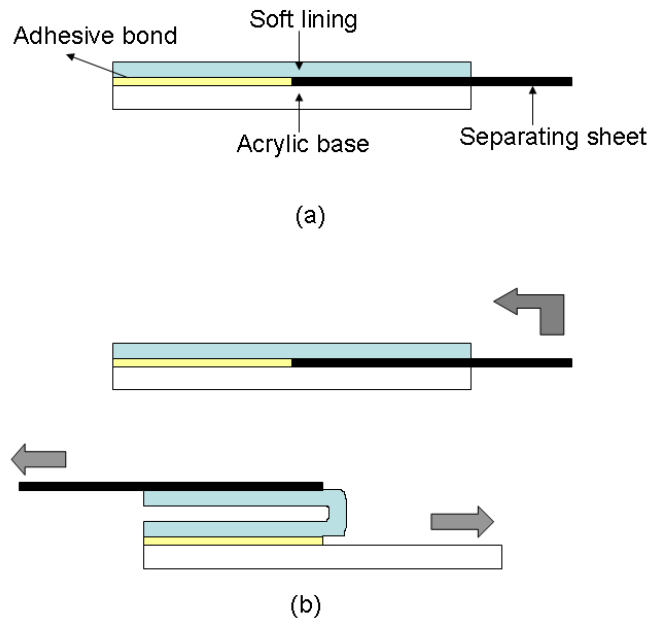
Figure 2-22: Schematic diagrams of: a) sample preparation for soft lining/acrylic denture base material and b) peeling direction (*153*).

In Figure 2-22 (a), an adhesive is applied over the acrylic denture base material. During the application of the soft lining, half the base area was covered with a thin clear plastic sheet in order to assist the separation between the soft lining and acrylic denture. The soft lining was bent at 180° and the adhesion was tested using an Instron at cross head speed of 10 mm/min (Figure 2-22 (b)). The highest force (N) obtained after the test was recorded, and was divided with the sample width (mm) in order to determine the bond strength between the materials. Using this method, the authors have successfully measured the bonding strength (N/mm) of soft lining for denture application (*153*).

The versatility and simplicity of the peel test would seem to indicate that this test method has the potential to be used to measure the adhesion strength between electrospun membrane and substrate or between electrospun membrane and electrospun membrane. The deposition of electrospun membranes onto substrates have been reported by a number of studies (*1, 11-12, 14, 93, 154*). Grafe *et al.* (*1, 11*) reported that layering electrospun membrane onto cellulose substrates can increase the filtration efficiency for submicron contaminants by holding 2.5 times more mass dust compared to a pure cellulose filtration media. The fabrication of a double layered electrospun membranes was reported by Na *et al.*

47

(*139*), where they studied the effect of hot pressing on the tensile properties of the membranes.

The enhanced properties of electrospun/substrate systems are already recognized (*1, 11-12, 14, 93, 154*), however the adhesion strength between the electrospun membrane and the substrate is not discussed. The importance of adhesion was reported by Zhu *et al.* (*93*) and Kim *et al.* (*154*), where they observed that electrospun membranes have poor adhesion to substrates and they were easily peeled off after testing. Hence, an investigation on the adhesion strength will be carried out in the current study, particularly for the bi-layer electrospun membranes.

2.7   Potential applications of electrospun nanofibre membranes

Electrospun nanofibre membranes are characterized by their higher surface area per mass (depending on fibre diameter) compared to bulk fibres and film (*130, 155*), their light weight (*4*) and their small pore sizes (*3*). Due to these unique properties, recent studies have employed electrospun membranes in various applications such as filtration (*1-3, 6, 9, 112, 156*), biomaterials (*2-3, 6, 8, 112*), protective clothing (*2, 12, 14*) and electronic applications (*2, 6, 112*).

2.7.1   Filtration

Electrospun nanofibre membranes have been reported to provide good properties for filtration applications. Truong *et al.* (*157*) reported that the incorporation of aliquat 336 into the electropsun copolymer Poly(vinylidene fluoride)-hexafluoropropylene (copolymer PVDF) has successful removed the toxic metal cadmium from hydrochloric acid solutions.

Gopal *et al* (*9, 131*) investigated the solid-liquid separation using electrospun polyvinylidene fluoride (PVDF) nanofibre membranes. The fibre diameter of electrospun PVDF was approximately 380 nm and the pore diameter was in a range of 4-10.6 µm. The authors found that the electrospun PVDF membranes were able to remove 5-10 µm particles without damaging the membrane's structure or surface. The authors suggested that the electrospun membranes have the potential to be used as a pre-filter for ultrafiltration in order to minimize fouling formation (*9*).

The same authors also studied the solid-liquid separation using electrospun polysulfone (PS) membranes (*131*). The smallest pore of electrospun PS membranes was 1.2 µm and the resultant average fibre diameter was 470 nm. They measured the separation factor (SF) of these membranes using equation 2.4,

$$S.F = \left(1 - \frac{C_{permeate}}{C_{feed}}\right) \times 100\% \qquad \text{equation 2.4}$$

where $C_{permeate}$ and C_{feed} are the concentrations of permeate solution and feed solutions, respectively (*131*).

From equation 2.4, the authors observed that the electrospun PS removed more than 99% of particles in the size range of 7 to 10 µm. For particles ranging in size from 0.1 to 3 µm, the membranes were found to remove 84-94%. For separation of fine particles such as 0.1 and 0.5 µm, the flux was observed to decrease with time and the membrane eventually was permanently fouled. Possible reasons for the low flux and permanent membrane fouling were due to direct interception, inertial impaction and diffusion. Direct interception occurs when a particle collides with the fibres. Inertial impaction occurs if the particle in the liquid fails to pass through the tortuous path of random oriented fibre in the membrane. This could cause the particles to attach onto a fibre surface. Diffusion (Brownian motion) occurs when extremely small particles (usually less than 1 µm) flow through the membrane regardless of the liquid flow. These particles are likely to be retained by adsorptive forces (*131*). The ability of electrospun membrane to remove solid particles from liquid has already been investigated by recent studies (*9, 131*). Hence, the feasibility of the membrane to be employed as a water filter for industrial wastes will be explored in the current study.

Apart from liquid filtration, electrospun nanofibre membrane can also be used for high efficiency particulate air (HEPA) and ultra low penetration air (ULPA) filter membranes (*40, 158*). Heikkila *et al.* (*158*) tested the filtration efficiency of electropsun polyamide 66 membrane using submicron particles of approximately 0.16 µm. They observed the incorporation of polyamide 66 as a coating (from 0.1 to 0.2 g/m^2) onto nonwoven substrates improved the filtration

efficiency of particles from 60-80%. However, the increased of filtration efficiency, resulted in pressure drop increases (*158*).

2.7.2 Biomaterials

The potential electrospun fibre is being investigated to be used as biomaterials. The electrospun scaffold acts as a temporary extra cellular matrix (ECM), which permits the growth and proliferation of cells. The feasibility of electrospun membranes for cell regeneration has been carried out by a number of researchers (*6, 8, 128, 159-161*).

Li *et al.* (*128*) fabricated a nanofibrous scaffold from a copolymer poly(D,L-lactide-*co*-glycolide) (PLGA) for the growth of two types of cells fibroblasts and bone marrow-derived mesenchymal stem cells (MSCs). The high surface area-to-volume ratio of the electrospun PLGA scaffolds were found to promote cell growth and good cell attachment (Figure 2-23) (*128*) .
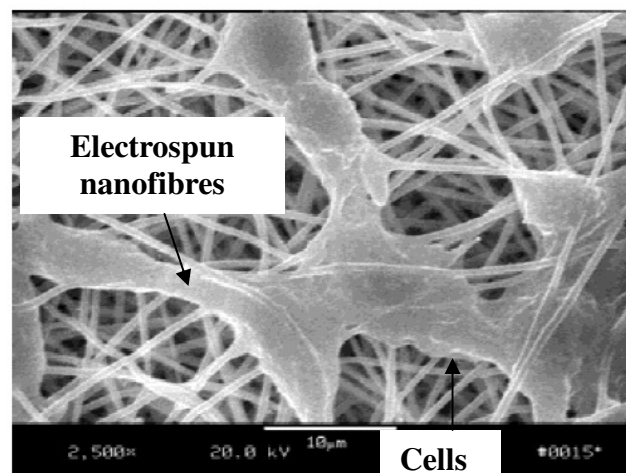
Figure 2-23: SEM image showing cells growing on PLGA electrospun nanofibrous scaffold after 3 days of culture (*128*).

Randomly oriented electrospun membranes were reported to provide promising properties for wound dressings. Wound dressings are particularly used for protection against dehydration and infection of wound from the environment, as well as to assist in the regeneration of tissue (*162-164*). Ruiz-Cardona *et al.* (*165*) reported that wound dressing materials should exhibit the following properties: able to control evaporative water loss, be permeable to selected gasses, be impermeable to bacteria and have good adhesion to skin. The feasibility of

electrospun polyurethane (PU) membranes to be employed as wound dressing materials has been investigated by Khil *et al.* (*163*). They observed that electrospun PU nanofibre membranes controlled evaporative water loss from the wound and provided excellent oxygen permeability and fluid drainage.

The beneficial effects on wound healing using electrospun nanofibre membranes have also been observed by Chen *et al.* (*166*). A composite nanofibre polyethylene oxide (PEO) with collagen and chitosan was found to promote wound healing as well as cell migration and proliferation. They also concluded that the composite electrospun membranes exhibited better wound healing performances than the gauze and commercial collagen sponge (*166*).

2.7.3   Energy applications

A number of studies have reported that the high surface area and porosity of electrospun nanofibre membranes can also be used in photovoltaic cells (*6*), batteries (*64, 66*) and membrane fuel cell (*6, 167*) applications.
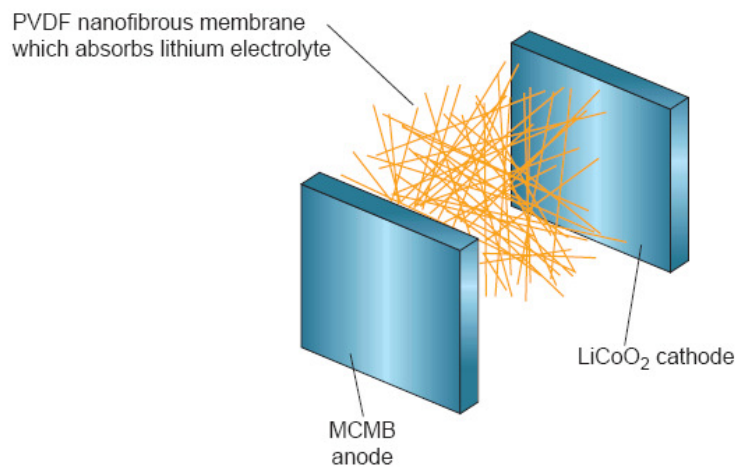
Figure 2-24: Electrospun PVDF nanofibre used as separator in a polymer battery. The PVDF nanofibres are sandwiched in between a mesocarbon microbead (MCMB) anode and a LiCoO$_2$ cathode (*6*).

Figure 2-24 illustrates the use of a high porosity electrospun PVDF membrane, which allows a high uptake of lithium electrolyte (approximately 350 wt%) and reduces the electrolyte leakage. In addition, the high surface area of electrospun PVDF nanofibre membrane allows ion conductivity in the battery and improved energy density per unit weight compared to traditional batteries (*6, 64*).

Electrospun PVDF membranes were also impregnated with Nafion for direct methanol fuel cell (DMFC) applications (*167*). Nafion provides a high crossover of methanol fuel from anode to cathode, resulting in fuel waste and polarization loss at the cathode. Choi *et al*. (*167*) reported that the incorporation of electrospun nanofibrous PVDF onto Nafion membrane gave lower methanol crossover while maintaining proton conductivity than the uncoated Nafion (*167*).

2.7.4 Protective fabrics

Protective fabrics have been used widely in a number of applications. As reported by Graham *et al.* (*4*), protective fabrics have potential to be in aerosol protection. The authors designed a protective fabric comprised of one or more layers of electrospun nanofibres on a nonwoven substrates with good aerosol barrier properties (*4*).

Further studies on electrospun membranes for protective fabrics were investigated by Gibson *et al.* (*12-13*) and Lee *et al.* (*14*). Gibson *et al.* (*12*) reported that the electrospun membranes exhibited higher breathability and aerosol filtration efficiency compared to the commercial textiles or membranes used in protective fabrics.

2.7.5 Sensors

The unique properties of electrospun nanofibre membranes such as high surface area and porosity provide better performance for sensor applications. Ramakrishna *et al.* (*2*) reported the incorporation of electrospun nanofibres into sensors for use in gas, chemical, optical and biological sensing (*2*).

As described earlier in Chapter 2, electrospun membranes are characterized using a number of measurement techniques. In the current study, some of the techniques used to characterize the physical and chemical properties of electrospun membranes include scanning electron microscopy (SEM), white light profilometry, capillary flow porometry, fourier transform infrared spectroscopy (FTIR), X-ray diffraction (XRD), tensile test, peel test and liquid filtration. The principle and theoretical background of the techniques are outlined below.

3.1 Scanning electron microscopy (SEM)

Figure 3-1 illustrates the schematic diagram of SEM which consists of an electron gun, a series of electromagnetic lenses and aperture (*144*). An electron beam is emitted from an electron gun. The electron beam goes through several electromagnetic lenses, including condenser lenses and objective lens. When the high electrons strike on the specimen surface, they produce inelastic scattering. During the inelastic scattering, an incident electron transfers kinetic energy to an electron in a specimen. With a sufficient kinetic energy, this electron will become secondary electrons (SE). The secondary electrons (SE) are then collected by a detector and amplified by an amplifier to produce image (*144*).
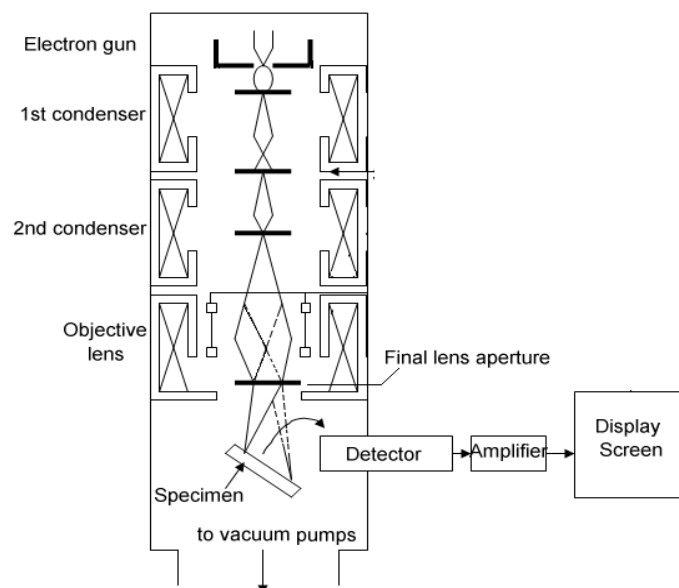
Figure 3-1: Schematic diagram of scanning electron microscope (*168*).

3.2 White light profilometry

The surface roughness of electrospun membranes can be measured using a non-contact technique known as white light profilometry. The basic principles and components of the white light profilometry are illustrated in Figure 3-2. It consists of a white light source (quartz-halogen), lens, spectrophotometer, a signal processing system and image analysis software. White light is focused through a lens that imparts a high level of axial chromatic aberration onto the sample surfaces. As the white light is scanned across the sample, the light is reflected from the sample surface to a spectrophotometer. The software selects the wavelength that is focused on the surface point. The relative height of the surface points forms a profile, which determines the surface roughness and topography of a material (*169*).

This technique can also be used to measure the thickness of electrospun membrane. For the thickness measurement, a flat surface such as glass slide is used as a zero point or base in order to differentiate between the electrospun membrane surface and the flat surface. The white light profilometry is used to scan across the flat surface and electrospun membrane. A large step change from the flat surface to electrospun surface gave sufficient information on the electrospun membrane thickness.
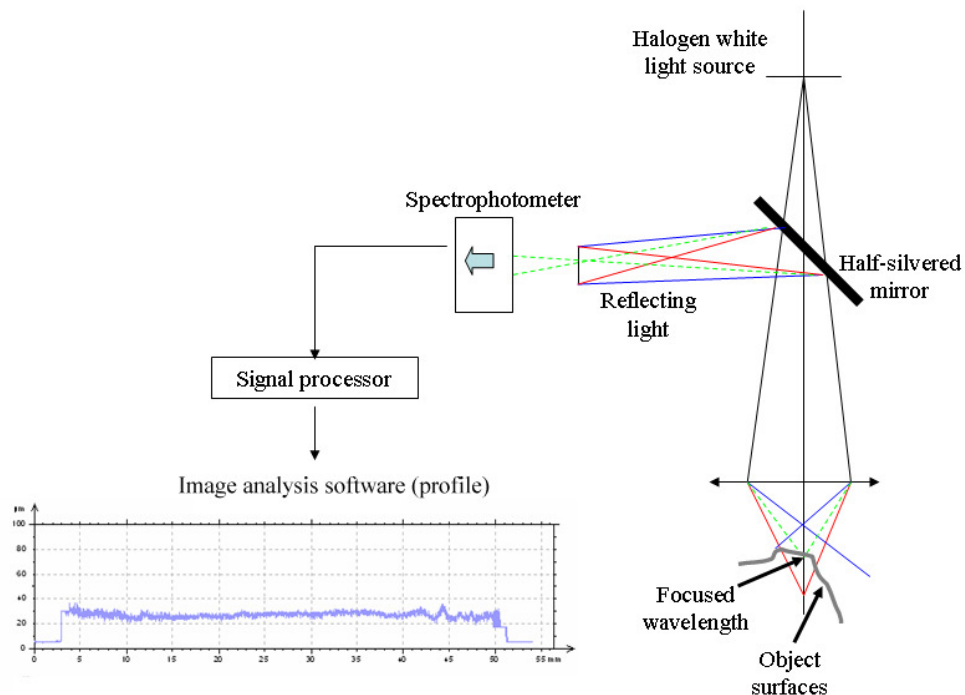
Figure 3-2: Schematic diagram of white light system (*169*).

3.3 Water contact angle (surface wettability) and surface energy

The wetting propensity of surfaces has been used in many technological fields such as painting, gluing, inking etc. One of the common methods used to determine wetting properties is the measurement of a water contact angle. The theory behind water contact angle has been described by a number of researchers. Figure 3-3 illustrates the Young theory, which is one of the earliest theories on wettability (*37*).
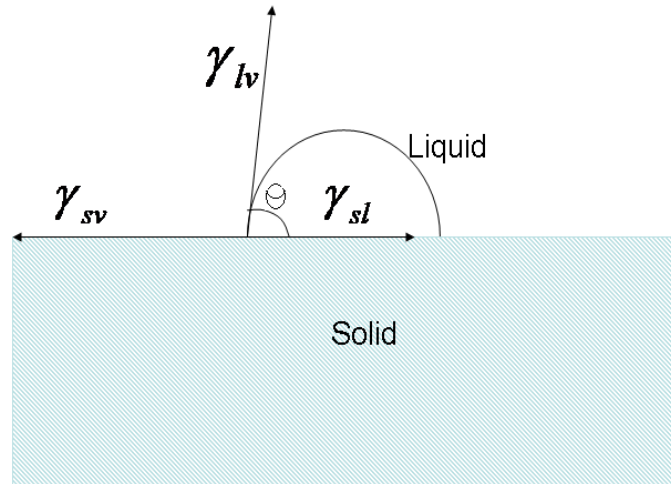
Figure 3-3: Schematic diagram of the water contact angle as proposed by Thomas Young (*37*).

In Young's theory, a drop of liquid is placed onto a solid surface. The drop shape alters due to an interfacial surface tension, until reaching equilibrium. The equilibrium is based upon three-phases (solid/liquid, solid/vapour and liquid/vapour interfaces), which can be determined using equation 3.1,

$$\gamma_{sv} - \gamma_{sl} = \gamma_{lv} \cos\theta \qquad\qquad \text{equation 3.1}$$

where γ_{sv} is the surface tension at solid/vapour interface, γ_{sl} is the surface tension at the solid/liquid interface, γ_{lv} is the surface tension at the liquid/vapour interface and θ is the equilibrium (Young) contact angle.

In the theory, the solid surface should be homogenous, rigid, solid and smooth. In addition, the liquid/solid interaction should not result in swelling of the solid, penetration of liquid into the solid or restructuring of solid. However, this theory is not applicable for electrospun membranes because the membrane

surfaces are not homogenous. The membranes have high surface roughness with porous structures.

For materials with rougher surfaces and porous structure, there are two possible theories: 1) Wenzel theory and 2) Cassie and Baxter theory (*37, 170-171*).

In the Wenzel theory, a drop is penetrated into the rougher surface and the equation is shown as,

$$\cos\theta_w = r\cos\theta_y \qquad\qquad \text{equation 3.2}$$

where r is the roughness factor, θ_w is the Wenzel angle and θ_y is the Young angle (based upon equation 3.1).

In equation 3.2, r (roughness factor), can be calculated using equation 3.3,

$$r = \frac{B}{A} \qquad\qquad \text{equation 3.3}$$

where B and A are the rough and smooth solid surfaces from the same materials.

Based upon equations 3.2 and 3.3, Wenzel noted that the Wenzel angle (θ_w) increases with roughness, if the Young angle (θ_y) is greater than 90°. If the Young angle (θ_y) is less than 90°, the increase in surface roughness reduces the Wenzel angle (θ_w). In other words, a material with hydrophilic surface will become more hydrophilic, if the surface roughness increases. In the case of a hydrophobic material, an increase in surface roughness gives higher hydrophobicity of the material (*170, 172*)

For porous materials, the water contact angle is usually based on Cassie and Baxter theory. In this theory, an apparent contact angle can be measured using equation 3.4,

$$\cos\theta_w = f_1 \cos\theta_R - f_2$$ equation 3.4

where θ_w is the apparent receding contact angle for the porous surface, θ_R is the solid/liquid receding contact angle, f_1 is the total area of solid/liquid interface and f_2 is the total area of liquid/air interface in a plane geometrical area to the rough surface (*171*).

Based on the Cassie and Baxter theory, Quéré and Reyssat (*172*) predicted that a material with a porous structure provides an air gap between the water droplet and the porous surface, as shown in Figure 3-4. The air gap prevents the water droplet from penetrating through the material surfaces. Hence, the water droplet can only sit on the surfaces with higher contact angle (*172*).
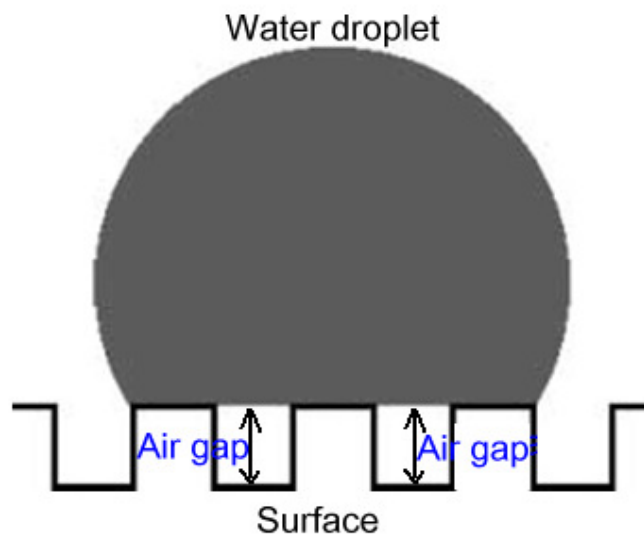
Figure 3-4: Water contact angle on porous material predicted by Quéré and Reyssat (*172*).

Several theories on wetting properties have been described in the section. For electrospun membranes, the selection of theory will be based on the membrane properties and morphological structures of the membrane. The accumulation of electrospun fibres forms a membrane with high surface roughness and porous

structures. Therefore, Wenzel theory and Cassie and Baxter theory are two relevant theories for electrospun membranes, which can be used in the study.

3.4 Capillary flow porometry

The pore sizes (diameter) from porous materials such as electrospun membranes can be measured using a number of techniques such as bubble point measurement, gas or vapour adsorption, extrusion porosimetry and intrusion porosimetry. In this current study, a capillary flow porometry has been used to measure the pore sizes of electrospun membranes.

Capillary flow porometry applies the same principle as liquid extrusion porosimetry. In a capillary flow porometry measurement, a non-reacting gas (air of N_2) flows through a dry sample and then through the same sample after it has been wetted with a liquid with known surface tension. As the gas flows through the wetted sample with increasing pressure, it starts forcing the liquid from the largest pore (bubble point) towards the smallest pore. The flow for dry sample (dry curve) and wet sample (wet curve) is plotted (Figure 3-5) to determine the bubble point, pore distribution and mean flow pore diameter. In Figure 3-5, the dry curve shows gas permeability of the material, whereas the wet curve indicates the liquid permeability of the material. Half dry flow indicates 50% of the flow through the dry sample at the same pressure. The intersection between half-dry and wet curve indicates the mean flow pore diameter of the sample.

The bubble point is measured using the Washburn equation (equation 3.5) (*173*),

$$D = \frac{4\gamma\cos\theta}{\Delta p} \qquad\qquad \text{equation 3.5}$$

where D is pore sizes (diameter), ΔP differential pressure (Psi), γ surface tension of the wetting agent (dynes/cm) and θ contact angle of wetting agent onto the material surface (°).

The pore distribution of a sample is measured using equations 3.6 to 3.8.

$$D = \frac{Q}{d_p - d_c}$$
equation 3.6

where D is the pore size (diameter) distribution (µm), Q is the incremental of filter flow (%), d_p and d_c are the previous and current maximum pore diameter (bubble point) (µm), respectively.

The Q, incremental of filter flow can be measured using equation 3.7,

$$Q = Q_c - Q_p$$
equation 3.7

where Q is the incremental of filter flow (%), Q_c and Q_p are the previous and current filter flow (%). The previous (Q_p) or current (Q_c) filter flow were measured by using equation 3.8,

$$Q_l = (Q_w - Q_d) \times 100\%$$
equation 3.8

where Q_l is the filter flow (current or previous) (%), Q_w and Q_d are the wet and dry flows (l/min) taken from a plot shown in Figure 3-5.
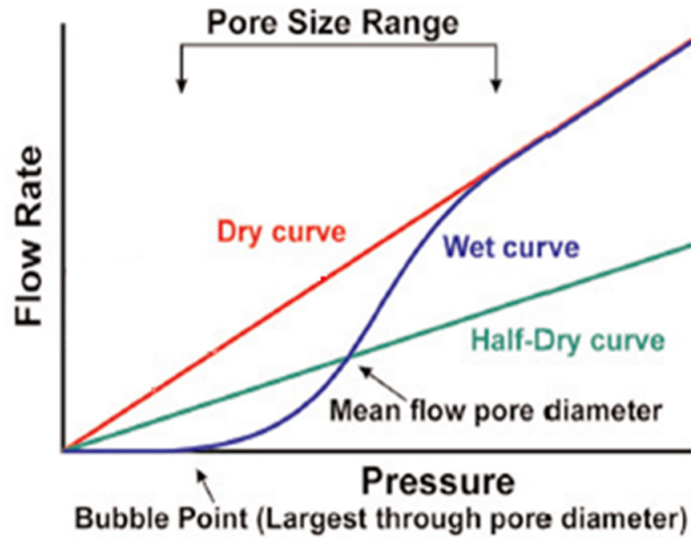
Figure 3-5: A typical plot of wet and dry curves measured by the capillary flow porometry (*174*).

The capillary flow porometry can only measures the throat pores (Figure 3-6 (a)), but not the blind pores (Figure 3-6 (b)).
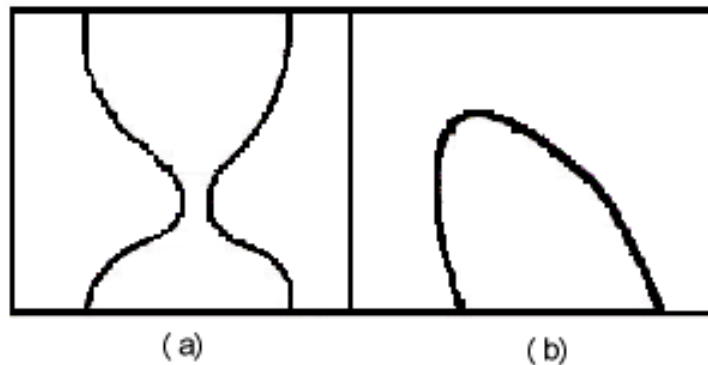
Figure 3-6: Schematic diagrams of: a) Pore throat b) Blind pore (*174*).

3.5 BET (Brunauer, Emmet, Teller) gas adsorption

BET gas adsorption is an ideal method to measure the surface area of materials including electrospun membranes. In BET system, the amount of inert gas (N_2) absorbed by a material is measured. The amount of gas absorbed by the material surface is a function of its vapour pressure as related to its equilibrium vapour pressure. The BET isotherm is determined using equation 3.9 (*127, 175-176*).

$$\frac{p_v}{W(p_0 - p_v)} = \frac{1}{W_m C} + \frac{(C-1)}{W_m C}\left[\frac{p_v}{p_0}\right]$$

equation 3.9

where W is the amount of absorbed gas in moles, W_m is the amount of gas to form a monolayer in moles, p_v and p_0 are the gas vapour pressure (Pa) and the equilibrium vapour pressure (Pa), respectively. C is a constant rate related to the absorption energy of the gas molecule to a solid substrate.
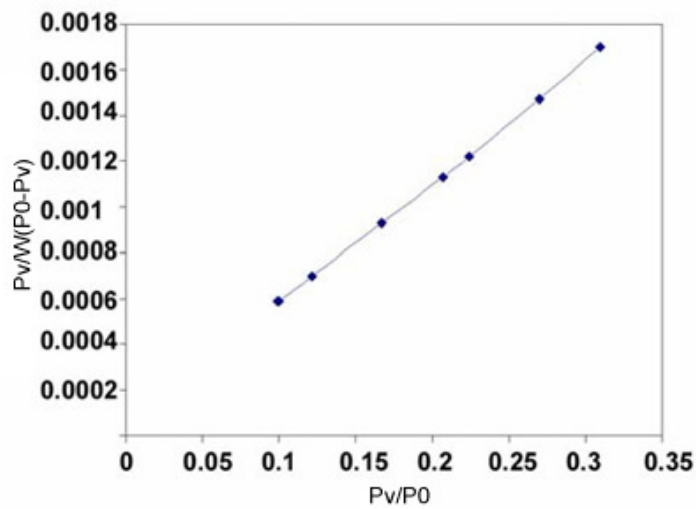
Figure 3-7: Typical plot of the BET isotherm (*127, 176*).

The specific surface area of a material, is determined by plotting $\frac{p_v}{W(p_{0-}p_v)}$

against $\frac{p_v}{p_0}$ (Figure 3-7) (*176*).

From the slope and intercept of the line, the W_m can be determined. Using the W_m values, the specific surface area of a material can be measured using equation 3.10 (*127*).

$$S = W_m N\alpha / m$$

equation 3.10

where S is the specific surface area (m^2/g), N is the Avogadro number (6.022 x 10^{23}) atoms or molecules/mole, α is the cross sectional area of the absorbed gas molecule (cm^2) and m is the mass of the material tested (g).

3.6 Fourier transform infrared (FTIR) spectroscopy

Infrared (IR) spectroscopy has been used widely to characterize chemical structures of polymers. This technique is based upon the vibrations of atoms of a molecule (*32*). An infrared spectrum is obtained by exposing the infrared through a sample and determining what fraction of the incident radiation is absorbed at a particular energy. The frequency at which any peak in the absorption spectrum appears is corresponded to the frequency of a part of sample molecules (*32*).

The infrared spectroscopy is usually carried out using the Fourier-transform infrared (FTIR) spectrometers (*177*). Figure 3-8 illustrates basic components of the FTIR spectrometer, which consist of interferometer, detector, amplifier, analogue/digital converter and computer. The radiation from the source is passed through an interferometer to the sample before reaching a detector. Data received from the amplified is converted to digital form using an analogue-to-digital converter. The data is then transferred to the computer for Fourier transformation to take place (*177*). Result obtained from the FTIR spectroscopy is shown in Figure 3-9.
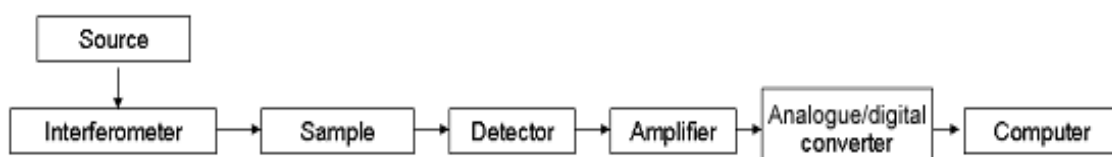
Figure 3-8: Schematic diagram of typical FTIR spectroscopy (*177*)

Figure 3-9 illustrates a typical IR spectrum for poly (vinylidene fluoride)-hexafluoropropylene. From the spectrum, the functional groups and vibration mode of the polymer can be determined using Table 3-1.

Figure 3-9: A typical plot FTIR spectrum for poly(vinylidene fluoride)-hexafluoropropylene

Table 3-1: Some examples of functional groups based upon infrared spectra (*178*).

Functional group		Types of vibration	Frequency (cm^{-1})	Wavelength (μ)
C-H	Alkanes	stretch	3000-2850	3.33-3.51
	-CH$_3$	bend	1450 and 1375	6.90 and 7.27
	-CH$_2$-	bend	1465	6.83
	Alkenes	stretch	3100-3000	3.23-3.33
		out-of-plane bend	1000-650	10.0-15.3
	Aromatics	stretch	3150-3050	3.17-3.28
		Out-of-plane stretch	900-690	11.1-14.5
	Alkyne	stretch	3300	3.03
	Aldehyde		2900-2800	3.45-3.57
			2800-2700	3.57-3.70
C=C	Alkenes		1680-1600	5.95-6.25
	Aromatic		1600 and 1475	6.25 and 6.78
C≡C	Alkynes		2250-2100	4.44-4.76
C=O	Aldehyde		1740-1720	5.75-5.81
	Ketone		1725-1705	5.08-5.87
	Carboxylic acids		1725-1700	5.80-5.88
	Ester		1750-1730	5.71-5.78
	Amide		1670-1640	6.00-6.10
	Anhydride		1810 and 1760	5.52 and 5.68
C-O	Alcohols, Ethers, Esters, carboxylic acids, anhydrides		1300-1000	7.69-10.0
O-H	Alcohols, Phenols			
	Free		3650-3600	2.74-2.78
	H-bonded		3500-3200	2.86-3.13
	Carboxylic acids		3400-2400	2.94-4.17
N-H	Primary and secondary Amines and Amide	stretch	3500-3100	2.86-3.23
C-N	Amines		1350-1000	7.4-10.0
C≡N	Nitriles		2260-2240	4.42-4.46
N=O	Nitro (R-NO$_2$)		1550 and 1350	6.45 and 7.40
S=O	Sulfoxides		1050	9.52
	Sulfones, Sulfonyl Chlorides and		1375-1300 and	7.27-7.69 and
	Sulphates, Sulphonamides		1200-1140	8.33-8.77
C-F	Fluoride		1400-1000	7.14-10.0

3.7 Wide angle X-ray diffraction (XRD)

Wide-angle X-ray diffraction (WAXD) is a good technique to identify the size and shape of crystallites in solid polymers (*175*). Figure 3-10 illustrates a typical WAXD used to determine the crystallographic structure of a polymer sample.
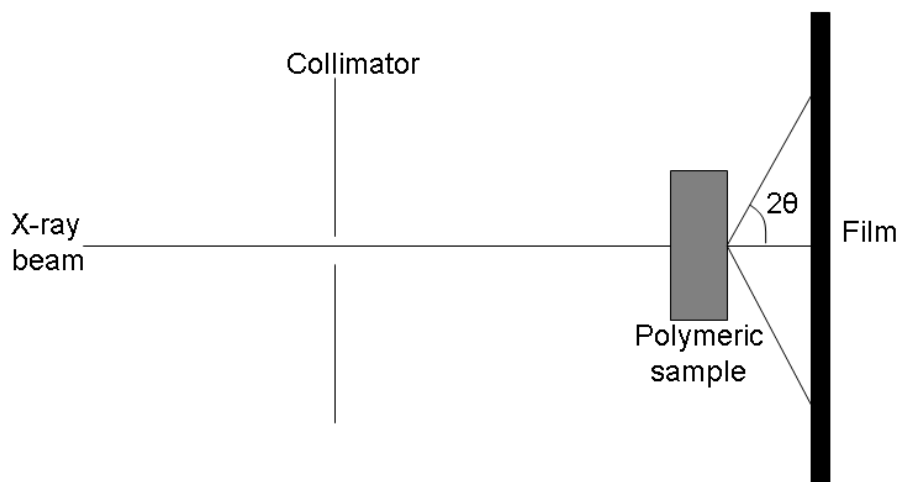
Figure 3-10: Schematic diagram of wide angle X-ray diffraction (*175*).

An X-ray beam is allowed to impinge on the polymer sample. The intensity of the scattered X-rays is determined as a function of the diffraction angle (2θ) (*175*). In the scattering pattern shown in Figure 3-11, a sharp peak indicates the crystalline region of the sample, whereas a broad peak indicates the amorphous phase of the sample (Figure 3-11) (*32, 175*).
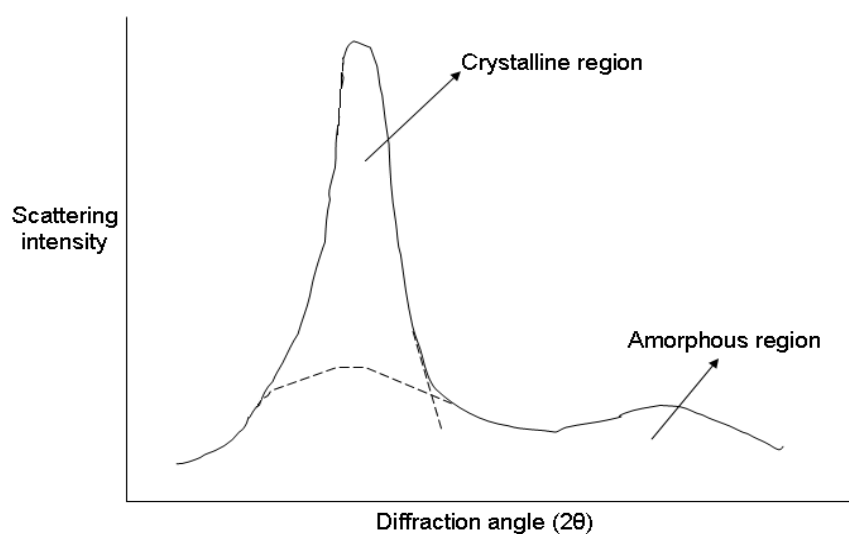
Figure 3-11: A typical plot of scattering intensity versus direction angle obtained from the wide angle x-ray diffraction (WAXD) (*175*).

From the plot shown in Figure 3-11, the spacing between two adjacent planes (*d*-spacing) can be determined using Bragg's equation shown in equation 3.11 (*33, 35*).

$$n\lambda = 2d\sin\theta \qquad\qquad \text{equation 3.11}$$

where integer *n* is the number of wavelengths path difference for scattering from adjacent plane (also known as order of diffraction/reflection), λ is the wavelength of the X-ray, *d* is the distance between two crystal planes, 2θ (Bragg's angle) is the angle between the incoming and outgoing beams from the same plane.

3.8 Tensile test

Figure 3-12 depicts a typical tensile test of materials (*179*). A load is applied in order to produce a given elongation of the materials. The tensile properties (such as stress, strain and modulus) of the tested materials are obtained from a load versus elongation graph (Figure 3-13 (a)) and a stress versus strain curve (Figure 3-13 (b)).
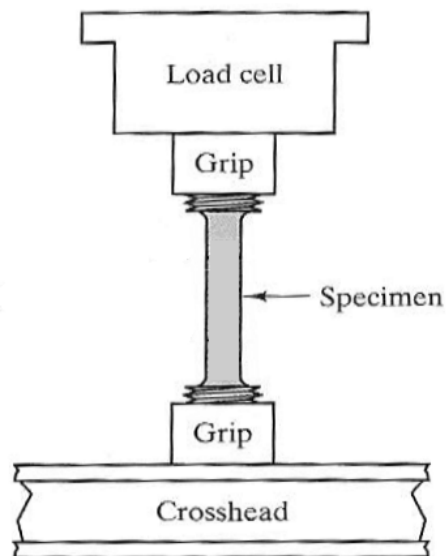
Figure 3-12: Schematic diagram of tensile test (*179*).
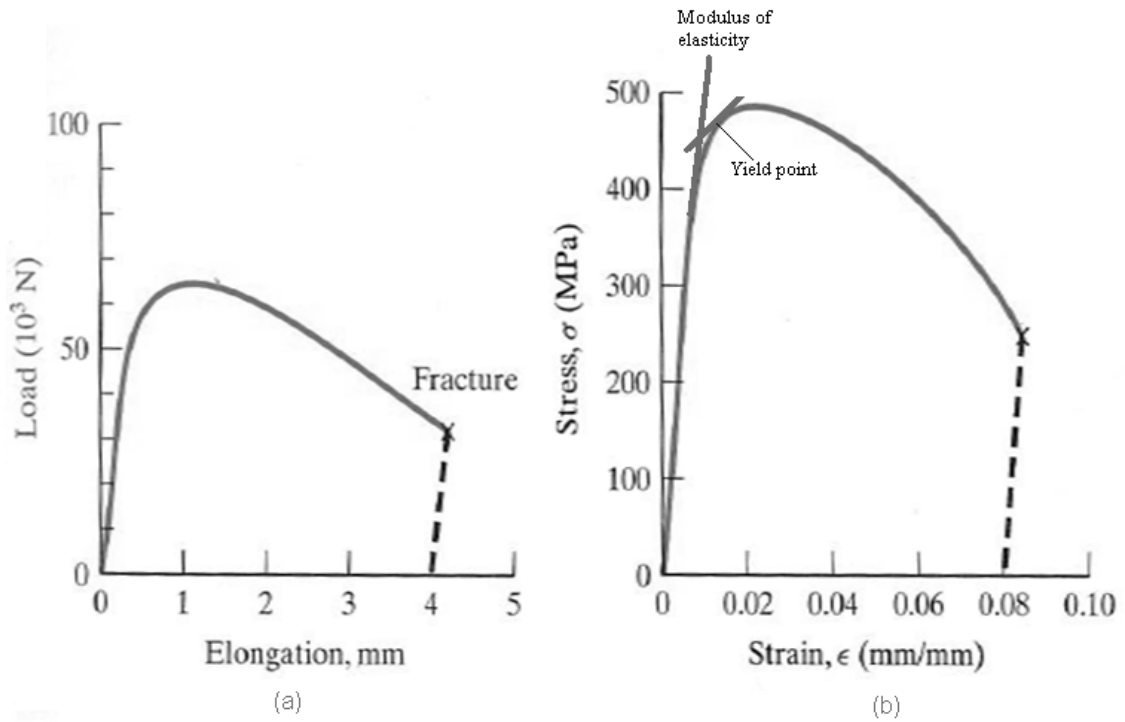
Figure 3-13: Typical plots of: a) load versus elongation and b) stress versus strain (*179*).

Stress can be defined as the force applied on the cross sectional area of a material (*179-180*). From the load versus elongation curve (Figure 3-13 (a)), stress of material can be calculated using equation 3.12.

$$\sigma = \frac{P}{A_0}$$
equation 3.12

where σ is stress (MPa), P is the load (N) applied on the sample and A_0 is the cross sectional area through the sample.

Tensile strain is elongation of a material as a fraction of the material's original length (*179-180*). From the load versus elongation curve (Figure 3-13 (a)), the tensile strain can be calculated using equation 3.13 and 3.14.

$$\in = \frac{l - l_0}{l_0} \qquad\qquad \text{equation 3.13}$$

$$= \frac{\Delta l}{l_0} \qquad\qquad \text{equation 3.14}$$

where l is the length at a given load (mm), l_0 is the original length at zero stress and Δl is the elongation of the sample (mm).

In Figure 3-13 (b), yield point refers to plastic deformation (permanent deformation) under applied load (*181*), whereas modulus of elasticity (Young's modulus) is the slope of the stress-strain curve in the elastic region. Young's modulus indicates the stiffness of materials and can be measured using equation 3.15.

$$E = \frac{\sigma}{\in} \qquad\qquad \text{equation 3.15}$$

where E is modulus of the material (MPa), σ and $\in$ are stress and strain, respectively, taken from the stress-strain slope.

Based on equations 3.12 to 3.15, the tensile strength, modulus and strain of a material can be determined.

3.9 Peel test

Peel test is commonly used to measure the adhesion strength between two bonded materials. There are a number of standard test methods for peel test listed in the American Society for Testing and Materials (ASTM) and International Organization for Standardization (ISO) such as T-peel test panel and test specimen (ASTM D1876), Roller peel test (ASTM D3167), climbing drum peel test (ASTM D1781), 180º peel test (ASTM D903), 90º peel test (ASTM D6862-04), T-peel test for flexible-to-flexible bonded assemblies (ISO 11339:2010), Peel test for a flexible-bonded-to-rigid test specimen assembly Part 2: 180 degree peel (ISO 8510-2:2006) and Determination of adhesion to a rigid substrate: 90 degree peel

method (ISO 813:2010). In the current study, the most relevant standard method is 180º peel test because the bi-layer membranes are flexible in bending.

The peel strength of a bonded material can be determined using equation 3.16 (*145, 151*),

$$\text{Peel strength (N/mm)} = \frac{F}{W} \qquad\qquad \text{equation 3.16}$$

where F is the average load to separate a bonded material (either two bonded flexible materials or flexible/non-flexible material) (N) and W is the width of the sample (m).

Kinloch *et al.*(*145, 151*) reported that, stress distribution in a peel test is very complex especially when cracks are located at the bi-material interfaces. Several approaches have been reported to determine the peel cracks, however due to the difficulty in defining the peel failure using stress distribution, a fracture-mechanic method was implemented, which can be determined by measuring the fracture energy (*G*) (*145, 151*). Fracture energy (*G*) can be defined as the energy needed to propagate a crack through a unit area of the joint (*151*). The measurements of fracture energies are varied depending upon the type of test used. For example, in the T-peel test (Figure 3-14), two thin strips are peeled apart at a constant peeling angle (90°). The applied forces (P) move in the direction of two peeling lengths. The fracture energy for the test is determined by equation 3.17 (*182-186*),

$$G_c^{\infty E} = 2\frac{P}{b} \qquad\qquad \text{equation 3.17}$$

where $G_c^{\infty E}$ is the energy needed to propagate a crack through a unit area of the joint (J/m^2), P is the average force (N) and b is the width of sample (m).
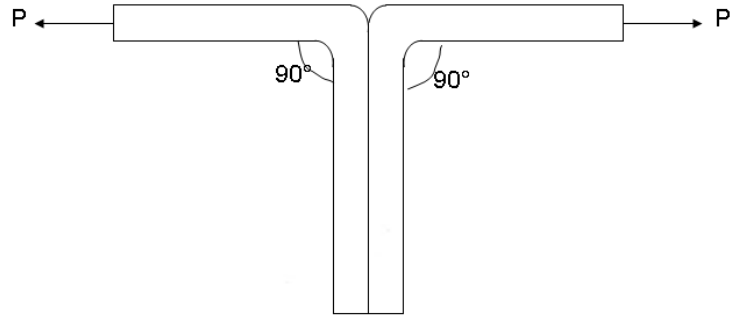
Figure 3-14: Schematic diagram of T-peel test.

Kinloch and Williams (*151*), reported that the thickness of the strip is not considered in the result because they assume that the strip is perfectly flexible in bending. (*151*).

When a strip is peeled away from a stable or rigid strip at an angle θ by a force P (Figure 3-15), the fracture energy is determined by using equation 3.18 and 3.19.
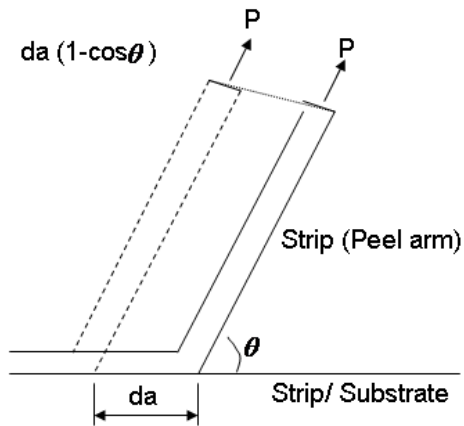
Figure 3-15: Schematic diagram of basic peel test.

$$G_c^{\infty E} = \frac{Pda(1-\cos\theta)}{bda} \qquad \text{equation 3.18}$$

$$= \frac{P}{b}(1-\cos\theta) \qquad \text{equation 3.19}$$

where $G_c^{\infty E}$ is the energy needed to propagate a crack through a unit area of the joint (J/m^2), P is the average force (N), da is the peel length (m), b is the width of sample (m) and θ is the angle of peel (°).

Equations 3.18 and 3.19 can be applied for any types of peel tests such as the 180º peel test, 90º peel test, etc.

3.10 Liquid filtration

3.10.1 Membrane for filtration

Membranes are mostly used as filter mediums. Membranes are relatively thin, semi-permeable and flexible sheets, which are made by several processes and materials to produce different structures. They can be porous or non-porous depending upon the separation processes for example microfiltration (MF), ultrafiltration (UF) and nanofiltration (NF) (*175, 187-191*). The fundamental separation process using membrane consists of two main phases: 1) feed and 2) product (permeate), as shown in Figure 3-16. Feed refers to the input or upstream side phase, whereas permeate refers to the product or downstream side (*175*). Separation is achieved because membranes have the ability to transport one component from a mixture of various components.
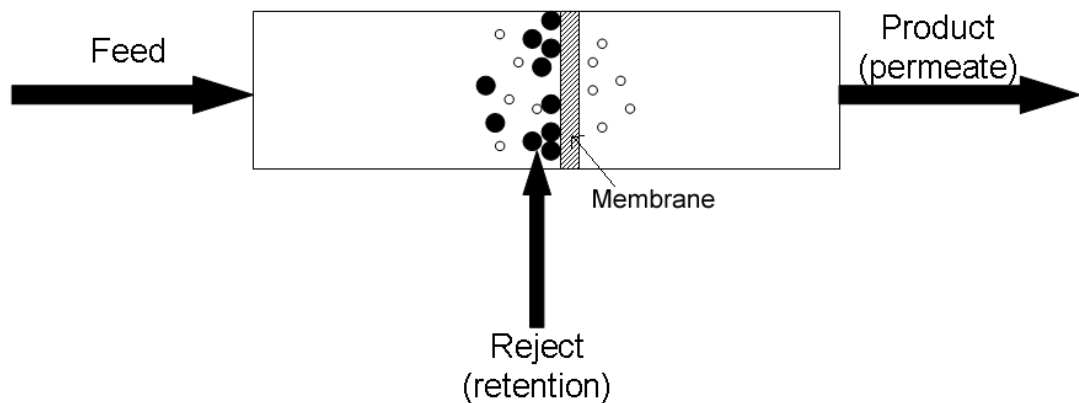
Figure 3-16: Schematic diagram of a fundamental separation process using microfiltration (*175*).

Membrane morphologies can be classified as symmetric (Figure 3-17 (a)) or asymmetric (Figure 3-17 (b)). Membranes based on symmetric structures act as depth filters and retain particles within the structures. For asymmetric structures, the membrane acts as a surface filter that retains particles on the membrane surfaces. The particles are removed by shear force applied by the moving feed solution over the membrane surfaces (*175, 192*).
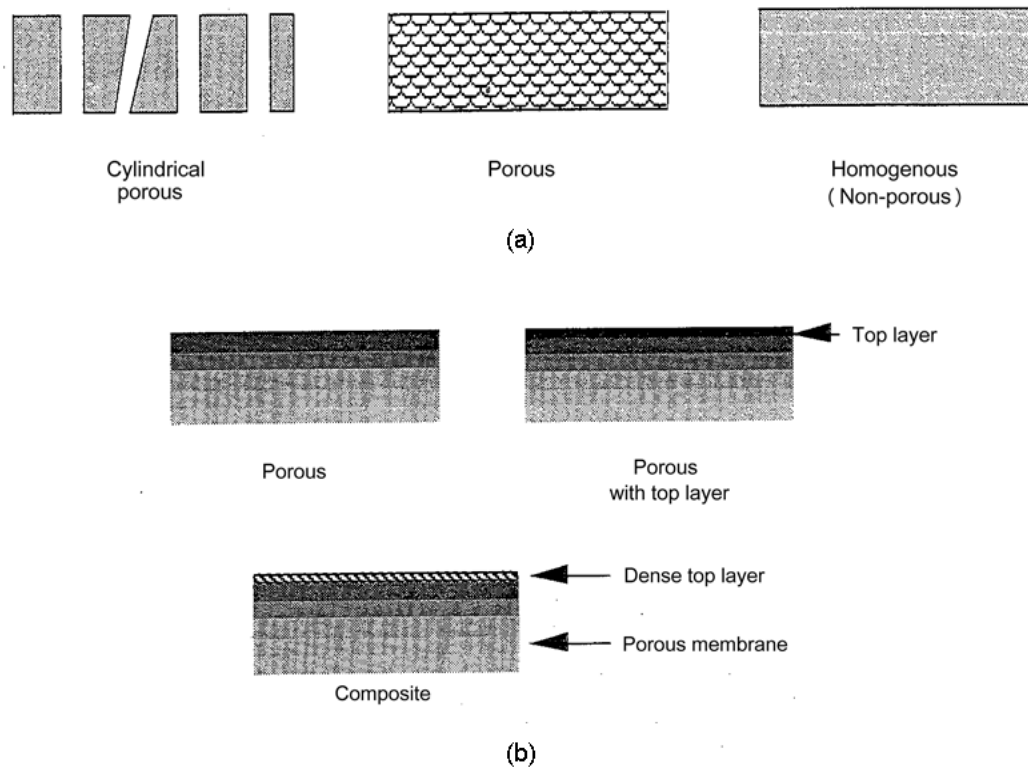
Figure 3-17: Schematic diagrams of: a) symmetric and b) asymmetric membranes (*175*).

3.10.2 Membrane configuration

Judd and Jefferson (*193*) reported that membrane morphologies influence the overall process performance. In filtration and separation processes, the optimal membrane configuration is characterised by membrane with higher surface area-to-volume ratio, low cost per unit membrane area, low energy expenditure per water volume, etc (*193*). Membrane with poor structures will lead to the formation of fouling.

Fouling is one of the major drawbacks in a membrane system which is caused by a strong interaction between membranes and components (such as biomaterials, colloids and metals) in the stream. The interaction forms a fouling layer onto membrane surfaces, reducing the fluid flux through the membrane. The reduction of flux will reduce the operation efficiency and increase the operating cost. Several methods have been identified to control fouling formation such as, membrane hydrophilicity and hydrophobicity (*194-195*), surface modification (*196-197*) and polymer modification.

Maximous *et al.* (*195*) reported that membranes with a hydrophobic surface have strong interaction with solutes and microbial cells. Therefore, a

72

hydrophobic membrane is expected to foul faster than the hydrophilic membrane. This was also observed by Howell *et al.* (*198*), who observed that a hydrophilic cellulosic membranes exhibited a lower fouling tendency than the hydrophobic polysulfone membranes. The feasibility of using hydrophilic membranes to reduce fouling has been reported by a number of studies (*199-202*). In contrast, some researchers have also reported that hydrophobic membranes provided less attachment to microbes, which resulted in lower fouling formation (*203-204*). Choo and Lee (*204*) found that a high hydrophobic fluoropolymer gave the lowest fouling tendency compared to cellulosic and polysulfone membranes. This could be attributed to small dispersive surface tensions on hydrophobic membrane materials that prevent the formation of fouling (*204*).

Surface modification is another technique used to minimise fouling tendency. In Figure 3-18, a PVDF microfilter was treated by grafting the membrane surface with 2-methacryloyloxyethyl phosphorycholine (MPC). The membrane showed an increase of flux by 86%, as compared to the uncoated membrane. (*191*). The hydrophobic membranes could also be grafted with hydrophilic monomers by the irradiation using an electron beam or photochemical method to reduce the fouling layer (*100, 196-197*).

Microfiltration PVDF membrane

Oxygen plasma etch

OH   OH   OH   OH   OH   OH

Ce^{4+}/MPC
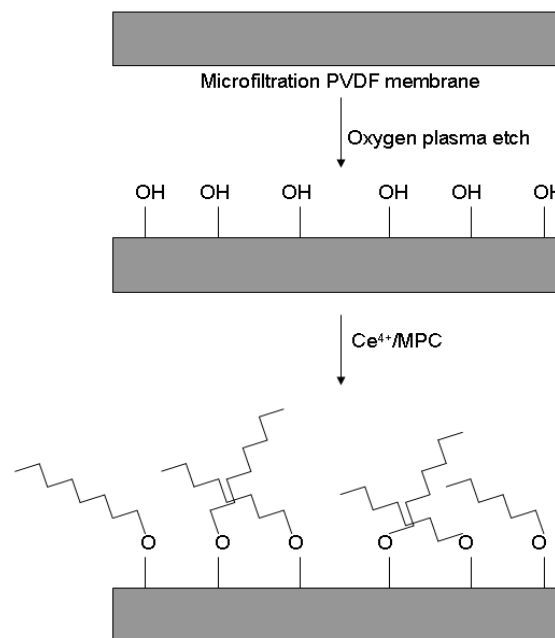
Figure 3-18: Surface modification of microfilter PVDF-2-methacryloyloxyethyl phosphorycholine (MPC) (*191*).

3.10.3 Transport properties and membrane selectively

Transport properties can be considered as one of the important parameters in membrane systems. Gopal *et al.* (*9*) reported that the transport properties and membrane selectively are significantly affected by the membrane performance such as flux. Flux can be defined as number of volume or mass of a specified component passing through a membrane surface area per unit time (*205*).

Transport properties of fluid through a porous membrane have been described by several theories such as Hagen-Poiseuille, Kozeny-Carman, etc (*175*). Those theories depend on pore structure, for example, the volume of flux (J) through parallel cylindrical pores (shown in Figure 3-17 (a)) can be determined by the Hagen-Poiseuille theory, as shown in equation 3.20.

$$J = \frac{\varepsilon r^2}{8\eta\tau} \times \frac{\Delta P}{\Delta x}$$
equation 3.20

where ε is the surface porosity (%), r is the pore radius (mm), $\dfrac{\Delta P}{\Delta x}$ is the driving force where ΔP is the pressure different (N/m^2) and Δx the membrane thickness (m), η is the liquid viscosity (Pa.s) and τ is the tortuosity factor (*175*).

For non-parallel pores, the volume of flux (J) can be determined using the Kozeny-Carman theory, as shown in equation 3.21 (*175*)

$$J = \frac{\varepsilon^3}{K\eta S^2 (1-\varepsilon)^2} \times \frac{\Delta P}{\Delta x}$$
equation 3.21

where ε is the volume fraction of the pores, K is the Kozeny-Carman constant (which depends on the shape of the pores and the tortuosity), η is the liquid viscosity (Pa.s), S is the internal surface area, ΔP is the pressure different (N/m^2) and Δx the membrane thickness (m).

It was also reported that the flux (J) through non-homogenous pores can be measured using equation 3.22 (*206*),

$$J = \frac{Q}{A \times T}$$

<div align="right">equation 3.22</div>

where Q is change of volume of liquid (ml or L), A is the area of membrane (m^2) and T is the permeation time (hr).

A number of flux theories have been discussed in this section. In this study, the theory shown in equation 3.22 is the most applicable theory for electrospun membranes. The accumulation of random oriented electrospun fibres forms a membrane with non-homogenous pores. By referring to equation 3.22, the flux (J) through the electrospun membrane can be determined.

Membrane selectivity is also one of the important parameters in membrane systems. Membrane selectivity is expressed as rejection coefficient in membrane process which can be measured using equation 3.23 (*175, 191*).

$$\% \text{ rejection} = \left(\frac{C_f - C_p}{C_f} \right) \times 100\%$$

<div align="right">equation 3.23</div>

where C_f is the concentration of feed and C_p is the concentration of permeate (product).

From the equation 3.23, the performance or efficiency of membranes can be obtained. Hence, the rejection coefficient (%) will be measured in the study.

CHAPTER 4 MATERIALS AND METHODS

4.1 Solution preparation

The initial stage of the project involved the optimisation of electrospinning conditions for the chosen hydrophilic and hydrophobic polymers. Two hydrophilic and two hydrophobic polymers were chosen. They were:

- Hydrophilic polymers: Nylon 6 and polyvinyl alcohol (PVA) and
- Hydrophobic polymers: polyacrylonitrile (PAN) and copolymer poly(vinylidene fluoride)-hexafluoropropylene (copolymer PVDF).

The polymers were dissolved at different concentrations in a suitable solvent prior to electrospinning as described below. All the polymers were used as received without further purification. Solvents were of analytical grade and were also used without further purification.

- Nylon 6 (Ultramide BS700, BASF) was dissolved in formic acid (BDH analytical grade) at concentrations 5, 12, 14, 16, 18, 20 and 25 %wt. The solutions were shaken on a shaker (Edmund Buhler 7400 Tubingen shaker) at room temperature for 2–3 days.

- PVA powder (Chem-Supply, Australia) with Molecular Weight (Mw) approximately 100,000 g/mol and degree of hydrolysis (DH) of 86–88% was dissolved in deionised water at concentrations 4, 6, 8, 10 and 12 %wt. The solutions were heated at 45°C for 3–4 hours with constant stirring, and then allowed to return to room temperature prior to electrospinning.

- PAN solutions were prepared by dissolving the PAN (Sigma Aldrich, Molecular Weight (MW) 150,000 g/mol) in dimethyl formamide (DMF; Merck) at concentrations 5, 9, 10, 11 and 13 %wt. The solutions were heated at 50°C for 4–5 hours with constant stirring, and then allowed to return to room temperature prior electrospinning.

- The copolymer PVDF-HFP powder (Kynar Flex® 2801, Arkema Inc.) was dissolved in N,N-dimethylacetamide (DMAc) (Sigma Aldrich) and acetone (Merck) in a ratio 2:1 (DMAc:Acetone). The solutions were prepared at concentrations 5, 10, 15, 20 and 25 %wt and were shaken (Edmund Buhler 7400 Tubingen) at room temperature for 1 day.

4.2 Solution viscosity

The solution viscosity of each polymer concentration was measured using a rotating viscometer (HA DV-III + Pro Viscometer, Brookfield Co.) with Rheocalc® software. The rotating speeds of viscometer spindle were different ranged from 10 to 40 rpm. All the solution was tested at room temperature. Five measurements were carried out for each solution concentration.

4.3 Electrospinning

4.3.1 Selection of optimal conditions for electrospinning
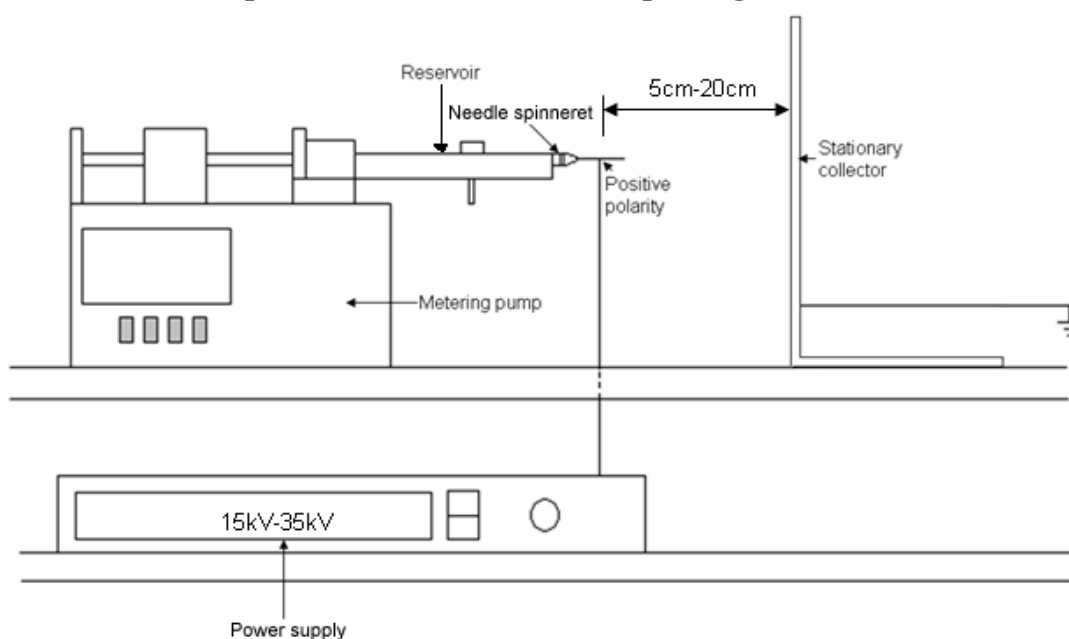
Figure 4-1: (a) Schematic diagrams of electrospinning system using stationary collector.

Figure 4-1(a) shows a schematic of the electrospinning system used to identify optimal electrospinning conditions for all polymers tested. It consisted of a single nozzle spinneret 23G (Terumo corporation, Ø0.65 mm) needle, delivery pump (Brain scientific), a vertical flat collector system and power supply. The needle tip-to-collector distances varied from 5 to 20 cm, in 5 cm increments. There was no further increased in distance to reduce the number of variables used in the study. Each polymer solution was electrospun at different voltages ranged from 9 to 35 kV. Pump flow rate was fixed at 0.2 ml/h in order to reduce the number of variables in the study. Electrospinning was carried out at room temperature (ranged from 20 to 23°C) with relative humidity ranging from 40 to

60%. The electrospun membrane was deposited onto a grounded vertical flat aluminium foil for 3 minutes with positive polarity at the needle tip. The 3 minutes electrospinning time was selected because it allowed the formation of electrospun fibres. Fibres fabricated less than 3 minutes exhibited poor structures and droplets due to the start up effect of the electrospinning system.

For each variable, the resultant fibres were characterized according to nature of fibre (such as continuous or droplets), fibre shape, coverage area, membrane structure and solution electrospinnability. The criteria for optimal electrospinning conditions were uniform cylindrical fibres, large coverage area and uniformity of membrane coverage. Any conditions fall outside these criteria will not be further optimized.

4.3.2 Fabrication of single layer electrospun membrane
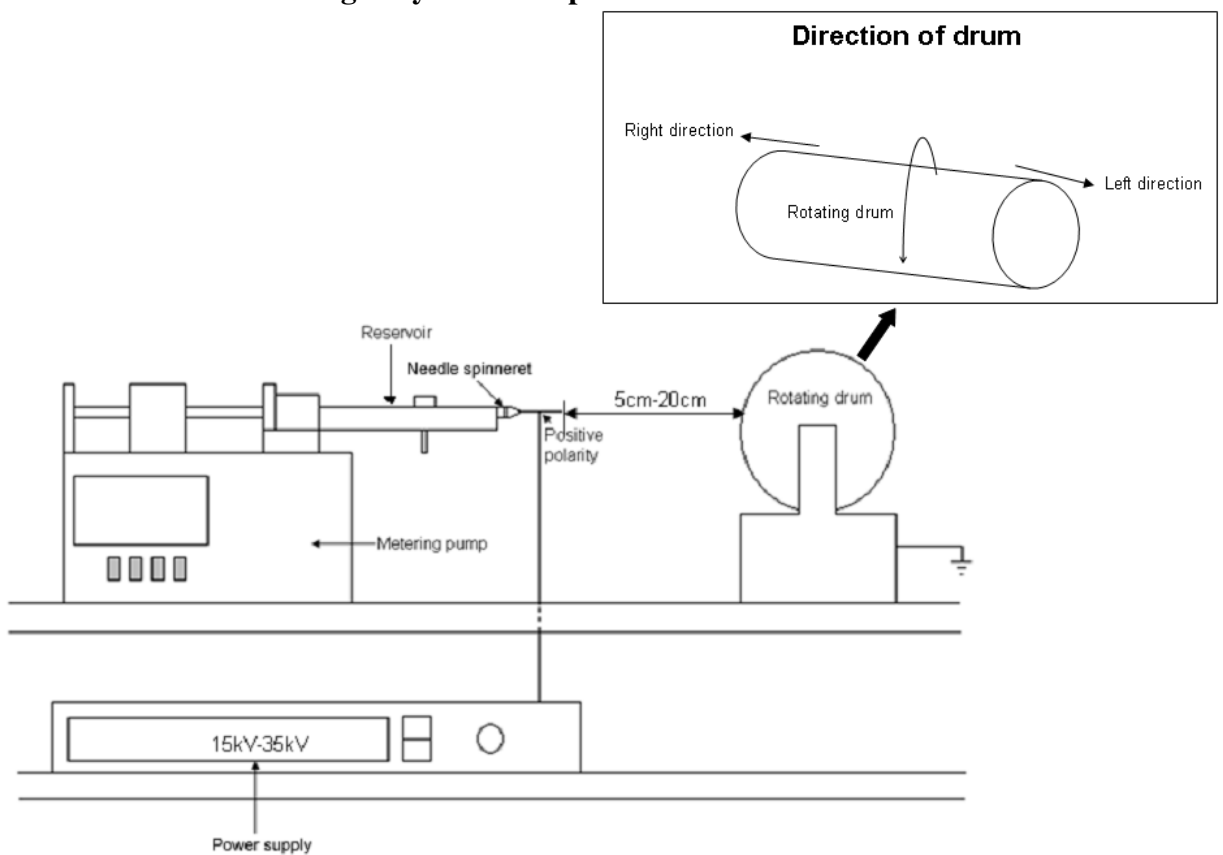
(b)

Figure 4-1: (b) Schematic diagrams of electrospinning system using rotating drum.

The optimal conditions identified above were used to fabricate large size of electrospun membranes (approximately 32 cm (length) x 20 cm (wide)) as illustrated in Figure 4-1 (b). To obtain a comparable membrane size for all

78

polymers tested, each polymer was electrospun on a rotating drum using the drum setting as shown in Table 4-1. The membrane was collected onto an aluminium foil placed on the rotating drum mandrel with diameter of 95 mm and a drum speed of 30 mm/sec.

Table 4-1: Parameters of rotating drum for electrospun Nylon 6, PVA, PAN and copolymer PVDF (see Figure 4-1 (b))

Electrospun nanofibre membrane	Left direction (mm)	Right direction (mm)
Nylon 6	130	140
PVA	50	140
PAN	130	170
Copolymer PVDF	50	170

Each electrospun membrane was characterized for membrane thickness, surface topography (surface area and roughness), surface wettability, pore size of electrospun membranes. IR (infrared) and wide angel X-ray diffraction were also used to identify changes in crystal phases of polymer after electrospinning.

4.3.3   Fabrication of bi-layer electrospun membrane

The same electrospinning parameters above (Section 4.3.2) were used for the fabrication of bi-layer electrospun membranes. The collector system is outlined in Section 4.3.2. Two different types of bi-layer electrospun membranes were prepared: 1) homogenous bi-layer and 2) heterogeneous bi-layer. The fabrication details are described below in Table 4-2.

Table 4-2: Homogeneous and heterogeneous bi-layer electrospun membranes.

Sample type	Top layer	Bottom layer	Spinning time (hr)	
			Top layer	Bottom layer
Homogeneous bi-layer				
1. hydrophilic/hydrophilic	Nylon 6	Nylon 6	22	22
2. hydrophilic/hydrophilic	PVA	PVA	22	22
3. hydrophobic/hydrophobic	PAN	PAN	14	14
4. hydrophobic/hydrophobic	Copolymer PVDF	Copolymer PVDF	26	26
Heterogeneous bi-layer				
1. hydrophobic/hydrophilic	PAN	Nylon 6	14	22
2. hydrophobic/hydrophilic	Copolymer PVDF	Nylon 6	26	22
3. hydrophobic/hydrophilic	PAN	PVA	14	22
4. hydrophobic/hydrophilic	Copolymer PVDF	PVA	26	22

Homogeneous and heterogeneous bi-layer membranes were fabricated in two step processes outlined below:

a) Fabrication of bottom layer

The bottom layer membrane was electrospun for 14 to 26 hours depending on polymer type, as indicated in Table 4-2. The membrane was then dried at room temperature for a day prior to deposition of the top layer.

b) Fabrication of top layer

The top layer membrane was deposited directly on top of the bottom layer (14 to 26 hours) and was then dried at room temperature for a day prior to testing.

The bi-layer membranes were characterized for membrane thickness, surface wettability (water contact angle), pore size of electrospun membranes. The membranes were also tested for tensile properties, adhesion strength and liquid filtration. IR (infrared) and wide angle X-ray diffraction (WAXD) were again used to monitor chemical structures and crystal phases of the bi-layer membranes.

4.4 Fibre and membrane characterisation

4.4.1 Fibre diameter and morphological structures

Fibre and membrane morphologies were characterized using Field Emission Scanning Electron Microscope-FESEM (Philips XL30). Samples were cut with dimension of 5 mm x 5 mm and were attached onto a scanning electron microscope (SEM) stub using carbon tape. The sample was then iridium coated using a sputter coater (Polaron) at 50 to 60 mA for 10 to 15 seconds prior to measurements. Nanofibre diameter was determined by taking the average of fifty measurements chosen at random from the sample.

4.4.2 Membrane coverage area measurement

An electrospun nanofibre membrane deposited onto an aluminium foil was scanned over a transparent grid with an area of 1 cm^2 per grid. The scanned coverage area was then measured using the ImageJ software. Three area measurements were taken for each membrane.

4.4.3 Thickness measurement

Single and bi-layer membrane thicknesses were measured using two methods: 1) a simple electronic digital micrometer (Kincrome) with the lower limit approximately 4µm and 2) white light profilometry (Cotec Altisurf 500 white light). In the case of micrometer, ten thickness measurements were taken at random locations and then averaged.

For the thickness measurement using white light profilometry, a flat glass slide was used as a zero point or base. The electrospun membrane was placed on top of the glass. White light was scanned across the electrospun glass slide from A to B to C, as shown in Figure 4-2, with a resolution of approximately 1000 data points/mm with an accuracy of approximately 0.05µm. A lower probe sensor (which is in a range of 9.2 nm-300 µm) was selected in the study in order to prevent the white light from passing through the glass. A line measurement was performed across the sample, as illustrated in Figure 4-2. This allowed a good profile of membrane thickness to be measured. Membrane thickness was quoted as the average of ten lines across ten different places of electrospun membrane.
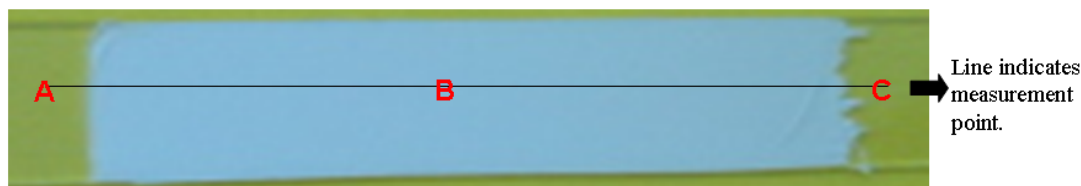
Figure 4-2: Photograph of a typical electrospun membrane onto a glass slide. The green regions (labelled A and C) and white region (labelled B) correspond to the glass and electrospun membrane respectively.

4.4.4 Surface wettability (water contact angle measurement)

The surface wettabilities (water contact angles) of single and bi-layer electrospun membranes, and commercial Nylon membrane were determined using a water contact angle measurement. The water contact angle was tested with a pocket Goniometer PG-3 (Fibro system) using a 4 µl drop of deionised water. The contact angle was measured using PG software at 5 seconds after the drop was applied. An average of ten measurements was measured per sample.

4.4.5 Surface roughness measurement

The surface roughness of the electrospun membrane was compared to that of a film cast on glass from the same electrospinning solution. The cast film was dried at room temperature for 2–3 days. The dried film was then peeled off the glass for surface roughness measurement. The roughness of the electrospun membrane and film surface was measured using a white light profilometry (Cotec Altisurf 500 white light) with a lower probe sensor (a range of 9.2 nm–300 µm). Ten measurements were taken for all samples. The surface roughness was determined automatically by the profilometry software using standard method (ISO 4287).

4.4.6 Surface area measurement of electrospun membrane

For surface area measurement, 0.02 g of electrospun membrane was degassed overnight at 25°C and N_2 gas was used to analyse the BET surface area using a Micrometric TriStar system. Three samples were tested for each electrospun membrane.

4.4.7 Pore size measurements

The pore sizes of single and bi-layer electrospun membranes, and commercial Nylon membranes were measured using capillary flow porometry with the lower limit of approximately 0.03 µm pore size (Porous Materials Inc.). These membranes were tested under dry and wet conditions. For wet conditions, the membrane was saturated with a defined surface tension of wetting agent galwick (surface tension, γ= 15.6 dynes/cm). The pore sizes were derived from the differences between the dry and wet curves.

4.4.8 Fourier Transform Infrared spectroscopy (FTIR)

The functional groups of single and bi-layer electrospun membranes were characterized using a Fourier Transform Infrared spectroscopy (FTIR) (PerkinElmer Spectrum One). The FTIR spectra of electrospun membranes were compared with the bulk polymers and cast films.

4.4.9 X-ray diffraction

The wide-angle X-ray diffraction (WAXD) was carried out using an X-ray diffractometer (Bruker AXS D8) with a Cu Kα radiation source (wavelength (λ) =1.54 Å). Cast films, single layer and bi-layer membranes (15 mm x15 mm) were attached separately onto a glass slide and were scanned in the range of 10° to 30° of 2θ at room temperature. For the heterogeneous bi-layer membranes, each membrane was tested at different side (for example, hydrophilic/hydrophobic and hydrophobic/hydrophilic). An empty glass slide was also scanned as the control.

The d-spacing of diffraction peaks were determined using Diffrac plus EVA (Bruker AXS) using equation 4.1,

$$d = \frac{\lambda}{2\sin\theta} \qquad\qquad \text{equation 4.1}$$

where d is d-spacing (nm), λ is the average wavelength of radiation (nm) and θ is the X-ray diffraction angle (°).

4.5 Tensile test

The tensile strengths of random oriented bi-layer electrospun membranes were tested using a uniaxial tensile test. Five samples from each bi-layer membrane were stamped out using a dog-bone shaped template (shown in Figure 4-3). The test was carried using an Instron mechanical testing device with a 10 N load cell and an extension rate of 10 mm/min. Samples were conditioned for 48 hours at 20°C and 65% relative humidity prior to testing. The highest peak stress (MPa), modulus (MPa) and elongation at break (%) were determined and used in the study.
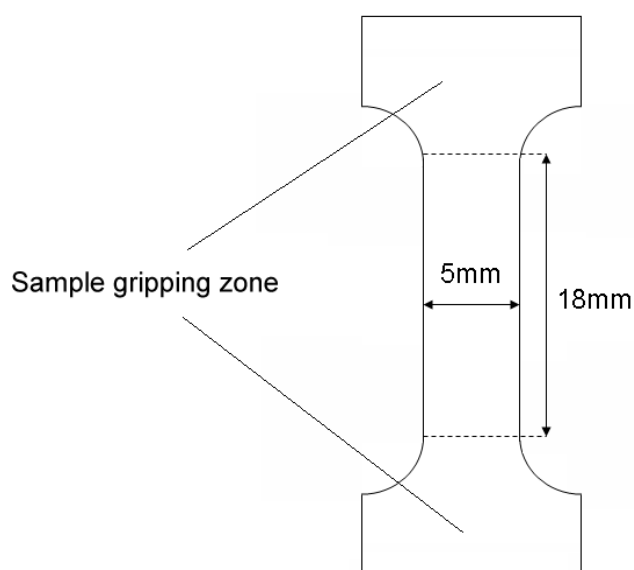
Figure 4-3: Typical sample template used for tensile test.

4.6 Peel test

The 180° peel test was used to measure the adhesion strength between the two layers of the bi-layer electrospun membrane. Samples for the peel test were assembled in a similar fashion as outlined in section 4.3.3, except with the following modifications. The initial step involved the collection of the bottom layer membrane on top of an aluminium foil for 14 to 26 hours, as shown in Figure 4-4 (a). The membrane was then dried for 24 hours in order to remove any excess solvent. Half of this membrane was covered up with an aluminium foil in order to assist with the separation of the top and bottom layer during the peel test as shown in Figure 4-4 (b). The top layer was then deposited onto the bottom layer for 14 to 26 hours as shown in Figure 4-4 (c). The bi-layer was dried again for

another 24 hours and was conditioned for 48 hours at 20°C and 65% relative humidity prior to testing.
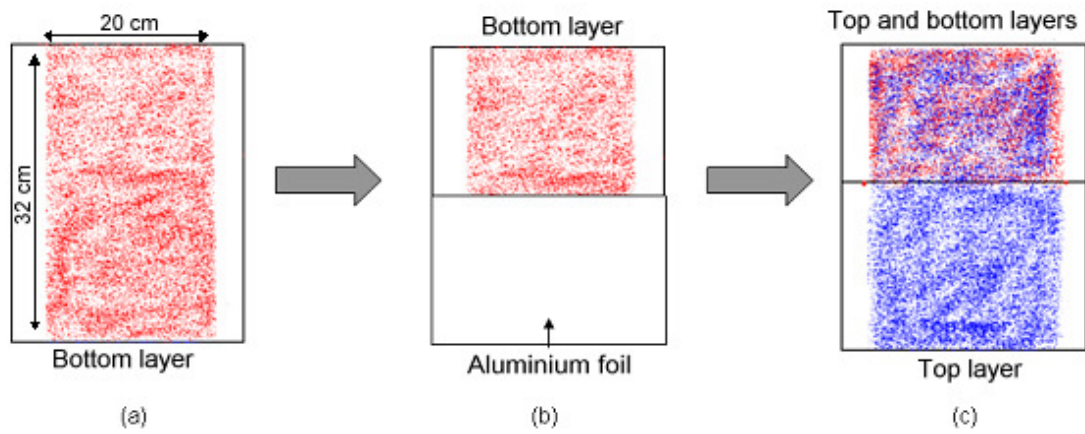
Figure 4-4: Schematic diagram of the fabrication steps used to fabricate a sample for the 180° peel test. a) bottom layer electrospun membrane on aluminium foil, b) aluminium foil over the bottom layer and c) fabrication of top layer.
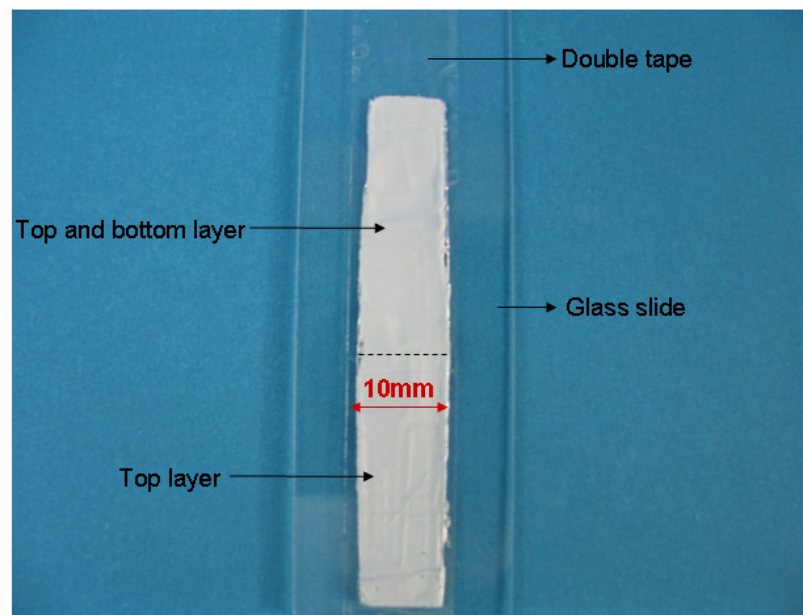
Figure 4-5: Photograph of sample for peel test prior to mounting in grips.

The membranes were cut into rectangular strips of 10 mm wide and 100 mm length. In Figure 4-5, the bottom layer was attached to the surface of glass slide using a double sided tape. The bottom layer membrane/glass slide was clamped via the bottom grip, while the top layer membrane was folded over 180º and clamped with the top grip, as shown in Figure 4-6. The adhesion between the two membranes (top and bottom layer) was tested using a 10 N load cell with a 10

mm/min crosshead speed and a gauge length of 36 mm. Based on the Chapter 3, the peel strength P and fracture energy ($G^{\infty E}$) were measured using equations 3.16 and 3.19, respectively.
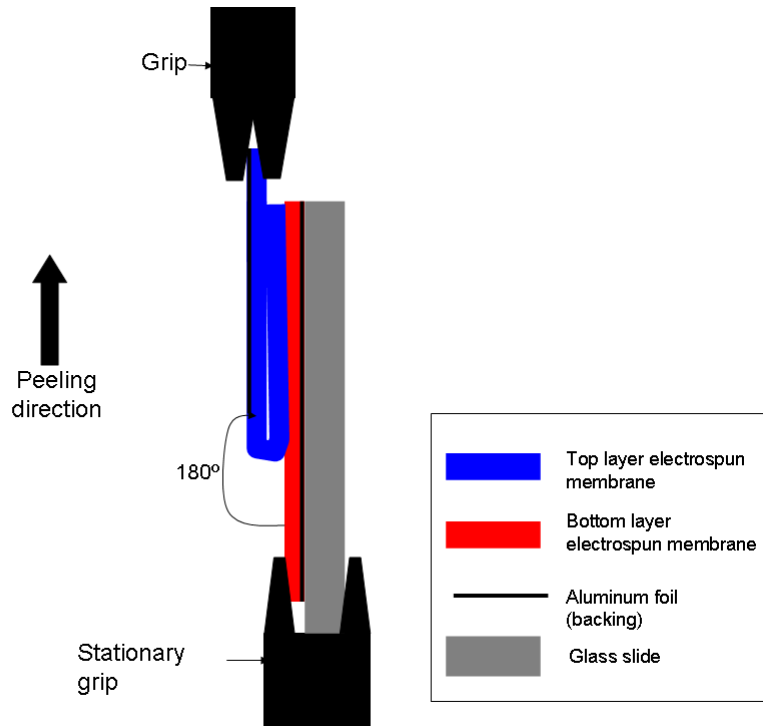
Figure 4-6: Schematic diagram of 180º peel test used in the study.

4.7 Liquid filtration test

The homogeneous and heterogeneous bi-layer membranes were tested for the removal of suspended solids from textile effluent. The testing conditions were as follows:

4.7.1   Pre-filtered Effluent

Effluent from textile dye bath was supplied by Dyechem Industries Pty.Ltd, Australia. The effluent was taken directly from pigment padding and consisted of pigment, acrylic binder and waxes. The concentrated effluent was diluted with deionised water, 10:1 (deionised water : pigment) and pre-filtered using cellulose filter paper (Whatman, Grade 1, particle size retention approximately 11 µm) to remove large solids.

4.7.2 Membrane filtration

A 30 ml of pre-filtered effluent and deionised water (control) were filtered using bi-layer membranes (Ø54 mm). The test was carried out using a simple laboratory filtration system shown in Figure 4-7. Three different pressures (5, 12 and 20 psi) were applied for each filtration. For each pressure, three samples were tested. The separation time was recorded using a HP webcam. The changes of weight for pre-filtered effluent and deionised water (control) through the bi-layer membrane were measured using a laboratory electronic weighing balance with an accuracy of 0.001g. The permeate flux of the membranes was measured using equation 4.2 as proposed by recent study (*206*).

$$J = \frac{Q}{A \times T}$$
<div style="text-align: right">equation 4.2</div>

where Q is change of volume of liquid (ml or L), A is the area of membrane (m^2) and T is the permeation time (hr).

The membrane flux was then compared to a standard commercial filter membrane (Nylon from GE water & Process Technologies).
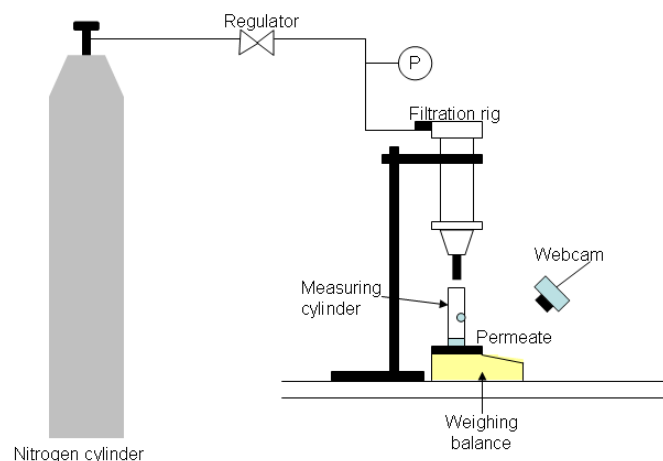
Figure 4-7: Schematic of filtration apparatus.

4.7.3 Characterization of pre-filtered effluent and permeate

The pre-filtered effluent (before filtration) and permeate (after filtration) were measured for turbidity, chemical oxygen demand (COD), pH and conductivity. The results were also compared to permeate from the commercial

filter membrane (Nylon from GE water & Process Technologies). The information on the commercial filter membrane is outlined below.

Product part number: 1215310

Product model: N00HY320F2

Pore size: 0.45 µm

Membrane thickness: 115 µm

Details on the pH, conductivity, turbidity and chemical oxygen demand (COD) tests used in the current study are shown in sections 4.7.3.1 to 4.7.3.2.

4.7.3.1 pH values and conductivity

Three samples (permeate) from each applied pressure (5, 12 and 20 psi) were measured for pH and conductivity. The pH values and conductivity of the samples were measured using pH meter (Radiometer Analytical S.A) and conductivity meter (WTW company), respectively. The results were then compared with pre-filtered effluent.

4.7.3.2 Turbidity and chemical oxygen demand (COD)

These samples were also tested for turbidity and chemical oxygen demand (COD). For turbidity test, 15 ml of permeate was analysed using a turbidimeter (HACH 2100). For COD, 20 µl of permeate was pipetted into a COD reagent (solution range from 0 to 1500ppm from HACH company) and heated at 150°C for 2 hours in a COD reactor (HACH) to permit reaction between the permeate and the reagent. The solutions were analysed using a spectrophotometer (HACH DR/4000) and the results were recorded and compared with pre-filtered effluent.

The percentage of turbidity (%) was calculated using the equation of separation factor as proposed by recent studies (*9, 131*). The separation factor was calculated using equation 4.3,

$$SF = \left[1 - \frac{C_{permeate}}{C_{feed}}\right] \times 100\% \qquad\qquad \text{equation 4.3}$$

where SF is the separation factor (%), $C_{permeate}$ and C_{feed} are the permeate concentration and feed (pre-filtered effluent) concentration, respectively.

The separation factor (SF) is usually measured using UV-visible spectrophotometry. In the UV-visible spectrophotometry, the concentration of permeate ($C_{permeate}$) and feed (C_{feed}) can be directly determined. However, the presence of particles in both concentrations interfere with the UV results. Thus, the turbidity values (NTU) were extrapolated to determine the separation factor (equation 4.3).

CHAPTER 5 FABRICATION AND CHARACTERISATION OF SINGLE LAYER ELECTROSPUN NANOFIBRE MEMBRANES

5.1 Nylon 6

5.1.1   Effect of concentration on viscosity

Nylon 6 a hydrophilic polymer was dissolved at different concentrations in order to identify the effect of concentrations on viscosity and fibre morphology. Figure 5-1 shows the effect of solution concentration on the viscosity of Nylon 6 solutions. Solution viscosity increased from 30 to 4925 cPs with increasing solution concentration from 5 to 25 %wt. This increase of viscosity with a higher concentration was described in Simha's early theory (*207*). In this theory, the transition from a dilute to a concentrated polymer solution is due to the overlapping of polymer chains in the polymer solution. In the dilute solution, there is no significant chain overlap or interaction, and the chains exist as separate entities or globules as shown in Figure 5-2 (a). When the concentration increases, these chains begin to overlap and the globules start to touch the adjacent molecule boundaries (Figure 5-2 (b)). At higher concentrations, the solution has greater polymer chain entanglement which results in a higher solution viscosity (Figure 5-2 (c)) (*207*).
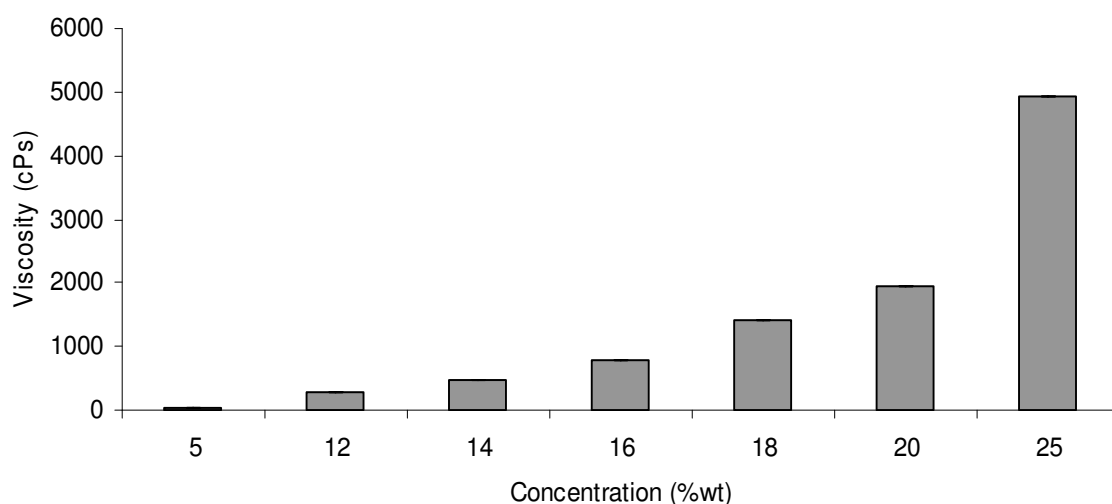
Figure 5-1: The effect of solution concentration on viscosity for Nylon 6 dissolved in formic acid. Values represent the average of 5 measurements for each concentration. Error bars were neglected due to the low standard deviation.
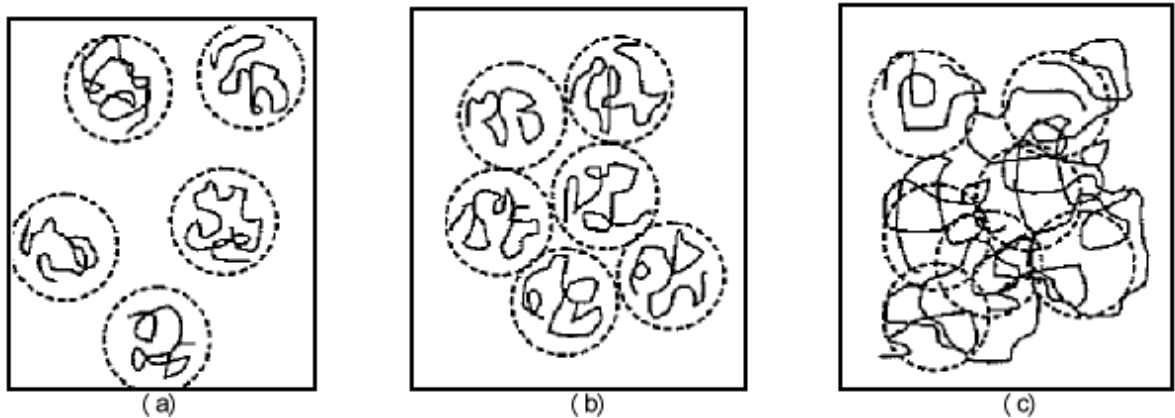
Figure 5-2: Schematic diagrams of polymer solution in different concentration regimes, a) less viscous b) mid-range viscosity and c) highly viscous solution (*112, 207*).

5.1.2   Effect of concentration on fibre and membrane morphologies

Changing the solution concentration was observed to affect the resultant fibre diameter of electrospun Nylon 6. Results presented in Figure 5-3 (a) show an increase in resultant fibre diameter with respect to the polymer concentration. When the concentration increased from 12 to 25 %wt, the fibre diameter was observed to increase approximately from 95 to 776 nm. At higher concentrations, the charged jets were expected to have greater resistance towards thinning of the jets, which resulted in the larger fibre diameter. The results were also in agreement with others studies (*45, 99, 103*). They observed that the fibre diameter of electrospun Nylon 6 increased with an increase of solution concentrations (*45, 99, 103*).

As the concentration increased from 12 to 25 %wt, the membrane coverage area reduced from 214 cm^2 to 69 cm^2 (Figure 5-3 (b)). A possible explanation could be due to the bending instabilities of jets during electrospinning. When the charged jets have higher resistance to stretch, they travel a greater linear distance before forming a bending instability (*42*). As a result, a smaller coverage area was formed. In addition, the thicker fibres resulted in dense membrane structures (Figure 5-4 (a-g)).
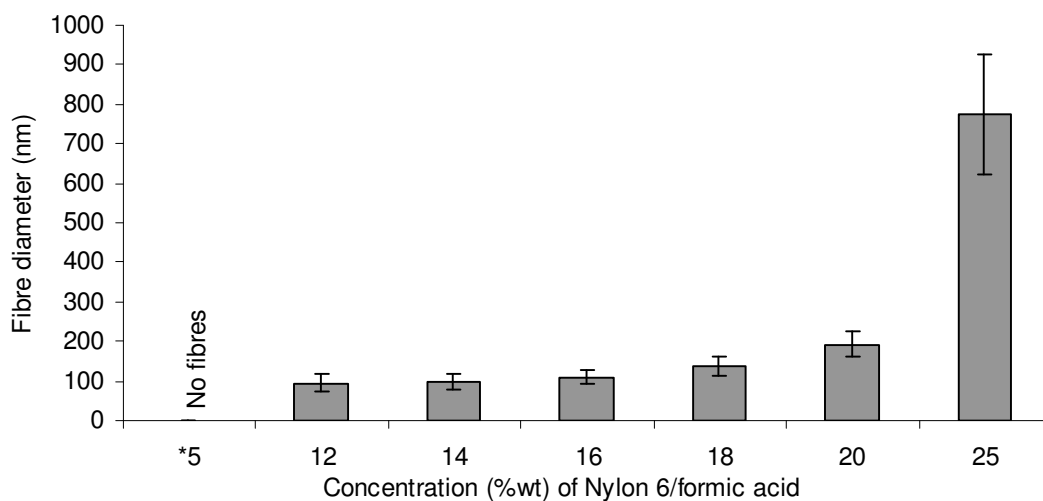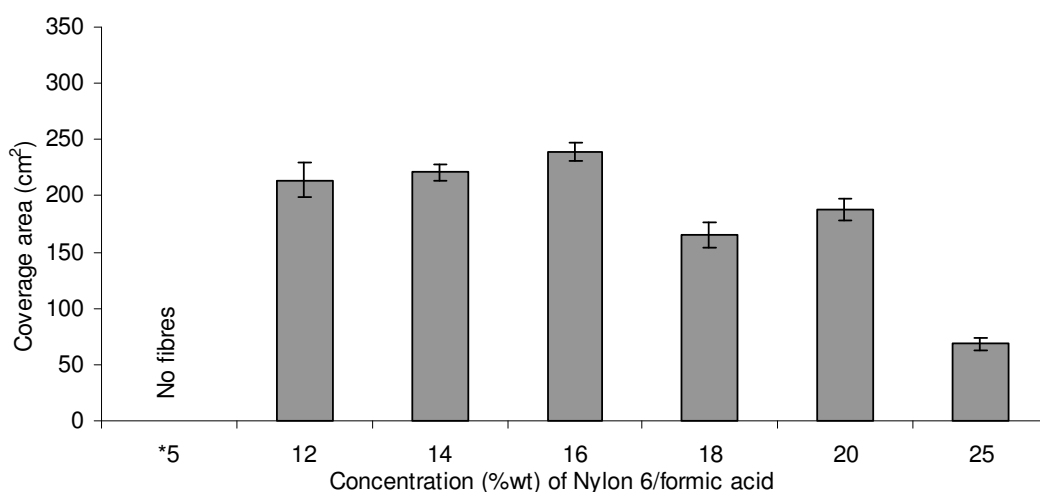
Figure 5-3: Typical plots of: a) concentration versus fibre diameter and b) concentration versus membrane coverage area. Values represent the average of 50 and 3 measurements for fibre diameter and membrane coverage area, respectively. Electrospinning voltage and distance were 35 kV and 20 cm, respectively, for Nylon 6 in formic acid.

* No fibres were observed.

The solution concentration was also found to influence the morphological structure of electropun Nylon 6 nanofibres. (Details on the morphological structures of electrospun Nylon 6 at different concentrations can be found in Appendix I). Figure 5-4 (a) shows that the 5 %wt concentration produces droplets. The formation of droplets was caused by the low viscosity of Nylon 6 solution (approximately 30 cPs). This would be a situation where a solution with low viscosity has minimal chain overlap, which limits the polymer chain

entanglement in polymer solution. This resulted in small droplets rather than uniform fibres. It was found that the size of the droplets was approximately 369 ± 247 nm, which was greater than the diameter of fibres.
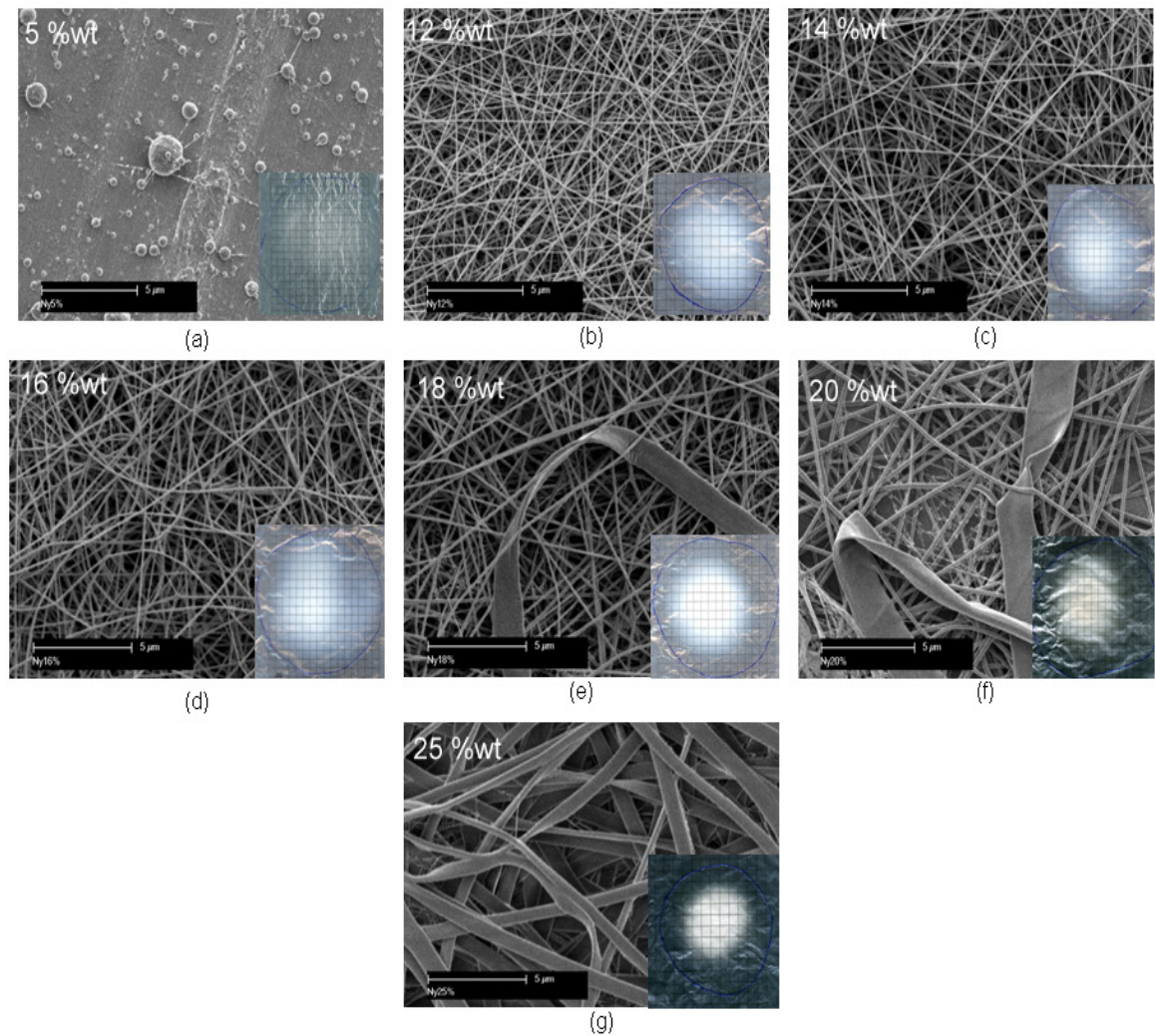
Figure 5-4: Typical SEM images of electrospun Nylon 6 at different concentrations. a) 5 %wt, b) 12 %wt, c) 14 %wt, d) 16 %wt, e) 18 %wt, f) 20 %wt and g) 25 %wt. For SEM images (a-g), the inset represents typical membrane coverage area at different concentrations. Electrospinning voltage and distance were 35 kV and 20 cm, respectively, for Nylon 6 in formic acid.

As the Nylon 6 concentration increased from 5 to 12 %wt, the transition from droplets to cylindrical fibres was observed (Figures 5-4 (a-b)). The formation of uniform cylindrical fibres was expected due to sufficient polymer chain entanglement of Nylon 6 at 12 %wt. Uniform cylindrical fibres were also observed at 14 and 16 %wt, (Figure 5-4 (c-d)). A further increase in concentration, from 18 to 20 %wt gave a mixture of cylindrical fibres and flat-ribbon fibres

(Figure 5-4 (e-f)). At 18 %wt, the diameter of cylindrical fibres was approximately 138 nm, whereas the width of the flat ribbon fibres was about 613 nm. For 20 %wt, the fibre diameters were 193 nm and the flat-ribbon fibres were approximately 703 nm. At 25 %wt, membranes with flat-ribbon fibres were formed (Figure 5-4 (g)). The formation of flat-ribbon fibres has been reported in the past by Koombhongse *et al.* (*208*). They assumed that the uneven evaporation of solvent between the surface and the core of the charged jet formed flat-ribbon fibres. The outer surface of the jet evaporated faster than the core, forming skin on the jet surface. As the solvent evaporated from the jet core, the atmospheric pressure tended to collapse the charged jet, forming a ribbon-like fibre (*208*).

In Figures 5-4 (b-d), Nylon 6 concentrations at 12 %wt, 14 %wt and 16 %wt form uniform cylindrical fibres. When the resultant fibre diameter at 12 %wt, 14 %wt and 16 %wt were plotted in histograms format (Figure 5-5 (a-c)), fibres at 16 %wt exhibited the lowest standard deviation. This implies that these fibres are more uniform than fibres at 12 %wt and 14 %wt. At 16 %wt concentration, the solution was expected to have higher polymer chain entanglement which resulted in uniform fibres as compared to fibres at 12 %wt and 14 %wt concentrations. The average fibre diameter of electrospun Nylon 6 at 16 %wt concentration was slightly larger than fibres at 12 %wt and 14 %wt. It was expected that the charged jets at 16 %wt to have greater resistance towards thinning of the jets, which resulted in larger fibre diameters compared to those at lower concentrations. Due to its fibre uniformity and large coverage area, 16 %wt concentration was selected for further experimentation particularly on the effects of applied voltages and needle tip-to-collector distances on the fibre and membrane morphologies.
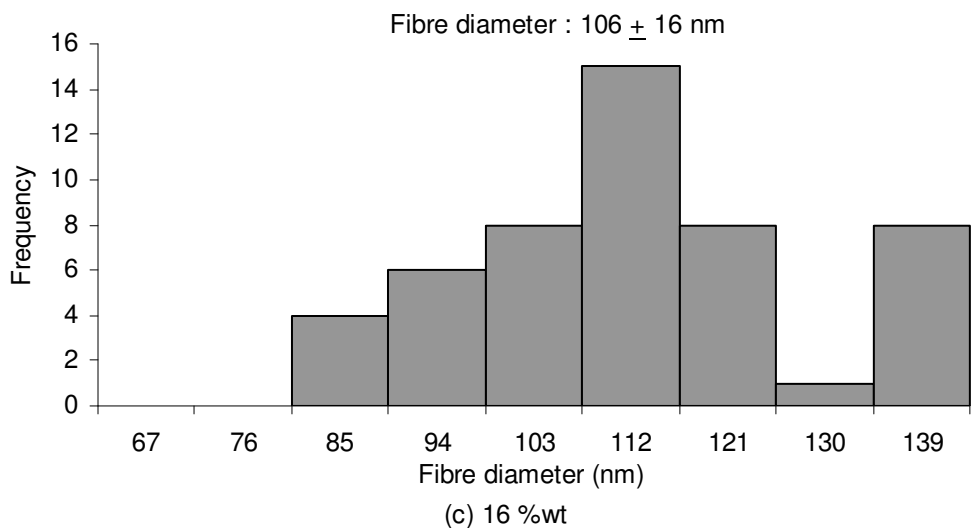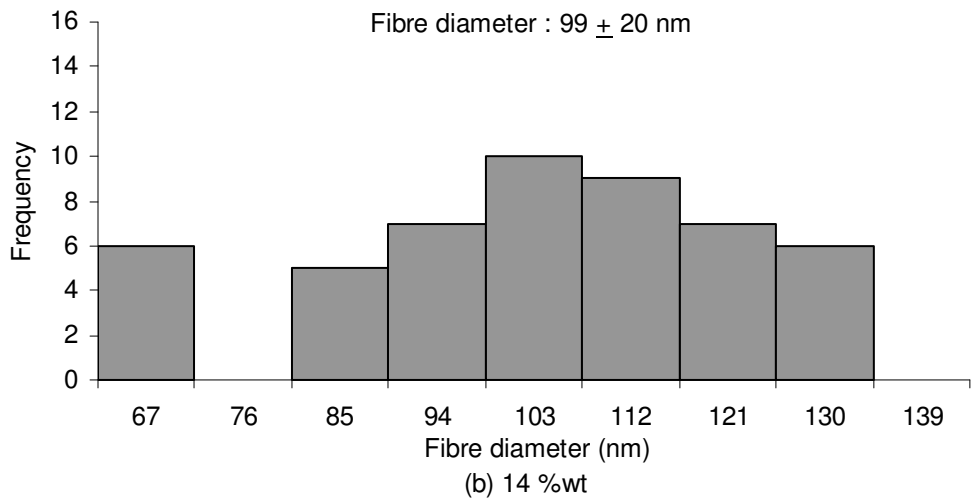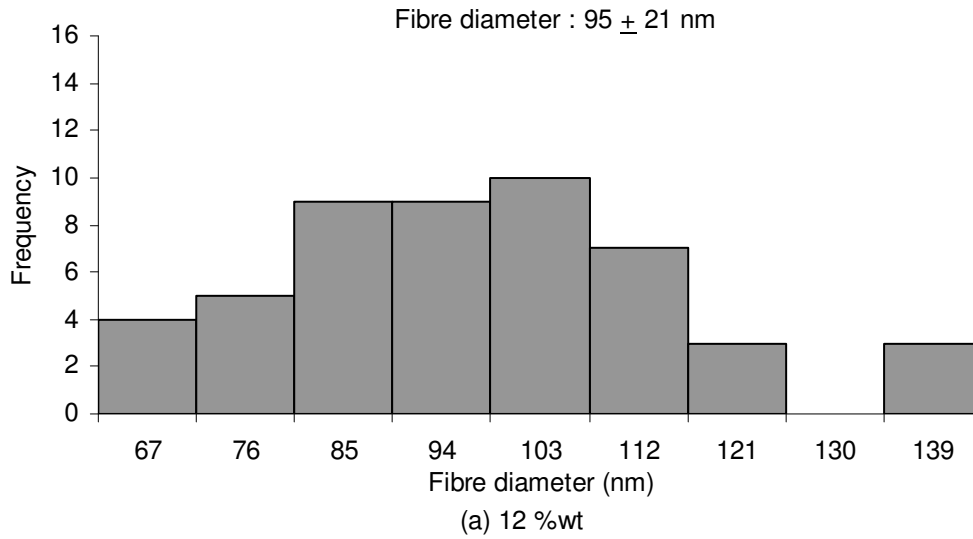
Figure 5-5: Plots of fibre distribution for electrospun Nylon 6 at different concentrations. a) 12 %wt, b) 14 %wt and c) 16 %wt. Electrospinning voltage and distance was 35 kV and 20 cm, respectively, for Nylon 6 in formic acid.

5.1.3 Effect of applied voltage on fibre and membrane morphologies

(a)

(b)
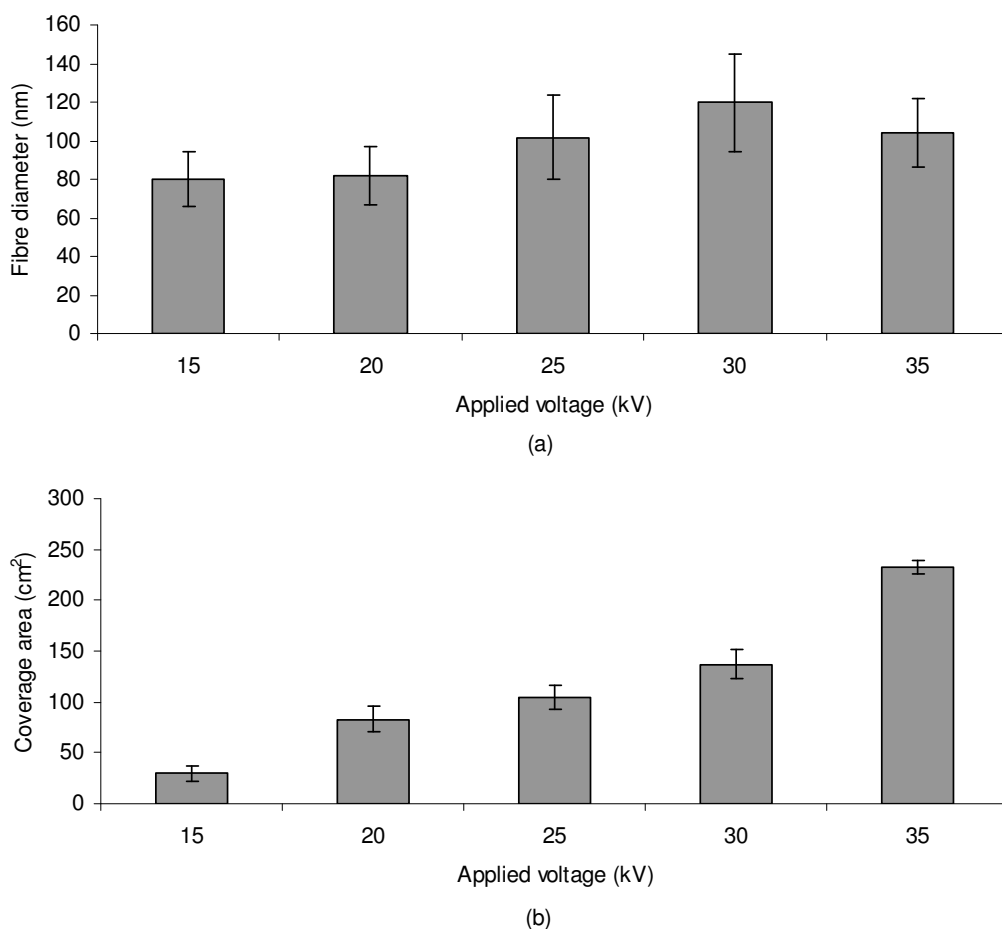
Figure 5-6: Typical plots of: a) applied voltage versus fibre diameter and b) applied voltage versus membrane coverage area. Values represent the average of 50 and 3 measurements for fibre diameter and membrane coverage area, respectively. Solution concentration and distance were 16 %wt and 20cm, respectively, for Nylon 6 in formic acid.

In Figure 5-6 (a), the average fibre diameters of electrospun Nylon 6 show a slight increase from 80 to 106 nm with the increase of applied voltage. This phenomena has been described by Ojha *et al.* (*45*), where the authors reported that an increase in voltage increased the electrostatic forces, which could eject more solution from the needle tip. As a result, an increase in fibre diameter was observed for electrospun Nylon 6 (*45*).

Increasing the voltages was also observed to increase the electrospun Nylon 6 coverage area (Figure 5-6 (b)). At 15 kV, the electrospinning jets had just enough electric field strength to eject the Taylor cone Nylon 6 jets at the needle tip. As a result, membranes with small area and fewer fibres were deposited (Figure 5-7 (a)). When a higher voltage was applied (above 20 kV), the stronger

electric field was able to draw out more fibres, resulting in a larger coverage area (Figure 5-7 (b-e)). These results contrasted with an earlier study done by Supaphol *et al.* (*41*). They reported that an increase in voltages reduced the Nylon 6 membrane coverage area. The disagreement could be attributed to the difference in polymer concentration where the authors used 32 %, whereas the current study used 16 %wt concentration for Nylon 6 solution. At 16 %, the charged jets would have bigger bending instabilities when the applied voltage increases. As a result, a large coverage area can be obtained at higher voltage. For 32 %, the solution was thicker than the 16 %. When a thick solution is electrospun at higher voltage, the charged jets would have higher resistance to stretch and thus travel linearly before forming a bending instability. This resulted in small coverage area at higher voltage.
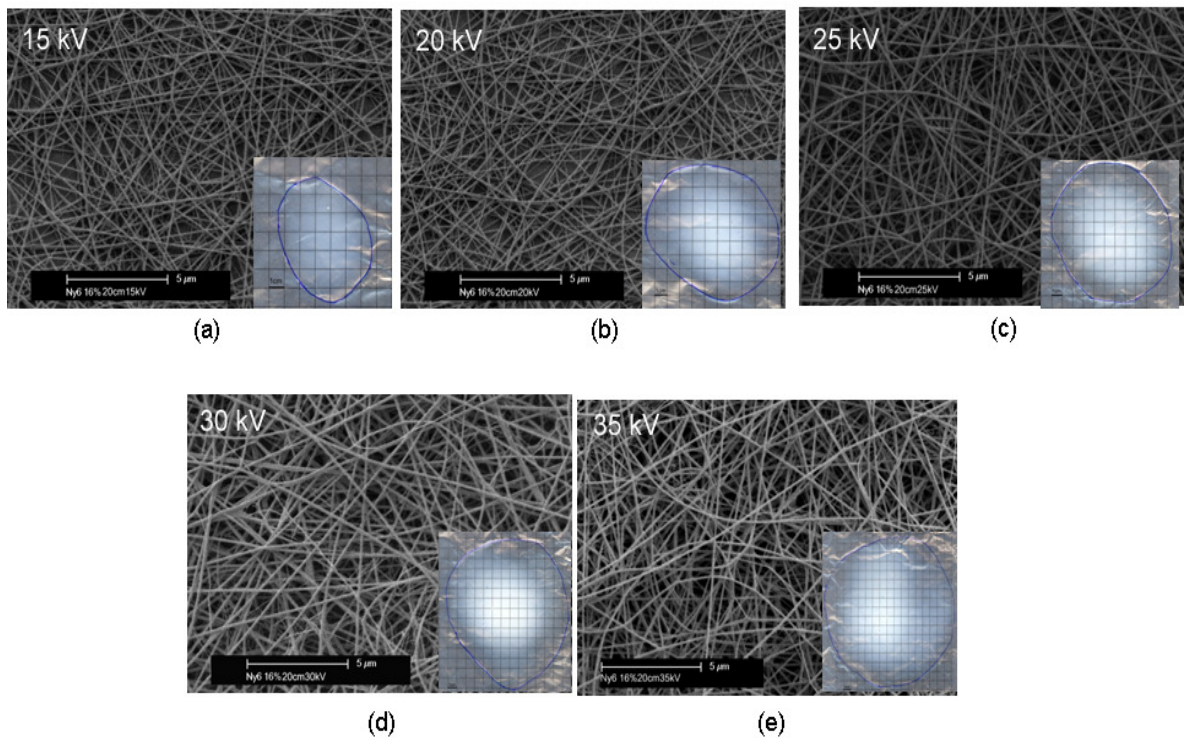
Figure 5-7: Typical SEM images of electrospun Nylon 6 at different voltages. a) 15 kV, b) 20 kV, c) 25 kV, d) 30 kV and e) 35 kV . For SEM images (a-e), the inset represents typical membrane coverage areas at different voltages. Electrospinning distance and concentration were 20 cm and 16 %wt, respectively, for Nylon 6 in formic acid.

In Figures 5-6 (a-b) and 5-7 (a-e), the optimal voltage was found at 35 kV because it produced uniform cylindrical fibres and large coverage area. However, the 35 kV tended to cause clogging at the needle tip. This was attributed to a rapid

evaporation of the solvent at higher voltage. Thus, further experiments were carried out in order to identify an ideal applied voltage without clogging. The applied voltage was reduced from 35 to 30 kV.

It was found that voltage above 32 kV caused clogging at the needle tip. The experiment showed that voltages at 32, 31 and 30 kV provided continuous jets without any clogging. The average fibre diameters at 30, 31 and 32 kV were approximately 120, 115 and 109 nm, respectively. For membrane coverage areas, the areas at 30, 31 and 32 kV were approximately 137, 173 and 240 cm^2, respectively. This shows that 32 kV produced a larger coverage area and uniform cylindrical fibres. The combination of uniform cylindrical fibres, larger coverage area and the absence of needle clogging meant that the 32 kV was chosen as the best voltage in the study. The voltage was used for further experimentation on the effect of needle tip-to-collector distance.

5.1.4 Effect of needle tip-to-collector distance on fibre and membrane morphologies

From Figure 5-8 (a), it was observed that the electrospun Nylon 6 showed a decrease in fibre diameter when the needle tip-to-collector distance increased from 5 to 20 cm. When a short distance was used (particularly at 5 cm), fibres with poor uniformity and larger diameter were obtained (Figure 5-9 (a)). This was attributed to poor solvent evaporation from the electrospinning jets at shorter distances, which resulted in non-uniform fibres being accumulated on the grounded collector plate. These fibres were also found to form smaller coverage areas (Figure 5-8 (b)) and dense membrane structures (Figure 5-9 (a)).

At greater distances (more than 5 cm), the Nylon 6 jets had longer flight times enabling the jets to be stretched before depositing on the collector. This resulted in smaller fibre diameters as compared to fibres at 5 cm (Figure 5-8 (a)). Similar results were also found in another study (*45*). Ojha *et al.* (*45*) reported that an increase in needle tip-to-collector distance reduced the resultant fibre diameter of electrospun Nylon 6. An increase in needle tip-to-collector distance was also expected to increase the bending instability of the Nylon 6 jets, which could form membranes with larger coverage areas. As a result, at 20 cm the coverage area was the largest (approximately 240 cm^2), but had fewer fibres as compared to the other distances (Figures 5-9 (a-d)).

(a)

Figure 5-8: Typical plots of: a) needle tip-to-collector distance versus fibre diameter and b) needle tip-to-collector distance versus membrane coverage area. Values represent the average of 50 and 3 for fibre diameter and membrane coverage area, respectively. Solution concentration and applied voltage were 16 %wt and 32 kV, respectively, for Nylon 6 in formic acid.

Figure 5-9: Typical SEM images of electrospun Nylon 6 at different needle tip-to-collector distance. a) 5 cm, b) 10 cm, c) 15 cm and d) 20 cm. For SEM images (a-d), the inset represents typical membrane coverage areas at different needle tip-to-collector distances. Electrospinning voltage and concentration were 32 kV and 16 %wt, respectively, for Nylon 6 in formic acid.

From results presented in Figures 5-8 (a-b) and 5-9 (a-d), the best distance was found to be 20 cm because of the uniformity of fibre diameter and larger coverage area.

5.2 Polyvinyl Alcohol (PVA)

5.2.1 Effect of concentration on viscosity

Polyvinyl alcohol is the other hydrophilic polymer used in the study. PVA solution viscosity was graphed against concentration in Figure 5-10. Viscosity was observed to increase with increasing solution concentration. As mentioned earlier in Section 5.1.1, the increase of viscosity was due to the overlapping of polymer chains in the polymer solution.
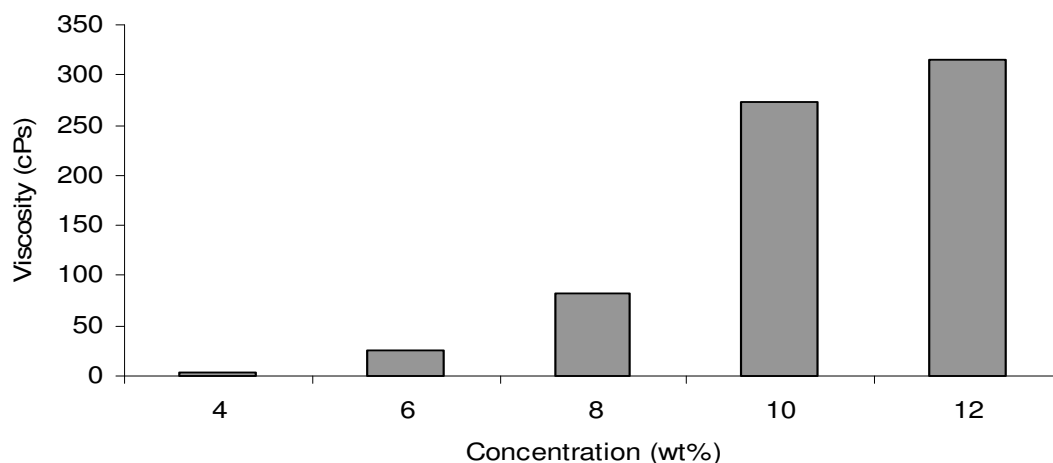
Figure 5-10: The effect of solution concentration on viscosity for PVA dissolved in deionised water. Values represent the average of 5 measurements for each concentration. Error bars were neglected due to the low standard deviation.

5.2.2 Effect of concentration on fibre and membrane morphologies

Within the limits of the voltages and distances studied, increasing PVA concentration from 4 to 12 %wt was found to increase the average fibre diameters of the electrospun PVA (Figure 5-11 (a)). At higher concentrations, the electrospun jets were expected to have higher resistance to being stretched, which resulted in bigger fibre diameters. This result was also in agreement with Zhang *et al.* (*46*), where it was observed that the resultant diameters of electrospun PVA fibres increased with increasing concentrations of polymer solutions.

In Figure 5-11 (b), the coverage area of electrospun PVA decrease from 145 cm^2 to 60 cm^2 when the concentration increased from 4 to 12 %wt. When the concentration increased, the PVA jets travelled further linearly before forming a bending instability. As a result, a dense membrane with smaller coverage area was deposited on the grounded collector (Figures 5-11 (b) and 5-12 (a-e)).

Between 4 to 8 %wt, beaded fibres were also observed. This shows that the PVA polymer solutions have poor chain entanglement at these concentrations. In Figures 5-11 (a) and 5-12 (a-c), the diameters of fibres at 4, 6 and 8 %wt were approximately 109, 180 and 219 nm, respectively. The diameters of beads at 4 and 6 and 8 %wt were approximately 539, 706 and 793 nm, respectively. As the concentration increased from 8 to 12 %wt, the PVA solution was presumed to have adequate polymer chain entanglement which resulted in uniform cylindrical fibres (Figure 5-12 (d-e)). In Figures 5-11 (a), the average fibre diameters at 10 %wt is about 259 nm, whereas the diameter at 12 %wt is 310 nm. (Details on the morphological structures of electrospun PVA can be found in Appendix I).

(a)

(b)

Figure 5-11: Typical plots of: a) concentration versus fibre diameter and b) concentration versus membrane coverage area. Values represent the average of 50 and 3 measurements for fibre diameter (excluding beads) and membrane coverage area, respectively. Electrospinning voltage and distance were 25 kV and 20 cm, respectively, for PVA in deionised water.
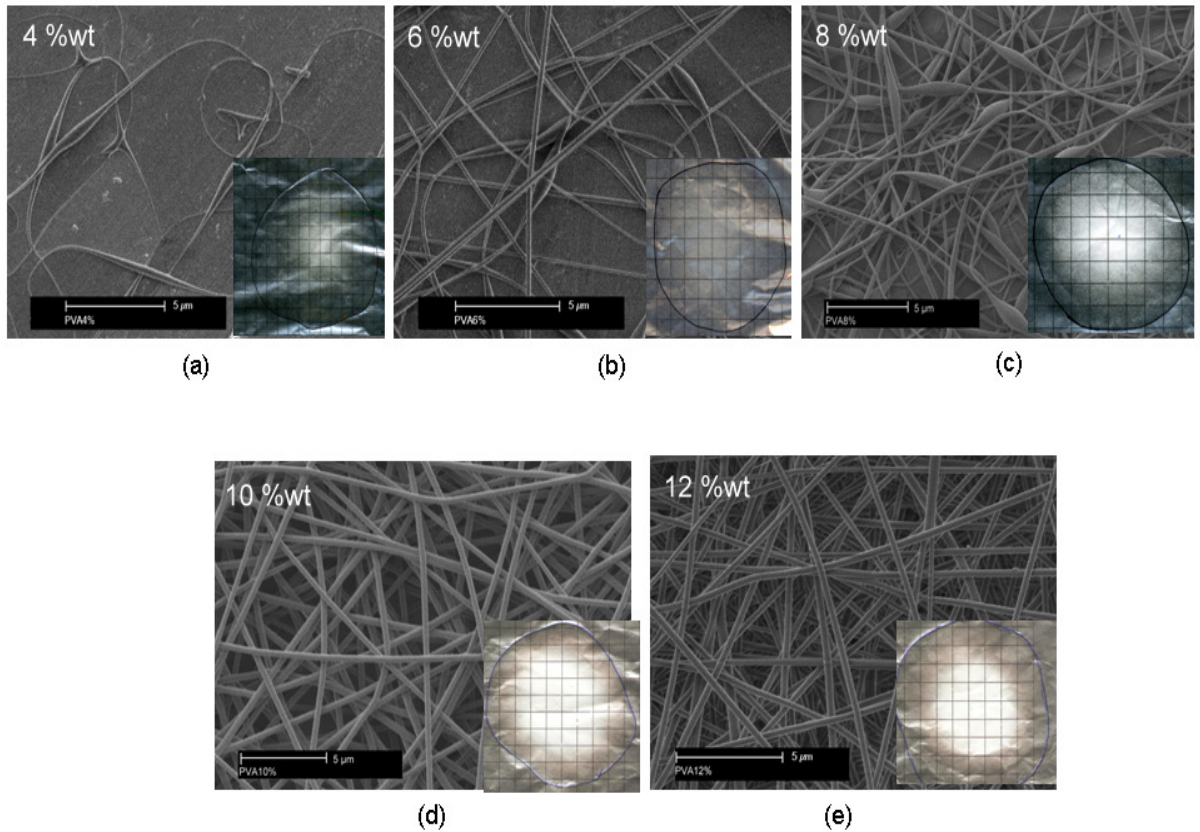
Figure 5-12: Typical SEM images of electrospun PVA at different concentrations. a) 4 %wt, b) 6 %wt, c) 8 %wt, d) 10 %wt and e) 12 %wt. For SEM images (a-e), the inset represents typical membrane coverage areas at different concentrations. Electrospinning voltage and distance were 25 kV and 20 cm, respectively, for PVA in deionised water.

Results presented in Figures 5-11 (a-b) and 5-12 (a-e) show that the fibres fabricated at 10 and 12 %wt are uniform with cylindrical structures. When both concentrations were correlated to coverage area, the 10 %wt produced larger area (approximately 74 cm^2) compared to 12 %wt (approximately 60 cm^2). Hence, the 10 %wt was selected for further study as an optimal concentration for PVA because it formed uniform cylindrical fibres as well as producing the large coverage area with uniform fibre distribution.

5.2.3 Effect of applied voltage on fibre and membrane morphologies

The 10 %wt PVA in deionised water concentration was electrospun at different applied voltages ranging from 15 kV to 35 kV. In Figure 5-13 (a), the increase of applied voltage does not affect the average fibre diameter of electrospun PVA. A possible reason could be due to the formation of multiple jets during electrospinning that could form a comparable fibre diameter at any

voltages. However, the results were in contrasted with a recent study done by Zhang *et al.* (*46*). It was reported that the average fibre diameters of electrospun PVA was slightly increased with increasing applied voltage. The disagreement could be attributed to the difference in applied voltage where the authors used 5kV to 15kV, whereas the current study used higher voltages in a range of 15kV to 35 kV. When a high voltage is applied to the PVA solution, multiple jets could form during the electrospinning. These multiple jets could have similar fibre diameter at any voltages.
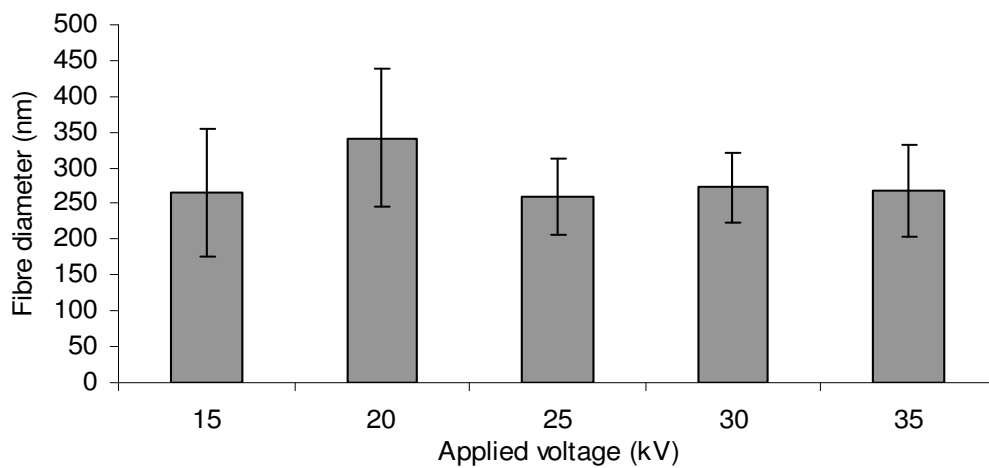
(a)
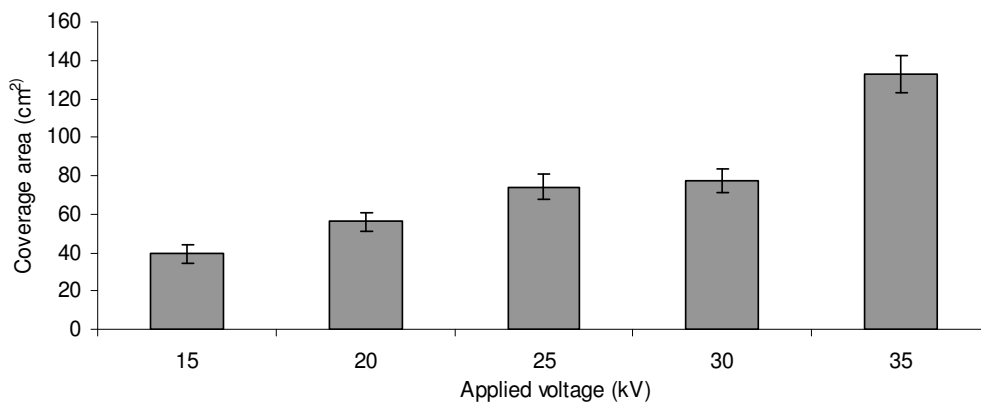
(b)

Figure 5-13: Typical plots of: a) applied voltage versus fibre diameter and b) applied voltage versus membrane coverage area. Values represent the average of 50 and 3 measurements for fibre diameter and membrane coverage area, respectively. Solution concentration and distance were 10 %wt and 20 cm, respectively, for PVA in deionised water.

The coverage area of electrospun PVA was found to increase with increasing voltage (Figure 5-13 (b)). When a higher voltage is applied, jets with bigger bending instabilities could form. This will result in a large coverage area

for electrospun PVA. In Figure 5-14 (a-c), uniform membranes are deposited particularly below 25 kV. At 30 to 35 kV, uneven membranes are deposited (Figure 5-14 (d-e)). This could be due to the formation of an unstable electrospinning jet at the higher voltages. From Figure 5-13 (b), it can be seen that 35 kV gives the largest coverage area, but the membrane has uneven structures (Figure 5-14 (e)). This falls outside the criteria of optimal conditions as defined earlier. Therefore, 25 kV was selected as the best option for further study because this voltage produced membranes with uniform cylindrical fibres, large coverage area and uniform fibre distribution.

Figure 5-14: Typical SEM images of electrospun PVA at different voltages. a) 15 kV, b) 20 kV, c) 25 kV, d) 30 kV and e) 35 kV. For SEM images (a-e), the inset represents typical membrane coverage areas at different applied voltages. Electrospinning distance and concentration were 20 cm and 10 %wt, respectively, for PVA in deionised water.

5.2.4 Effect of needle tip-to-collector distance on fibre and membrane morphologies

At the shorter needle tip-to-collector distances (below 10 cm), PVA formed larger fibres with diameters ranging from 292 to 486 nm (Figure 5-15 (a)). The formation of larger fibre diameter is due to poorly developed whipping instability, which results in inadequate stretching of the fibres. The morphological structures

of the fibres are shown in Figure 5-16 (a-b).When the distance increased from 10 to 20 cm, solvent (deionised water) from the PVA jets had sufficient time to evaporate, resulting in fibre with fine diameters and uniform cylindrical shape. The average fibre diameter at 20 cm was approximately 259 nm, which was half the diameter size of fibres produced at 5 cm (Figure 5-15 (a)).
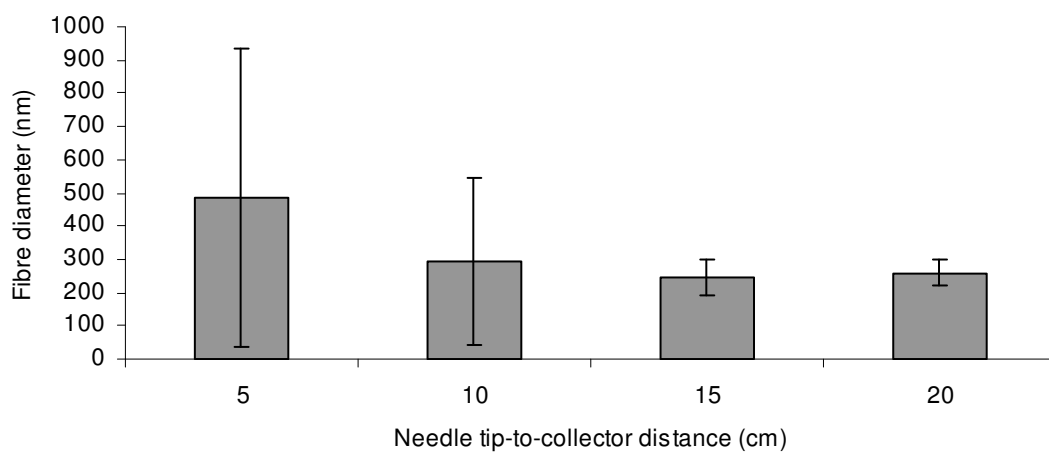
(a)
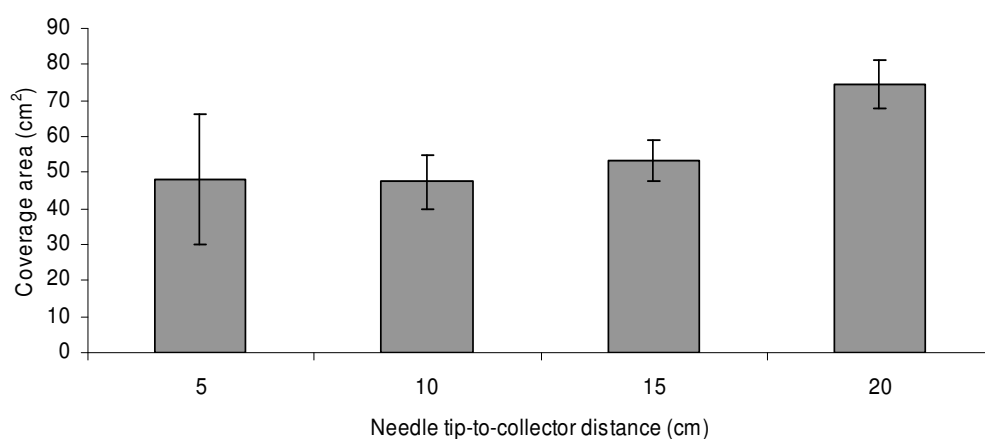
(b)

Figure 5-15: Typical plots of: a) needle tip-to-collector distance versus fibre diameter and b) needle tip-to-collector distance versus membrane coverage area. Values represent the average of 50 and 3 for fibre diameter and membrane coverage area, respectively. Solution concentration and applied voltage were 10 %wt and 25 kV, respectively, for PVA in deionised water.
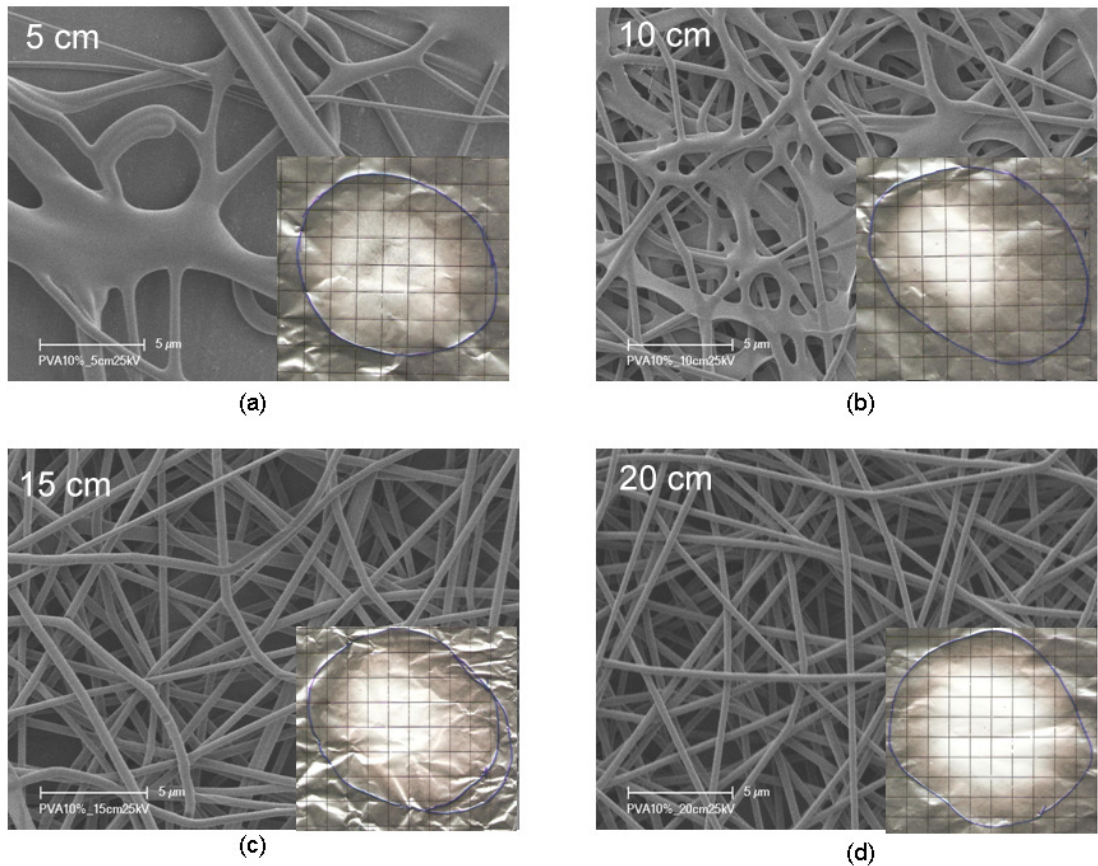
Figure 5-16: Typical SEM images of electrospun PVA at different distance. a) 5 cm, b) 10 cm, c) 15 cm and d) 20 cm. For SEM images (a-d), the inset represents typical membrane coverage areas at different needle tip-to-collector distances. Electrospinning voltage and concentration were 25 kV and 10 %wt, respectively, for PVA in deionised water.

The increase of needle tip-to-collector distance was also found to increase membrane coverage area (Figure 5-15 (b)). At the larger distances, the bending instabilities of the PVA jets were expected to increase causing a larger coverage area (Figure 5-16 (c-d)). From the results shown in Figures 5-15 (a-b) and 5-16 (a-d), the 20 cm appeared to provide the optimal electrospinning distance for electrospun PVA.

5.3 Polyacrylonitrile (PAN)

In Sections 5.1 to 5.2, the optimal electrospinning conditions for hydrophilic electrospun Nylon 6 and PVA membranes have been identified. This section investigates the optimal conditions for hydrophobic electrospun PAN membranes.

5.3.1 Effect of concentration on viscosity

In Figure 5-17, the PAN solution showed an increase in viscosity as the concentration increased from 5 to 13 %wt. In Simha's Theory, the increase of viscosity was due to the overlapping of polymer chains in the polymer solution, outlined in Section 5.1.1.
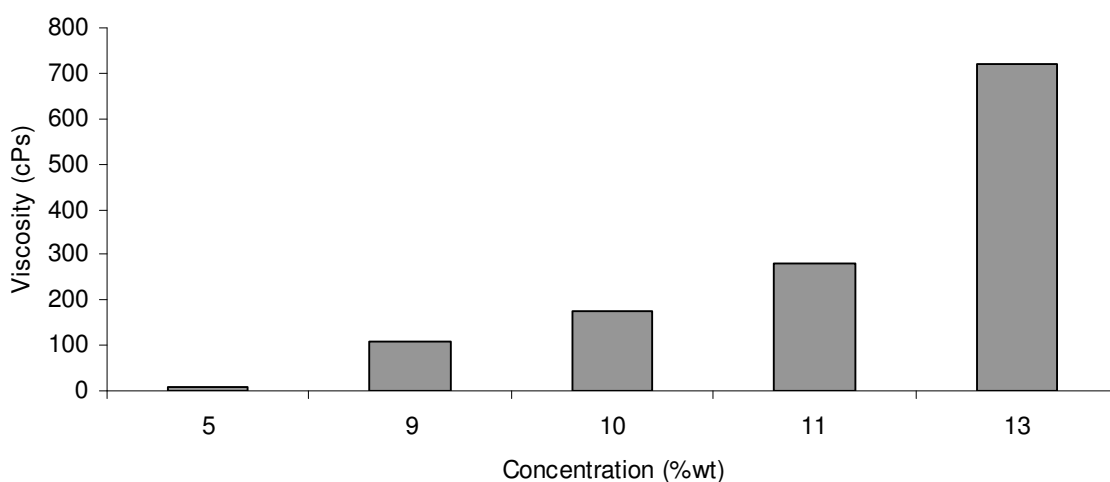
Figure 5-17: The effect of solution concentration on viscosity of PAN in dimethyl formamide (DMF). Values represent the average of 5 measurements for each concentration. Error bars were neglected due to the low standard deviation.

5.3.2 Effect of concentration on fibre and membrane morphologies

Figures 5-18 (a-b) show that an increase in concentration increased the average fibre diameter and also reduced the membrane coverage area for electrospun PAN. In Figures 5-19 (a-b), solutions with concentration below 9 %wt, resulted in beaded fibres. (The morphological structures of electrospun PAN can also be found in Appendix I). In Figure 5-18 (a), the average fibre diameter at 5 %wt was approximately 261 nm. The diameter of beads at 5 %wt was 1.2 μm. For 9 wt%, the average fibre diameter was around 346 nm and the bead diameter was 4.7 μm. PAN concentrations at 10 %wt, produced uniform cylindrical fibres

with diameter of 624 nm (Figure 5-19 (c)). At higher concentration (particularly above 11 %wt), the solution was too viscose for electrospinning effectively, producing a mixture of blobs and fibres as shown Figures 5-19 (d-e). At 13 %wt, even fewer fibres were observed, which resulted in a less dense membrane with much larger diameter (approximately 2.6 µm). In Figures 5-19 (d-e), the diameter of blobs at 11 and 13 %wt were about 12.1 and 39 µm, respectively.

(a)

(b)
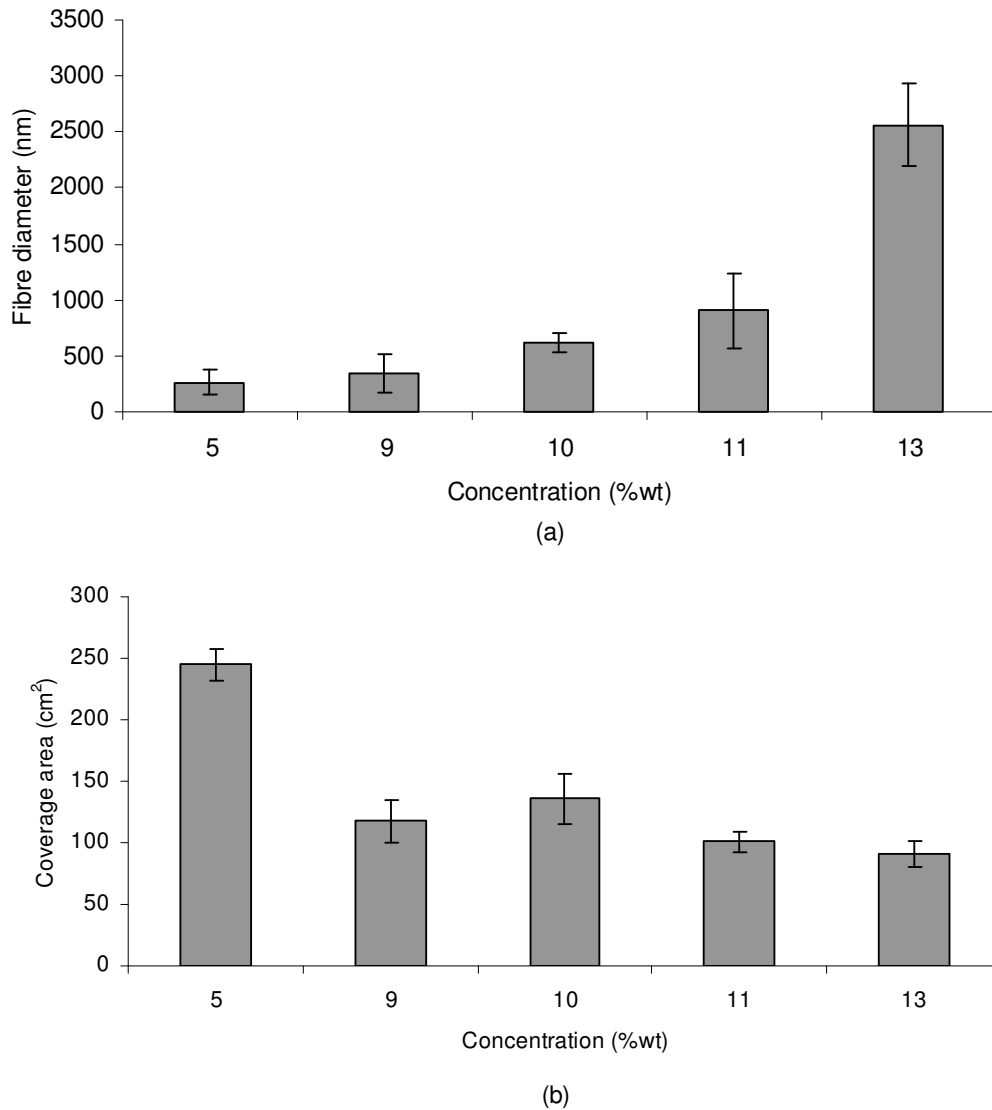
Figure 5-18: Typical plots of: a) concentration versus fibre diameter and b) concentration versus membrane coverage area. Values represent the average of 50 and 3 for fibre diameter (excluding beads and droplets) and membrane coverage area, respectively. Electrospinning voltage and distance were 20 kV and 20 cm, respectively, for PAN in dimethyl formamide (DMF).
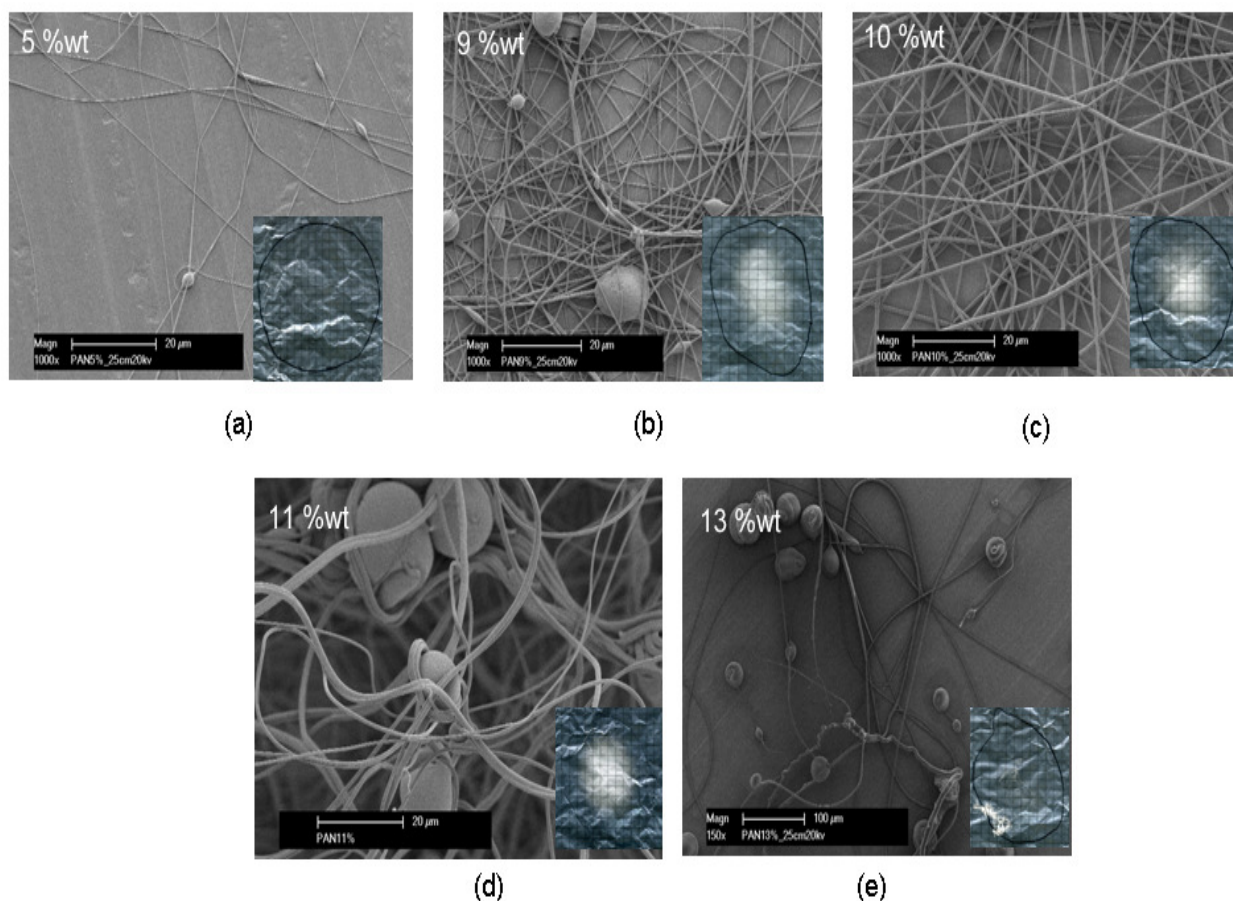
Figure 5-19: Typical SEM images of electrospun PAN at different concentrations. a) 5 %wt, b) 9 %wt, c) 10 %wt, d) 11 %wt and e) 13 %wt. For SEM images (a-e), the inset represents typical membrane coverage areas at different concentrations. Electrospinning voltage and distance were 20 kV and 20 cm, respectively, for PAN in dimethyl formamide (DMF).

From Figures 5-18 (a-b) and 5-19 (a-e), uniform cylindrical fibres can only be produced at 10 %wt. Thus, 10 %wt of PAN in dimethyl formamide (DMF) was selected as the optimal concentration for PAN solutions. Further experimental was carried out at this concentration.

5.3.3 Effect of applied voltage on fibre and membrane morphologies

Results presented in Figure 5-20 (a) show that the resultant fibre diameters for PAN are broadly comparable over the voltages studied. It was expected that the formation of multiple jets during electrospinning could produce a comparable fibre diameter for electrospun PAN at any voltages. The results were in contrasted with a recent study done by Jalili *et al.* (*58*). The authors reported that the PAN fibre diameter decreased with an increase in applied voltage. The disagreement could be due to electrospinning conditions used by the authors. The authors

110

applied different flow rates (2 to 12 ml/hr) at different voltages (10 to 20 kV), which exhibited different results compared to the current study. For current study, the flow rate was fixed (0.2 ml/hr) at any voltages.

In Figure 5-20 (b), the membrane coverage area showed an increase as the applied voltage increased from 15 to 35 kV. When a higher voltage was applied, jets with bigger bending instabilities could form. This will result in a large coverage area for electrospun PAN.
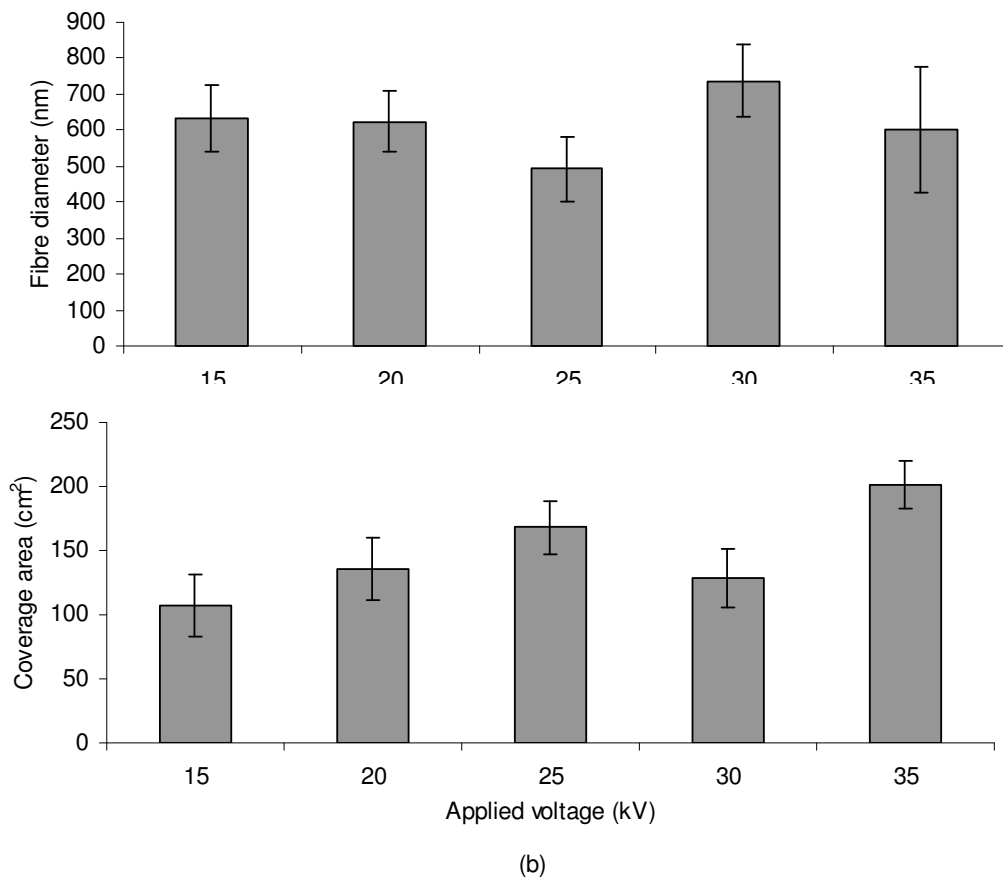
Figure 5-20: Typical plots of: a) applied voltage versus fibre diameter and b) applied voltage versus membrane coverage area. Values represent the average of 50 and 3 measurements for fibre diameter and membrane coverage area, respectively. Solution concentration and distance were 10 %wt and 20 cm, respectively, for PAN in dimethyl formamide (DMF).

Figures 5-21 (a-e) are the SEM images of electrospun PAN at different field strengths range of 15kV/20cm to 35kV/20cm. However, after 3 minutes electrospinning time resulted in the formation of beaded fibres. Typical beaded fibres are shown in Figure 5-22 (a-b). The formation of beaded fibres was also

observed by a recent study (*58*). Jalili *et al.* (*58*) reported that when a high electric field (above than 11kV/15cm) was applied to the PAN solution, a number of beaded fibres was created. At higher electric field, a Taylor's cone was no longer suspended at the needle tip because charged jets were pulled out faster than the supply. As a result, the charged jets were ejected directly from the needle tip. These jets hit the internal needle wall which resulted in beaded fibres for electrospun PAN (*58*). The evidence of this finding was shown by Deitzel *et al.* (*51*). The authors were able to capture an image of jets hitting the internal needle wall at high voltage. This image can be found in Chapter 2, Section 2.3.2.1.
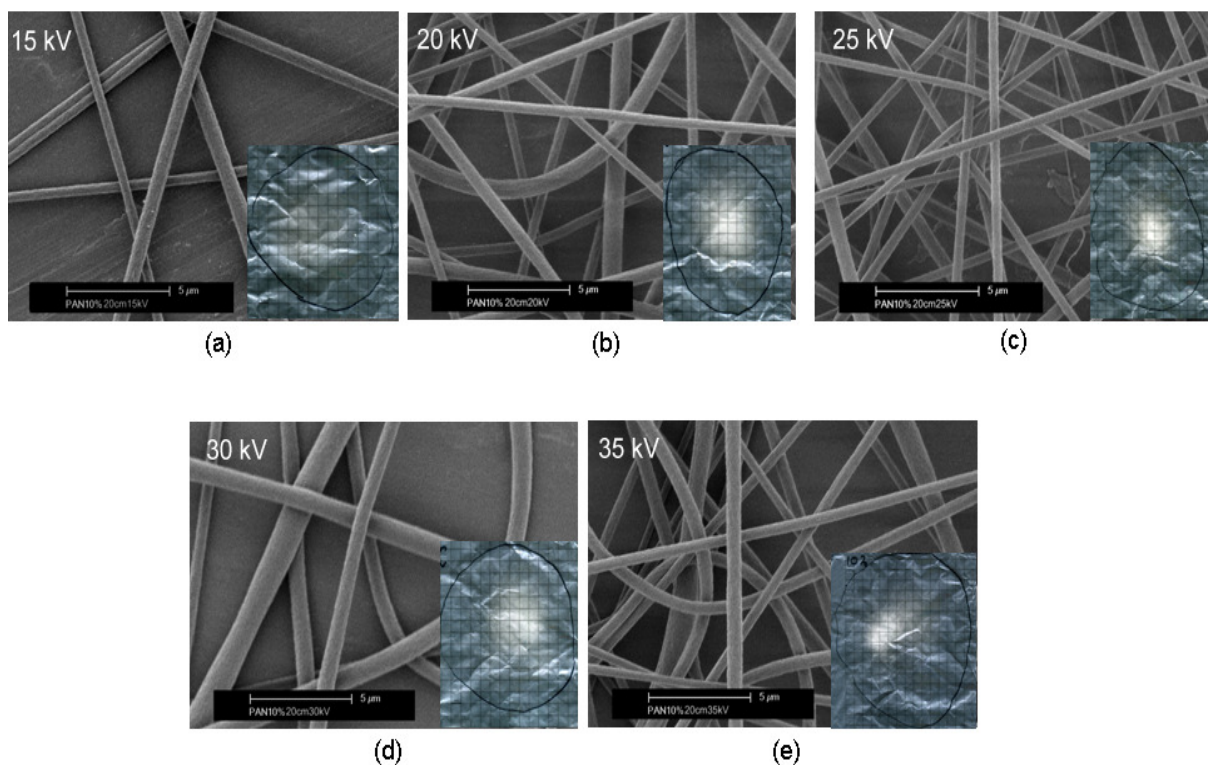
Figure 5-21: Typical SEM images of electrospun PAN at different voltages. a) 15 kV, b) 20 kV, c) 25 kV, d) 30 kV and e) 35 kV. For SEM images (a-e), the inset represents typical membrane coverage areas at different applied voltages. Electrospinning distance and concentration were 20 cm and 10 %wt, respectively, for PAN in dimethyl formamide (DMF). The electrospinning time is 3 minutes.
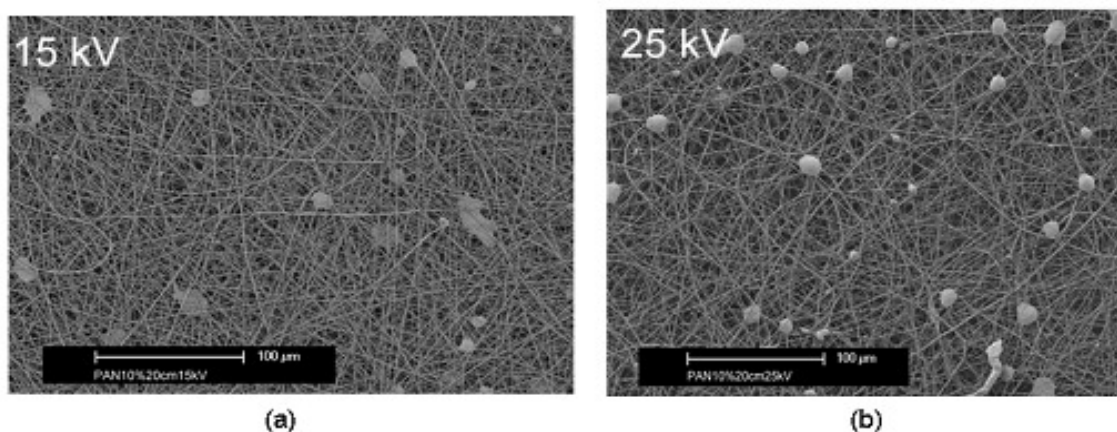
Figure 5-22: Typical SEM images of beaded electrospun PAN at: a) 15 kV and b) 25 kV. Electrospinning distance and concentration were 20 cm and 10 %wt, respectively, for PAN in dimethyl formamide (DMF). The electrospinning time is 8 minutes.

In the current study, the applied voltages were reduced to 10 and 9 kV in order to obtain uniform cylindrical fibres throughout the electrospinning period. At 10 kV, beaded fibres were observed after 3 minutes electrospinning time (Figure 5-23 (a)). The average fibre diameter and bead diameter were approximately 643 nm and 3μm, respectively. When the voltage reduced to 9 kV, the PAN jets were continuously ejected from a stable Taylor cone. This resulted in bead-free fibres for electrospun PAN throughout the electrospinning (Figure 5-23 (b)). The average fibre diameter at 9 kV was approximately 677 nm and the membrane coverage area was 141 cm^2.
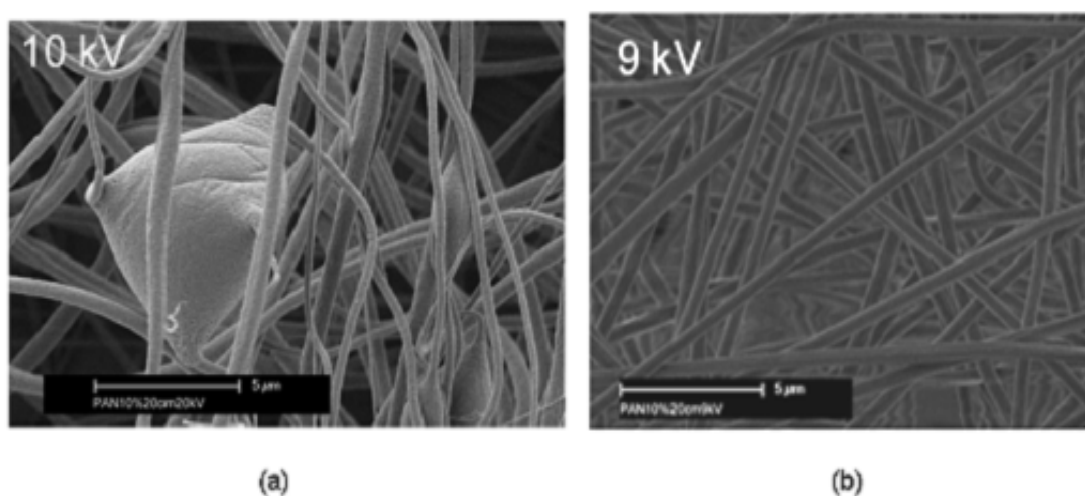
Figure 5-23: Typical SEM images of electrospun PAN at: a) 10 kV and b) 9 kV. The images were. Electrospinning distance and concentration were 20 cm and 10 %wt, respectively, for PAN in dimethyl formamide (DMF). The electrospinning time is 8 minutes.

From these experiments, 9 kV was selected as an optimal voltage due to the formation of uniform cylindrical fibres throughout the electrospinning time. The 9 kV was then used for the subsequent experiments.

5.3.4 Effect of needle tip-to-collector distance on fibre and membrane morphologies

An increased in electrospinning distance was observed to reduce the resultant fibre diameter and increased the coverage area of electrospun PAN (Figures 5-24 (a-b)). At shorter distances particularly at 5 cm, solvent from the PAN jets had insufficient flight time to evaporate the DMF solvent, which resulted in non uniform fibres, as shown Figure 5-25 (a).

As the distance increased from 5 to 20 cm, the PAN jets have sufficient flight time to be stretched and the DMF solvent to evaporate, which resulted in fibre with finer diameter and uniform cylindrical fibres (Figures 5-25 (b-d)). The increased of needle tip-to-collector distance was expected to increase the bending instabilities of the PAN jets, resulting in the larger coverage area.

In Figures 5-24 (a-b) and 5-25 (a-d), 20 cm was found to create uniform cylindrical fibres with a large coverage area. Hence, the distance 20 cm was chosen as an optimal distance for electrospun PAN.
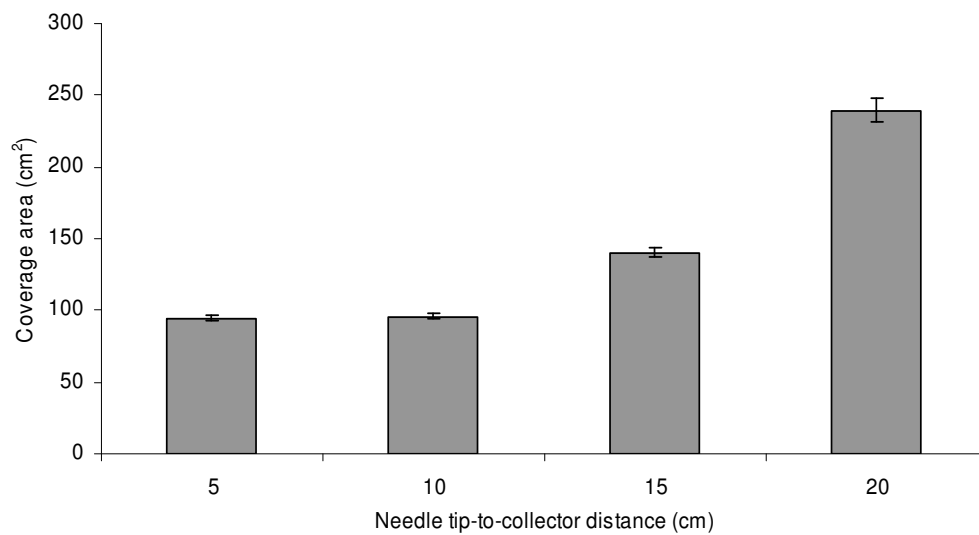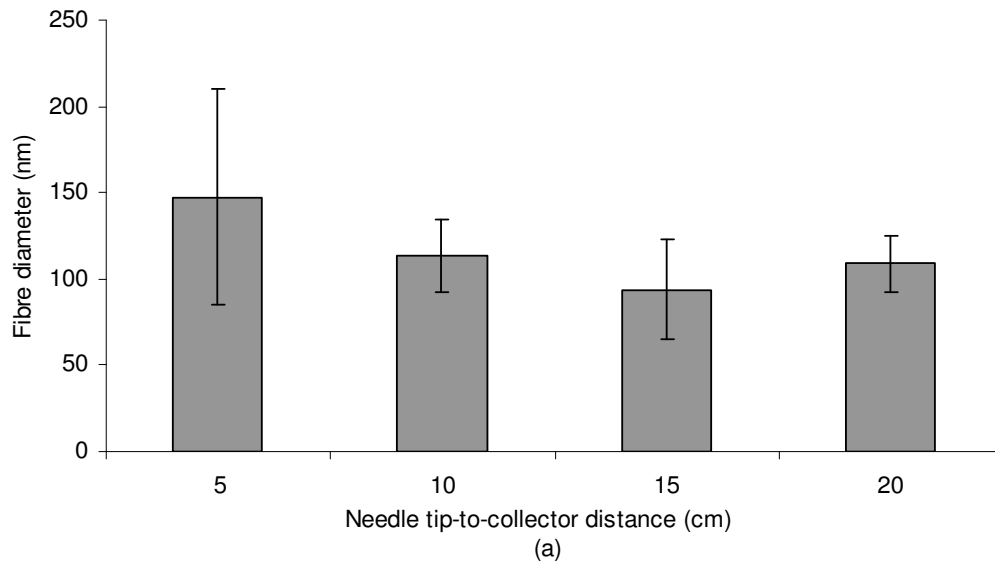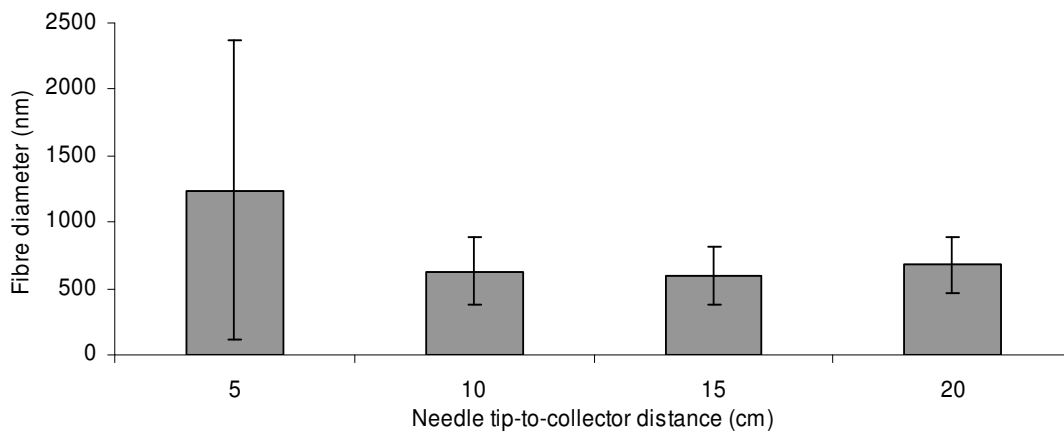
(a)
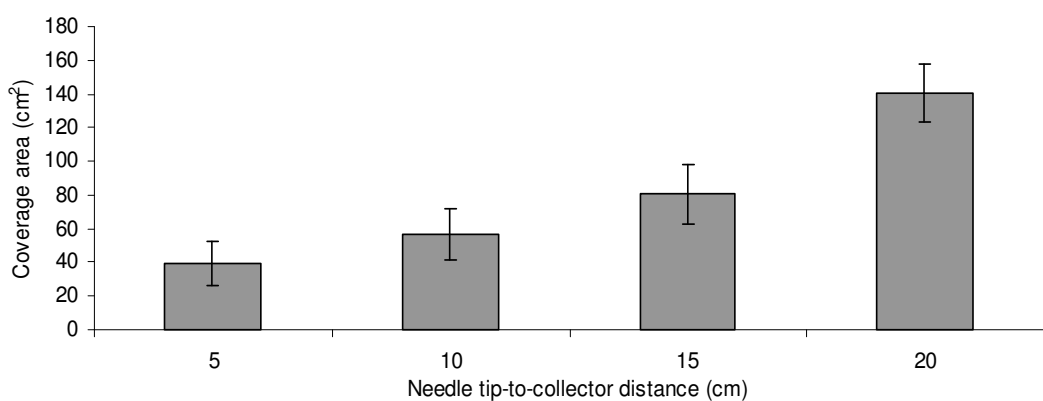
(b)

Figure 5-24: Typical plots of: a) needle tip-to-collector distance versus fibre diameter and b) needle tip-to-collector distance versus membrane coverage area. Values represent the average of 50 and 3 for fibre diameter and membrane coverage area, respectively. Solution concentration and applied voltage were 10 %wt and 9 kV, respectively, for PAN in dimethyl formamide (DMF).
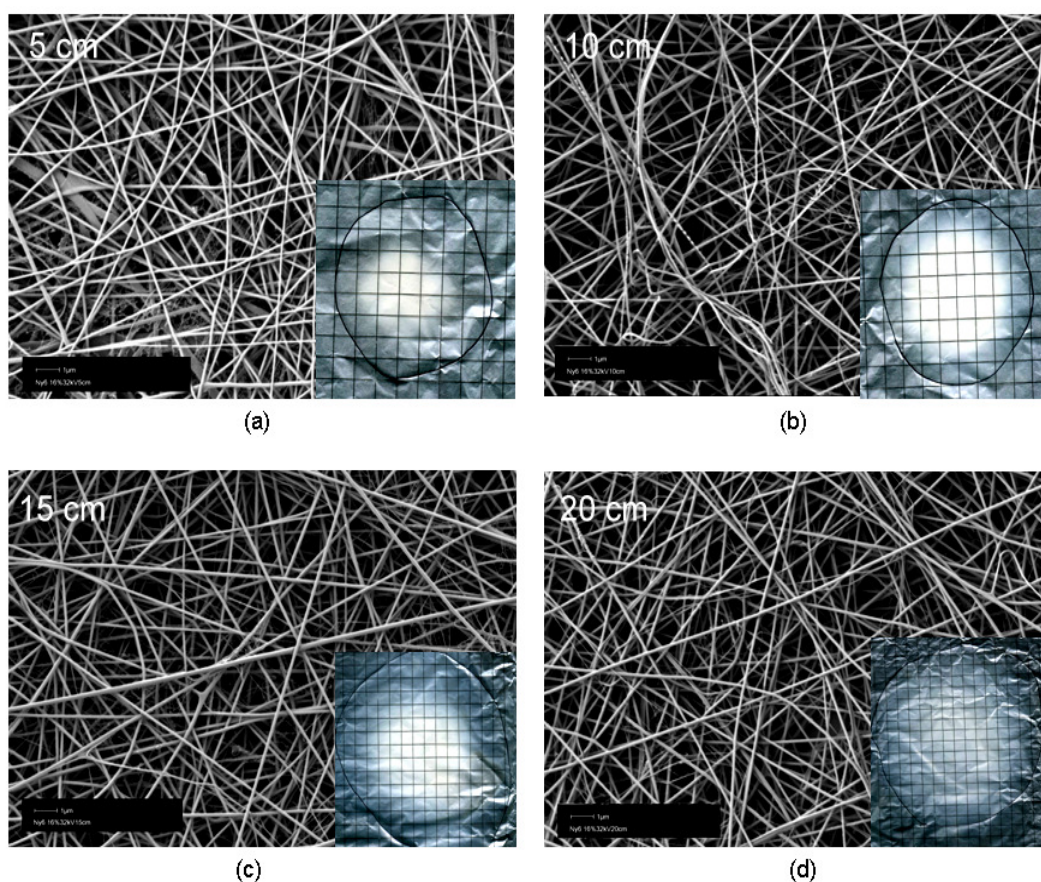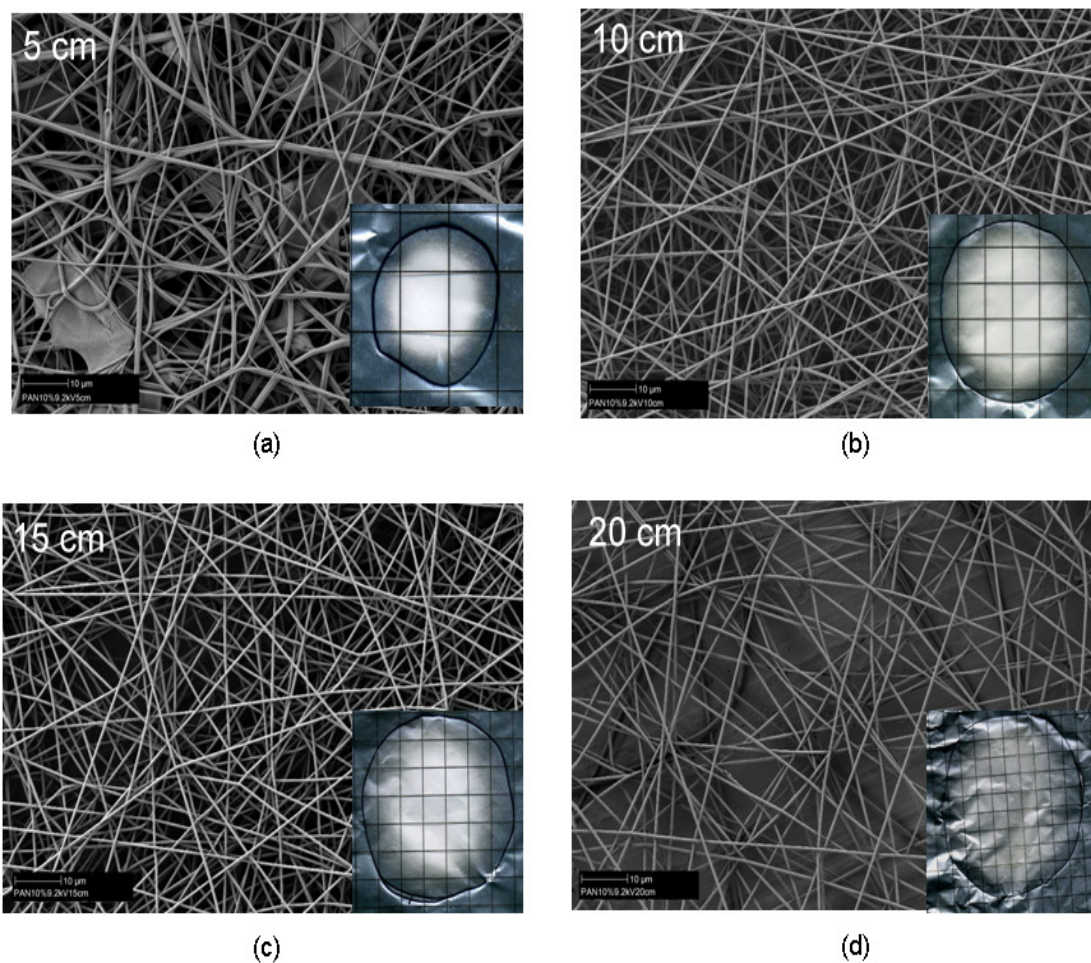
Figure 5-25: Typical SEM images of electrospun PAN at different needle tip-to-collector distance. a) 5cm, b) 10cm, c) 15cm and d) 20cm. For SEM images (a-d), the inset represents membrane coverage areas at different needle tip-to-collector distance. Electrospinning voltage and concentration were 9 kV and 10 %wt, respectively, for PAN in dimethyl formamide (DMF).

5.4 Copolymer Polyvinylidene Fluoride-Hexafluoropropylene (copolymer PVDF)

The optimal electrospinning conditions for hydrophilic polymers such as Nylon 6 and PVA and hydrophobic PAN have been identified (Sections 5.1-5.3). In this section, the behaviour of the second hydrophobic polymer, copolymer PVDF was investigated with respect to its propensity to produce electrospun fibre membranes.

5.4.1 Effect of concentration on viscosity

Figure 5-26 illustrates the effect of concentration on solution viscosity. The viscosity was observed to increase from 3 to 378 cPs with an increase of concentration from 5 to 25 %wt. The behaviour is similar to those of the previous polymers.
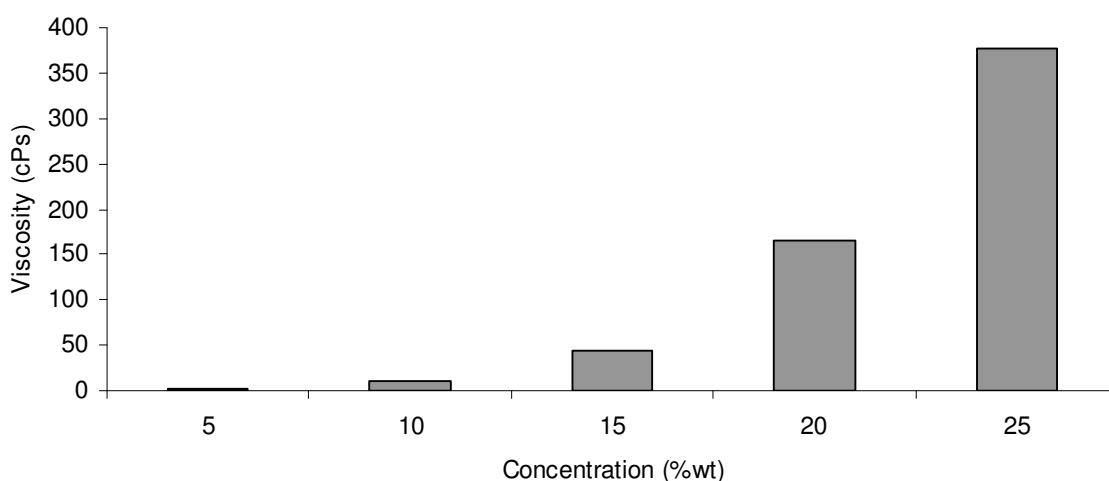
Figure 5-26: The effect of solution concentration on viscosity of copolymer PVDF in dimethyl acetamide (DMAc)/Acetone (2/1). Values represent the average of 5 measurements for each concentration. Error bars were neglected due to the low standard deviation.

5.4.2 Effect of concentration on fibre and membrane morphologies

The formation of electrospun copolymer PVDF varied depending on the concentration used. As shown in Figures 5-27 (a-b), an increase in concentration from 5 to 25 %wt resulted in larger fibre diameters with smaller coverage area. Similar findings were also observed by recent studies (*66*). It was found that the average fibre diameter of electrospun copolymer PVDF increased with increasing the solution concentration (*66*).
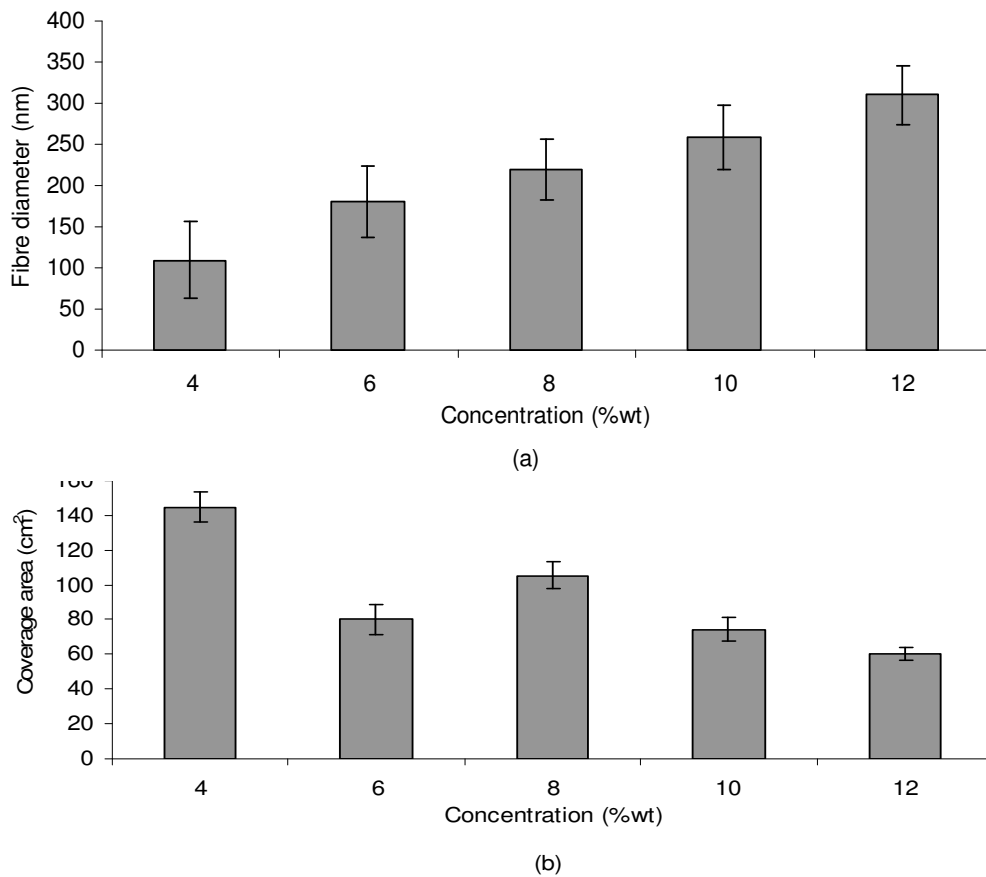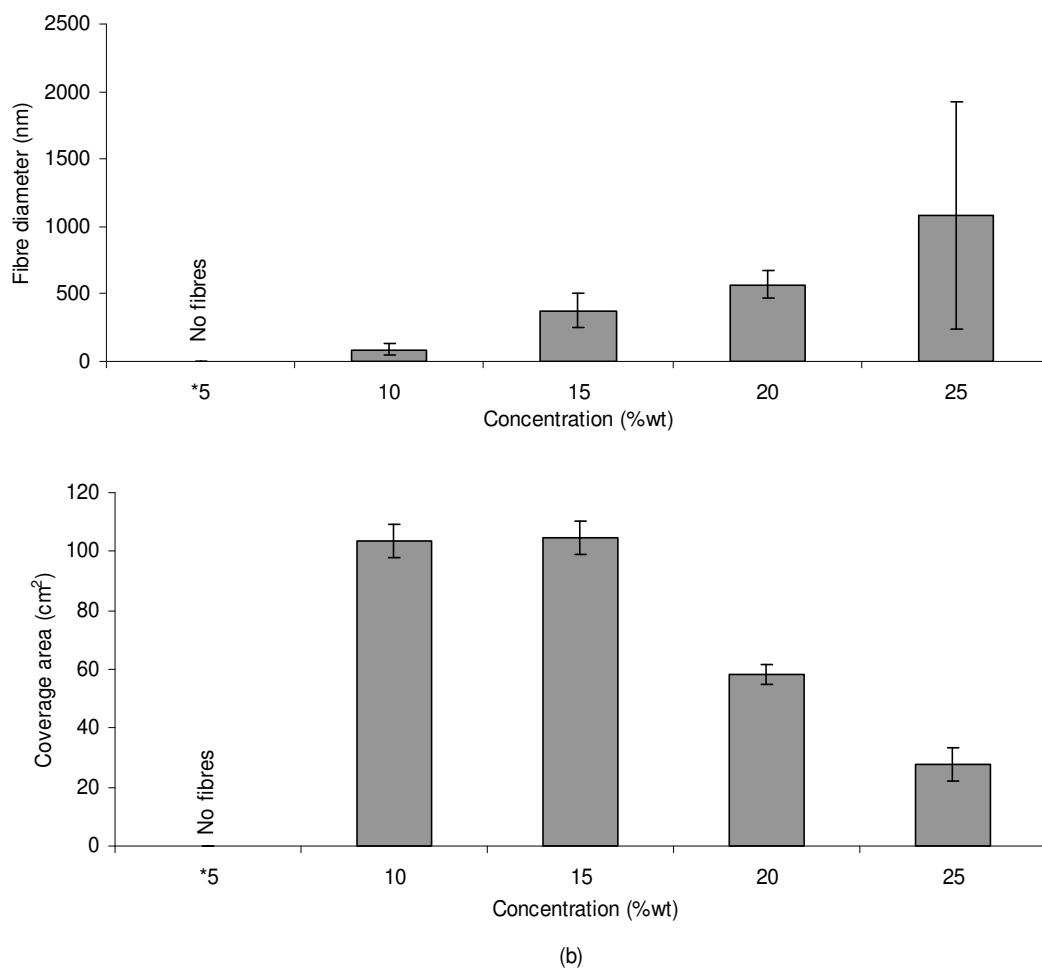
Figure 5-27: Typical plots of: a) concentration versus fibre diameter and b) concentration versus membrane coverage area. Values represent the average of 50 and 3 measurements for fibre diameter (excluding beads) and membrane coverage area, respectively. Electrospinning voltage and distance were 15 kV and 20 cm, respectively, for copolymer PVDF in dimethyl acetamide (DMAc)/Acetone (2/1).

*No fibres were observed.

Changing the solution concentration also resulted in the formation of different fibre morphologies. At 5 %wt concentration, droplets were produced instead of fibres due to its low viscosity of about 3 cPs. As described earlier in Section 5.1.2, a solution with lower viscosity has minimal chain overlap, which limits polymer chain entanglement in the solution. As a result, only droplets were deposited on the collector plate rather than fibres (Figure 5-28 (a)). In Figure 5-28 (a), the diameter of droplets was approximately 567 nm. As the concentration increased up to 10 %wt, a mixture of droplets and fibres were observed (Figure 5-28 (b)). This indicates that when the solution viscosity

increased, the solution was sufficiently viscous to prevent the break-up of the charged jet into droplets. The droplets were also bigger (approximately 1.6 µm) than the droplets at 5 %wt. This could be due to the increase of solution viscosity. In Figures 5-27 (a) and 5-28 (b), the average fibre diameter at 10 %wt was around 89 nm. At 15 %wt, only beaded fibres are observed (Figure 5-28 (c)). When the concentration increased up to 20 %wt, the solution viscosity increased to about 166 cPs. At this concentration, the copolymer PVDF in solution had greater chain entanglement, which resulted in uniform cylindrical fibres (Figure 5-28 (d)). In Figure 5-28 (e), the 25 %wt concentration was too viscose for electrospinning, which resulted in a mixture of coalesced fibres and branched fibres. The formation of coalesced fibres and branched fibres produced the smallest coverage area compared to other membranes at lower concentrations (Figure 5-27 (b)). A summary on the morphological structures of electrospun copolymer PVDF can be found in Appendix I.
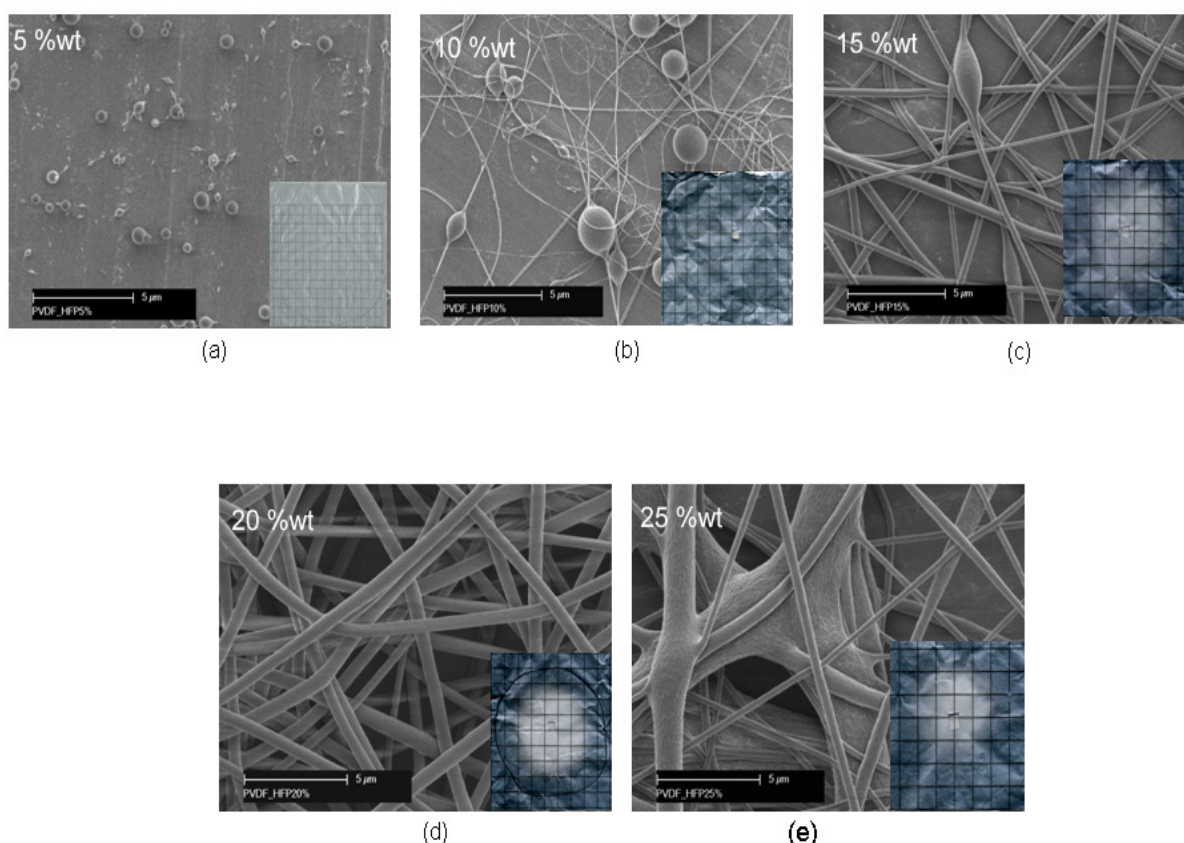
Figure 5-28: Typical SEM images of electrospun copolymer PVDF at different concentrations. a) 5 %wt, b) 10 %wt, c) 15 %wt, d) 20 %wt and e) 25 %wt. For SEM images (a-e), the inset represents membrane coverage areas at different concentrations. Electrospinning voltage and distance were 15 kV and 20 cm, respectively, for copolymer PVDF in dimethyl acetamide (DMAc)/Acetone (2/1).

From results presented in Figures 5-27 (a-b) and 5-28 (a-e), only 20 %wt concentration produced uniform cylindrical fibres. Hence, the optimal concentration for the subsequent electrospinning of copolymer PVDF solutions was 20 %wt.

5.4.3 Effect of applied voltage on fibre and membrane morphologies

Figure 5-29 (a) shows the effect of voltage on fibre diameter of copolymer PVDF. The electrospun copolymer PVDF showed a comparable fibre diameter over the voltages studied. It was expected that the formation of multiple jets during electrospinning could produce a comparable fibre diameter for electrospun copolymer PVDF.

(a)

(b)
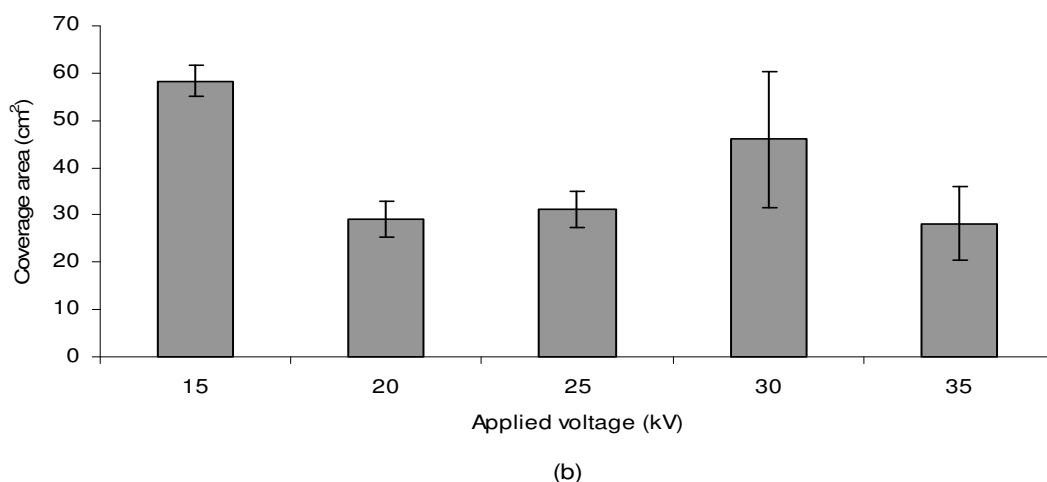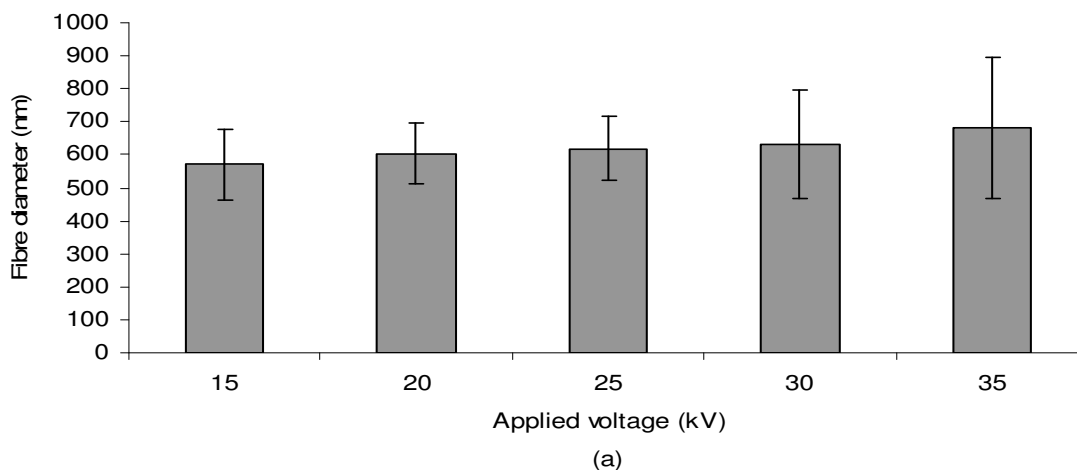
Figure 5-29: Typical plots of: a) applied voltage versus fibre diameter and b) applied voltage versus membrane coverage area. Values represent the average of 50 and 3 measurements for fibre diameter and membrane coverage area, respectively. Solution concentration and distance were 20 %wt and 20 cm, respectively, for copolymer PVDF in dimethyl acetamide (DMAc)/Acetone (2/1).

In addition, the increase of voltages resulted in a reduction of coverage area for electrospun copolymer PVDF (Figure (5-29 (b)). This could be due to the unstable charged jet at the higher voltage.

In Figures 5-30 (a-c), applied voltages below 25 kV formed uniform cylindrical fibres as well as a uniform membrane. When the applied voltage increased above 30 kV, the copolymer PVDF jets became unstable. This resulted in poor membrane uniformity and larger fibre diameters (5-30 (d)). At 35 kV, coalesced fibres were observed, indicating poor solvent evaporation of the DMAc/acetone mix (Figure 5-30 (e)).
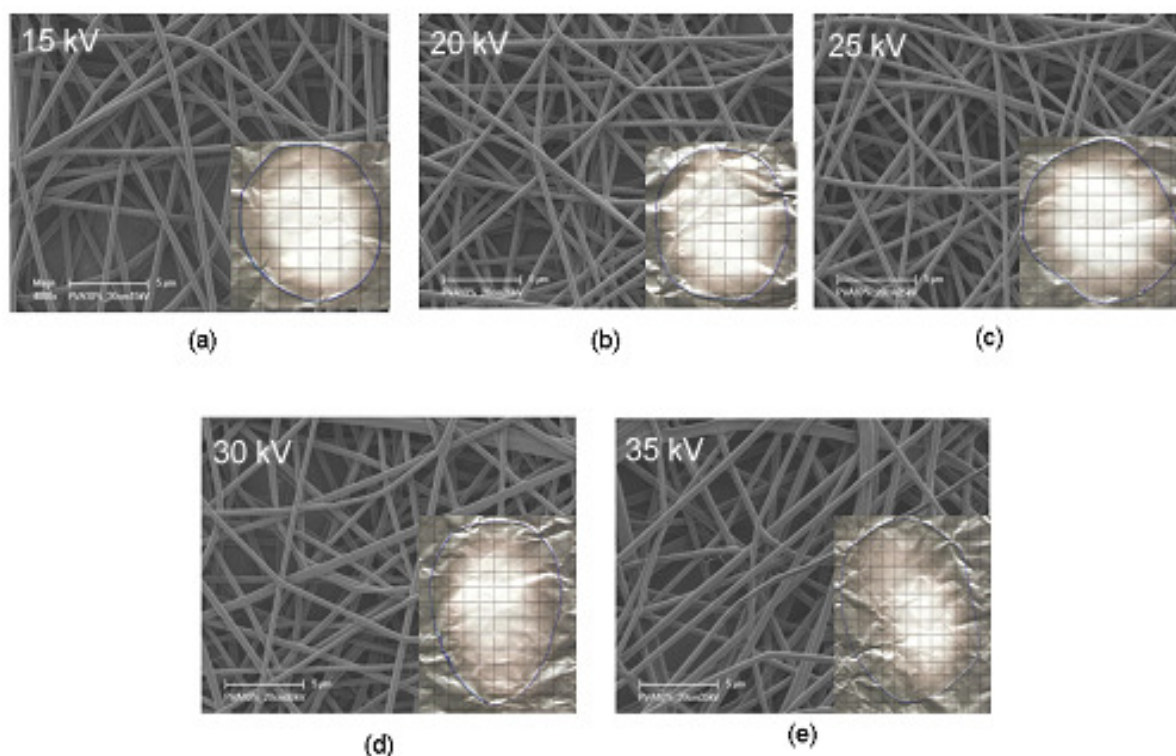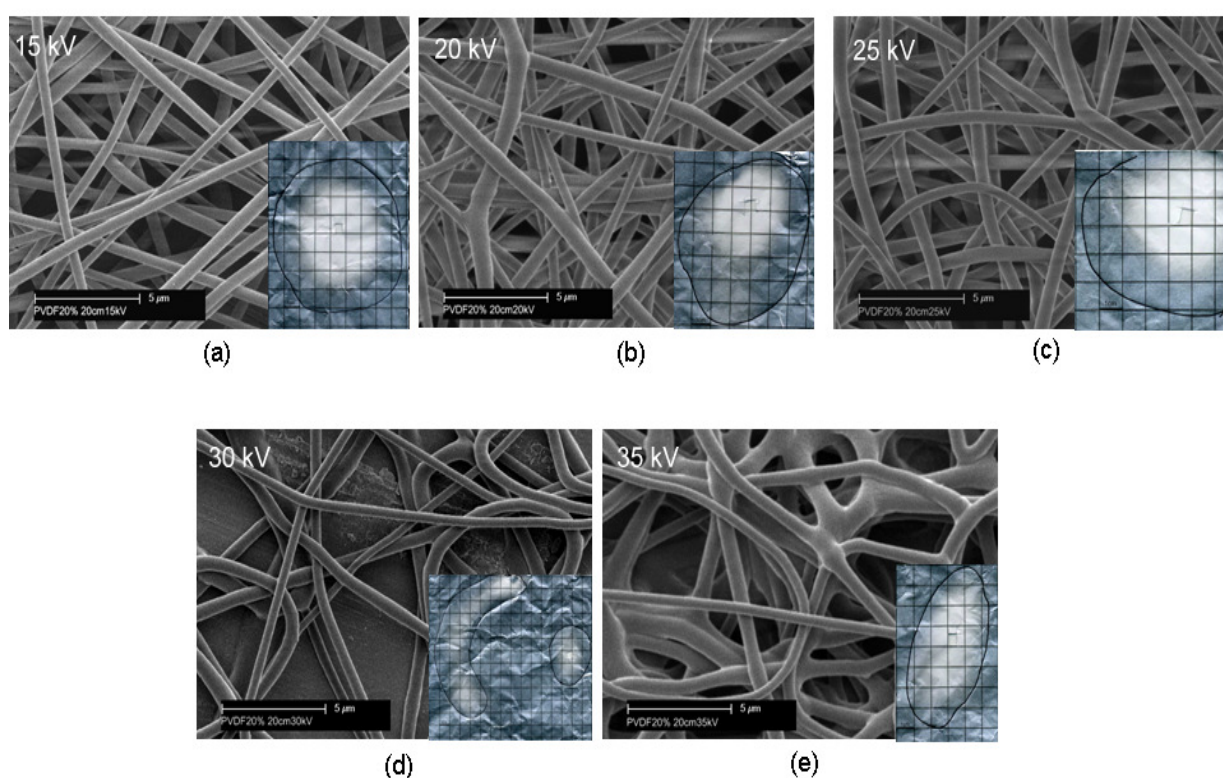

Figure 5-30: Typical SEM images of electrospun copolymer PVDF at different voltages. a) 15 kV, b) 20 kV, c) 25 kV, d) 30 kV and e) 35 kV. For SEM images (a-e), the inset represents membrane coverage areas at different applied voltages. Electrospinning distance and concentration were 20 cm and 20 %wt, respectively, for copolymer PVDF in dimethyl acetamide (DMAc)/Acetone (2/1).

Results presented in Figures 5-29 (a-b) and 5-30 (a-e) indicate that uniform cylindrical fibres with a large coverage area occurred at 15 kV. Hence 15 kV was chosen as an optimal applied voltage for copolymer PVDF solution in subsequent experiments.

5.4.4 Effect of needle tip-to-collector distance on fibre and membrane morphologies

The needle tip-to-collector distance also affected the resultant fibre diameter and coverage area of the electrospun copolymer PVDF (Figures 5-31 (a-b)). A reduction in fibre diameter was observed (from 2.6 µm to 570 nm) when the electrospinning distance increased from 5 cm to 20 cm. At 5 cm and 10 cm, membranes with wet fibres and non-uniform structures were observed (Figures 5-32 (a-b)), indicating poor solvent evaporation of the DMAc/acetone mix at shorter distances (less than 10 cm).
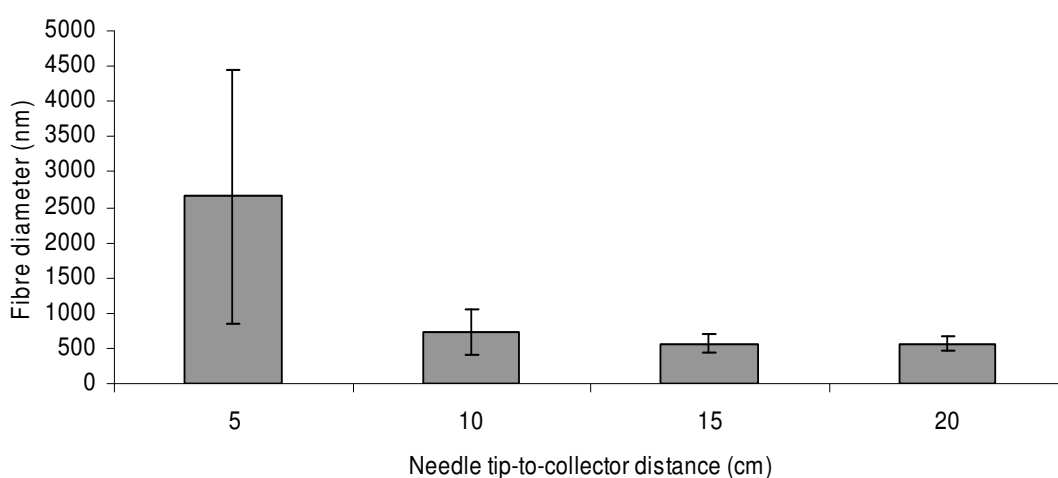
(a)
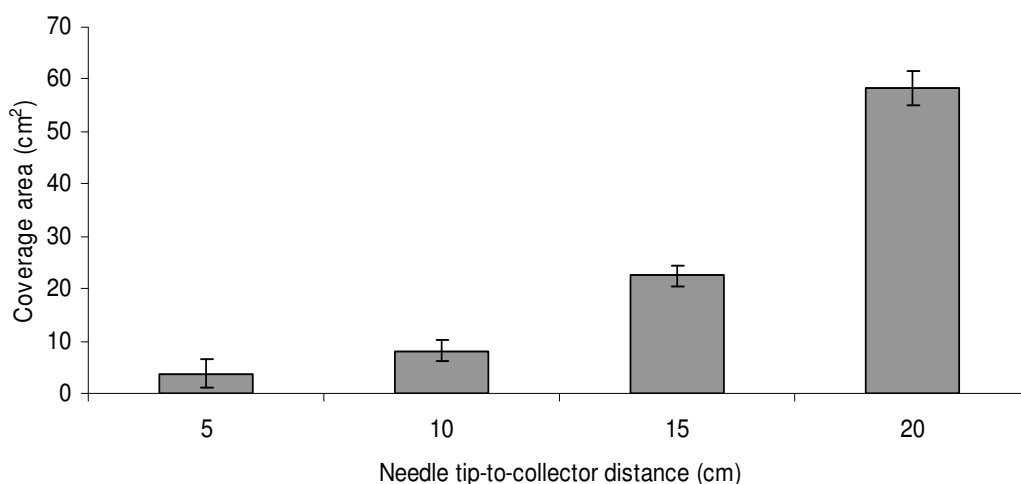
(b)

Figure 5-31: Typical plots of: a) needle tip-to-collector distance versus fibre diameter and b) needle tip-to-collector distance versus membrane coverage area. Values represent the average of 50 and 3 for fibre diameter and membrane coverage area, respectively. Solution concentration and applied voltage were 20 %wt and 15 kV, respectively, for copolymer PVDF in dimethyl acetamide (DMAc)/Acetone (2/1).

As the distance increased up to 15 cm, some cylindrical fibres were fused to the adjacent fibres (Figure 5-32 (c)). At 20 cm, the solvent had sufficient flight time to evaporate which resulted in fibres with fine diameters and uniform cylindrical shapes, shown in Figure 5-32 (d). At the longer distances (at 15 to 20 cm), the bending instabilities of the jets were expected to increase, thus forming larger coverage areas compared to the shorter distances (Figure 5-31 (b)).
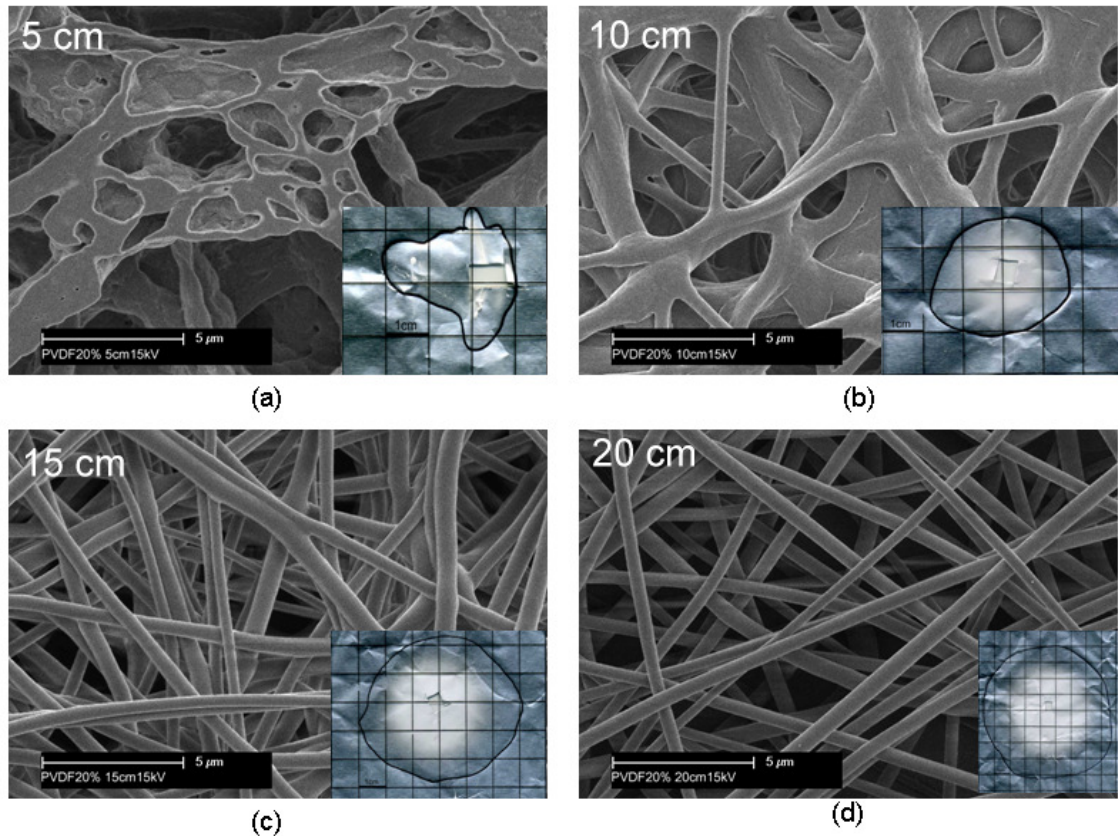
Figure 5-32: Typical SEM images of electrospun copolymer PVDF at different needle tip-to-collector distance. a) 5 cm, b) 10 cm, c) 15 cm and d) 20c m. For SEM images (a-d), the inset represents membrane coverage areas at different needle tip-to-collector distances. Electrospinning voltage and concentration were 15 kV and 20 %wt, respectively, for copolymer PVDF in dimethyl acetamide (DMAc)/Acetone (2/1).

In Figures 5-31 (a-b) and 5-32 (a-d), 20 cm was selected as the optimal distance for electrospun copolymer PVDF because it forms uniform cylindrical fibres and large coverage area as compared to other electrospinning distances.

5.5 Optimal Conditions for Electrospun Nylon 6, PVA, PAN and copolymer PVDF

Results presented in Sections 5.1 to 5.4 showed that the average fibre diameter of hydrophilic electrospun Nylon 6 and PVA and hydrophobic electrospun PAN and copolymer PVDF increased with increasing concentration. The increase of fibre diameter was also observed to reduce the coverage area of all polymers tested.

The current study also found that the effects of applied voltage on the fibre diameter and membrane coverage area were different depending on the polymer used. The increased of voltage was found to increase the fibre diameters for electrospun Nylon 6, whereas fibre diameter was largely unaffected in the case of PVA, PAN and copolymer PVDF. There are different opinions explaining the effects of applied voltage on fibre diameter (*41, 46, 63, 106-109*). Some studies reported that the increase of applied voltage increased the resultant average fibre diameter for electrospun ethyl-cyanoethyl cellulose, polyethylene oxide (PEO), poly (D,L-lactic acid) and poly(L-lactic acid) (PLLA). Other studies reported that the increase of applied voltage reduced the average fibre diameter of electrospun acrylic and polystyrene (*39, 51, 58, 104-105*). Tan *et al.* (*54*) observed that the effect of applied voltage on electrospun poly(L-lactid acid) P(LLA) fibre diameter was insignificant. The increased of voltage was also observed to form larger coverage area for electrospun Nylon 6, PVA and PAN membranes. For electrospun copolymer PVDF membrane, the increase of voltages resulted in a reduction of coverage area of the membrane.

All the polymers tested showed similar results on the effects of needle tip-to-collector distance on fibre diameter and membrane coverage area. The increased of needle tip-to-collector distance reduced the average fibre diameter of electrospun Nylon 6, PVA, PAN and copolymer PVDF. At longer distance, all the polymers tested produced larger coverage area.

Based on results in Sections 5.1 to 5.4, the optimal conditions for electrospun Nylon 6, PVA, PAN and copolymer PVDF are summarized in Table 5-1. The conditions particularly concentrations and applied voltages, were different depending on polymers used. A distance of 20 cm was found to give an optimal electrospinning distance for all polymers tested because the polymer jets had sufficient flight time to evaporate which resulted in uniform cylindrical fibres

and larger whipping to produce a large coverage area with uniform membrane structures. The coverage areas of electrospun Nylon 6, PVA, PAN and copolymer PVDF membranes varied from 58 to 240 cm^2.

Table 5-1: Optimum electrospinning conditions

Polymer	Solvent	Dielectric constant for solvent at 25°C (*112*)	Concentration (%)	Voltage (kV)	Fibre diameter (nm)	Coverage area (cm^2)
Nylon 6	Formic acid	58.5	16	32	109 $\pm$ 16	240 $\pm$ 8
PVA	Deionised water	78.5	10	25	259 $\pm$ 39	74 $\pm$ 7
PAN/	Dimethyl formamide (DMF)	36.7	10	9	677 $\pm$ 205	141 $\pm$ 17
Copolymer PVDF	Dimethyl acetamide (DMAc)/	37.8	20	15	570 $\pm$ 105	58 $\pm$ 3
	Acetone (2/1)	20.7				
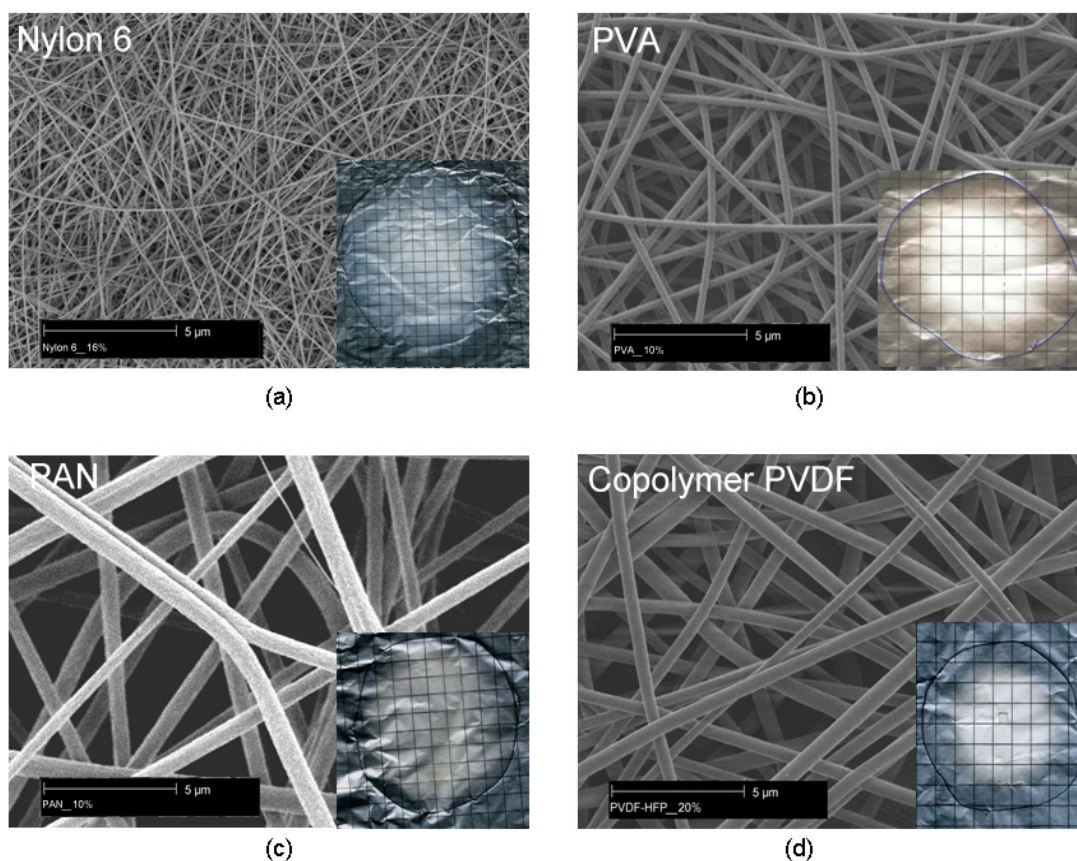
Figure 5-33: Typical SEM images of the optimal electrospun nanofibres. For SEM images (a-d), the inset represents coverage area of electrospun membranes for, a) Nylon 6, b) PVA, c) PAN and d) copolymer PVDF.

Table 5-1 and Figures 5-33 (a-d) also show that the hydrophilic electrospun membranes of Nylon 6 and PVA exhibit smaller average fibre diameter compared to the hydrophobic polymer membranes of copolymer PVDF and PAN. This could be due to the dielectric constants of solvents used in the study. Son *et al.* (*209*) reported that solvents with higher dielectric constants produced finer fibre diameter than solvents with lower dielectric constants. The dielectric constant indicated the polarity of solvent. Solvents with higher dielectric constants were expected to have a greater net charge density in solution. When the charges carried by the jets increased, higher elongation forces were imposed on the jets at that electrical field strength. As a result, smaller diameters for electrospun fibres were obtained (*209*). In the current study, solvents for Nylon 6, PVA and PAN were formic acid, deionised water and *N,N*-dimethlyformamide (DMF), respectively. The dielectric constants for the solvents at 25°C were 58.5 (formic acid), 78.5 (water) and 36.7 (DMF) (*112, 210*). For copolymer PVDF, a mixture of *N,N*-dimethylacetamide (DMAc) and acetone was used to dissolve the polymer. The dielectric constant for the mixture was unknown. However, the dielectric constants for DMAc and acetone at 25°C were 37.8 and 20.7, respectively (*210*). Solvents with higher dielectric constants such as formic acid and water could have greater net charge density for the Nylon 6 and PVA solutions. This resulted in greater elongation of the Nylon 6 and PVA jets during electrospinning. The elongation of those jets produced finer fibre diameters for electrospun Nylon 6 and PVA compared to the electrospun PAN and copolymer PVDF fibres.

In addition, the membrane morphologies were expected to affect the physical properties of the membrane such as thickness, surface area and roughness, surface wettability (water contact angle) and pore size. These membranes were also tested for chemical structure in order to identify any changes in the chemical structures of polymers during the electrospinning.

5.6 Membrane Thickness and Pore size

5.6.1 Membrane thickness measured by a non- destructive white light profilometry

A micrometer is a fast and easy instrument to measure thicknesses of materials such as electrospun membranes. However, it requires direct contact with the membrane which involves applying a force on the membrane surface to determine the thickness. This is particularly a problem for soft electrospun membranes with open architecture, which may result in significant membrane compression. Hence, a non contact method had found to measure membrane thickness. White light profilometry fitted the criteria and the technique was used to measure thickness. As mentioned in Chapter 4, a flat glass slide was used as a zero point or base in order to differentiate between the electrospun membrane surface and the flat base. A large vertical step change from the glass surface is equivalent to the thickness of the electrospun membrane. A comparative study was then performed between the white light profilometry technique and measurements with a micrometer. The results are tabulated in Table 5-2.

Table 5-2: The thicknesses, fibre diameter and range of pore sizes for electrospun Nylon 6, PVA, PAN and copolymer PVDF. The membrane thicknesses were measured by white light profilometry and a digital micrometer.

Electrospun membrane	Fabrication period (hour)	Fibre diameter (nm)	Range of pore sizes (µm)	Thickness (µm)	
				White light profilometry	Digital micrometer
Nylon 6	22	109 $\pm$ 16	0.13-0.41	40 $\pm$ 3	30 $\pm$ 6
PVA	22	259 $\pm$ 39	0.47-1.74	42 $\pm$ 6	33 $\pm$ 3
PAN	14	677 $\pm$205	0.5-3.65	51 $\pm$ 6	35 $\pm$ 9
Copolymer PVDF	26	570 $\pm$105	0.67-3.03	45 $\pm$ 9	34 $\pm$ 3
*Glass slide	-	-	-	1100 $\pm$ 1	1100 $\pm$ 1

* Control

Table 5-2 demonstrated that the micrometer gave lower values for all membranes tested when compared to the values obtained from the white light profilometry method. The different in value between the white light profilometry and micrometer for the electrospun Nylon 6, PVA, PAN and copolymer PVDF were approximately 10, 9, 16 and 11 µm respectively. The results indicated that

the membranes were compressed by the micrometer. Figures 5-34 (a-b) illustrate small region of an electrospun membrane before and after measurement with a micrometer. The raised edges of the electrospun membrane were not used because the membrane structure was distorted while the sample was transferred from its backing aluminium foil to glass slide.

An indentation is clearly observed where the micrometer measurement was taken. This indentation depth confirmed that the micrometer reduce the thickness of the electrospun nanofibre membranes. In Figure 5-34 (b), the indentation depth is approximately 16 µm.

These results indicated that a non-contact method such as white light profilometry can be used successfully to measure the thickness of easily compressed electrospun membranes. A number of advantages were observed using this technique,

1. The non-destructive white light profilometry was able to scan over the electrospun membrane surfaces without damaging the membrane structures. Thus, the membrane can be reused for other measurements.

2. This technique does not compress a sample and therefore it is more suitable for spongy materials with open pore structures.

3. White light profilometry can measure electrospun thicknesses in the nanometer range (down to 50 nm), which is beyond the limit of a micrometer. The minimum measurement of the micrometer is approximately 4 µm.
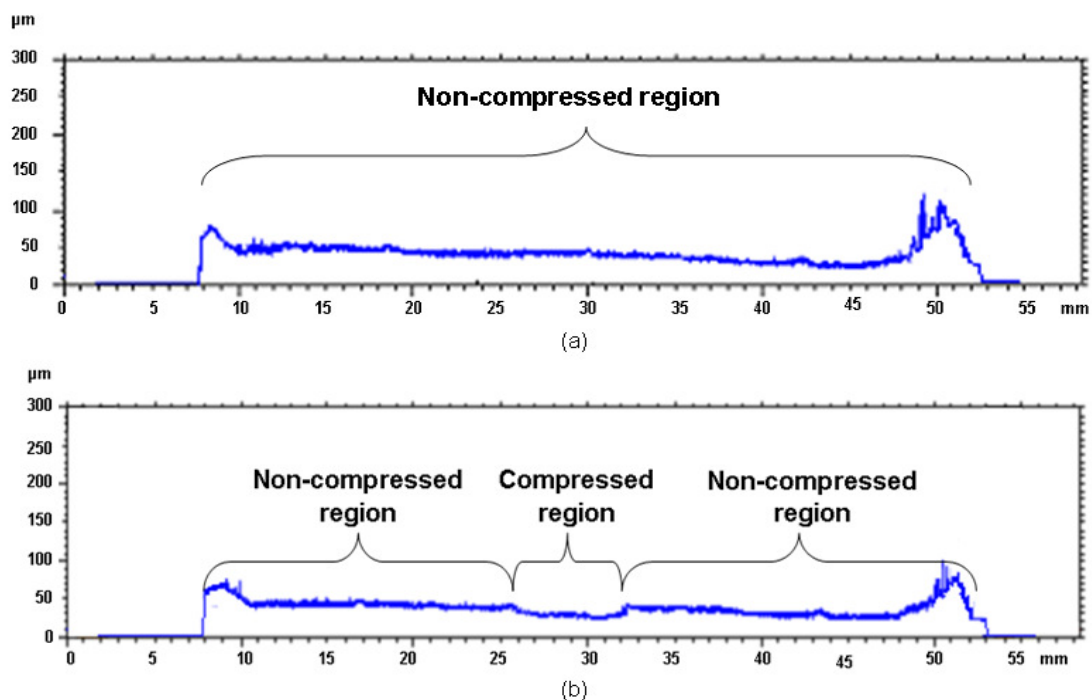
Figure 5-34: A typical profile obtained from white light profilometry for electrospun membrane, a) before and b) after measurement with a micrometer.

In Table 5-2, the fabrication times for electrospun Nylon 6, PVA, PAN and copolymer PVDF are different in order to form comparable thicknesses for all the electrospun membranes. However, the membrane thicknesses were relatively uncontrollable using electrospinning. Hence, the membrane thicknesses as measured by the white light profilometry varied in a range of 40 to 51 µm. These membranes were then tested for surface roughness, surface wettability (water contact angle) and chemical structures.

5.6.2   Membrane pore size

As shown in Table 5-2, membranes with finer fibre diameters such as electrospun Nylon 6 and PVA exhibited smaller pore sizes, whereas membranes with bigger fibre diameters such as electrospun PAN and copolymer PVDF exhibited larger pore sizes. In addition, electrospun PAN and copolymer PVDF membranes demonstrated broader range of pore sizes than the electrospun Nylon 6 and PVA membranes. This could be to the high variability of PAN and copolymer PVDF fibre diameters as compared to Nylon 6 and PVA.

Apart from the fibre diameter, membrane density could affect the membrane pore sizes. The accumulation of random oriented fibres could form a non uniform membrane density. The non uniform membrane density will affect

the pore sizes of the membrane. The membrane density and pore sizes can be controlled by controlling the orientation of fibres onto collector. However, this work is beyond the scope of the current study and should be investigated in prospective studies.

Table 5-2 also showed that membranes with finer fibre diameters and smaller pore sizes such as electrospun Nylon 6 and PVA membranes required longer electrospinning times in order to obtain the same thickness membrane. For membranes with larger fibre diameters and pore sizes such as electrospun PAN required shorter electrospinning times to produce a membrane of the same thickness. Although the electrospun copolymer PVDF membrane exhibited larger fibre diameters and pore sizes, the membrane was slower to spin as compared to other electrospun membranes. This is probably because the concentration of copolymer PVDF solution was considerably higher (approximately 20 %wt) compared to the other polymer solutions. The solution concentrations for Nylon 6, PVA and PAN were 16 %wt, 10 %wt and 10 %wt, respectively.

5.7 Determination of Surface Topography

Figures 5-35 (a-d) illustrate the surface roughness of the electrospun membranes as measured by the white light profilometry. Electrospun Nylon 6 membrane was found to exhibit the lowest surface roughness, followed by the electrospun PVA, copolymer PVDF and PAN membranes. Membranes with finer fibre diameters and pore sizes such as Nylon and PVA (as shown earlier in Table 5-2) were presumably to give lower surface roughness as compared to those with bigger fibre diameters and pore sizes such as PAN and copolymer PVDF.
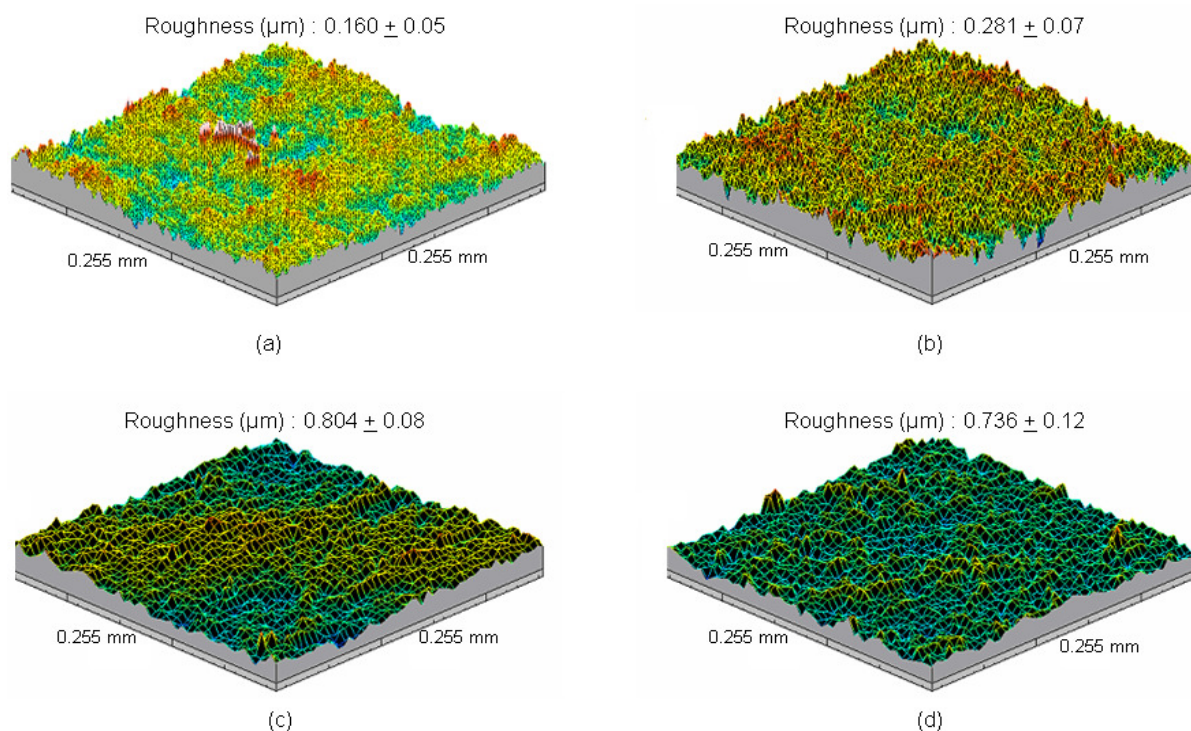
Figure 5-35: Typical area of 3D surface roughness measured by white light profilometry for electrospun nanofibre membranes. a) Nylon 6 b) PVA c) PAN and d) copolymer PVDF.

For membrane surface areas (BET (Brunauer, Emmet, and Teller) surface area), electrospun Nylon 6 and PVA exhibited higher surface areas than the copolymer PVDF. In Figure 5-36, the surface area for electrospun Nylon 6, PVA and copolymer PVDF are 25, 14 and 3 m^2g, respectively. It was expected that the finer fibre diameters of electrospun Nylon 6 and PVA gave higher BET surface areas compared to the bigger fibre diameters of copolymer PVDF membrane.
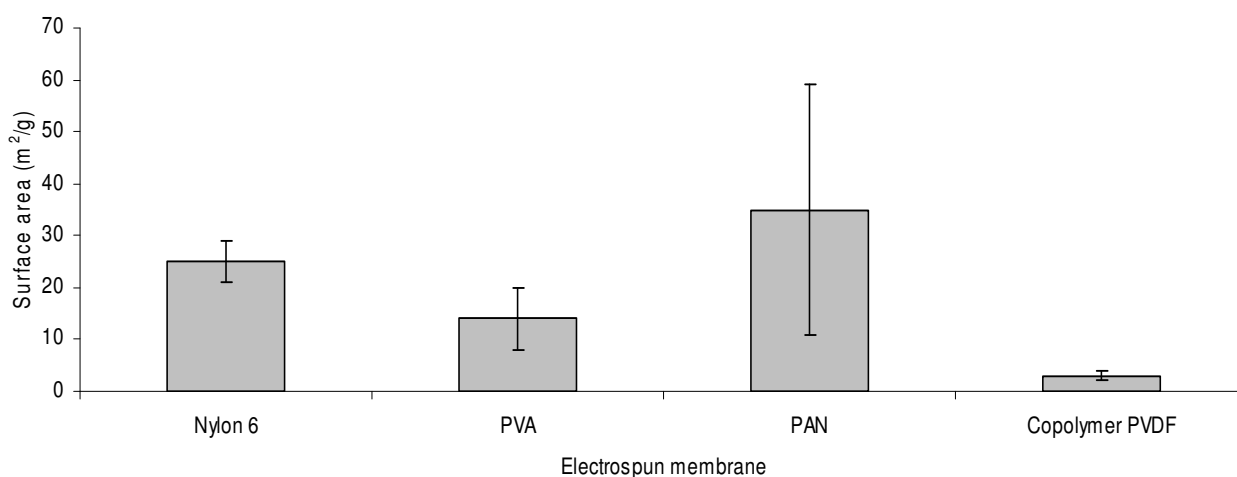
Figure 5-36: BET surface areas for the four electrospun membranes

PAN with the largest fibre diameter, however exhibited the highest BET surface area (approximately 35 m^2/g) as compared to other membranes. Further examination of membrane structure using scanning electron microscopy (SEM) was carried out in order to understand this observation. SEM analysis indicated wrinkle structures on the PAN fibre surface (Figure 5-37 (a)). The presence of the wrinkle structures was found to increase the BET surface area of PAN. The formation of wrinkle structure was also observed in recent studies for electrospun PAN and Polystyrene (*208, 211-212*). They reported that the formation of wrinkle structure was likely due to the buckling instability of the skinned charged jets. Solvent evaporation led to the formation of the skin on the outer surface of the polymer jets. As the solvent evaporated from the core of the jets, the core pulled radically inward, resulting in a wrinkle structure on the outer surface of the jets (*208, 211-212*). In addition, a large variation in BET surface area was observed for electrospun PAN membrane. A possible reason of this was due to a high variation in fibre diameter (677 $\pm$205 nm). The high variation in fibre diameter forms non-uniform wrinkle structures on the fibre surfaces.

For the other electrospun membranes such as Nylon 6, PVA and copolymer PVDF, no such wrinkle structures only smooth surfaces were observed on the fibre surface (Figures 5-37 (b-d)).
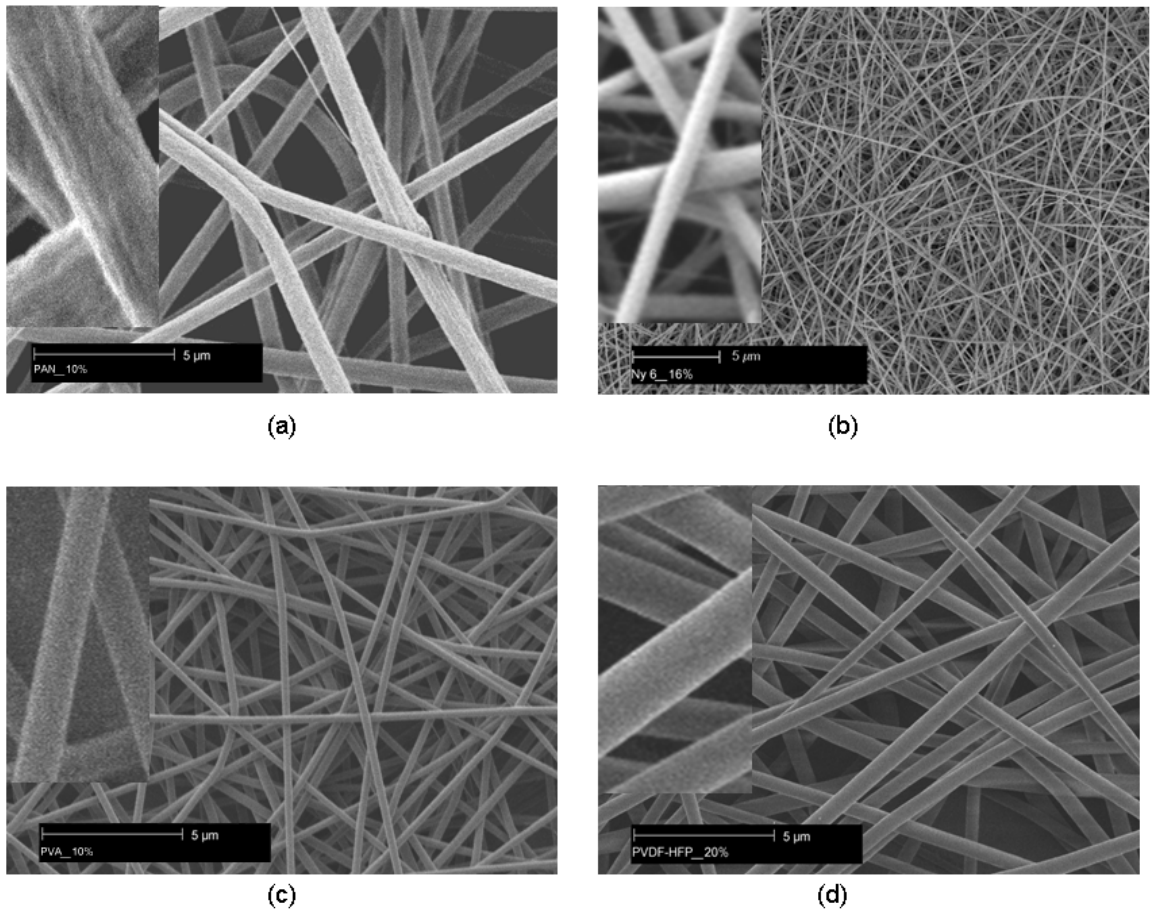
Figure 5-37: SEM images of typical: a) wrinkle structures on electrospun PAN, smooth structures on b) electrospun Nylon 6, c) electrospun PVA and d) electrospun copolymer PVDF.

5.8 FTIR analysis of electrospun membranes, cast films and bulk polymers.

Figure 5-38 (a) illustrates the FT-IR spectra of Nylon 6 polymers from a bulk polymer, cast film and electrospun membrane. Although the spectra were similar, there were some differences in detail. The differences were observed in the region 650 to 1500 cm^{-1} (Figure 5-38 (a)). A possible reason could be due to the changes in crystal structure of polymers after electrospinning compared to the bulk polymer and cast film. Recent study reported that Nylon 6 has two common crystalline forms, α- and γ-crystal phases (*213*). The authors reported that the α-crystal phases appeared at various peaks such as 1413, 1039 and 927 cm^{-1} and the vibration types of those peaks were CH$_2$ scissors, CH$_2$ twist-wag and CO-NH, respectively. For γ-crystal phases, the peaks can be appeared at 1000 and 975 cm^{-1} (CO-NH) (*213*). In the current study, the Nylon 6 bulk polymer and cast film showed peaks at 1413 and 927 cm^{-1}, indicating the α-crystal phases (Figure 5-38 (a)). When electrospinning the same solution used for the cast film, the electrospun membrane showed γ-crystal phases with the peak at 975 cm^{-1} (Figure 5-38 (a)). However, peak at 1000 cm^{-1} was not observed for electrospun membrane. A possible reason of this is due the orientation of polymer chains upon crystallization of electrospun Nylon 6 fibres. Raghavendra *et al.* (*214*) reported that the polymer chains orientation was influenced by several factors such as melt temperature, draw force and stress force on melts (*214*). In the current study, the orientation of polymer chains (Nylon 6) was influenced by rapid evaporation of solvent from the electrospun fibres. As reported by previous study, the polymer chains orientation of their sample was influenced by heat and rapid cooling using liquid nitrogen (*213*). This shows that the electrospun Nylon 6 nanofibres have different chains orientation as compared to Nylon 6 used in the previous study. Due to the differences, peak at 1000 cm^{-1} did not appear in the IR spectra for electrospun Nylon 6. In addition, the formation of γ-crystal for electrospun Nylon 6 nanofibres was observed by Liu *et al.* (*137*).
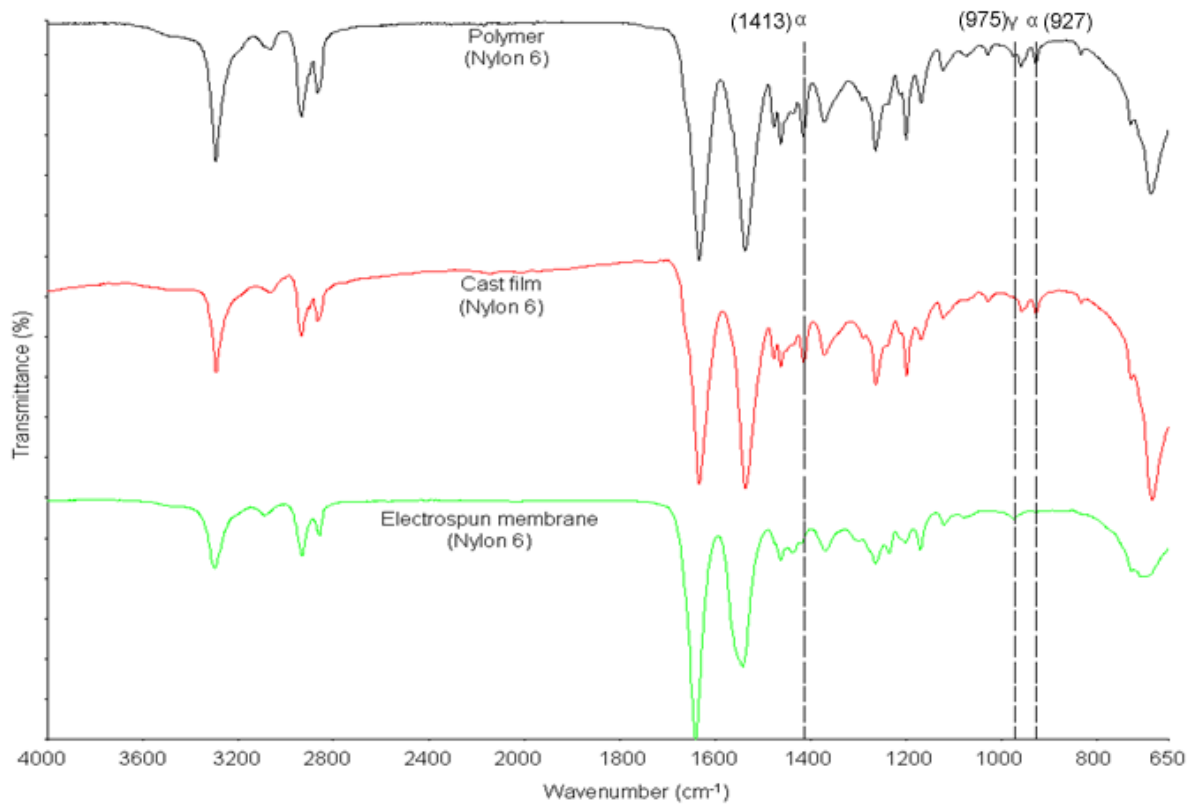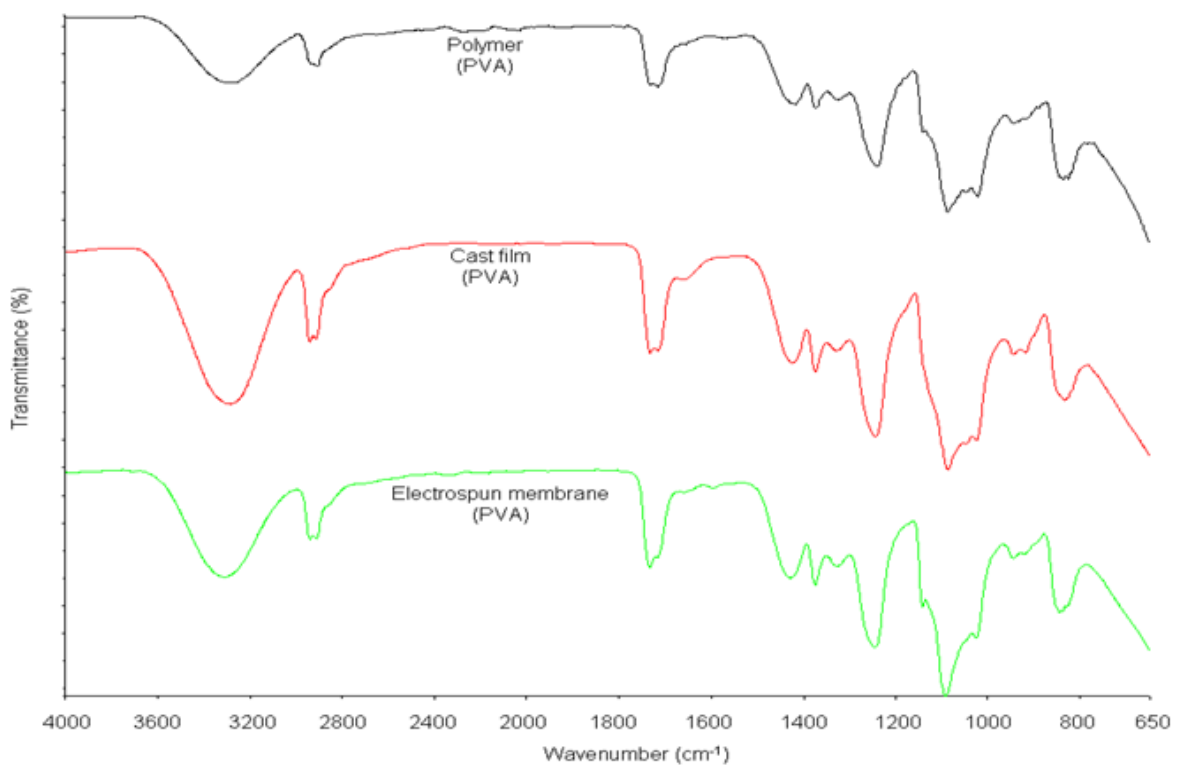
Figure 5-38: FT-IR spectra for polymers, cast films and electrospun nanofibre membranes. a)

Nylon 6, and b) PVA
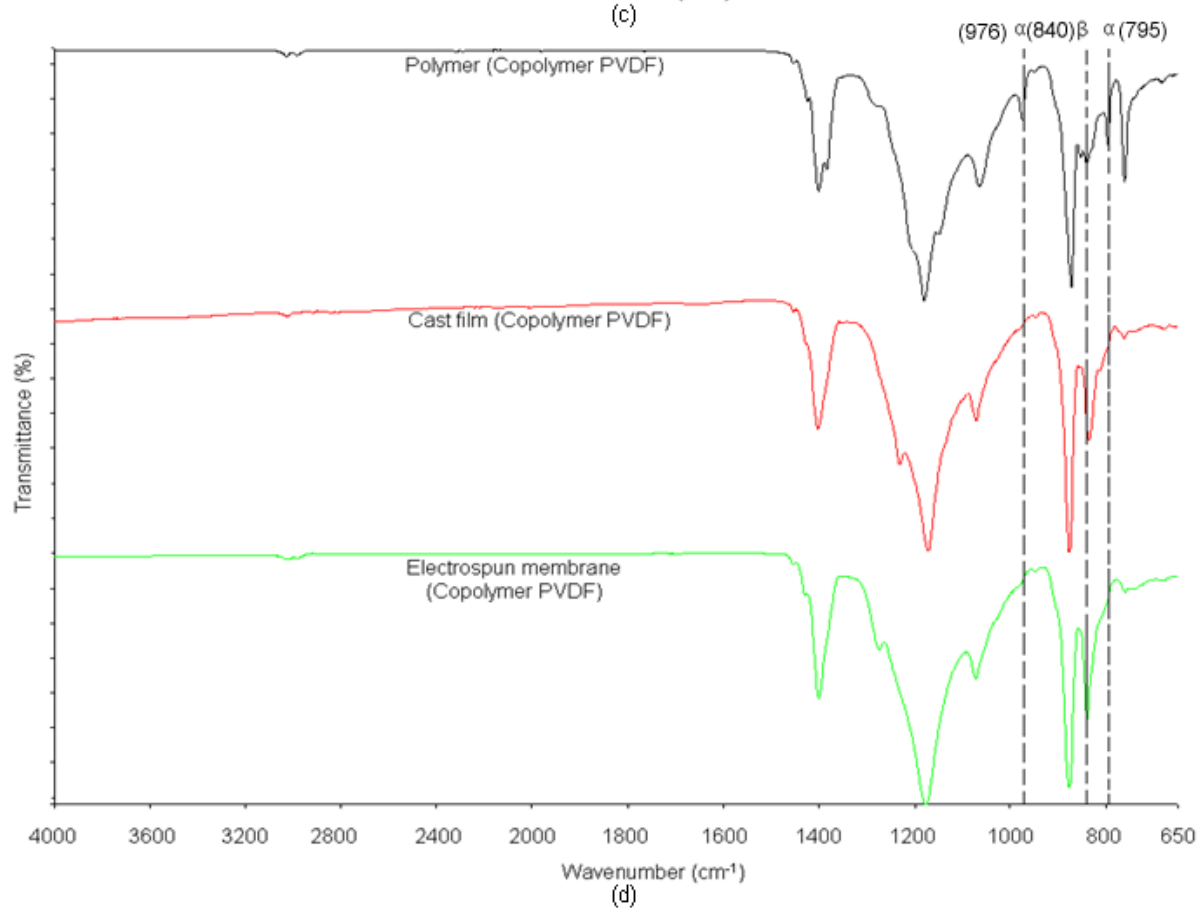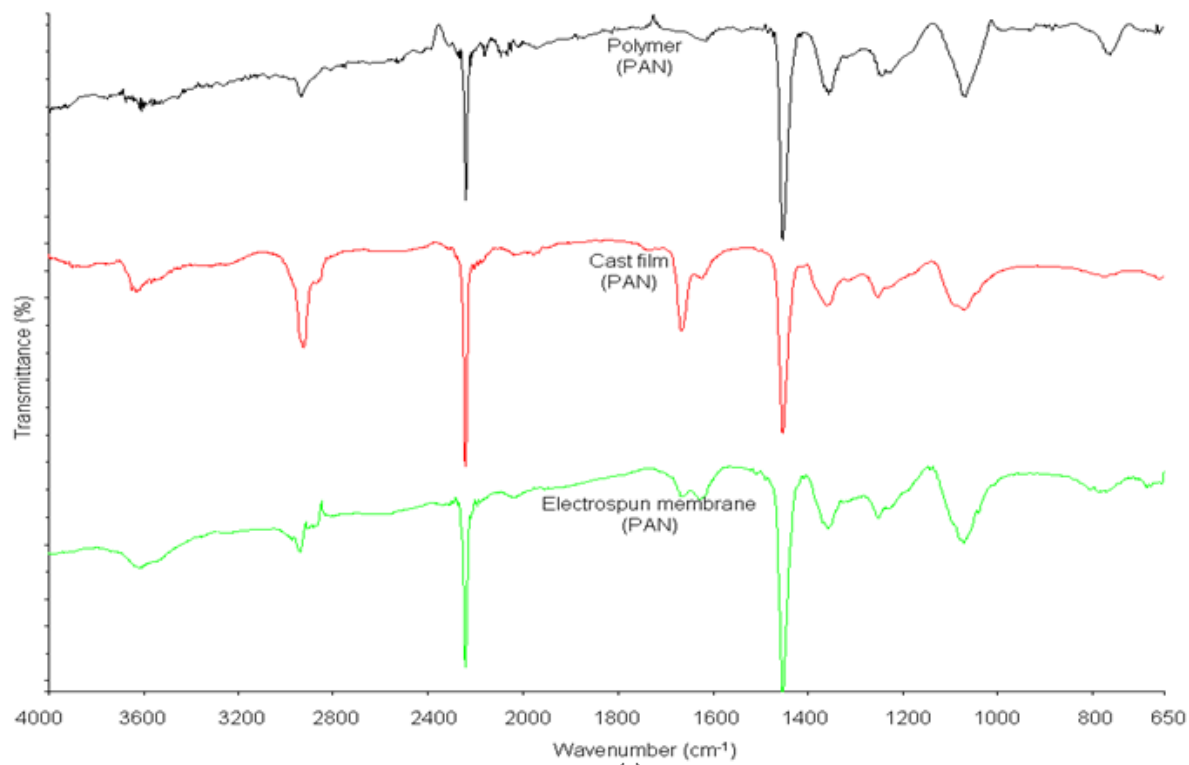
Figure 5-38: FT-IR spectra for polymers, cast films and electrospun nanofibre membranes. c) PAN and d) copolymer PVDF.

In Figure 5-38 (b), the FTIR spectra of PVA bulk polymer, cast film and electrospun PVA membranes are slightly different in region 1000 to 1200 cm^{-1}. Possible reasons of the differences are due to two factors: 1) changes in polymer chain orientation and 2) the presence of residual solvent for PVA cast film and electropsun PVA. When the bulk PVA is dissolved and prepared for cast film and electrospun membrane, the polymer would undergo different arrangement of polymer chains. For electrospun PVA fibres, the orientation of polymer chains is based on a rapid evaporation of solvent (water) from the PVA fibres. For PVA cast film, the polymer chains orientation is dependent on drying at room temperature. Due to the differences, the bulk PVA, cast film and electrospun PVA exhibited different IR spectra. In addition, the presence of residual solvent (water) in the PVA cast film and electrospun PVA could also contribute to the difference in the IR spectra.

For PAN, the FTIR spectra for the bulk polymer, cast film and electrospun membrane were observed to be slightly different from 1600 to 3000 cm^{-1} (Figure 5-38 (c)). It was expected that the orientation of polymer chains and the presence of residual solvent (dimethyl formamide) in the samples influenced the difference in the spectra.

The peaks detected for copolymer PVDF polymer, cast film and electrospun membrane were slightly different from 650 to 1380 cm^{-1} (Figure 5-38 (d)). A number of studies reported that, peak changes in the IR spectra indicate different crystal phases for electrospun PVDF fibres (*63, 215-216*). They reported that peaks at 613, 795 and 976 cm^{-1} were associated with the α - crystal phases of PVDF. The peaks at 613, 795 and 976 cm^{-1} were due to CF$_2$ bending and skeletal bending, CH$_2$ rocking and CF-out-of plane deformation, respectively. For β - crystal phase, the peaks appeared at 1279 (CF-out-of plane deformation), 840 (CH$_2$ rocking), 510 cm^{-1} (CF$_2$ bending), etc (*63, 215-216*). In the current study, the bulk polymer of copolymer PVDF exhibited a mixture of α - crystal with peaks 795 and 976 cm^{-1} and β -crystal at 840 cm^{-1}. For cast film and electrospun membranes β -crystal phase was observed at 840 cm^{-1}. The formation of β - crystal phases for cast film and electrospun membranes could be due to a number of factors: 1) dissolving copolymer PVDF in solvent(s) at room temperature and 2) electrospinning process. Similar results were also found by

recent studies (*63, 217*). Gregorio Jr. *et al.* (*217*) observed that the β-crystal of PVDF was obtained after diluting PVDF polymer in *N,N*-dimethyl acetamide (DMAc) at temperature below 70°C. Nasir *et al.* (*63*) reported that electrospinning limited the development of the crystal phase of electrospun PVDF nanofibres, which resulted in the formation of β-crystal phases for the fibres.

Further experiments using the wide angle X-ray diffraction (WAXD) were also carried out in order to confirm changes in crystal phases for bulk polymers, cast films and electrospun membranes of Nylon 6 and copolymer PVDF.

5.9 Wide angle X-ray diffraction analysis of electrospun membranes, cast films and bulk polymers.

From the FTIR results (Sections 5.8), it was found that there were changes in crystal phases from bulk polymers to electrospun membranes for Nylon 6 and copolymer PVDF. To confirm these results, a wide angle X-ray diffraction (WAXD) test was carried out of the bulk polymer, cast film and electrospun membrane. Figures 5-39 (a-d) show the diffraction peaks and *d*-spacing of polymers, cast films and electrospun membranes for Nylon 6, PVA, PAN and copolymer PVDF.

In Figure 5-39 (a), two strong diffraction peaks were observed for Nylon 6 bulk polymer and cast film, whereas one peak was observed for electrospun Nylon 6. The Nylon 6 bulk polymer exhibited diffraction peaks at 20.5° and 24.2°, and the cast film had diffraction peaks at 20.5° and 24.4°. Electrospun Nylon 6 membrane only showed a peak at 21.7°. Recent studies reported that the α-crystal of Nylon 6 at room temperature appeared at approximately 21° and 24° and were indexed as the 200 and 002/202 planes, respectively. In the γ-phase, the peaks appeared at 22° and 23° and were indexed as 001 and 200/201 planes, respectively (*137, 218*). The α-crystal phase has a monoclinic structure and the hydrogen bonds are formed between anti-parallel chains (*218*). For the γ-crystal phase, the hydrogen bonding direction is about 60° from the original hydrogen bonding direction of the α-crystal phase. This forms a hexagonal or pseudo-hexagonal packing (*137*).   Based on these results in recent studies, the current study demonstrated the α-crystal phases for Nylon 6 bulk polymer and cast film, whereas electrospun Nylon 6 membrane showed γ-crystal structure. The α-crystal phases of Nylon 6 polymer and cast film, as well as γ-crystal of electrospun Nylon 6 were also observed in the IR spectra of Nylon 6 (Section 5.8). In Figure 5-39 (a), electrospun Nylon 6 membranes show broader and lower intensities as compared to Nylon 6 polymers and cast films. Liu *et al.* (*137*) reported that a broad peak of electrospun Nylon 6 indicated the semi-crystalline structure of the membrane. A rapid solidification of polymer jets retarded the development of crystallinity of the electrospun Nylon 6 (*137*).
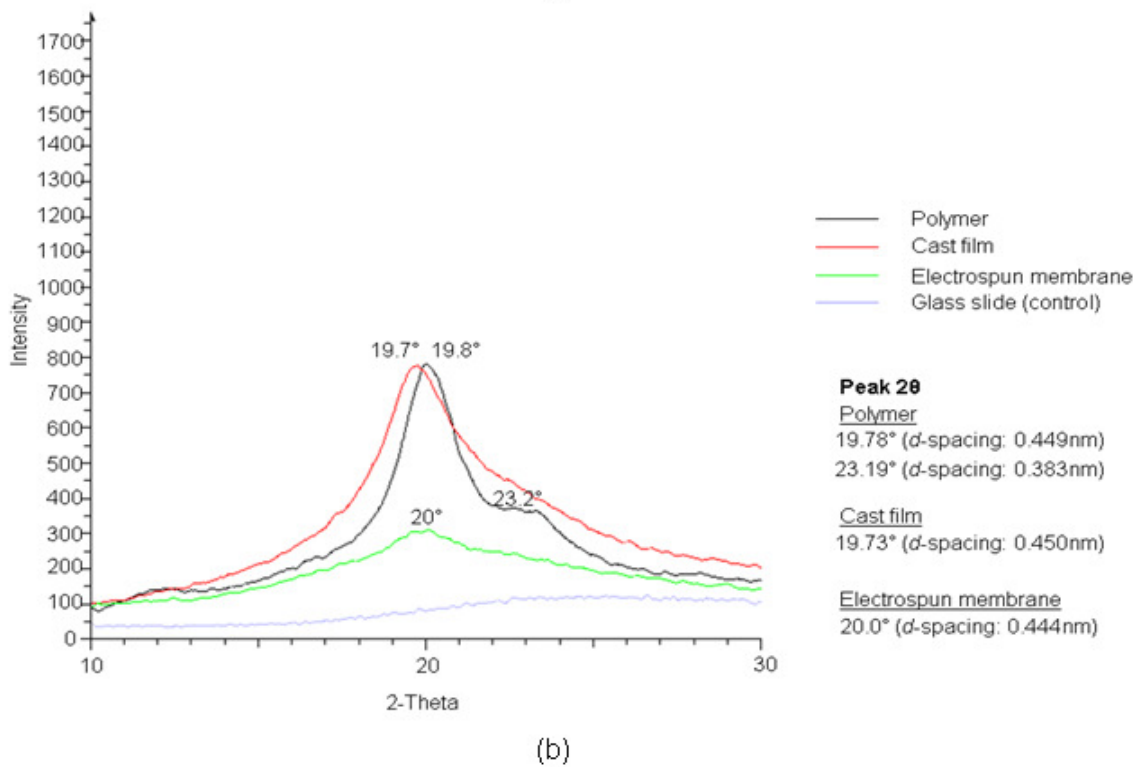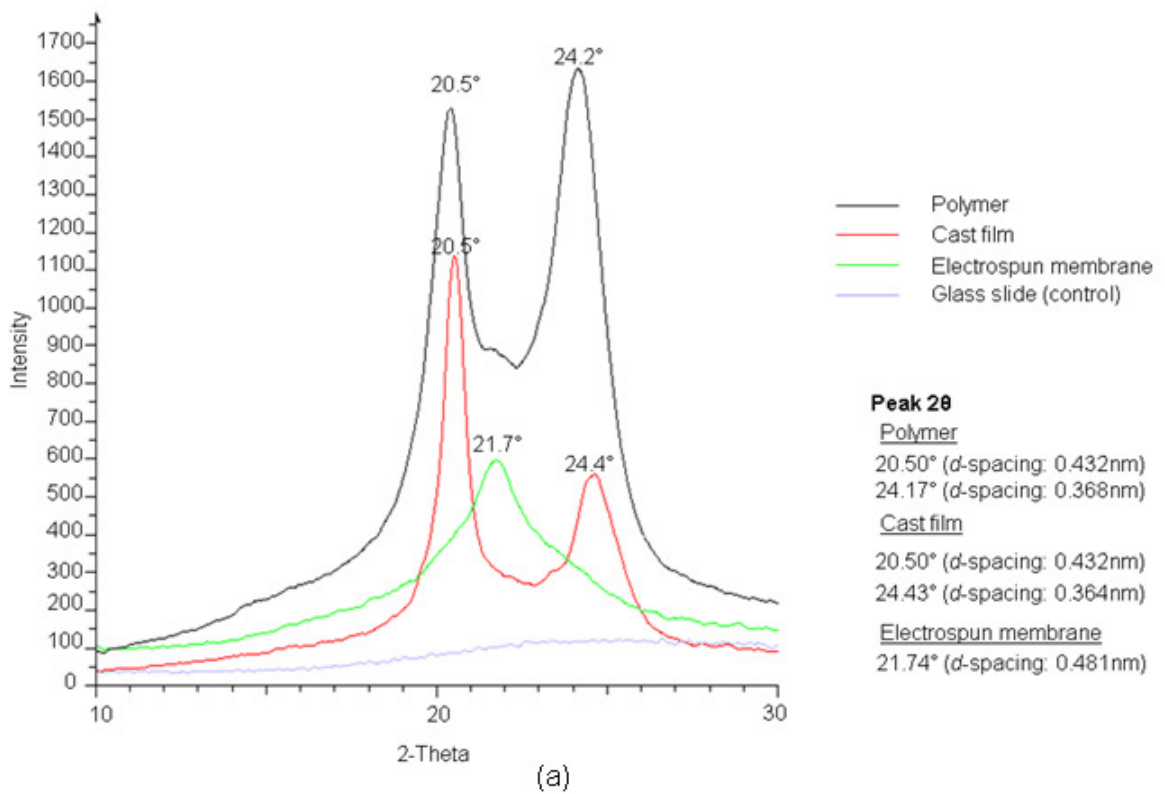
Figure 5-39: X-ray diffraction patterns for single layer electrospun membranes. a) Nylon 6 and b) PVA.
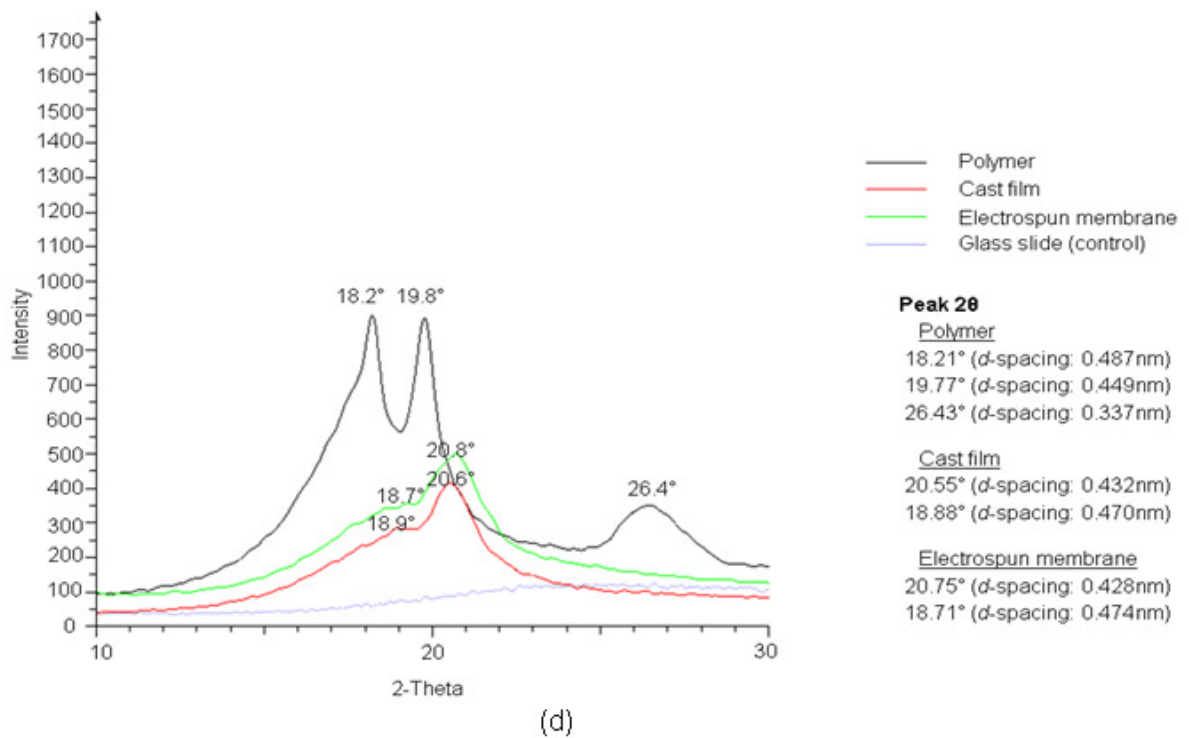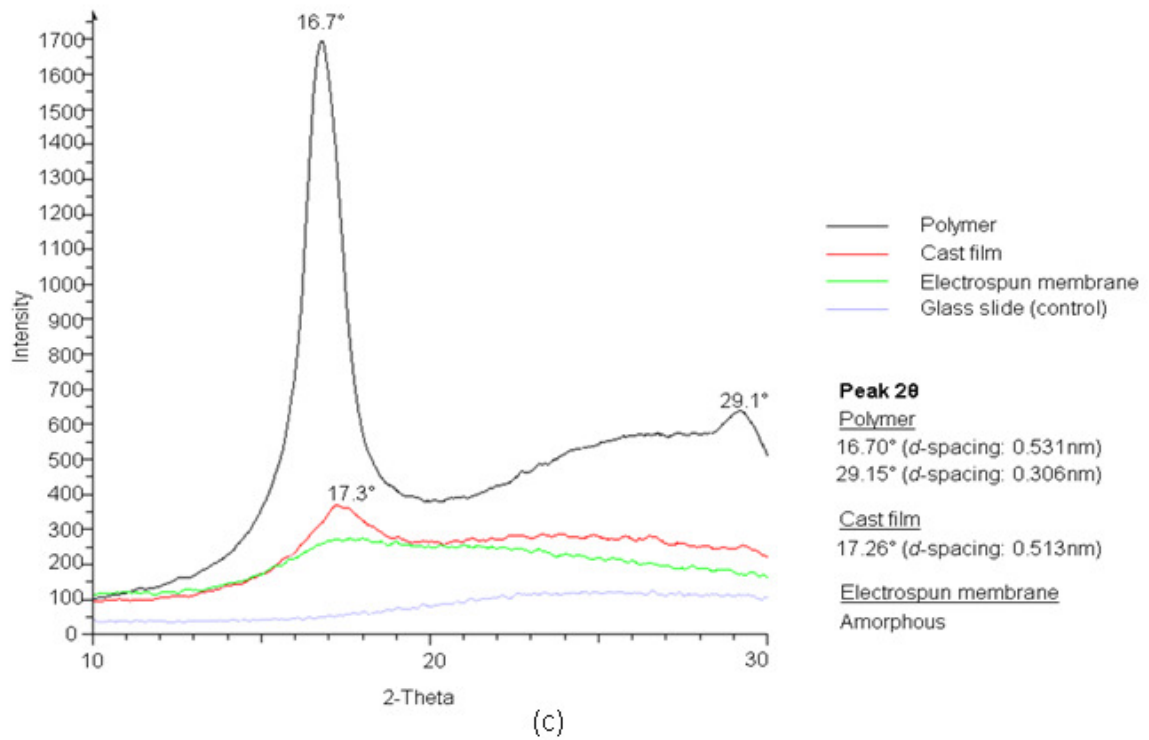
Figure 5-39: X-ray diffraction patterns for single layer electrospun membranes. c) PAN and copolymer PVDF

For PVA, the bulk polymer showed a strong diffraction peak at 19.8° and a shoulder peak at 23.2° (Figure 5-39 (b)). For cast film the diffraction peak was observed at 19.7°. A broad diffraction peak at 20.0° was also found for electrospun PVA membrane. As with electrospun Nylon 6, a rapid solidification of PVA jets limited the development of crystallinity in the electrospun PVA. This could result in semi-crystalline electrospun PVA membrane. The semi-crystalline nature of electrospun PVA membrane was also reported by Shao *et al.* (*219*), where they found a single peak of electrospun PVA membrane at 20.0° and the peak was indexed as the 101 plane.

In Figure 5-39 (c), the PAN bulk polymer shows two diffraction peaks at 16.7° and 29.1°. The PAN cast film exhibits broad diffraction at 17.3°. For electrospun PAN, no diffraction peak was observed, indicating that the electrospun PAN membranes were fully amorphous.

Three diffraction peaks were observed for copolymer PVDF bulk polymer. In Figure 5-39 (d), the bulk polymer exhibited strong diffraction peaks at 18.2°, 19.8° and 26.4°. For cast film, a strong diffraction peak was observed at 20.6° and a shoulder peak was observed at 18.9°. Similar to cast film, electrospun copolymer PVDF exhibited a strong diffraction peak at 20.8° and a shoulder peak at 18.7°. Recent studies reported that the diffraction peaks of the α - crystal structure were approximately 18° and 27° and were indexed as the 020 and 111 planes, respectively (*215, 220*). The β-crystal phases were found at 20.0° and 21.0°, and were indexed as the 200/110 planes. The β-crystal phases involved in different chain conformations such as planar zigzag, leads to an orthorhombic cell for the β-phase. Monoclinic form the α-crystal phases (*215*). Based upon their results, the bulk polymer for copolymer PVDF exhibited a mixture of α - and β - crystal phases with diffraction peaks of 18.2° (α - phase $\approx 18°$) and 19.8° (β - phase $\approx 20°$). The cast film and electrospun copolymer PVDF had β-crystal phases, where both film and electrospun membrane showed a peak at 20.8° (β - phase $\approx 21°$) These results were confirmed by the FTIR analysis, as shown in Section 5.8.

5.10 Determination of Surface Wettability

Electrospun membranes with different fibre diameters, surface roughness and surface chemistry were found to give different surface wettability. As shown in Table 5-3, the electrospun Nylon 6 and PVA membranes give water contact angles below 90º. Within 5 seconds, complete wetting of the surface was observed on the hydrophilic electrospun Nylon 6 and PVA membrane surfaces as well as on their cast films. PVA gave lower water contact angle than the Nylon 6 because the water droplet was directly spread over the PVA membrane surfaces after the droplet was applied.

Table 5-3: Characterization of electrospun membranes and polymer cast films.

Sample type	Contact angle at 5 seconds (º)	Surface roughness (µm)	Average of fibre diameter (nm)
Electrospun nanofibrous membrane			
Nylon 6	42 ± 6	0.16 ± 0.05	109 ± 16
PVA	17 ± 3	0.28 ± 0.07	259 ± 39
PAN	129 ± 6	0.80 ± 0.08	677 ± 205
PVDF-HFP	135 ± 6	0.74 ± 0.12	570 ± 105
Cast film			
Nylon 6	44 ± 5	0.09*	NA
PVA	15 ± 6	0.08*	NA
PAN	55 ± 3	0.07*	NA
PVDF-HFP	126 ± 3	0.10*	NA

* Standard deviations were neglected due to the low values.

Poor wettability was observed for hydrophobic copolymer PVDF polymer. In Table 5-3, the electrospun copolymer PVDF membranes and cast film showed water contact angle exceeding 90º. Copolymer PVDF, with the functional group of $-CF_2$, was found to prevent water droplets from penetrating the membrane surfaces. This resulted in a high water contact angle for electrospun copolymer PVDF membrane and cast film. Within 5 seconds, the water contact angles of electrospun copolymer PVDF membrane and film were 135º and 126º, respectively. This result also shows that the difference in contact angles between electrospun copolymer PVDF and cast film is minimal.

In the case of electrospun PAN, it was expected that the surface roughness exhibited a higher water contact angle for the membrane. In Table 5-3, the water contact angle for electrospun PAN is approximately 129°, whereas the PAN cast

film exhibited a water contact angle lower than 90º. This can be explained due to the formation of wrinkle structures on the PAN fibre surface (see Section 5.7). The most likely explanation can be found in a recent publication by Quéré and Reyssat (*172*), where they described the importance of micro-textures such as the lotus leaf effect and man-made synthetic etching in enhancing the chemical hydrophobicity. In the current study, the nano-texture of the PAN wrinkle structures increased its apparent membrane roughness. The increase in membrane roughness was found to give the higher water contact angles compared to a smooth surface of PAN film.

For electrospun Nylon 6 and PVA membranes, the effect of surface roughness on water contact angle was comparable to the cast films. This indicates that the membrane surface roughness has minimal effect on the contact angle for electrospun Nylon 6 and PVA.

CHAPTER 6 FABRICATION AND CHARACTERISATION OF BI-LAYER ELECTROSPUN NANOFIBRE MEMBRANES

As described in Chapter 4, the bi-layer membranes were fabricated in two forms, which were homogeneous bi-layer membranes (membranes composed of two identical polymers) and heterogeneous bi-layer membranes (membranes composed of two different polymers such as hydrophobic and hydrophilic). These bi-layer membranes were characterized for membrane thickness and surface wettability. The infrared (IR) and wide angle X-ray diffraction (WAXD) tests were carried out to monitor the chemical structures and crystal phases of bi-layer membranes after electrospinning. The tensile properties and adhesion strength between layers were also measured in the current study. The study also investigated the feasibility of using these membranes as a filter to remove textile effluent from aqueous solutions.

6.1 Membrane Thickness

The non-contact technique of white light profilometry has been already shown to successfully measure the thickness of single layer electrospun membranes. The same technique was used to measure the thickness of homogeneous and heterogeneous bi-layer membranes. As with single layer membranes, the bi-layer membrane was peeled off from its backing aluminium and was then placed on the glass slide for measurement. White light profilometry was then used to scan across the glass slide and the membrane surfaces. The peeled thickness (µm) of homogeneous and heterogeneous bi-layer membranes were measured and tabulated in Table 6-1.

Table 6-1: The thicknesses of homogenous and heterogeneous bi-layer electrospun membranes as measured by white light profilometry.

Sample type	Fabrication period (hour)	Wetting properties	Total thickness (µm)
Bi-layer homogeneous			
Nylon 6 (upper layer)/	22	Hydrophilic	82 ± 6
Nylon 6 (bottom layer)	22	Hydrophilic	
PVA (upper layer)/	22	Hydrophilic	85 ± 6
PVA (bottom layer)	22	Hydrophilic	
PAN (upper layer)/	14	Hydrophobic	99 ± 6
PAN (bottom layer)	14	Hydrophobic	
Copolymer PVDF (upper layer)/	26	Hydrophobic	93 ± 7
Copolymer PVDF (bottom layer)	26	Hydrophobic	
Bi-layer heterogeneous			
PAN (upper layer)/	14	Hydrophobic	93 ± 4
Nylon 6 (bottom layer)	22	Hydrophilic	
Copolymer PVDF (upper layer)/	26	Hydrophobic	83 ± 10
Nylon 6 (bottom layer)	22	Hydrophilic	
PAN (upper layer)/	14	Hydrophobic	92 ± 5
PVA (bottom layer)	22	Hydrophilic	
Copolymer PVDF (upper layer)/	26	Hydrophobic	89 ± 6
PVA (bottom layer)	22	Hydrophilic	

Results presented in Table 6-1 showed that the thicknesses of homogeneous varied in a range of 82 to 99 µm. The bi-layer Nylon 6/Nylon 6 exhibited the thinnest membrane as compared to other homogenous bi-layer membranes. A possible reason of this was be due to a thin layer of electrospun Nylon 6, which has already been discussed earlier in Section 5.6.1, Chapter 5. In addition, the thicknesses of the homogeneous bi-layer membranes were about twice thicker than the single layers.

For heterogeneous bi-layer membrane, the fabrication time was varied depending on polymer used. As shown in Table 6-1, the heterogeneous bi-layer membranes have greater thickness as compared to single layer membranes. The thickness of single layer membranes was in a range of 40 to 45 µm, whereas the thickness of heterogeneous bi-layers was far higher in a range of 83 to 93 µm.

Although the membrane thicknesses were different, this fundamental study has successfully fabricated homogeneous and heterogeneous bi-layer membranes, which has not been reported by other studies.

6.2 FTIR analysis of homogeneous and heterogeneous bi-layer membranes

The IR test was also carried out for the homogeneous and heterogeneous bi-layers in order to monitor chemical structures of polymer for the upper and bottom layers. In the current study, these structures have to be monitored in order to obtain similar chemical structures for the upper and bottom layers. In addition, a rapid evaporation of solvent from electrospun fibres could affect the crystal phases of the fibres. Thus, any changes in crystal phases can be identified using the IR. For the homogeneous and heterogeneous bi-layers, the IR spectra are illustrated in Figures 6-1 (a-d) and 6-2 (a-d).

Figure 6-1 (a) illustrates the IR spectra for the homogeneous bi-layer Nylon 6/Nylon 6. From the results, it shows that the IR spectra for the top and bottom layer are comparable. In addition, the IR spectra for homogeneous bi-layer Nylon 6/Nylon 6 are also similar to the single layer Nylon 6. This indicates that the bi-layer Nylon 6/Nylon 6 exhibited the same crystal phases (γ-crystal phases) as single layer.

In Figures 5-38 (b) and 6-1 (b), the single layer PVA and homogeneous bi-layer PVA/PVA membranes also showed the same spectra, indicating that these membranes have similar chemical structures after electrospinning.
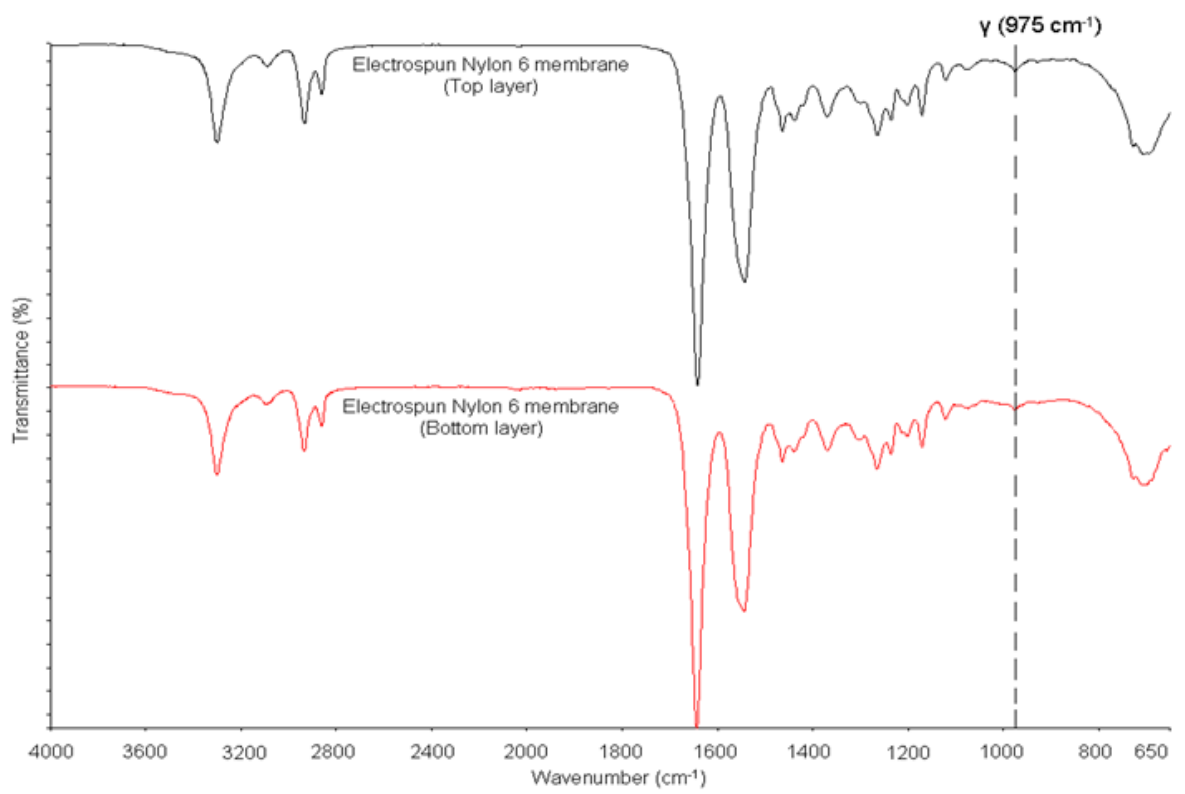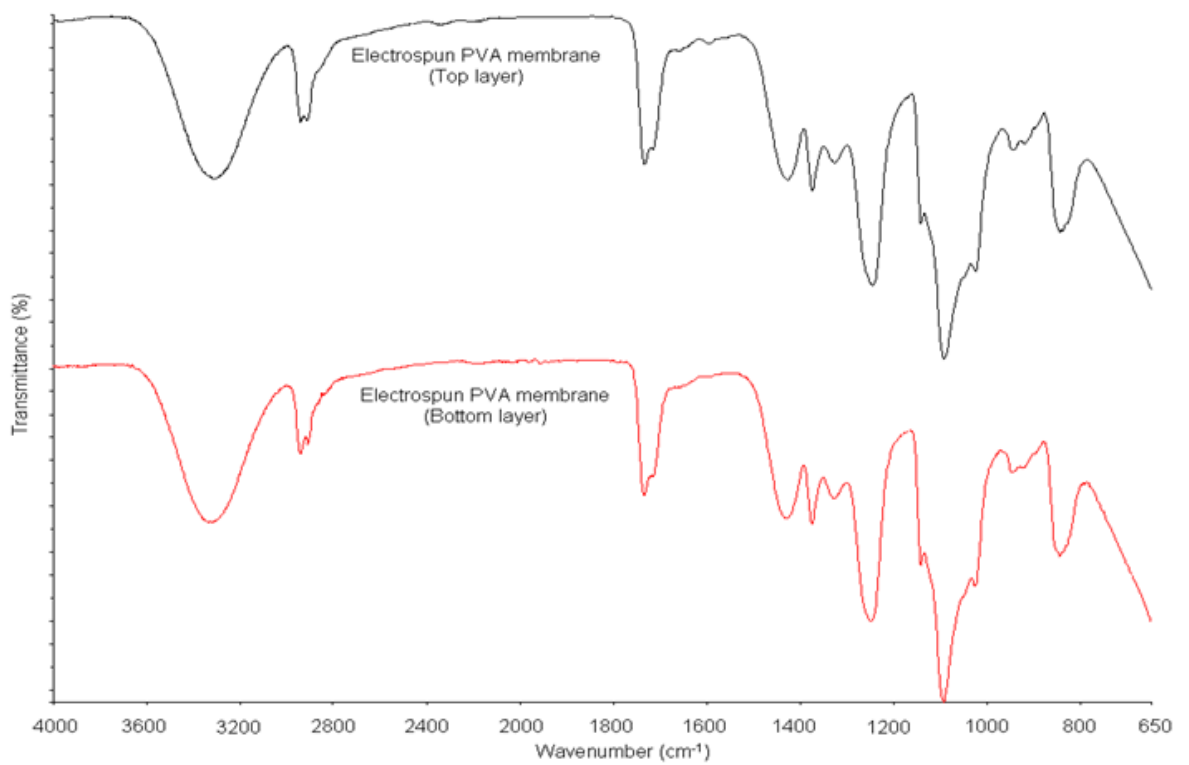
Figure 6-1: FT-IR spectra for homogeneous bi-layer electrospun nanofibre membranes for the top and bottom layer. a) Nylon 6/Nylon 6 and b) PVA/PVA.
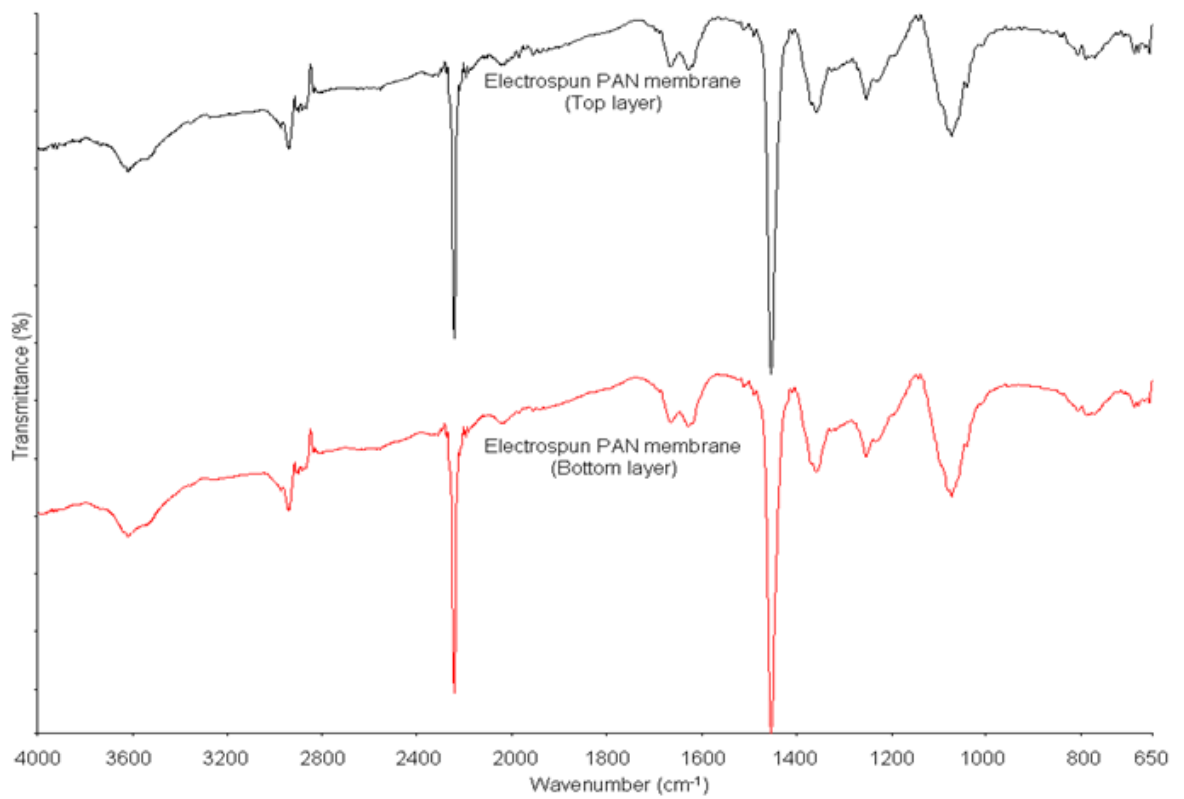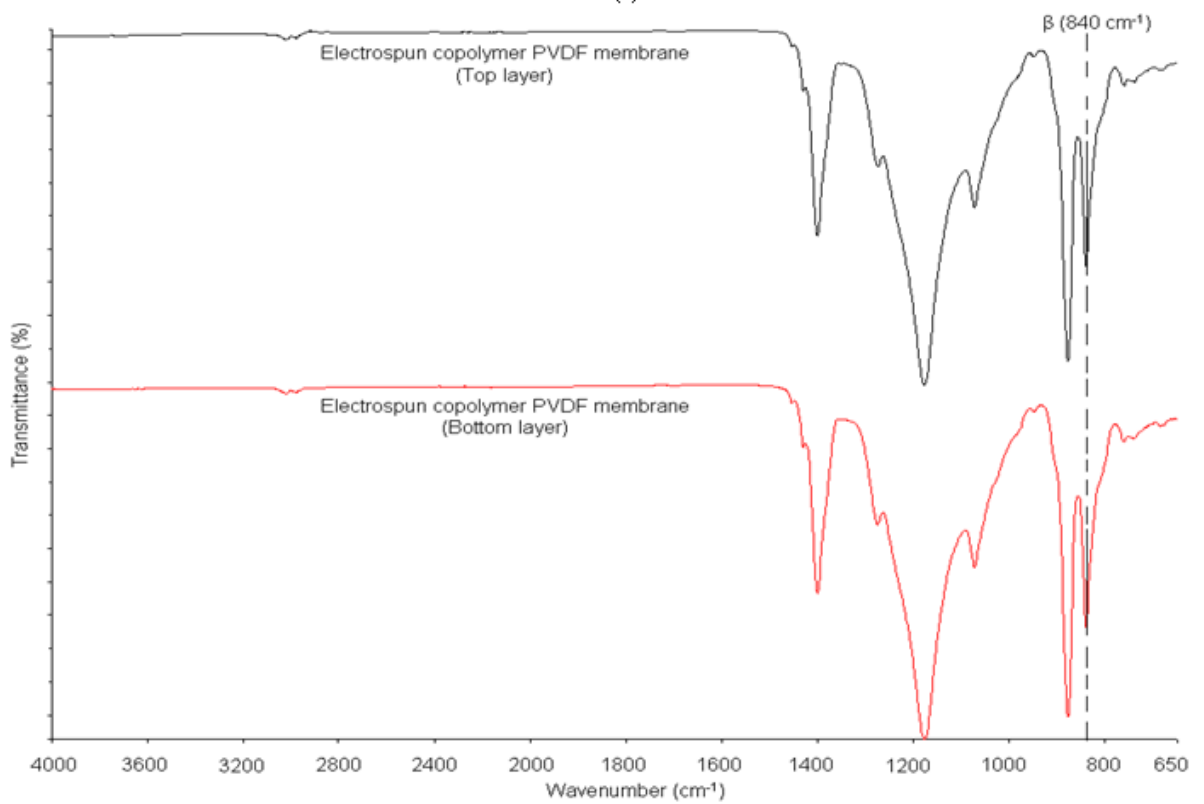
Figure 6-1: FT-IR spectra for homogeneous bi-layer electrospun nanofibre membranes for the top and bottom layer. c) PAN/PAN and d) copolymer PVDF/PVDF.

As with electrospun PVA, the homogeneous bi-layer PAN/PAN demonstrated the same spectra as the single layer electrospun PAN (Figure 5-38 (c) and 6-1 (c)).

In Figures 5-38 (d) and 6-1 (d), the homogeneous bi-layer copolymer PVDF/PVDF also showed the same spectra as the single layer copolymer PVDF. The homogeneous bi-layer copolymer PVDF/PVDF and single layer copolymer PVDF showed a comparable peak at 840 cm^{-1}, indicating the β-crystal phases of the polymer. Similar results were also observed by some studies, where they reported that peak at 840 cm^{-1} exhibited the β-crystal phases of PVDF (*63, 215-216*). The vibration type of the peak was CH$_2$ rocking (*63, 215-216*).

When the heterogeneous bi-layer membranes were tested, two distinct IR spectra were observed (Figures 6-2 (a-d)). The IR spectra for the heterogeneous bi-layer depend on the side from which the observation is made. This indicates that the IR spectra only show the surface effects of the membrane. In addition, the heterogeneous bi-layer membranes also retained the same crystal phases as other membranes (Figure 6-2 (a-b and d)). From the FTIR analysis, it can be summarized that;

1) the electrospinning retained the same chemical structures and crystal phases for the top and bottom layers of the homogeneous bi-layer membrane.

2) the electrospinning retained the same chemical structures and crystal phases for the single layer and heterogeneous bi-layer membranes

To confirm the crystal phases of the bi-layer Nylon 6/Nylon 6 and copolymer PVDF/PVDF, these membranes were tested for the wide angle X-ray diffraction (WAXD).
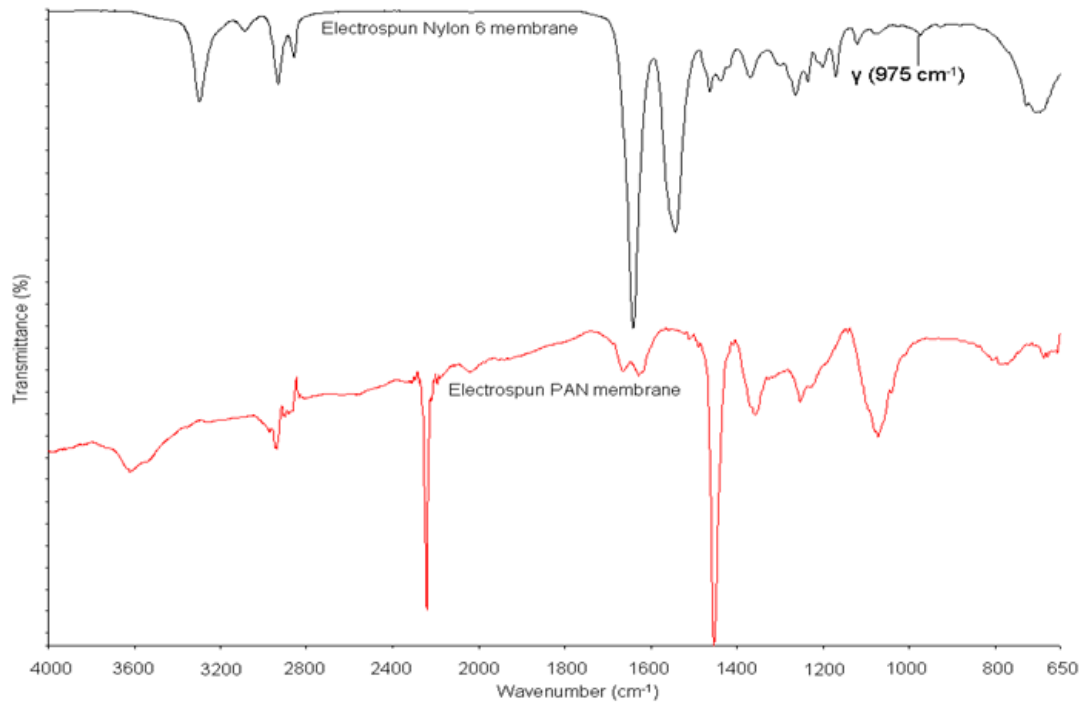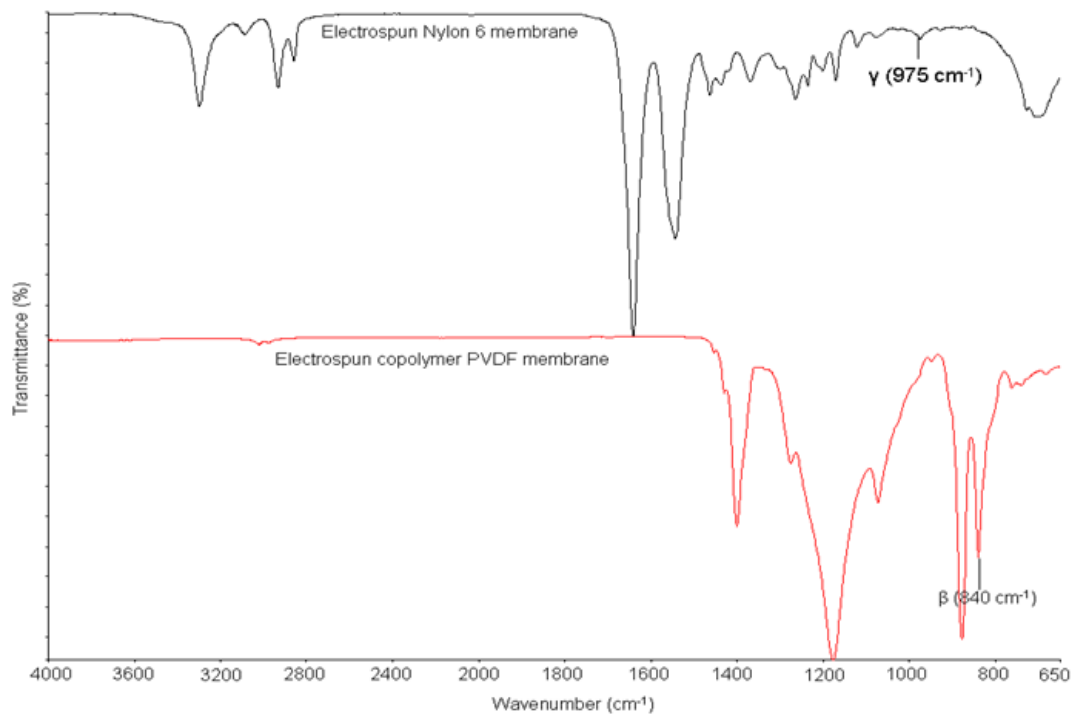
Figure 6-2: FT-IR spectral for heterogeneous bi-layer electrospun nanofibre membranes.
a) PAN/Nylon 6 and b) copolymer PVDF/Nylon 6.
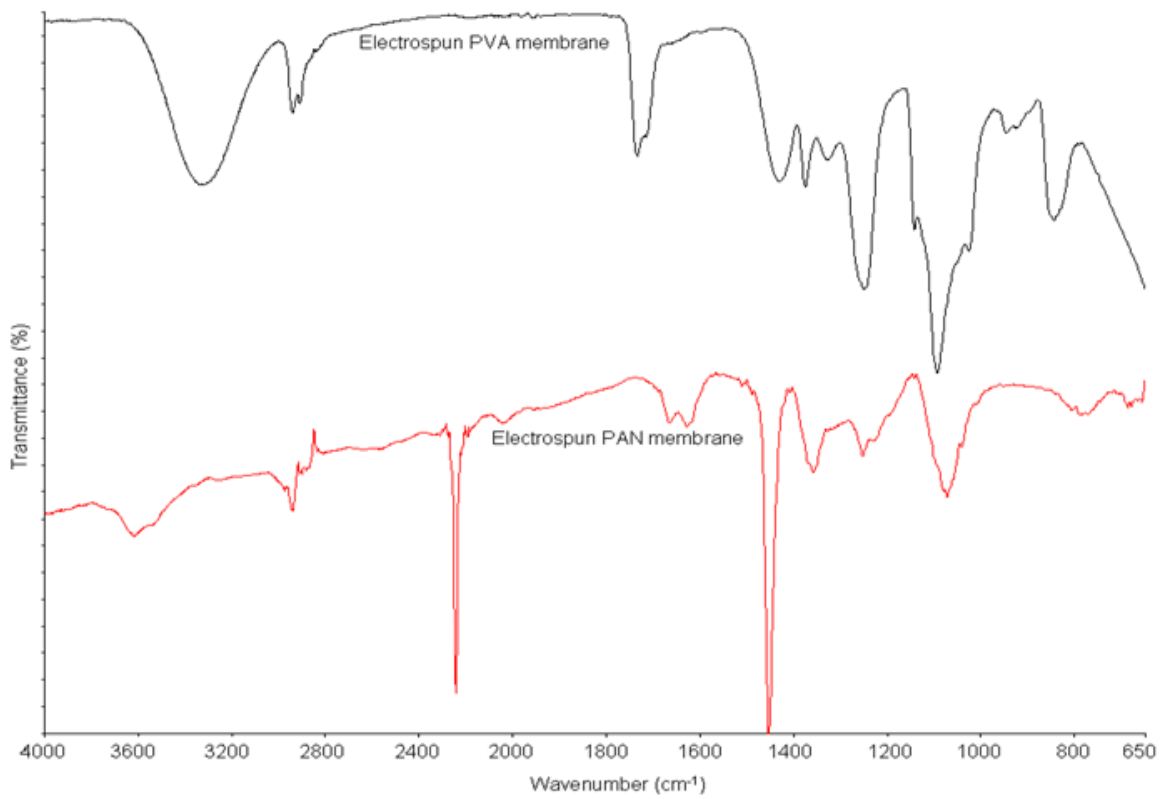
(c)
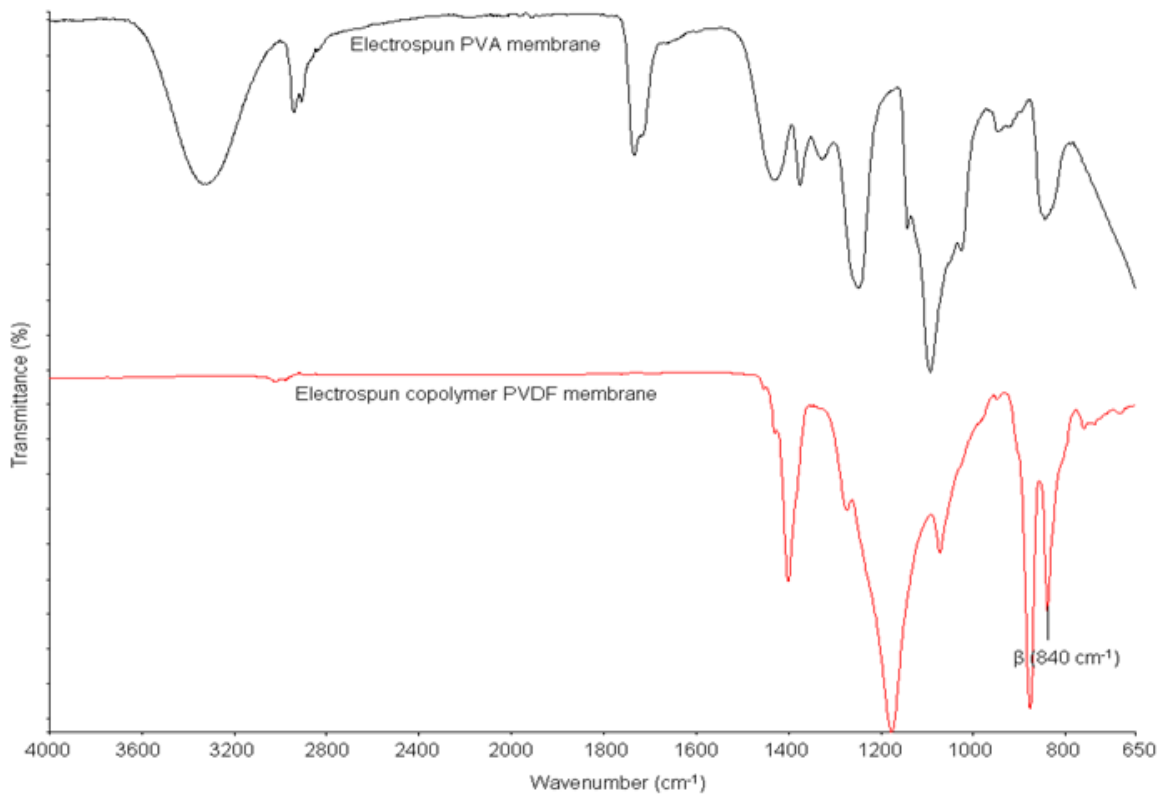
(d)

Figure 6-2: FT-IR spectral for heterogeneous bi-layer electrospun nanofibre membranes.

c) PAN/PVA and d) copolymer PVDF/PVA.

6.3 Wide angle X-ray diffraction analysis of homogeneous and heterogeneous bi-layer membrane

Figures 6-3 (a-d) show the diffraction peaks for homogenous and heterogeneous bi-layer electrospun membranes obtained from the wide angle X-ray diffraction. For homogeneous bi-layer membranes, these membranes showed similar diffraction peaks to the single layer membranes. In Figures 5-39 (a) and 6-3 (a-b), the diffraction peaks for homogeneous bi-layer Nylon 6/Nylon 6 and single layer Nylon 6 were identical, confirming that the 21.7° ($\approx 22°$) of 2θ is the peak of electrospun Nylon 6. Recent studies reported that diffraction peak at about 22° was indexed as 001 planes. This peak indicated the γ-crystal phase of Nylon 6 (*137, 218*). In the current study, the homogeneous bi-layer Nylon 6/Nylon 6 also exhibited γ-crystal phase with the diffraction peak at 22°. The γ-crystal phase of the membrane was also appeared in the FTIR spectra, Section 6.2.

Homogeneous bi-layer PAN/PAN membranes also exhibited similar peaks to the single layer electrospun PAN. In Figures 6-3 (a and c), the bi-layer PAN/PAN membranes show a broad peak, indicating the amorphous structure of the membranes.

The diffraction peaks for homogeneous PVA/PVA were similar to the single layer PVA membranes. In Figures 6-3 (c-d), the PVA/PVA membranes show a single peak at about 20°. Shao *et al.* (*219*) reported that a single peak of electrospun PVA membrane at 20.0° indicated the 101 planes.

As with other homogeneous bi-layer membranes, the homogeneous bi-layer copolymer PVDF/PVDF membrane exhibited similar diffraction peak to the single layer copolymer PVDF membrane (Figures 6-3 b and d). Recent studies reported that the β-crystal phases of PVDF were found at 20.0° and 21.0°, and were indexed as 200/110 planes. (*215, 220*). In the current study, the homogeneous bi-layer copolymer PVDF/PVDF also showed β-crystal phases with the diffraction peak at approximately 21°. The β-crystal phases of these membranes were also appeared in the FTIR spectra (Section 6.2).

For heterogeneous bi-layer membranes such as hydrophilic/hydrophobic and hydrophobic/hydrophilic, each membrane was tested for the top and bottom layers. The heterogeneous bi-layer Nylon 6/PAN was found to exhibit a clear diffraction peak at 21.7° (Figure 6-3 (a)). This shows that when exposing the

Nylon 6 top layer to the X-ray beam, the diffraction peak of Nylon 6 was clearly observed. In addition, the bi-layer Nylon 6/PAN exhibited a broad peak similar to the bi-layer PAN/PAN. This shows that the X-ray beam was able to diffract amorphous structures of the PAN bottom layer.

When the bi-layer Nylon 6/PAN was tested, the membrane exhibited two diffraction peaks (Figure 6-3 (a)). This indicates that when the PAN top layer was directly exposed to the X-ray beam, a diffraction peak of PAN was observed. The bi-layer PAN/Nylon 6 also showed a tendency to form a diffraction peak of Nylon 6 bottom layer. This indicates that the X-ray beam was also able to diffract the Nylon 6 bottom layer.

The diffraction peaks of heterogeneous bi-layer Nylon 6/copolymer PVDF membrane shown in Figure 6-3 (b) are more complex. The membrane exhibited a combination of peaks between the electrospun Nylon 6 and copolymer PVDF. A shoulder peak at about 21.7° was observed, showing the tendency to form a diffraction peak from the electrospun Nylon 6. The membrane also exhibited diffraction peaks at 20.7° and 18.7°, which confirmed the presence of electrospun copolymer PVDF.

When the bi-layer copolymer PVDF/Nylon 6 was tested, the diffraction peaks of electrospun copolymer PVDF were clearly observed. When exposing the copolymer PVDF top layer to the X-ray beam, it diffracts the crystal structures of electrospun PVDF (Figure 6-5 (b)). The membrane also showed a tendency to form a diffraction peak of Nylon 6 bottom layer.

Due to the complexity of the WAXD diffraction peaks, the crystal phases for the heterogeneous bi-layer membranes were not easy to determine. However, it can be determined using the FTIR test.
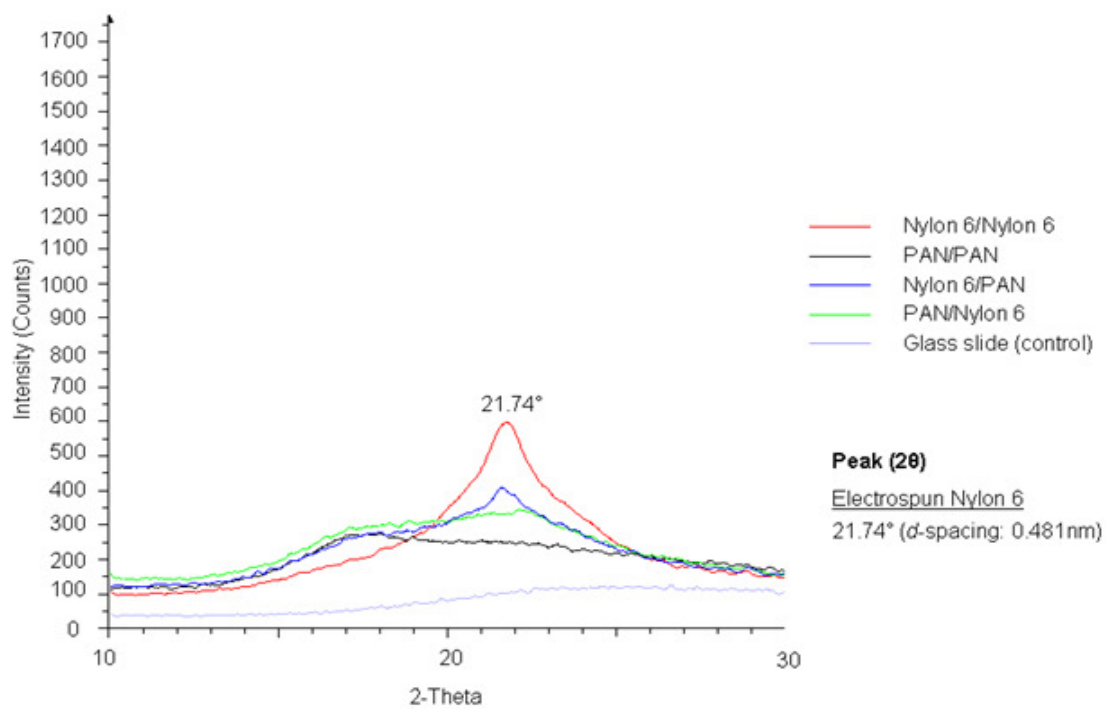
(a)
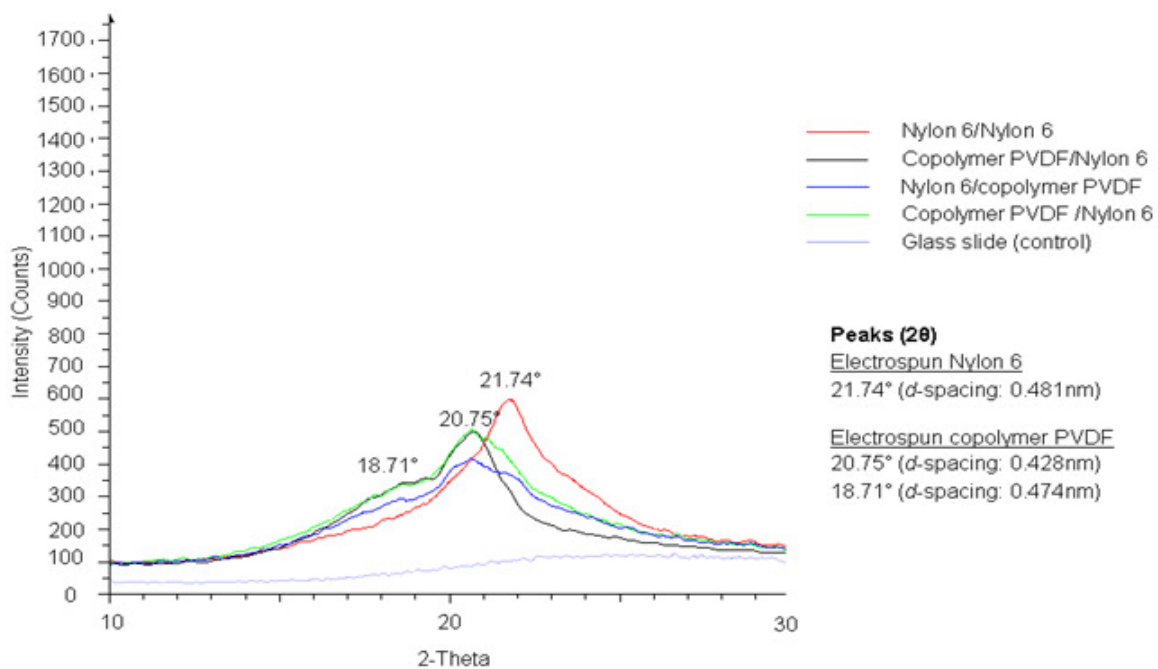
(b)

Figure 6-3: X-ray diffraction patterns for homogeneous and heterogeneous bi-layer membranes measured by the wide angle X-ray diffraction. a) Nylon 6/Nylon 6, PAN/PAN, Nylon 6/PAN and PAN/Nylon 6 and b) Nylon 6/Nylon 6, copolymer PVDF/PVDF, Nylon 6/copolymer PVDF, copolymer PVDF/Nylon 6
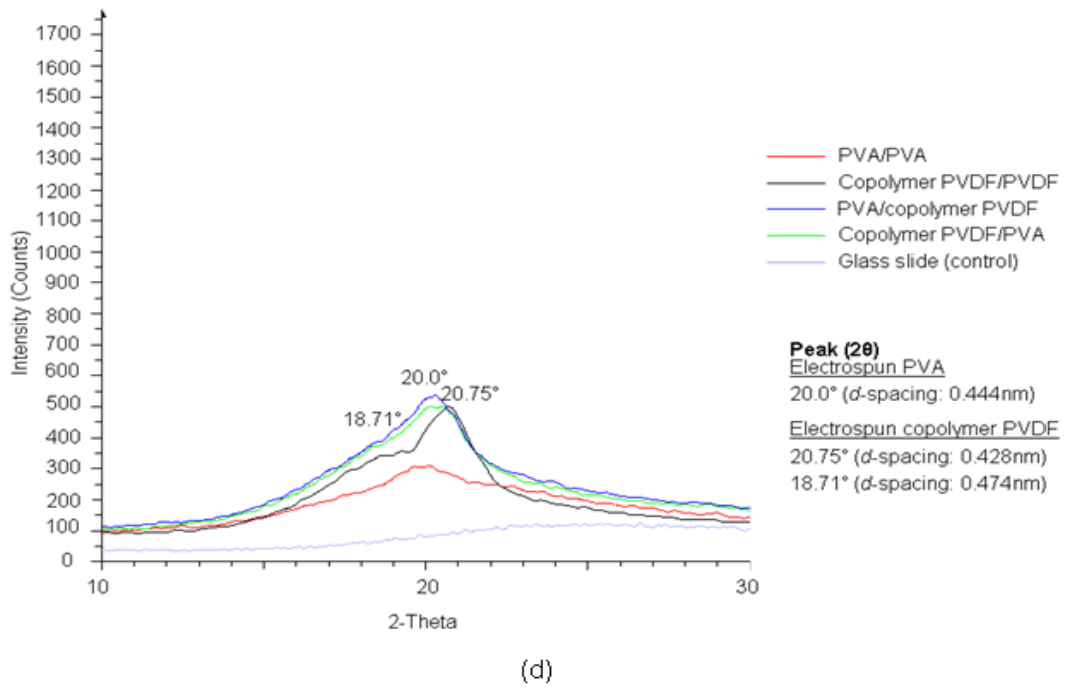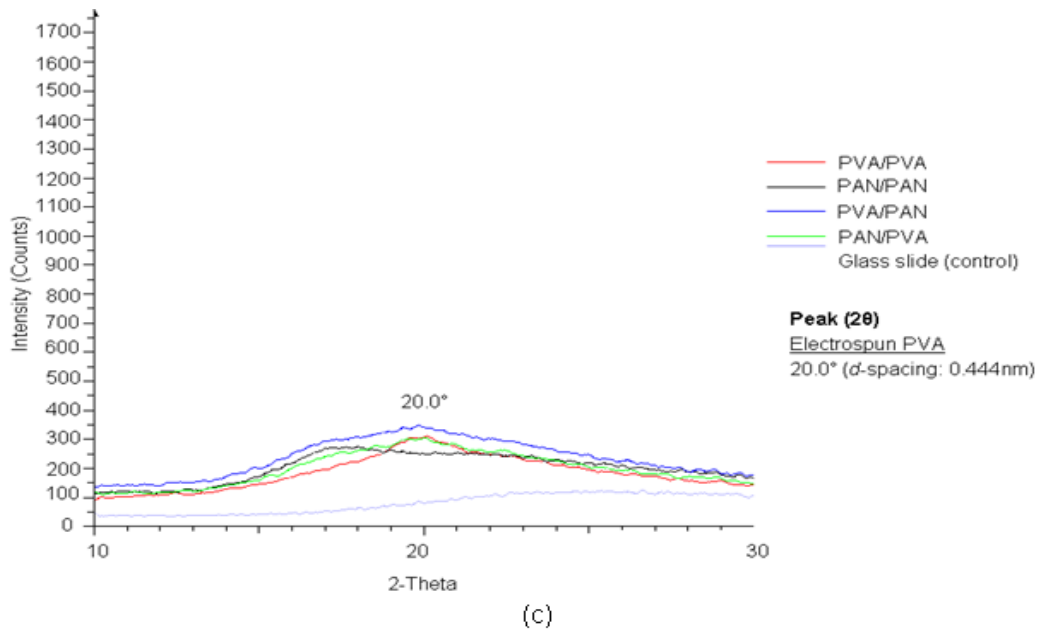
Figure 6-3: X-ray diffraction patterns for homogeneous and heterogeneous bi-layer membranes measured by the wide angle X-ray diffraction. c) PVA/PVA, PAN/PAN, PVA/PAN and PAN/PVA and d) PVA/PVA, copolymer PVDF/PVDF, PVA/copolymer PVDF and copolymer PVDF/PVA

6.4 Determination of Surface Wettability
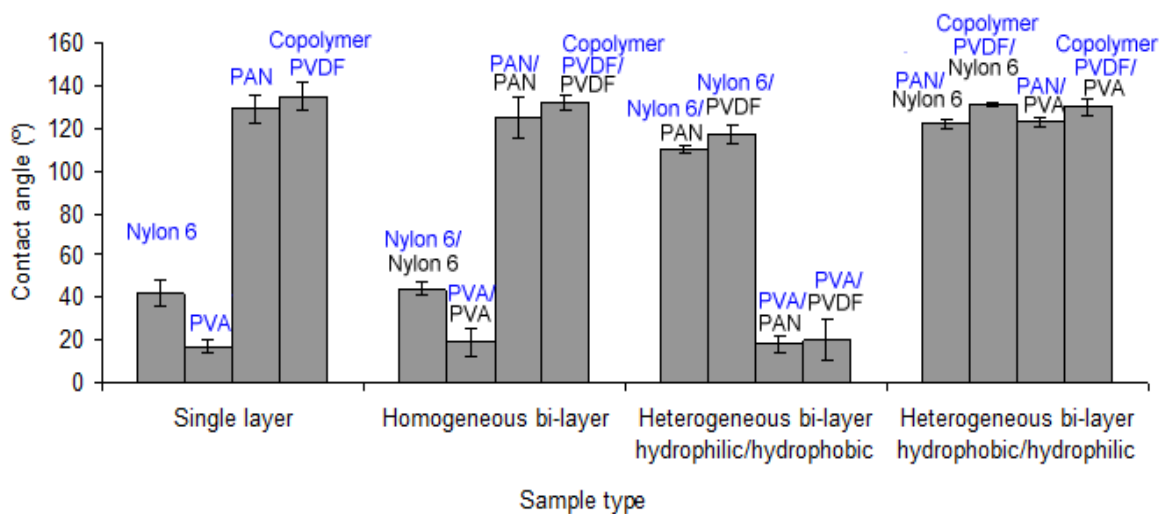
Figure 6-4: a) A plot of water contact angles for single layer, homogenous and heterogeneous bi-layer electrospun membranes. The droplet was applied on membranes written in blue. The measurement was taken at 5 seconds after the drop was applied.

As shown in Section 5.10 and Figure 6-4 (a), the single layer electrospun Nylon 6 and PVA are hydrophilic polymers, showing the water contact angles lower than 90°. The water contact angles for single layer electrospun Nylon 6 and PVA were approximately 42° and 17°, respectively. For single layer electrospun PAN and copolymer PVDF, both membranes exhibited water contact angles more than 90°. This shows that those membranes were hydrophobic, where the water contact angles for single layer PAN and copolymer PVDF were approximately 129° and 135°, respectively.

Similar to the single layer electrospun membranes, the homogenous bi-layer Nylon 6/Nylon 6 and PVA/PVA also exhibited hydrophilic properties. As a result, complete wetting of surfaces was observed on those membranes. In Figure 6-4 (a), the homogeneous bi-layer Nylon 6/Nylon 6 and PVA/PVA give water contact angle approximately 44° and 19°, respectively. Those values were also similar to the single layer Nylon 6 and PVA. For homogeneous bi-layer PAN/PAN and copolymer PVDF/PVDF, both membranes exhibited water contact angles more than 90°, consistent with their hydrophobic nature. The water contact angles for homogeneous bi-layer PAN/PAN and copolymer PVDF/PVDF were also similar to the single layer PAN and copolymer PVDF. In Figure 6-4 (a), the water

contact angles for homogeneous bi-layer PAN/PAN were approximately 125°. The nano-texture of wrinkle structures on the PAN fibre surface was presumed to give a higher water contact angles for single layer PAN and homogeneous bi-layer PAN/PAN membrane. Electrospun copolymer PVDF with its functional group of CF_2 was hydrophobic, producing water contact angles of 132° for homogeneous bi-layer copolymer PVDF/PVDF.
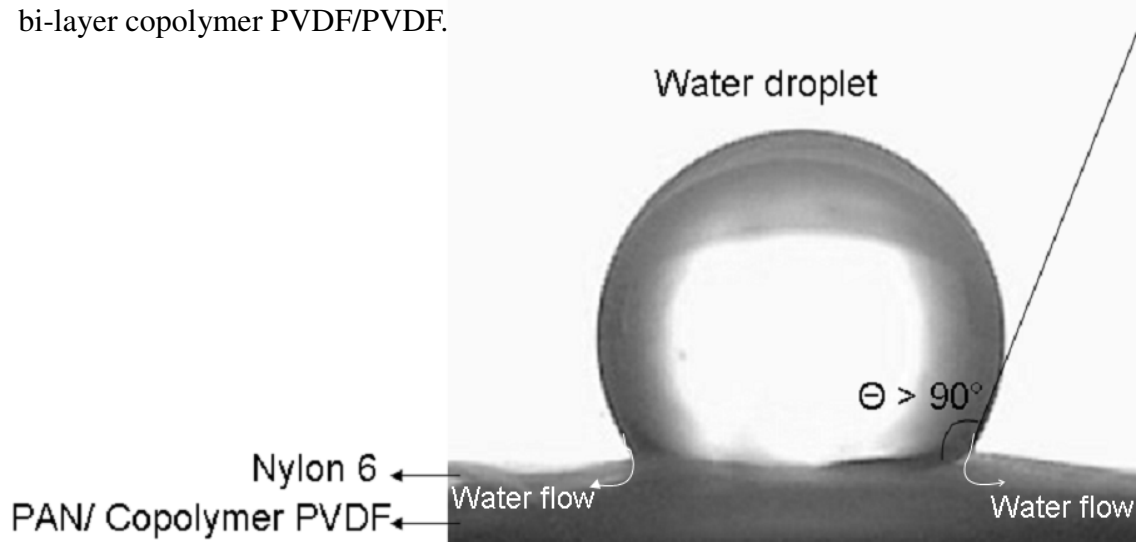
Figure 6-4: b) Photograph of water droplet on the bi-layer Nylon 6/PAN or Nylon 6/Copolymer PVDF. The photograph was taken at 5 seconds after the drop was applied.

A summary of the water contact angles for the heterogeneous bi-layer membranes is shown in Figure 6-4 (a). The heterogeneous bi-layer Nylon 6/PAN and Nylon 6/ copolymer PVDF membranes exhibited water contact angles more than 90°. A possible reason could be due to the presence of electrospun PAN and copolymer PVDF as base membranes. In Figure 6-4 (b), the droplet goes through the electrospun Nylon 6, but the electrospun PAN or copolymer PVDF prevents further downward movement of the droplet. As a result, the water contact angles for heterogeneous bi-layer Nylon 6/PAN and Nylon 6/ copolymer PVDF were approximately 110° and 117°, respectively, which were lower than the single layer PAN and copolymer PVDF as well as the homogeneous bi-layer PAN/PAN and copolymer PVDF/PVDF.

The heterogeneous bi-layer PVA/PAN and PVA/copolymer PVDF membranes were expected to give similar wetting behaviours to the bi-layer Nylon 6/PAN and Nylon 6/ copolymer PVDF membranes. However, the water contact angles for bi-layer PVA/PAN and PVA/copolymer PVDF were lower than the bi-

layer Nylon 6/PAN and Nylon 6/ copolymer PVDF membranes. The bi-layer PVA/PAN and PVA/copolymer PVDF exhibited contact angles of 18° and 20°, respectively. This low contact angles was due to the spreading and re-dissolving of water droplet over the PVA membrane surfaces, which resulted in lower water contact angles for the membrane (Figure 6-4 (c)). Results obtained in these cases were also similar to the single layer PVA and homogeneous bi-layer PVA/PVA. For bi-layer Nylon 6/PAN and Nylon 6/ copolymer PVDF, the contact angles are approximately 110° and 117°, respectively. As mentioned earlier, the PAN or copolymer PVDF bottom layer prevents further downward movement of droplet, which results in higher contact angles for the bi-layer Nylon 6/PAN and Nylon 6/ copolymer PVDF.
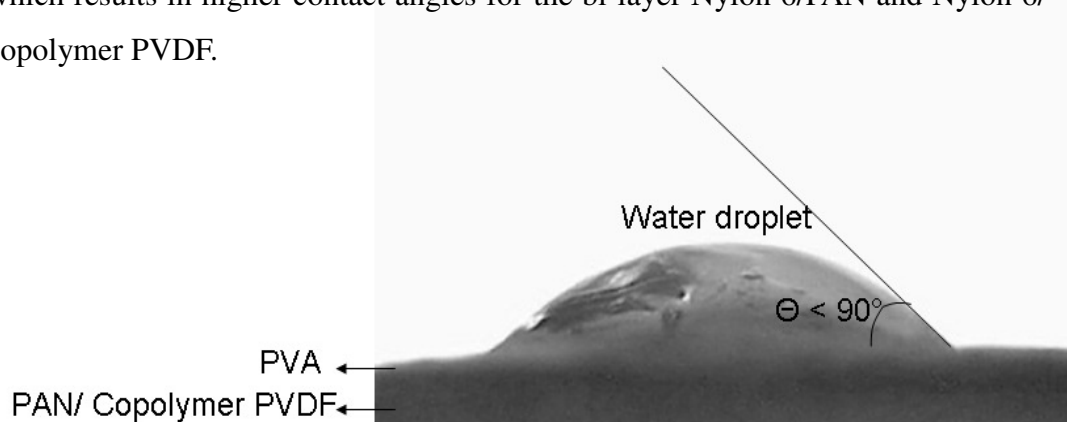
Figure 6-4: c) Photograph of water droplet on the bi-layer PVA/PAN or PVA/Copolymer PVDF. The photograph was taken at 5 seconds after the drop was applied.

For heterogeneous bi-layer PAN/Nylon 6, copolymer PVDF/Nylon 6, PAN/PVA and copolymer PVDF/PVA membranes, all exceeded 90°. In Figure 6-4 (a), the water contact angles for bi-layer PAN/Nylon 6, copolymer PVDF/Nylon 6, PAN/PVA and copolymer PVDF/PVA were approximately 122°, 131°, 123° and 130°, respectively. These values were also similar to the single layer and homogenous bi-layer PAN/PAN as well as the single layer and homogeneous bi-layer copolymer PVDF/PVDF. The presence of top layer electrospun PAN and copolymer PVDF prevented water droplets from directly penetrating through the membranes. This shows that the hydrophobic character of the top surfaces influenced the water contact angles for the bi-layer PAN/Nylon 6, copolymer PVDF/Nylon 6, PAN/PVA and copolymer PVDF/PVA.

6.5 Tensile Strength

In Sections 6.1 to 6.4, the physical properties of homogeneous and heterogeneous bi-layer membranes varied depending on the polymer used. Such variations were found to affect the tensile properties of the membranes. In order to gain a better understanding between tensile properties and physical properties of the membranes, this section is organized into two sub-sections: 1) tensile strength of homogeneous bi-layer membranes and 2) tensile strength of heterogeneous bi-layer membranes.

6.5.1 Determination of tensile strength for homogeneous bi-layer electrospun nanofibre membranes

As mentioned earlier in Chapter 4 (Section 4.5), the random orientated bi-layer membranes were stamped out using a dog-bone shaped template in order to measure the tensile strength of the membranes. The tensile properties (tensile strength, strain and modulus) of homogeneous bi-layer membranes are tabulated in Table 6-2.

Table 6-2: Tensile properties of homogeneous bi-layer electrospun Nylon 6/Nylon 6, PVA/PVA, PAN/PAN and copolymer PVDF/PVDF membranes.

Bi-layer homogeneous	Tensile stress, σ (MPa)	Tensile strain, ε (%)	Modulus, E (MPa)	Range of pore sizes (μm)
Nylon 6/Nylon 6	6.1 ± 1.3	23.4 ± 4.5	23.2 ± 1.8	0.05-0.26
PVA/PVA	3.5 ± 1.7	46.1 ± 8.4	18.3 ± 3.3	0.06-0.91
PAN/PAN	1.6 ± 1.0	43.3 ± 8.0	6.2 ± 5.6	0.56-2.69
Copolymer PVDF/PVDF	1.2 ± 1.2	196.8 ± 14.7	1.2 ± 1.1	0.20-2.00
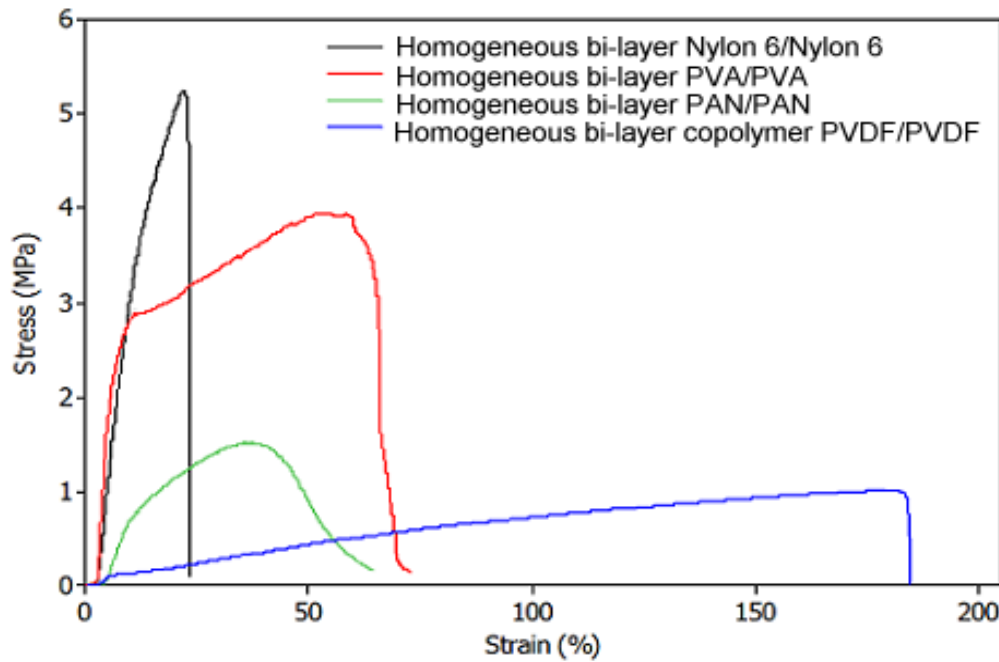
Figure 6-5: Typical plots of stress versus strain for homogeneous bi-layer electrospun Nylon 6/Nylon 6, PVA/PVA, PAN/PAN and copolymer PVDF/PVDF.

In Table 6-2, the tensile strength and modulus for homogeneous bi-layer Nylon 6/Nylon 6 are approximately 6.1 MPa and 23.4 MPa, respectively. It was expected that the fine pore sizes (in a range of 0.05-0.26 µm) of electrospun Nylon 6 and high fibre-to-fibre bonding in the Nylon 6 membrane gave a high tensile strength for the bi-layer Nylon 6/Nylon 6. The effect of pore sizes and porosity on the tensile strength has been described in earlier studies (*139, 142*). They reported that membranes with lower porosity (smaller pore sizes) limited the movement of electrospun fibres, which resulted in higher tensile strength. For electrospun membranes with higher porosity, the membrane was likely to undergo fibre movement and alignment, which resulted in lower tensile strength (*139, 142*). In Figure 6-5, the bi-layer Nylon 6/Nylon 6 exhibits a single slope as compared to others. The sharp slope indicates that the random orientated Nylon 6 fibres require a higher force to align these fibres in the loading direction. Due to its fine pore sizes and fibre-to-fibre bonding, the membrane restricted the movement of Nylon 6 fibres. As a result, the bi-layer Nylon 6/Nylon 6 membranes gave a sharp slope at higher stress and break at lower strain. In Figure 6-6 (a), bi-layer Nylon 6/Nylon 6 retains its random oriented structure, conforming that the membrane limits the movement of the fibres.

161
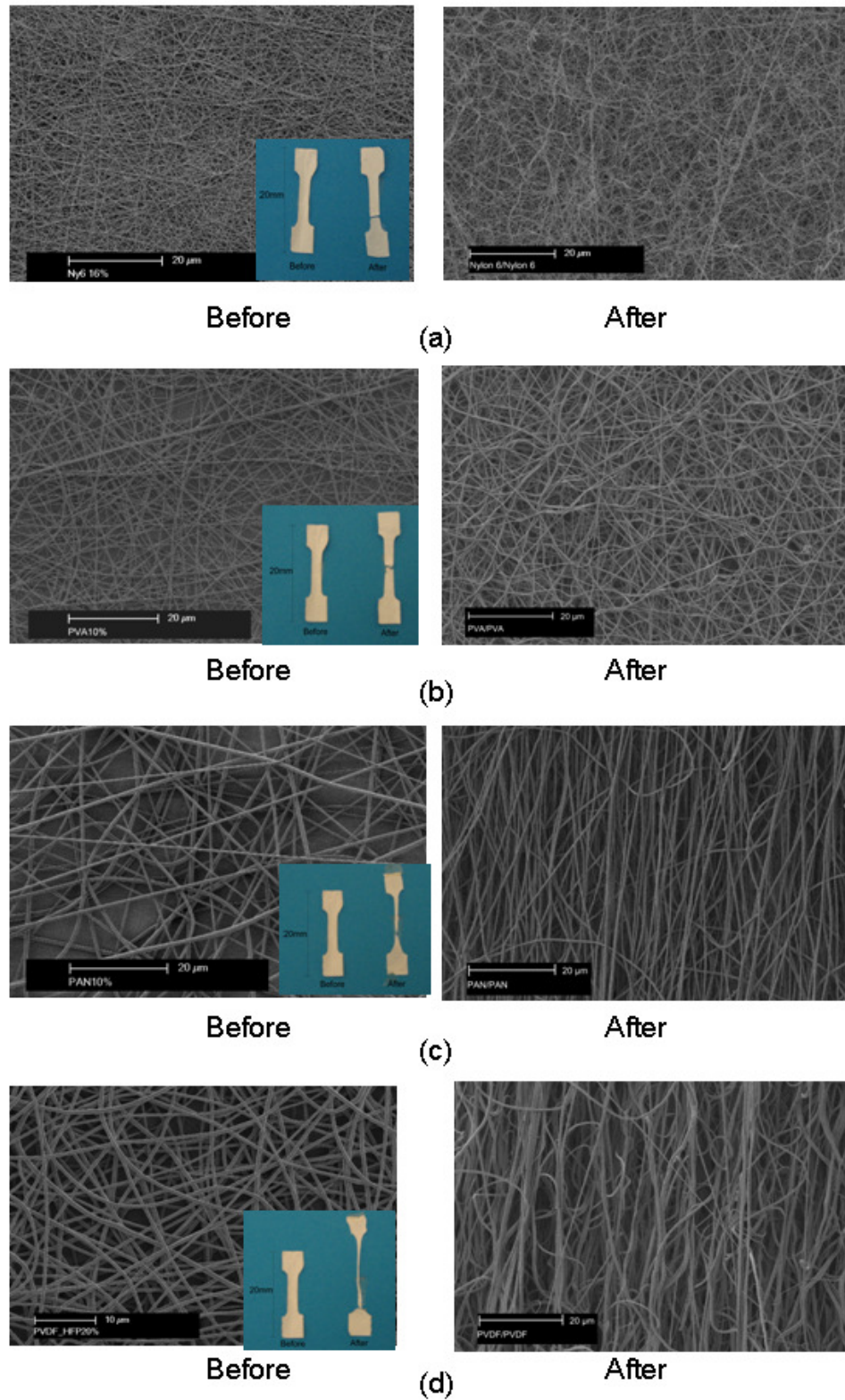
Figure 6-6: Typical SEM images and photographs for homogeneous bi-layer membranes before and after tensile test. a) Nylon 6/Nylon 6, b)PVA/PVA, c) PAN/PAN and d) copolymer PVDF/PVDF.

For homogeneous bi-layer PVA/PVA, the tensile strength and modulus are approximately 3.5 MPa and 18.3 MPa, respectively (Table 6-2). As with bi-layer Nylon 6/Nylon 6, small pore sizes and fibre-to-fibre bonding were presumed to give higher tensile strength and modulus for the bi-layer PVA/PVA. As shown in Figure 6-5, the bi-layer PVA/PVA membrane demonstrates two slopes. The first slope indicates a higher force to align PVA fibres in a loading direction, whereas the second slope indicates a slight movement of the membrane. Although the membrane had a slight movement, it was also found that the membrane retained its random oriented structure after the tensile test (Figure 6-6 (b)). This could be due to the membrane had strong fibre-to-fibre bonding, which restricted the alignment of PVA fibres in loading direction.

As shown in Table 6-2, the tensile strength and modulus for bi-layer PAN/PAN were approximately 1.6 MPa and 6.2 MPa, respectively. It was expected that the bigger pore sizes and poor fibre-to-fibre bonding in the PAN membrane provided a low tensile strength for the bi-layer PAN/PAN. Figure 6-5 shows two slopes for the bi-layer PAN/PAN. The first slope was considerably lower than the Nylon 6/Nylon 6 and PVA/PVA membranes. This could be due to poor fibre-to-fibre bonding of the membrane, which permits the alignment of PAN fibres in loading direction (Figure 6-6 (c)). When a high load was further applied, those fibres were continuously aligned and eventually broke at higher strain at approximately 43%. The alignment of PAN fibre was also observed to form necking after the tensile test. When the membranes were observed under the scanning electron microscopy (SEM), the PAN fibre diameter was found to reduce from 677 nm to 542 nm (Figure 6-6 (c)). This shows that the fibres are being stretched during the tensile test. The reduction in fibre diameter was also found for other electrospun fibres.

The homogenous bi-layer copolymer PVDF/PVDF also exhibited lower tensile strength and modulus at approximately 1.2 MPa and 1.2 MPa, respectively (Table 6-2). In Figure 6-5, the copolymer PVDF/PVDF membrane shows two slopes. Similar to other bi-layer homogeneous membranes, the first slope indicates a high force to align PVDF fibres in loading direction. Due to its poor fibre-to-fibre bonding in the membrane, the bi-layer copolymer PVDF/PVDF was observed to change from the random oriented fibres to aligned fibres (Figure 6-6 (d)). The alignment of the fibres was observed to form the second slope, as shown

in Figure 6-5. When a high load was further applied, the bi-layer PVDF/PVDF continued to align and eventually break at higher tensile strain at approximately 197%.

6.5.2 Determination of tensile strength for heterogeneous bi-layer electrospun nanofibre membranes

The tensile properties (stress, strain and modulus) of homogeneous bi-layer membrane have already been discussed in Section 6.5.1. In this section, the tensile properties (stress, strain and modulus) of heterogeneous bi-layer membranes will be examined.

In Table 6-3, the tensile properties for heterogeneous bi-layer membranes were dependent on the combination of polymers used. In Table 6-3, the tensile strain of bi-layer copolymer PVDF/PVA is approximately 202 %. As discussed earlier in Section 6.6.1, the alignment of PVDF fibres provided a high tensile strain for electrospun copolymer PVDF. Thus, a combination of electrospun PVDF and electropun PVA gave a high tensile strain for the bi-layer copolymer PVDF/PVA. The membrane also showed a higher tensile strength with approximately 3.5 MPa. However, the presence of electrospun copolymer PVDF in the bi-layer membrane was found to give low modulus for the membrane. The modulus of the membrane was only 11 MPa. In Figure 6-7, the heterogeneous bi-layer copolymer PVDF/PVA showed two slopes. The first slope indicates a high force to align the membrane, whereas the second slope indicates the alignment PVDF fibres under stress. The formation of these aligned fibres was due to poor fibre-to-fibre bonding of the electrospun PVDF. When the membrane is stretched in a loading direction, the electrospun PVDF fibres will continuously aligned. The alignment of the fibres forms necking for the PVDF membrane, as shown in Figure 6-8 (a). In addition, the bi-layer copolymer PVDF/PVA did not show any delamination, showing that the electrospun copolymer PVDF and PVA have similar strains to break.

Table 6-3: Tensile properties of heterogeneous bi-layer electrospun PAN/Nylon 6, copolymer PVDF/Nylon 6, PAN/PVA and copolymer PVDF/PVA.

Bi-layer homogeneous	Tensile stress, σ (MPa)	Tensile strain, ε (%)	Modulus, E (MPa)
PAN/Nylon 6 Copolymer	3.2 ± 1.1	107.6 ± 3.1	21.0 ± 2.6
PVDF/Nylon 6	2.6 ± 1.0	178.4 ± 8.3	19.5 ± 4.5
PAN/PVA	2.9 ± 1.0	85.0 ± 4.8	17.9 ± 6.7
Copolymer PVDF/PVA	3.5 ± 1.0	202.2 ± 9.2	10.9 ± 4.2
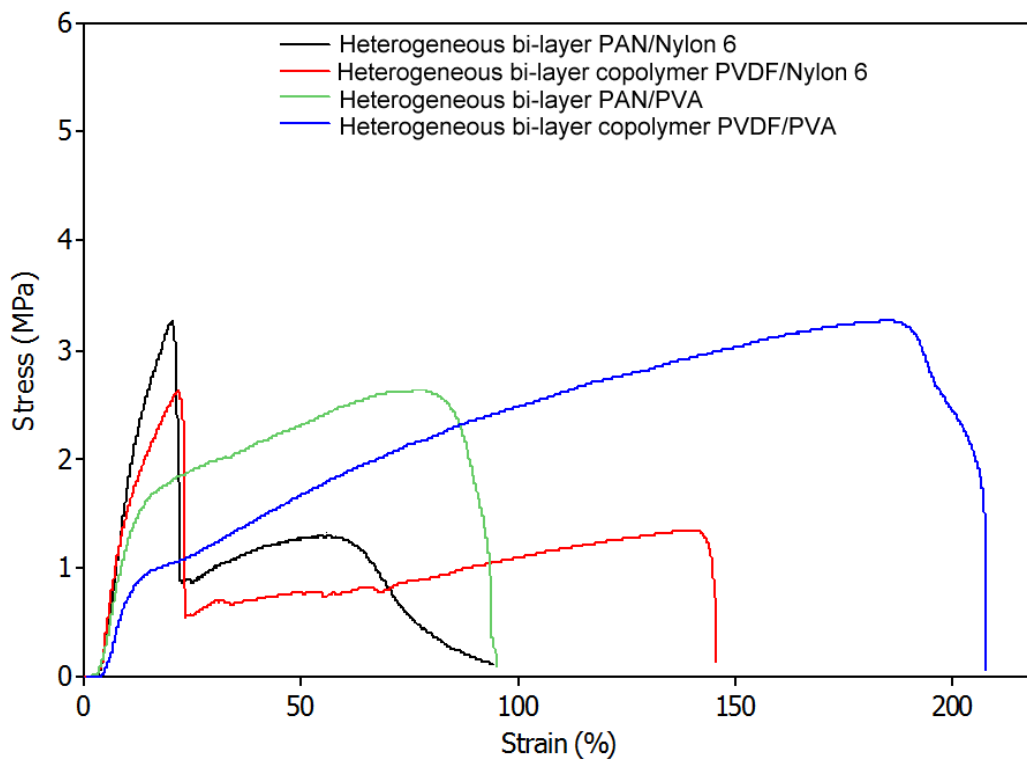
Figure 6-7: Typical plots of stress versus strain of heterogeneous bi-layer electrospun PAN/Nylon 6, copolymer PVDF/Nylon 6, PAN/PVA and copolymer PVDF/PVA.
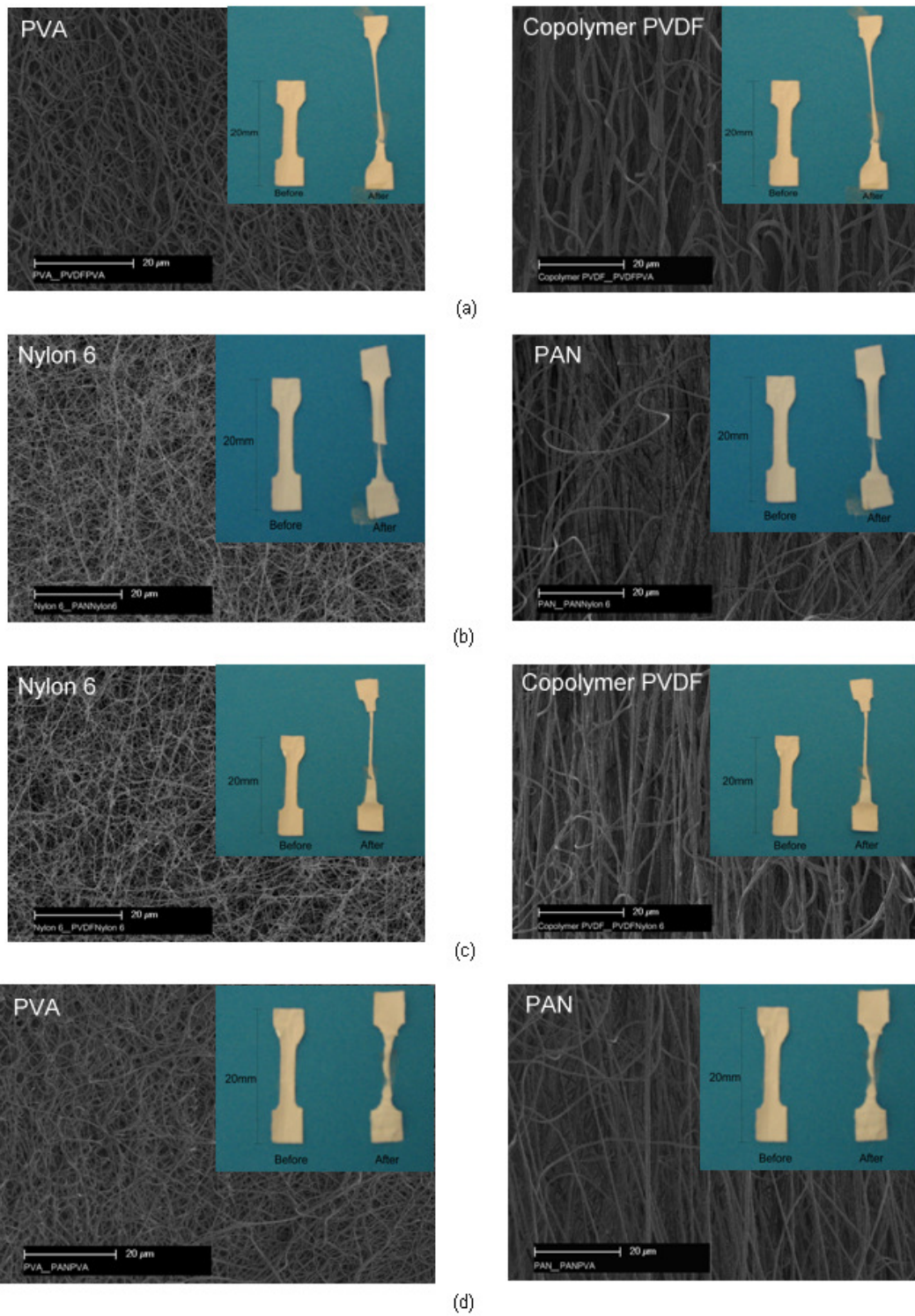
Figure 6-8: Typical SEM images and photographs for heterogeneous bi-layer membrane after tensile test. a) copolymer PVDF/PVA, b) PAN/Nylon 6, c) copolymer PVDF/Nylon 6 and d) PAN/PVA

The tensile properties (stress, strain and modulus) of bi-layer PAN/Nylon 6 were influenced by each layer (electrospun PAN and Nylon 6) in the membrane. The membrane showed the tensile strength of 3.2 MPa and modulus of 21 MPa (Table 6-3). The presence of electrospun Nylon 6 was found to contribute higher tensile strength and modulus for the bi-layer PAN/Nylon 6. In addition, the presence of electrospun PAN gave a higher strain (approximately 108 %) for the membrane. In Figure 6-7, the heterogeneous bi-layer PAN/Nylon 6 demonstrates two separate slopes. The first slope indicates a high force to align the membrane. As the membrane was further aligned, the electrospun Nylon 6 was found to break. As a result, a sharp drop was observed at lower strain approximately 20%. However, the presence of electrospun PAN allowed the extension of the bi-layer PAN/Nylon 6, resulting in the second slope for the membrane (Figure 6-7). In Figure 6-8 (b), the membrane was observed to delaminate after the tensile test, showing the poor adhesion between electrospun PAN and Nylon 6 layers.

Each layer from the heterogeneous bi-layer copolymer PVDF/Nylon 6 was also influenced the tensile strength, strain and modulus of the membrane. In Table 6-3, the membrane exhibited tensile strain of 178 %. It is understandable that the presence of electrospun copolymer PVDF enhanced the tensile strain of the membrane, whereas the presence of electrospun Nylon 6 enhanced the membrane tensile strength and modulus. As shown in Table 6-3, the membrane tensile strength and modulus are about 3 MPa and 20 MPa, respectively. As with bi-layer PAN/Nylon 6, the bi-layer copolymer PVDF/Nylon 6 exhibited two separate slopes (Figure 6-7). The first slope indicates a high force to align the membrane. Due to the low strain of electrospun Nylon 6, a sharp drop was observed at approximately 21%. The presence of electrospun copolymer PVDF gave further extension for the bi-layer copolymer PVDF/Nylon 6. This resulted in the second slope, as shown in Figure 6-7. The delamination of the membrane was also observed, showing the low adhesion between copolymer PVDF and Nylon 6 (Figure 6-8 (c)).

The tensile properties of bi-layer PAN/PVA was affected by the physical properties of electrospun PAN and PVA. In Table 6-3, the tensile strain and strength are approximately 85% and 2.9 MPa, respectively. For modulus, the membrane exhibited 18 MPa. Similar to the bi-layer copolymer PVDF/PVA, the bi-layer PAN/PVA demonstrates two slopes, where the first slope indicates a

higher force to align the bi-layer PAN/PVA membrane in loading direction and the second slope indicates the alignment of PAN and PVA fibres in the membrane (Figure 6-7). In Figure 6-8 (d), the membrane does not show any delamination, indicating that the electrospun PAN and PVA have similar strain to break.

Results presented in Table 6-3 show that the tensile properties for heterogeneous bi-layer membranes varied dependent on the combination of polymers used. However, the current study noted that the uncertainties for the membrane tensile stress are approximately 30%. Thus, further research is required to confirm the phenomenon. In addition, the tensile properties for the bi-layer Nylon 6/PAN, Nylon 6/copolymer PVDF, PVA/PAN and PVA/copolymer PVDF were not presented in the thesis because these membranes have the same properties to the bi-layer PAN/Nylon 6, copolymer PVDF/Nylon 6, PAN/PVA and copolymer PVDF/PVA, respectively.

The delamination of some bi-layer membranes shows the importance of adhesion strength between layers for the bi-layer membranes. Thus, a study on adhesion strength was carried out to understand this behaviour.

6.6 Adhesion Strength

The adhesion strength between layers in the bi-layer electrospun membranes was complex due to the difference in surface topography, porosity, fibre morphology and polymer used for the electrospun membranes. Hence, results presented in this section are mainly fundamental and more work is required to confirm the findings.

The 180° peel test was reported to be an ideal test method to measure adhesion strength between two flexible materials (*145, 221*). Electrospun membranes are generally flexible in nature, and thus the 180° peel test was chosen as a test method in the study.

A preliminary study to identify an ideal experimental system for the 180° peel test was carried out in the study. Figure 6-9 (a) illustrates the 180° peel test used initially, where the top layer is held by a moving grip and the bottom layer is held by a stationary grip.
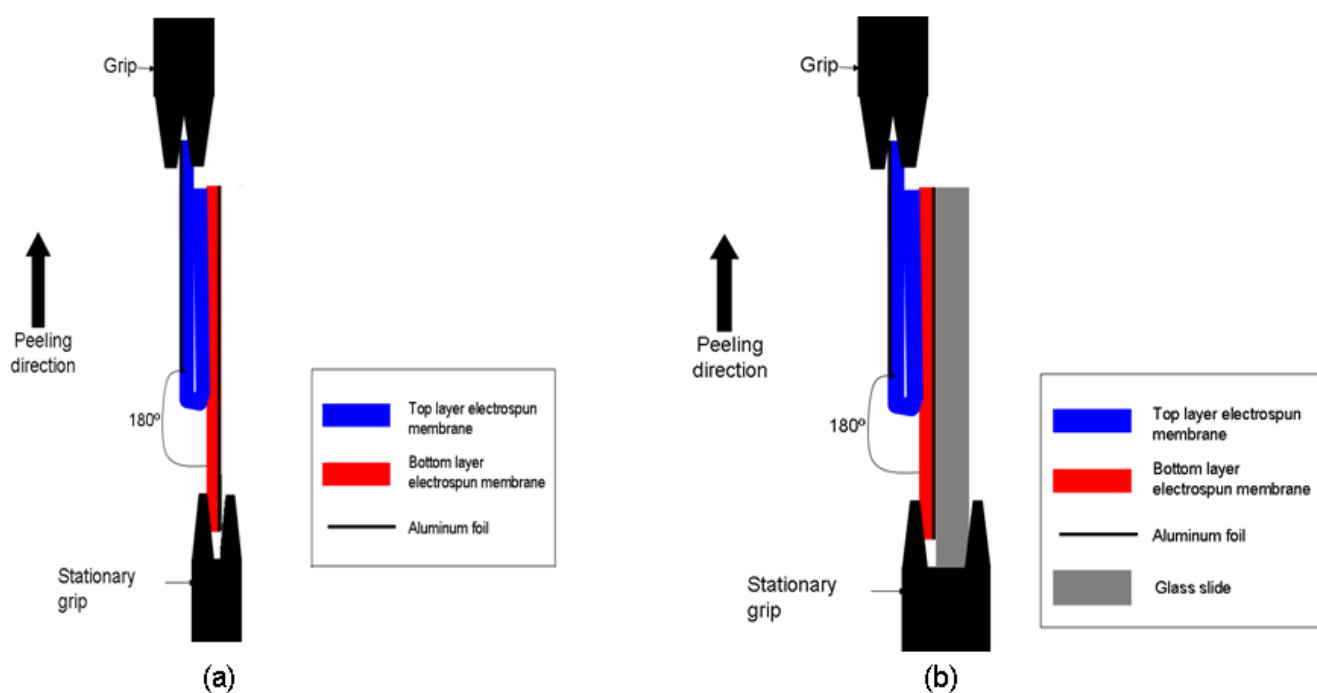
Figure 6-9: Schematic diagrams of peel test configuration used in the study, a) Without glass slide and b) with glass slide to prevent unnecessarily movement of bottom sample

A number of problems were encountered using this experimental procedure such as the high variability in adhesion strength (Table 6-4: without glass slide). The problem was due to the movement of the bi-layer membrane during the test, which in turn affected the peel angle and therefore the measured adhesion strength of the bi-layer membranes. The importance of the peel angle in peel test has been described by Kinloch *et al*. (*222*), where they demonstrated the effect of different peel angles on the measured adhesion strength between a polyethylene film and an aluminium foil. The adhesion strength between the polyethylene film and an aluminium foil was observed to reduce when the peel angle was reduced (*222*).

Table 6-4: Peel strength of typical bi-layer membranes using different systems.

Bi-layer membranes	Without glass slide Peel strength (mN/mm)	With glass slide Peel strength (mN/mm)
Nylon 6/Nylon 6	2.9 ± 2	1.7 ± 0.4
PAN/PAN	4.9 ± 3	3.7 ± 0.6
Copolymer	11.2 ± 4	4.8 ± 0.9
PVDF/PVDF		

The peel system shown in Figure 6-9 (a) was modified by attaching the bottom layer to a glass slide to prevent unnecessarily movement in order to obtain a constant peel angle (Figure 6-9 (b)). As shown in Table 6-4, the backing system was observed to reduce the variability (standard deviation) compared to results in the first system. Hence, the new configuration shown in Figure 6-9 (b) was used to measure the adhesion strength between two electrospun layers in the bi-layer systems.

In the study, the adhesion strength of bi-layer membranes was measured as peel strength (mN/mm) and fracture energy (J/mm^2). The peel strength and fracture energy were calculated using equations 4.2 and 4.3 in Chapter 4.

This section is divided into two parts: 1) Determination of adhesion strength on homogeneous bi-layer membranes and 2) Determination of adhesion strength on heterogeneous bi-layer membranes.

6.6.1 Determination of adhesion strength of homogeneous bi-layer membranes
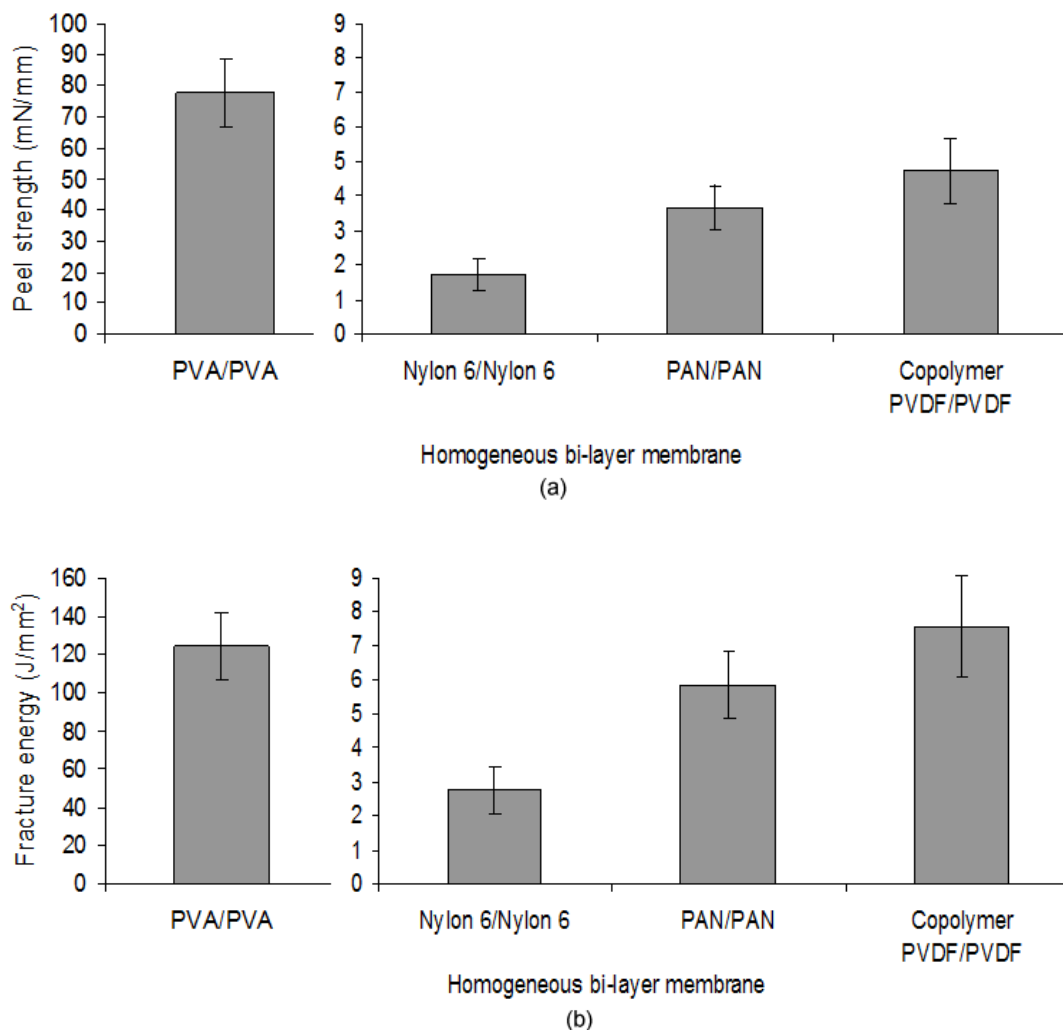
Figure 6-10: Plots of: a) adhesion strengths and b) fracture energy of homogeneous bi-layer electrospun membranes. Values represent 5 measurements.

Figures 6-10 (a-b) predict the adhesion strength and fracture energy of the homogenous bi-layer electrospun membranes. The homogenous bi-layer PVA/PVA exhibited the highest adhesion strength and fracture energy at about 78 mN/mm^2 and 124 J/mm^2 respectively compared to the other homogeneous bi-layer membranes. The high adhesion was probably due to the presence of residual water solvent from the electrospun PVA top layer. When the PVA top layer was electrospun, the residual water solvent has partially dissolved the surface of the PVA bottom layer. The top and bottom layers were then solidified together after the solvent evaporation.
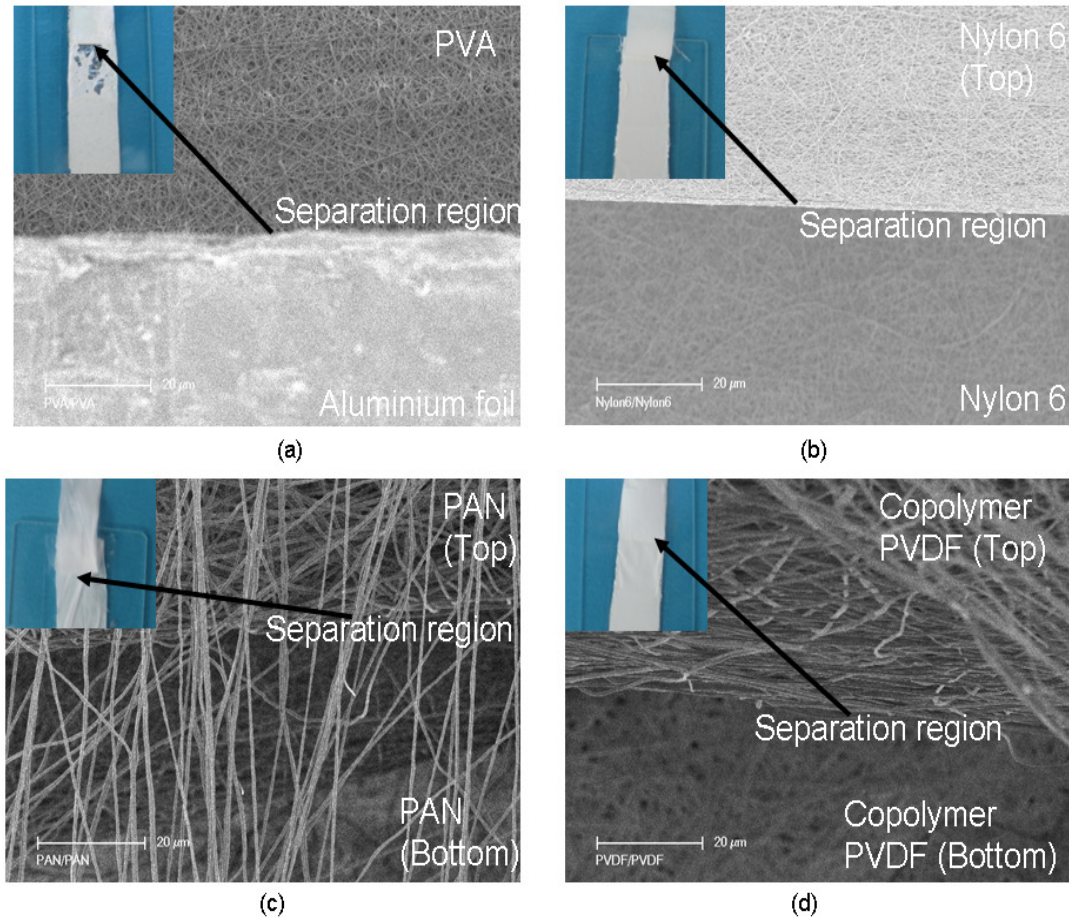
Figure 6-11: SEM images and photographs of membrane fracture for homogeneous bi-layer membranes. a) PVA/PVA, b) Nylon 6/Nylon 6, PAN/PAN and d) copolymer PVDF/PVDF. Arrows indicate the separation regions between the top and bottom layers after the peel test.

Figures 6-11 (a-d) illustrate membranes fracture for the homogeneous bi-layer membranes after peel test. In Figure 6-11 (a), the high adhesion of PVA/PVA layers causes some parts of the membrane to break and peel away from the backing aluminium foil.

For other homogeneous bi-layer membranes such as Nylon 6/Nylon 6, PAN/PAN and copolymer PVDF/PVDF, the adhesion strengths were approximately 17 to 46 times lower than the bi-layer PVA/PVA. The adhesion strength and fracture energy for bi-layer copolymer PVDF/PVDF were approximately 5 mN/mm and 8 J/mm^2, respectively. For bi-layer PAN/PAN, the adhesion strength was about 4 mN/mm and the fracture energy was 6 J/mm^2. The bi-layer Nylon 6/Nylon 6 exhibited the lowest adhesion strength (2 mN/mm) and fracture energy (3 J/mm^2) compared to other homogeneous bi-layer membranes.

The lower adhesion of the bi-layer Nylon 6/Nylon 6, PAN/PAN and copolymer PVDF/PVDF could be due to the physical bonding between the top and bottom layers of the membrane. In the study, the physical bonding refers to the adhesion due to contact areas between the top layer and bottom layer.

In Figure 6-10, the bi-layer copolymer PVDF/PVDF and PAN/PAN showed higher adhesions as compared to bi-layer Nylon 6/Nylon 6. These high adhesions could be due to two factors: 1) contact areas between fibres and 2) the presence of residual solvents in the membrane.

Membranes with large fibre diameter such as PAN (~677 nm) and copolymer PVDF (~570 nm) could give more contact areas with the same fibre diameter. For membranes with small fibre diameter such as Nylon 6 (~109 nm), it was expected that the membrane had less contact areas with the same fibre diameter, as compared to the large fibre diameter.

In addition, the presence of residual solvents in the bi-layer copolymer PVDF/PVDF, PAN/PAN could give higher adhesion as compared to the bi-layer Nylon 6/Nylon 6. The Nylon 6 solvent is much volatile than the solvents used for copolymer PVDF and PAN. Hence, this solvent was expected to evaporate before the Nylon 6 fibres deposited on the grounded collector. This resulted in the deposition of dried fibres in the membrane. These dried fibres exhibited poor attractive force between the top and bottom layer.

In Figures 6-11 (c-d), some fibres were pulled out from the bi-layer copolymer PVDF/PVDF and PAN/PAN. It is suggested that a friction between the top and bottom layers during the peel test generated electrostatic charges on the fibre surfaces. These charges were likely to pull and drag other fibres. The presence of electrostatic charges on fibres was also observed by Shashoua *et. al* (*223*). They reported that the abrasion of identical or different fibres generated electrostatic charges between the fibre surfaces. However, further research is required to confirm the phenomenon.

6.6.2 Determination of adhesion strength on heterogeneous bi-layer membranes

The adhesion strength of homogeneous bi-layers has been discussed in the previous section, where the bi-layer PVA/PVA membrane showed far higher adhesion strength (approximately 78 mN/mm^2) as compared to the bi-layer

copolymer PVDF/PVDF, PAN/PAN and Nylon 6/Nylon 6 membranes. For bi-layer copolymer PVDF/PVDF, PAN/PAN and Nylon 6/Nylon 6, the adhesion strengths were less than 7 mN/mm^2.

The adhesion strength of heterogeneous bi-layer membranes, that is, the adhesion strength between the hydrophilic and hydrophobic layers was also investigated using the peel test configuration shown in Figure 6-9 (b). The results are presented in Figures 6-12 (a-b). The adhesion strengths of heterogeneous bi-layer membranes are typically below 4 mN/mm with the fracture energies being typically below 6 J/mm^2. This shows that the adhesion strengths between the top and bottom layers for heterogeneous bi-layer membranes are considerably low. This low adhesion is probably due to the physical bonding between the top and bottom layer, where these layers are attached due to surface contact between fibres.

Figures 6-12 (a-b) also show that the adhesion strength and fracture energies for bi-layer hydrophilic/hydrophobic and hydrophobic/hydrophilic are similar. This indicates that the contact areas between the hydrophilic/hydrophobic and hydrophobic/hydrophilic are comparable. When these bi-layers have similar contact areas, they will exhibit similar attractive forces.

In addition, the bi-layer PVA/PAN, PAN/PVA, PVA/copolymer PVDF and copolymer PVDF/PVA were found to give higher adhesion as compared to the bi-layer Nylon 6/PAN, PAN/Nylon 6, Nylon 6/copolymer PVDF and copolymer PVDF/Nylon 6. It is suggested that the large fibre diameter of electrospun PVA (~259 nm) have more contact areas with electrospun PAN or copolymer PVDF compared to the small fibre diameter of electrospun Nylon 6 (~109 nm).
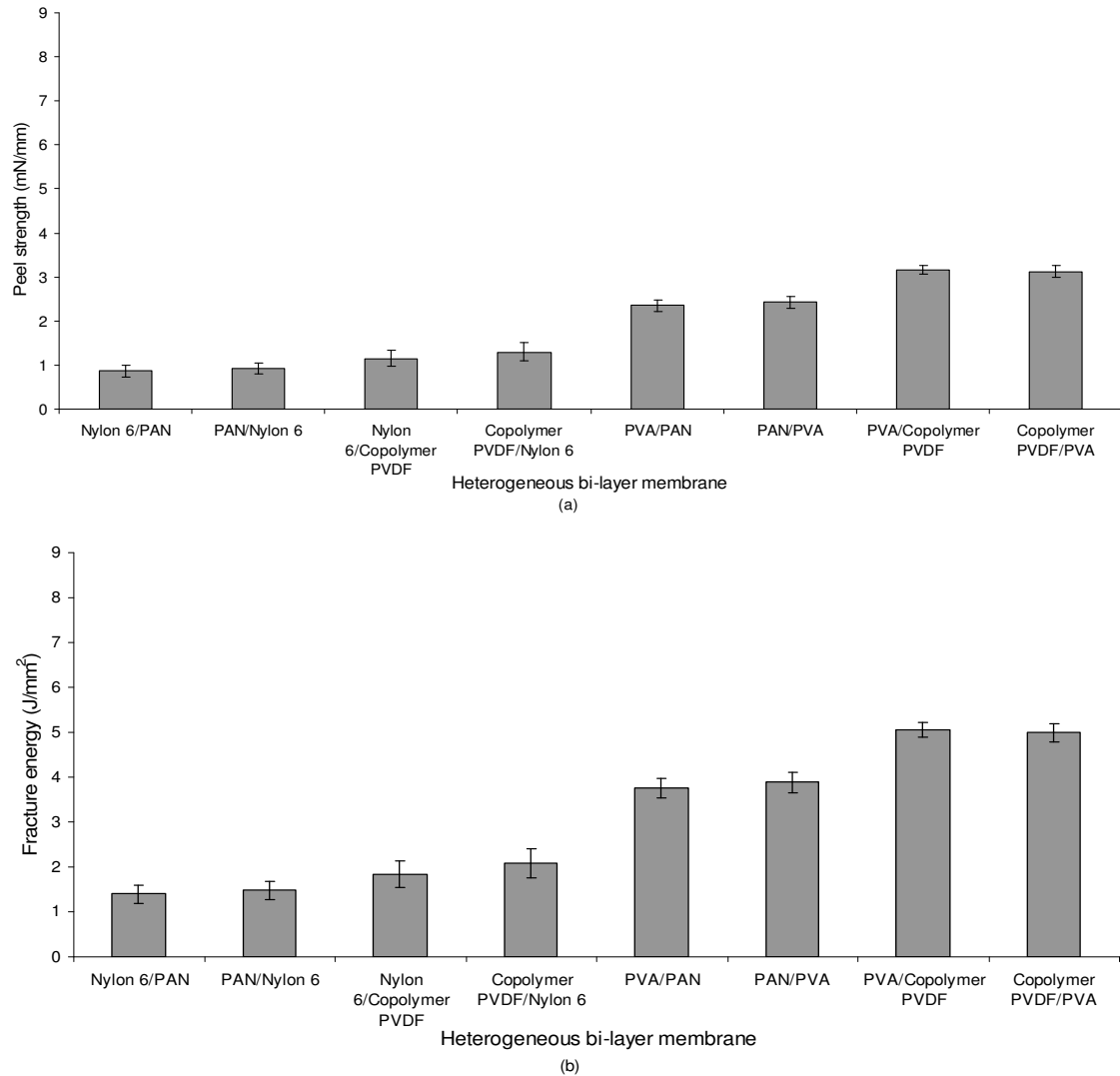
Figure 6-12: Plots of: a) adhesion strengths and b) fracture energy of heterogeneous bi-layer electrospun membranes. Values represent 5 measurements.

Figure 6-13 illustrates the typical membrane fracture after the peel test for heterogeneous bi-layer membranes. Some fibres were pulled away from the electrospun PAN and copolymer PVDF layers. As mentioned earlier in Section 6.6.1, a friction between the top and bottom layers during the peel test generated electrostatic charges on the fibre surfaces. These charges were likely to pull other fibres from both layers. The presence of electrostatic charges on fibres was also observed by Shashoua *et. al* (*223*), where they reported the abrasion of identical or different fibres generated electrostatic charges between the fibre surfaces.
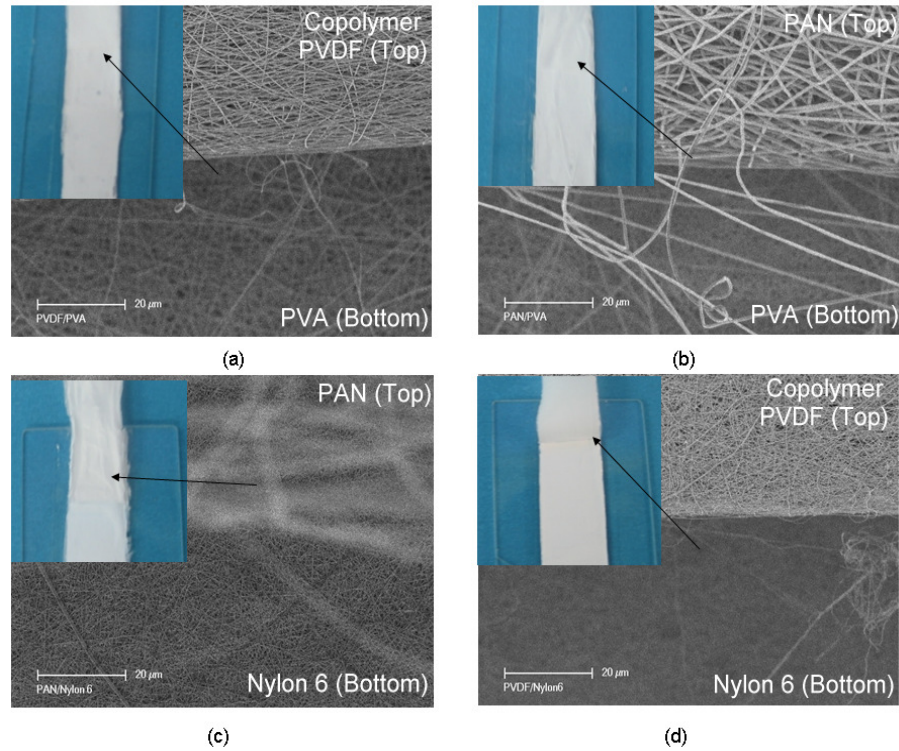
Figure 6-13: SEM images and photographs of membrane fracture for heterogeneous bi-layer membranes. a) copolymer PVDF/PVA, b) PAN/PVA, c) PAN/Nylon 6 and d) copolymer PVDF/Nylon 6. Arrows indicate the separation regions between layers after the peel test.

The current study has developed a new test method to measure adhesion strength between layers in the bi-layer membrane. In addition, the study was able to measure reproducible adhesion strengths for the homogeneous and heterogeneous bi-layer membranes using the method. However, factors affecting the adhesion strength between the top and bottom layer are required for further research.

6.7 Remediation of textile effluent using homogenous and heterogeneous bi-layer electrospun membranes

The physical properties of homogeneous and heterogeneous bi-layer membranes such as membrane thickness, chemical structures, surface wettability (water contact angle), tensile strength and adhesion strength have been investigated in the current study. This section discusses the ability of these membranes to be used as filter media for liquid filtration. The membranes were used to remove suspended solids from textile effluent by observing the changes in turbidity, chemical oxygen demand (COD), conductivity, pH values and fluxes. The results were then compared with a commercial filter media in order to access the feasibility of homogeneous and heterogeneous bi-layer membranes as filter media. However, the electrospun PVA was found to dissolve in water during the filtration. Hence, studies on the remediation of textile effluent using electrospun PVA membrane were not pursued in the current study. The study investigated other membranes such as electrospun Nylon 6, PAN, copolymer PVDF and commercial membranes for the remediation of textile effluent.

This section is divided into a number of sub-sections:

a) Characterization of homogeneous bi-layer membranes and commercial membrane

b) Flux of membranes

c) Properties of feed and permeate using homogeneous bi-layer and commercial membranes

d) Characterization heterogeneous bi-layer hydrophilic/hydrophobic and hydrophobic/hydrophilic membranes

e) Flux of the heterogeneous bi-layer membranes

Details on the sub-sections are outlined below.

6.7.1 Characterization of homogeneous bi-layer membranes and commercial membrane

Membranes properties (fibre diameter and pore sizes) are tabulated in Table 6-5. In the product specification, the average pore size of commercial Nylon membrane was reported to be 0.45µm (*10*). However, our measurements indicated a spread of pore sizes ranging from 0.17 to 2.5µm.

As with single layer electrospun membrane, the fibre diameter has affected the pore sizes of bi-layer membranes. The fine fibre diameter of electrospun Nylon 6 was found to give smaller pore sizes for the homogeneous bi-layer Nylon 6/Nylon 6. The homogeneous bi-layer PAN/PAN and copolymer PVDF/PVDF exhibit a broad range of pore sizes probably due to the high variability of PAN and copolymer PVDF fibre diameters as compared to the electrospun Nylon 6 membranes. Results presented in Table 6-5 also show that the pore sizes of homogeneous are smaller than the single layer membrane (Section 5.6). This could be due to the increase of membrane thickness for the bi-layer membranes.

Table 6-5 also shows that there is no fibre diameter for commercial Nylon 6. This indicates that the commercial Nylon is not a fibrous membrane, but it is a membrane filter. The morphological structures of the commercial Nylon 6 as well as the homogeneous bi-layer Nylon 6/Nylon 6, PAN/PAN and copolymer PVDF/PVDF are illustrated in Figures 6-14 (a-d).

Table 6-5: Properties of homogenous bi-layer membranes and commercial membrane.

Membrane	Fibre diameter (nm)	Average pore size shown in the product specification (µm) (10)	Pore size range measured in the study (µm)
Commercial Nylon	Nil	0.45	0.17 – 2.5
Nylon 6/ Nylon 6	109 $\pm$ 16	NA	0.05-0.26
PAN/PAN	677 $\pm$ 205	NA	0.56-2.69
Copolymer PVDF/PVDF	570 $\pm$ 105	NA	0.20-2.00

NA: Not applicable because these membranes were measured experimentally using capillary flow porometry
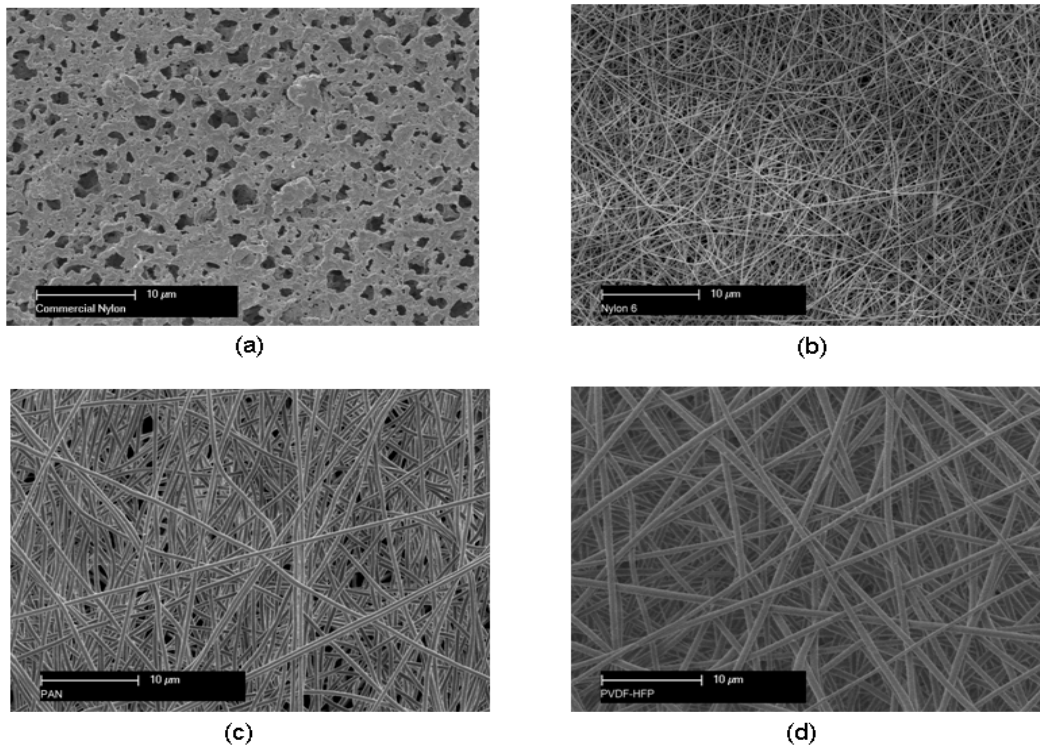
Figure 6-14: SEM images of membranes, a) Commercial Nylon, homogenous bi-layer electrospun, b) Nylon 6/ Nylon 6, c) PAN/PAN and d) copolymer PVDF/PVDF.

6.7.2 Flux of membranes

Figures 6-15 (a-d) show the plots of permeate fluxes of a control water sample (deionised water) and the textile effluent passing through a commercial Nylon membrane, homogenous bi-layer electrospun Nylon 6/Nylon 6, PAN/PAN and copolymer PVDF/PVDF membranes. The fluxes of all the membranes except bi-layer copolymer PVDF/PVDF increase with increasing amount of applied pressure from 5 to 20psi. Pressures higher than 20psi were not quantified because some electrospun membranes were damaged.

Figure 6-15 (a) illustrates flux of textile effluent and control (deionised water) at 5, 12 and 20 psi for commercial Nylon membrane. The membrane showed greater flux than the homogenous bi-layer Nylon 6/Nylon 6 because of larger pore sizes. Due to its larger pore sizes, more liquid and suspended solid particles passed through the commercial membrane. This explains the higher flux through the commercial membrane compared to the homogenous bi-layer Nylon 6/Nylon 6 membrane. As a result, the filtration time for commercial membrane was approximately 89% faster than the bi-layer Nylon 6/Nylon 6 (Figure 6-16). In

addition, an accumulation of green particles was observed on the commercial Nylon surfaces. This shows that the membrane was able to capture large solid particles from liquid (Figure 6-17 (a).

The homogenous bi-layer Nylon 6/Nylon 6 exhibited the lowest flux for both control sample (deionised water) and textile effluent compared to the other membranes (Figure 6-15 (b)). This is due to the fact that this membrane has the smallest pore sizes compared to the other membranes. Due to its small pore sizes, some of the suspended solid formed a cake on the membrane surface (Figure 6-17 (b)). This resulted in membrane fouling for the bi-layer Nylon 6/Nylon 6. Fouling is defined as blockage due to particles caught in the membrane or filter media (*175, 190*). As the feed flows through the membrane, the suspended solids start to accumulate and get embedded into the membrane pores, eventually blocking the flow. This blockage resulted in the reduction of the permeate flux as shown in Figure 6-16 (b). Due to the fouling, the filtration time for 30 ml effluent was approximately 45 minutes, which was longer compared to other membranes. Typical plots of flux versus time at 5 psi and 12 psi can be found in Appendix II.
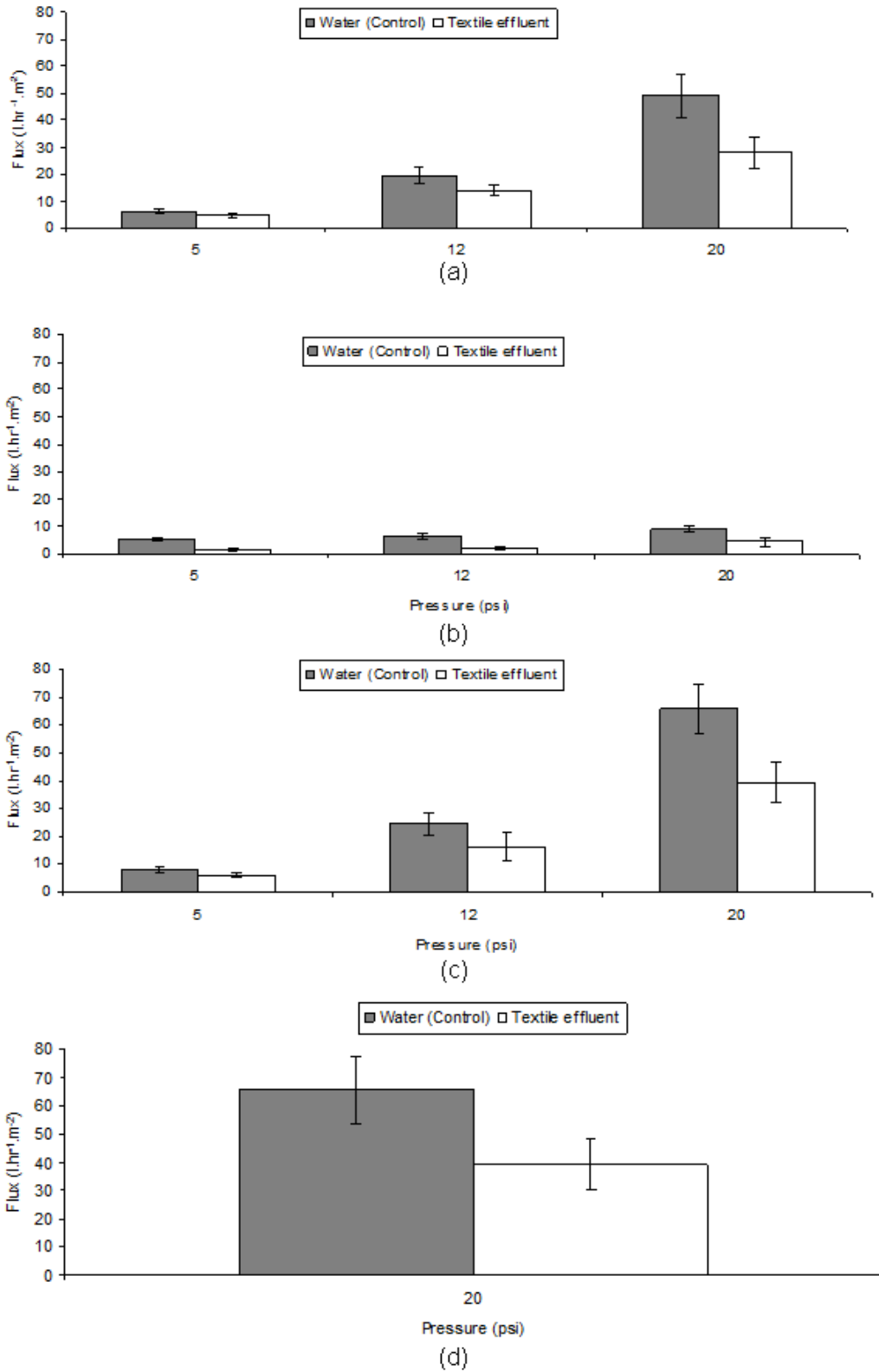
Figure 6-15: Plots of fluxes for control (deionised water) and effluent at different applied pressures for: a) commercial Nylon, homogenous bi-layer electrospun: b) Nylon 6/Nylon 6, c) PAN/PAN and d) PVDF/PVDF. Error bars indicate three samples for each test.
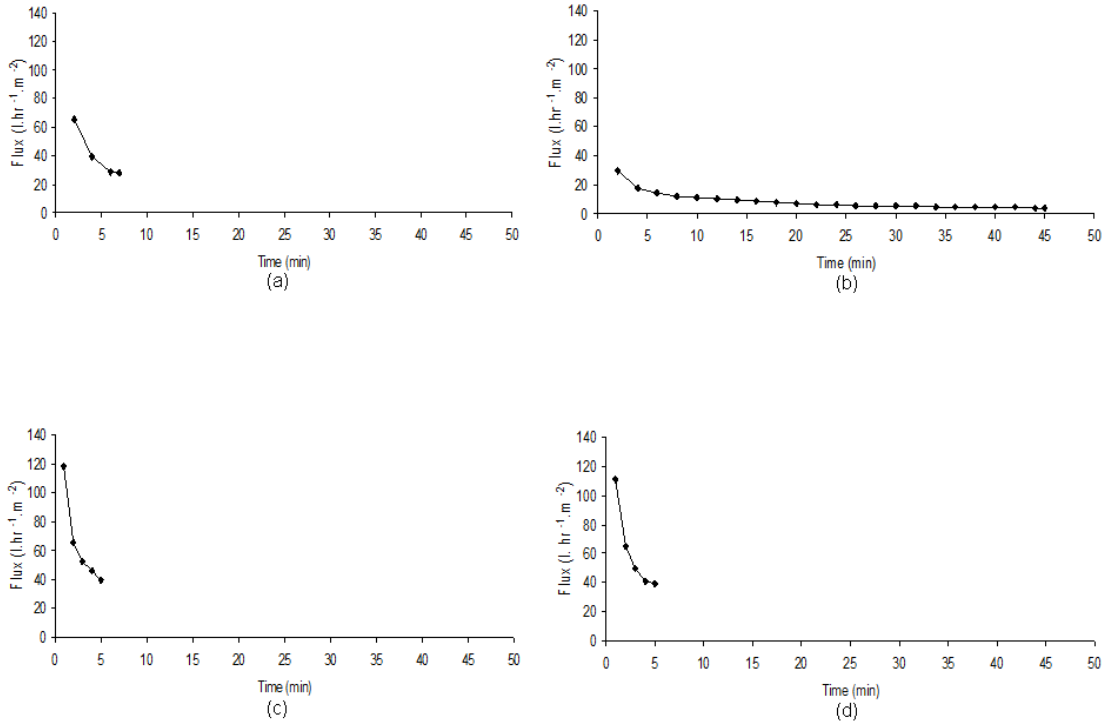
Figure 6-16: Typical plots of flux versus time for a) commercial membrane homogeneous bi-layer

b) Nylon 6/Nylon 6, c) PAN/PAN and d) copolymer PVDF/PVDF. Applied pressure was 20 psi.
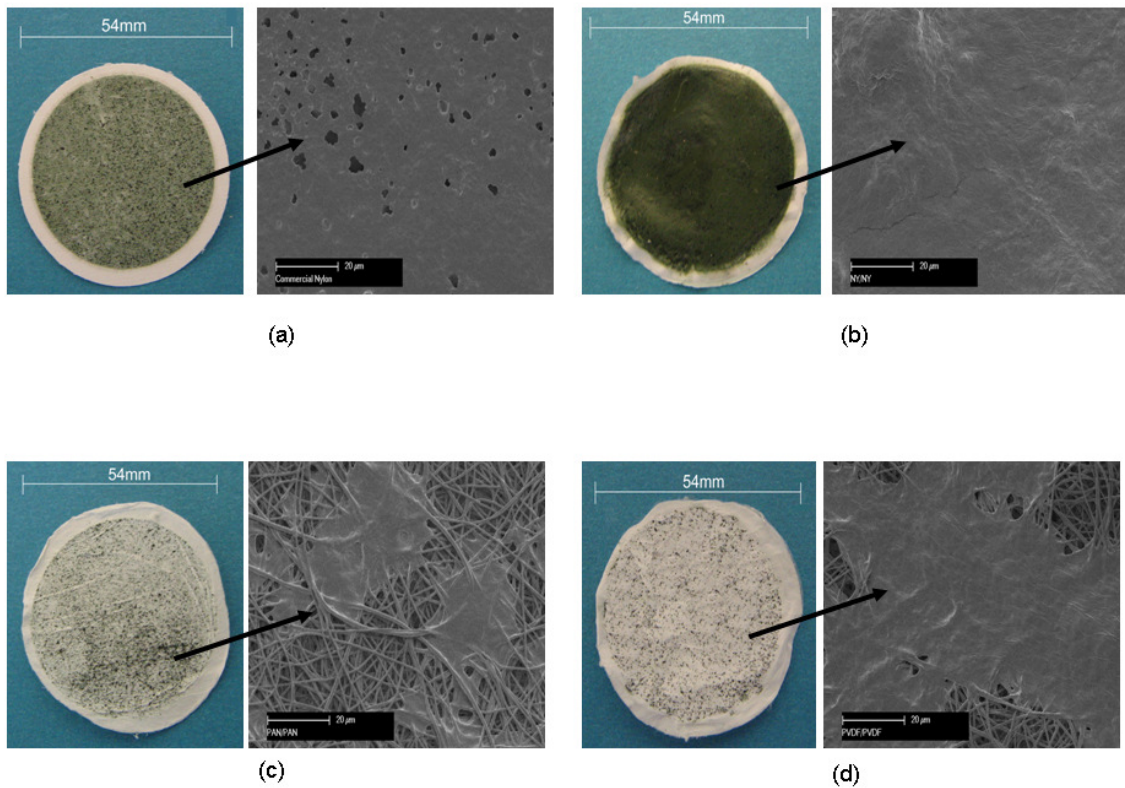
Figure 6-17: Photographs and SEM images of typical membranes after filtration. a) commercial

Nylon, homogenous bi-layer electrospun: b) Nylon 6/Nylon 6, c) PAN/PAN and d) PVDF/PVDF.

Applied pressure is 5 psi.

182

In the case of homogenous bi-layer electrospun PAN/PAN, both water control and effluent fluxes were higher than for the Nylon 6 bi-layer due to the larger pore diameter permitting more water and suspended solids to pass through the membrane (Figure 6-15 (c)). The larger pore diameter was observed to capture smaller amounts of suspended solids on the membrane surface (Figure 6-17 (c)). In addition, the initial and end fluxes for homogenous bi-layer PAN/PAN membrane was higher than the bi-layer Nylon 6/Nylon 6 because, the membrane did not suffer from membrane fouling to the same degree (Figure 6-16 (c)).

Both homogenous bi-layer copolymer PVDF/PVDF and bi-layer PAN/PAN have approximately the same membrane pore size. In addition, the bi-layer copolymer was also found to capture smaller amounts of solids, as shown in Figure 6-17 (d)). However, in the case of homogenous bi-layer copolymer PVDF/PVDF the transport of the water control and effluent sample through the membrane was inhibited particularly below than 20 psi (Figure 6-15 (d)). This was attributed to a larger contact angle of copolymer PVDF (approximately 132°), which restricted the flow sample through membrane pore (Figure 6-18). A similar situation occurs with PAN until the membrane wets out after 17 seconds. When the membrane wets out, it allows the transportation of solution at 5 and 12psi. For homogenous bi-layer Nylon 6/Nylon 6 and commercial Nylon, the lower contact angles (Figure 6-18) permit the flow of aqueous based permeate samples at 5psi, 12psi and 20psi.

Membrane fouling due to hydrophobicity has been reported in a number of studies (*195, 198*). However, the current study demonstrated that membrane fouling can be reduced by having larger pore sizes in the membrane. The larger pore sizes of the homogeneous bi-layer copolymer PVDF/PVDF and PAN/PAN allow more liquid to pass through the membranes. This results in the reduction of membrane fouling as compared to homogenous bi-layer Nylon 6/Nylon 6 membranes
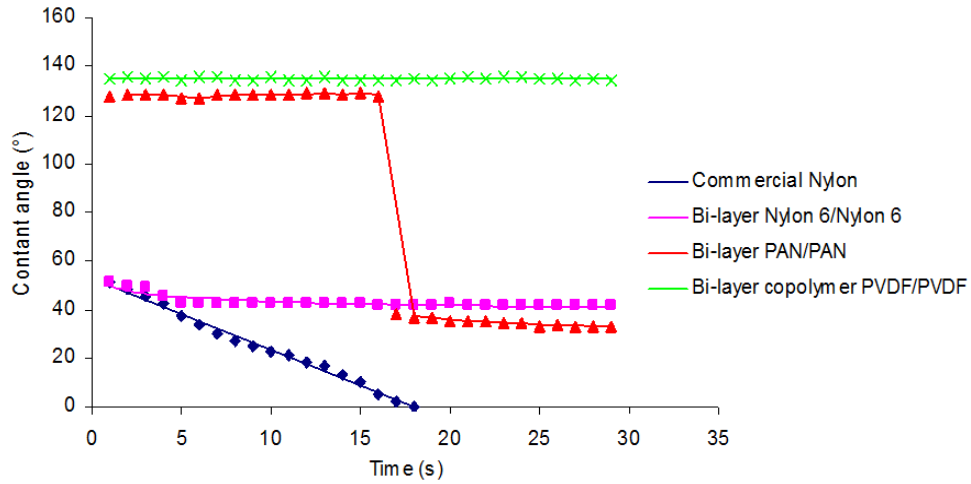
Figure 6-18: Water contact angles for commercial Nylon and homogenous bi-layer electrospun membranes.

6.7.3 Properties of feed and permeate

In Table 6-6, the commercial Nylon membrane removed 33 to 35% of suspended solids as pressure decreased from 20psi to 5psi, respectively. As previously mentioned, the presence of a large pore diameter allowed more suspended solids to pass though the membrane, resulting in a cloudy permeate as shown in Figure 6-19 (c). The large pore of the membrane was also found to give high values of COD in a range of 1920 to 2000 mg/L. In addition, there were no changes in pH values and conductivities. This indicates that the membrane is unable to reduce COD values as well as pH and conductivities.
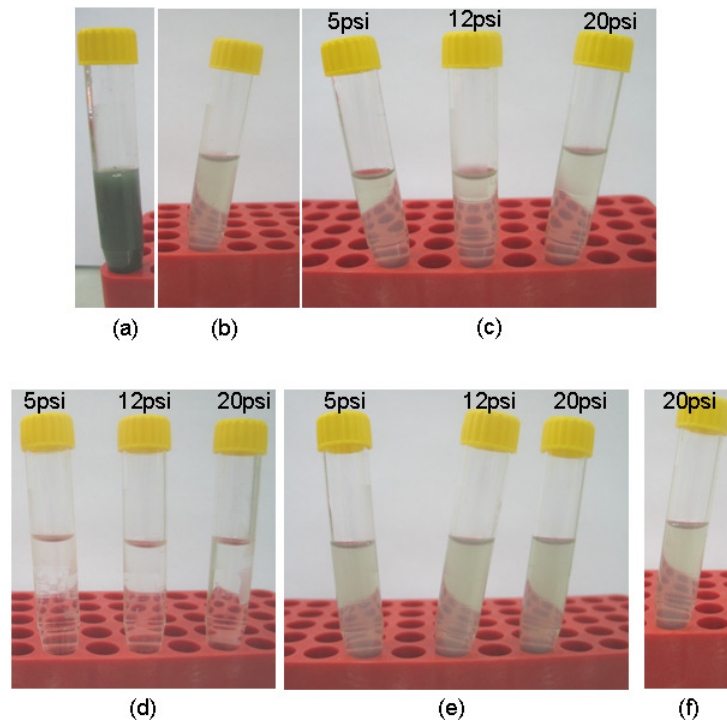
Figure 6-19: Photographs showing the clarity of: a) raw effluent, b) feed (pre-filtered effluent), permeate using: c) commercial Nylon, bi-layer homogenous electrospun: d) Nylon 6/Nylon 6, e) bi-layer PAN/PAN and f) copolymer PVDF/PVDF.

Although the homogenous bi-layer Nylon 6/Nylon 6 membrane exhibited the lowest fluxes, this membrane gave the best removal of suspended solids (approximately 99%) and also the best clarity (Figure 6-19 (d)). In Table 6-6, the COD values were only slightly affected by the applied pressure. The pH values and conductivities were also not affected by the filtration process. These results demonstrate that the structures of electrospun Nylon 6 nanofibres are still unable to improve the pH values and conductivities. The accumulation of the nanofibres forms different pore structures as compared to other materials such as ion exchange resins. Ion exchange resins are commonly used for water purification. Due to its highly developed pore structures, the ion exchange resins have the ability to improve pH values and conductivities of a liquid. The electrospun Nylon 6, however, shows excellent properties in the removal of suspended solids from a liquid. In Figure 6-19 (d), a clear liquid was observed after the filtration process.

Poor separation of suspended solids from effluent was also observed for homogenous bi-layer PAN/PAN. In Figure 6-19 (e), a cloudy permeate was observed after filtration, indicating that some suspended solid particles passed through the larger pores of the bi-layer PAN/PAN membrane. Regardless of

pressure used, the membrane exhibited poor solid removal (16 to 18%) and high COD values ranging from 2230 to 2340 mg/L (Table 6-6).

Similar results were obtained for homogenous bi-layer copolymer PVDF/PVDF. In Table 6-6, the membrane also gave a small reduction in suspended solids as well as high COD values. As a result, a cloudy permeate was observed for the membrane (Figures 6-19 (f)). No changes in pH values and conductivity were observed in the case of both membranes.

Table 6-6: Properties of feed and permeate using commercial Nylon, homogenous bi-layer Nylon 6/Nylon 6, PAN/PAN and copolymer PVDF/PVDF.

Parameter	Feed		Permeate									
	Raw pigment	Pre-filtered pigment	Commercial Nylon membrane			Bi-layer Nylon 6/Nylon 6 membrane			Bi-layer PAN/PAN membrane			Bi-layer PVDF/PVDF membrane
Applied pressure (psi)	NA	NA	5	12	20	5	12	20	5	12	20	20
Turbidity (NTU)	>4000	183 ± 1	119 ± 1	121 ± 2	123 ± 3	1.82 ± 0.1	1.85 ± 0.2	1.97 ± 0.2	150 ± 2	151 ± 3	154 ± 4	154 ± 3
Turbidity (%)	NA	NA	35	34	33	99	99	99	18	17	16	16
COD (mg/L)	Off scale	2370 ± 1	1920 ± 5	1940 ± 4	2000 ± 4	800 ± 4	820 ± 4	840 ± 5	2230 ± 6	2280 ± 7	2340 ± 7	2350 ± 7
pH	6.75 ± 0.1	7.36 ± 0.1	7.35 ± 0.3	7.35 ± 0.4	7.33 ± 0.5	7.35 ± 0.2	7.37 ± 0.3	7.37 ± 0.4	7.33 ± 0.4	7.32 ± 0.4	7.34 ± 0.4	7.33 ± 0.3
Conductivity (µS/m)	226 ± 1	223 ± 1	219 ± 2	219 ± 2	220 ± 3	218 ± 2	219 ± 1	219 ± 2	222 ± 3	222 ± 3	223 ± 1	222 ± 1

6.7.4 Characterization of the heterogeneous bi-layer hydrophilic/hydrophobic and hydrophobic/hydrophilic membranes

The pore sizes for homogeneous bi-layer membranes have been investigated (see Table 6-5). For heterogeneous bi-layer membranes, the pore sizes are tabulated in Table 6-7.

Table 6-7: Pore sizes of heterogeneous bi-layer membranes.

Bi-layer membrane	Range of pore sizes (µm)
Nylon 6/PAN	0.14-0.88
PAN/Nylon 6	0.16-0.77
Nylon 6/copolymer PVDF	0.15-0.96
Copolymer PVDF/Nylon 6	0.16-0.88

In Table 6-7, the ranges of pore sizes for the bi-layer Nylon 6/PAN and PAN/Nylon 6 are similar. Similar trend was also observed for the bi-layer Nylon 6/copolymer and copolymer PVDF/Nylon 6, where both membranes showed similar range of pore sizes.

In addition, the range of pore sizes for the heterogeneous bi-layer membrane is in between the pore sizes of each component in membrane. For example, the pore sizes for the copolymer PVDF/Nylon 6 was in a range of 0.16 to 0.88 µm, which was in between the pore size of single layer Nylon 6 (0.13 to 0.41 µm) and single layer copolymer PVDF (0.67-3.03 µm)

6.7.5 Flux of heterogeneous bi-layer membranes

Results presented in Figure 6-20 show that the permeate flux for homogeneous bi-layer Nylon 6/Nylon 6, heterogeneous Nylon 6/PAN and Nylon 6/copolymer PVDF are comparable, confirming that that the smaller pore diameter of Nylon 6 favoured quick fouling and lower flux as compared to the commercial membrane.
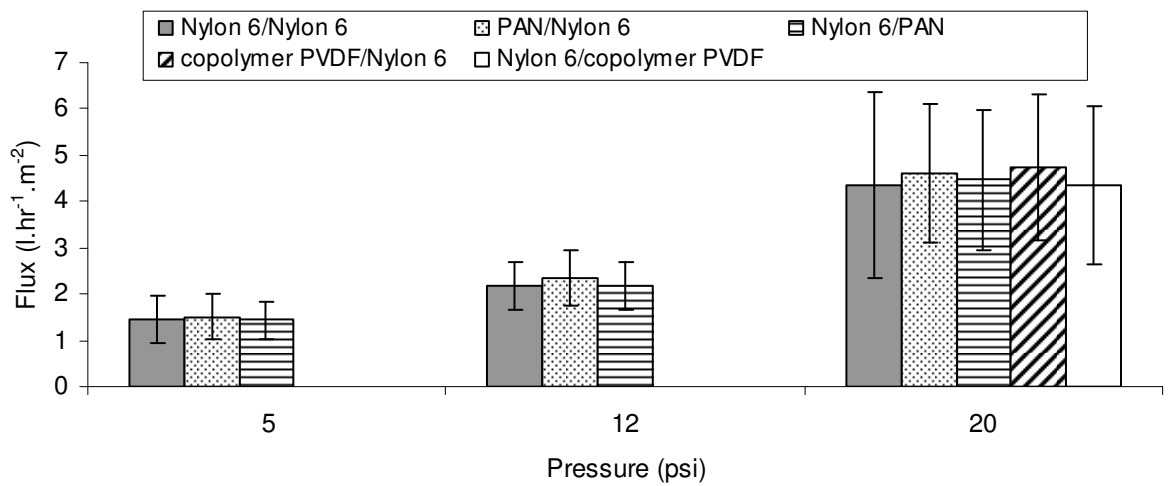
Figure 6-20: Plots of flux versus pressure for heterogeneous bi-layer membranes and homogeneous bi-layer Nylon 6/Nylon 6.
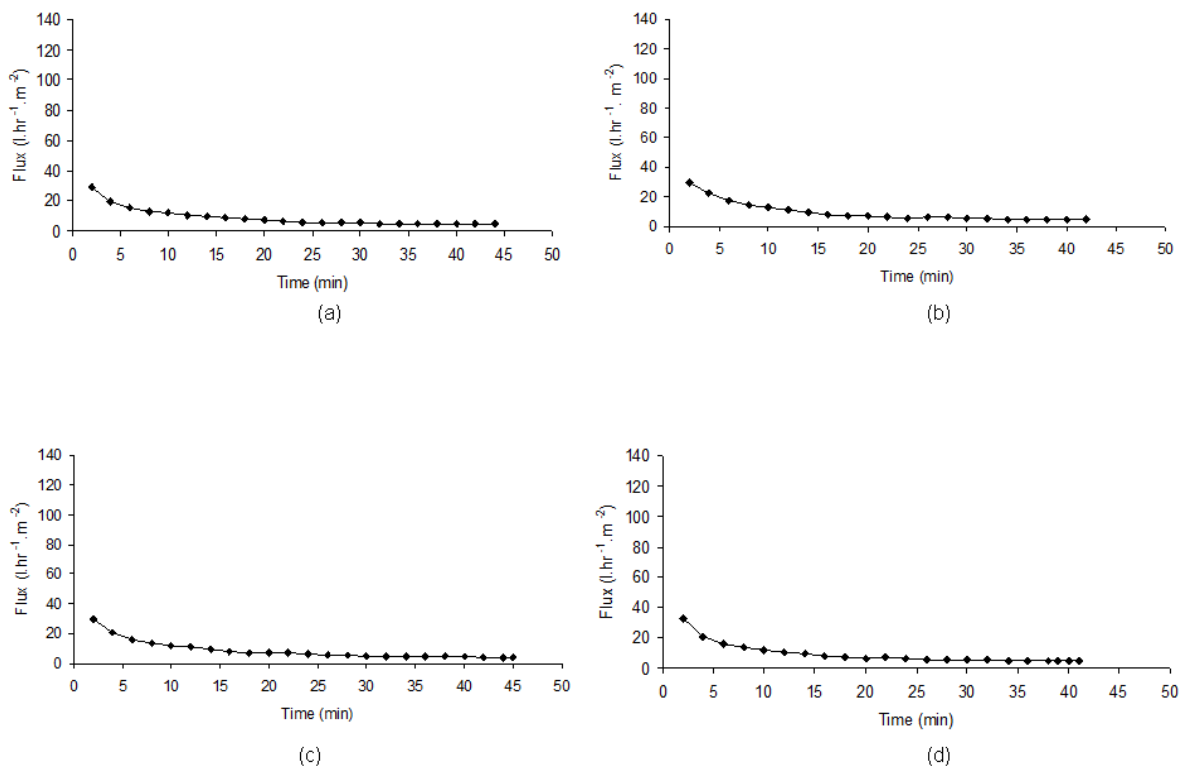
Figure 6-21: Typical plots of flux versus time for heterogeneous bi-layer: a) Nylon 6/PAN, b) PAN/Nylon 6, c) Nylon 6/copolymer PVDF and d) copolymer PVDF/Nylon 6. Applied pressure was 20 psi.

As with homogeneous bi-layer Nylon 6/Nylon 6, the permeate fluxes for the heterogeneous bi-layer Nylon 6/PAN and Nylon 6/copolymer PVDF were low due to membrane fouling. Due to the fouling, the filtration times for 30 ml effluent were approximately 42 to 45 minutes similar to the homogeneous bi-layer Nylon 6/Nylon 6 (Figures 6-16 and 6-21). As the feed flows through the membrane, the

solids start to accumulate and get embedded into the membrane pores. This results in the blockage of the flow.
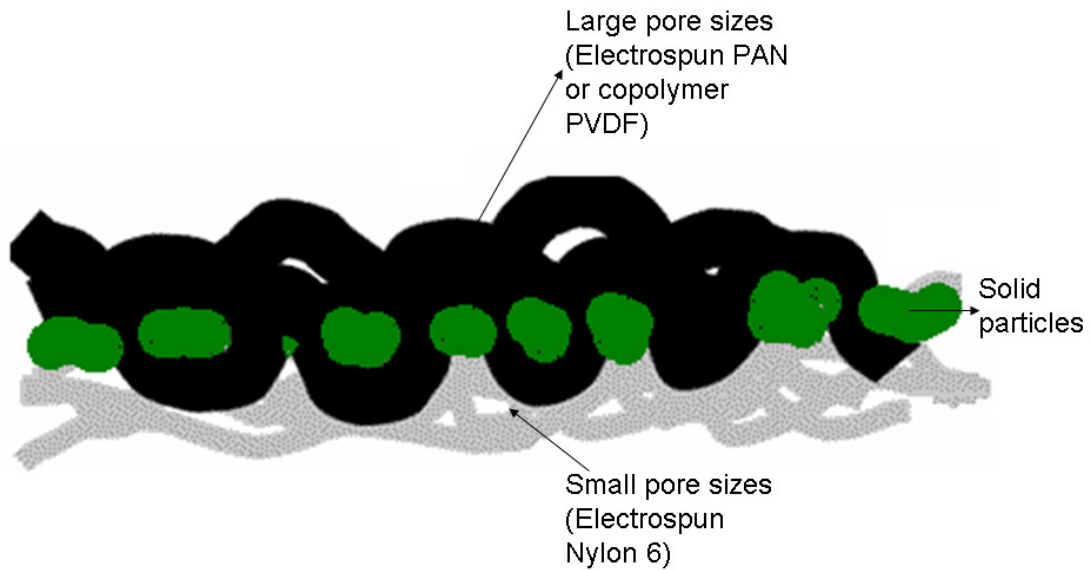
Figure 6-22: Schematic representation of heterogeneous bi-layer electrospun (large pore/small pore).

For bi-layer PAN/Nylon 6 and copolymer PVDF/Nylon 6, these bi-layers also exhibited low flux because of membrane fouling. The presence of large pore sizes did not facilitate the reduction of the membrane fouling. The solid particles were observed to trap in between the upper and bottom layer, as shown in Figure 6-22. This results in membrane fouling as well as blockage for the filtration process.

6.7.6 Properties of feed and permeate

The turbidity, COD, pH and conductivity of permeate samples were compared with the bi-layer Nylon 6/Nylon 6 (Table 6-8). Changing the bi-layer system with two different polymeric nanofibres maintains the same quality as the homogenous bi-layer Nylon 6/Nylon 6 at different applied pressures. As expected the smaller pore diameter contributed from Nylon 6 provides clear permeate with a 99% turbidity reduction (Figures 6-23 (b-c)). Increasing the applied pressures gave only a slight decrease in COD values, but it did not affect pH or conductivities of the permeate.
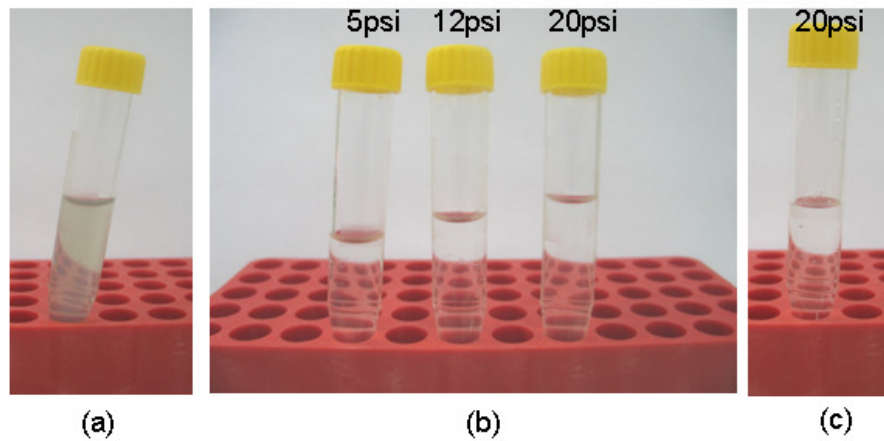
Figure 6-23: Photographs showing the clarity of: a) feed (pre-filtered effluent), permeate using: b) heterogeneous bi-layer electrospun PAN/Nylon 6 and c) heterogeneous bi-layer electrospun PVDF/Nylon 6.

From this experiment, it shows that the homogeneous and heterogeneous bi-layer electrospun membranes were able to remove suspended solids from textile effluent using a lab scale filtration system. However, more work is required to prevent membrane fouling using electrospun membrane, while achieving high quality of water.

Table 6-8: Properties of feed and permeate using homogenous bi-layer Nylon 6/Nylon 6, heterogeneous bi-layer Nylon 6/PAN, PAN/Nylon 6, Nylon 6/copolymer PVDF and copolymer PVDF/Nylon 6 membranes

Parameter	Feed	Permeate										
	Pre-filtered pigment	Bi-layer Nylon 6/Nylon 6 membrane			Bi-layer Nylon 6/PAN membrane			Bi-layer PAN/Nylon 6 membrane			Bi-layer Nylon 6/copolymer membrane	Bi-layer copolymer PVDF/Nylon 6 membrane
Applied pressure (psi)	NA	5	12	20	5	12	20	5	12	20	20	20
Turbidity (NTU)	183 ± 1	1.82 ± 0.1	1.85 ± 0.2	1.97 ± 0.2	1.81 ± 0.3	1.83 ± 0.2	1.89 ± 0.1	2.00 ± 0.1	1.83 ± 0.3	1.95 ± 0.2	2.05 ± 0.3	2.00 ± 1
Turbidity (%)	NA	99	99	99	99	99	99	99	99	99	99	99
COD (mg/L)	2370 ± 1	800 ± 4	820 ± 4	840 ± 5	820 ± 3	820 ± 5	850 ± 6	820 ± 3	820 ± 6	840 ± 3	840 ± 3	830 ± 8
pH	7.36 ± 0.1	7.35 ± 0.2	7.37 ± 0.3	7.37 ± 0.4	7.35 ± 0.1	7.37 ± 0.1	7.35 ± 0.1	7.32 ± 0.4	7.35 ± 0.3	7.35 ± 0.5	7.37 ± 0.5	7.32 ± 0.4
Conductivity (µS/m)	223 ± 1	218 ± 2	219 ± 1	219 ± 2	219 ± 1	219 ± 2	220 ± 2	220 ± 2	219 ± 3	219 ± 2	220 ± 1	220 ± 2

192

CHAPTER 7 CONCLUSION

Fundamental studies on homogeneous and heterogeneous bi-layer electrospun membranes have been carried out in this study. The study emphasizes the fabrication, characterization and performance of the membranes fabricated from hydrophilic and hydrophobic polymers using electrospinning. A preliminary study on the optimisation of electrospinning conditions for hydrophilic and hydrophobic polymers was undertaken prior to the fabrication of bi-layer membranes. The optimal conditions for each polymer were based upon solutions with good electrospinning-ability, uniform cylindrical fibres and membrane structures, as well as large coverage area.

Nylon 6 and polyvinyl Alcohol (PVA) were selected as hydrophilic polymers, whereas polyacrylonitrile (PAN) and copolymer Poly(vinylidene fluoride)-Hexafluoropropylene (copolymer PVDF) were selected for hydrophobic polymers. All the polymers tested were characterized with respect to their propensity to produce electrospun nanofibre membranes. The study demonstrated that the optimal electrospinning conditions such as applied voltage were different dependent on the polymer used. The optimal applied voltage for electrospun Nylon 6, PVA, PAN and copolymer PVDF were 32, 25, 9 and 15 kV, respectively. A distance of 20 cm was found to give optimal needle tip-to-collector distance for all polymers tested because the polymer jets had sufficient flight time to evaporate which resulted in uniform cylindrical fibres and membrane structures. The study found that the hydrophilic electrospun membranes of Nylon 6 and PVA exhibited smaller average fibre diameter compared to the hydrophobic polymer membranes of copolymer PVDF and PAN. The resultant average fibre diameters for electrospun Nylon 6, PVA, PAN and copolymer PVDF were 109 ± 16, 259 ± 39, 677 ± 205 and 570 ± 105 nm, respectively.

The resultant fibre diameters of electrospun Nylon 6, PVA, PAN and copolymer PVDF formed different pore sizes. Electrospun Nylon 6 and PVA, with finer fibre diameters, provided smaller pore sizes. The range of pore sizes for electrospun Nylon 6 measured by the capillary flow porometry was in a range of 0.13 to 0.41 µm. For electrospun PVA, the range of the membrane pore sizes was 0.47 to 1.74 µm. Membranes with larger fibre diameters such as electrospun PAN and copolymer PVDF produced bigger pore sizes. The range of pore sizes for

electrospun PAN was 0.5 to 3.65 µm, whereas for electrospun copolymer was 0.67 to 3.03 µm. In addition, the electrospun PAN and copolymer PVDF demonstrated broader range of pore sizes because of their high variability in fibre diameters. The study also showed that the fine fibre diameter and small pore sizes gave lower surface roughness for the electrospun Nylon 6 and PVA membranes as compared to the PAN and copolymer PVDF membranes. The membrane surface areas for electrospun Nylon 6 and PVA are much higher than the copolymer PVDF probably due to the fine fibre diameter of electrospun Nylon 6 and PVA. Membranes with larger fibre diameters, such as electrospun PAN should showed lower surface area. However, the presence of wrinkle structures on the PAN fibre surfaces provided high surface area for electrospun PAN membrane.

The study has developed a non-contact technique to measure the thickness of electrospun membranes using a white light profilometry. The initial study of this new technique has already been published in one of the refereed journals. A number of advantages were observed using this technique such as the use of white light to scan the sample does not damage and compress the sample. The white light profilometry can measure electrospun thicknesses in the nanometer range (down to 50 nm), which is beyond the limit of a micrometer. From the experimentations, the thickness of electrospun Nylon 6, PVA, PAN and copolymer PVDF is in a range of 40 to 51 µm.

From the FTIR analysis, it was found that the electrospinning was able to transform crystal phases of polymers such as Nylon 6 and PVDF. Changes in the crystal phases for the polymers were confirmed by the wide angle X-ray diffraction (WAXD) diffraction peaks.

For surface wettability, the electrospun Nylon 6 and PVA membranes gave complete wetting, showing that both polymeric membranes were hydrophilic. The copolymer PVDF prevented water droplets from penetrating through the membranes, showing the hydrophobic of the polymer. The presence of wrinkle structures on electrospun PAN surfaces was also observed to restrict the penetration of water droplets through the membrane.

From the results above, the physical properties of electrospun membranes were different dependent on the polymer used. For, bi-layer membranes, two forms of bi-layers were fabricated: 1) homogeneous (membranes composed of two identical polymers) and heterogeneous bi-layer membranes (membranes

composed of two different polymers such as hydrophobic and hydrophilic). Most of the properties of homogeneous bi-layers are comparable to the single layers, (except membrane thickness and pore sizes). The thicknesses of homogeneous and heterogeneous bi-layer membranes as measured by the non contact white light profilometry were in a range of 82 to 99 µm. For single layer, the thickness was less than 51 µm.

For the FTIR analysis, the IR spectra for homogeneous and heterogeneous bi-layers varied depending on polymer used. As with single layers, crystal phases of the bi-layer membranes were observed to change after electrospinning.

The study also showed that the homogeneous bi-layer membranes provided similar water contact angles to single layer membranes. However, water contact angles for heterogeneous bi-layer membranes varied depending on the polymer used. The heterogeneous bi-layer Nylon 6/PAN and Nylon 6/copolymer PVDF exhibited water contact angles more than 90°. This is due to the presence of electrospun PAN and copolymer PVDF as base membrane, which prevents further downward movement of the droplet. However, the presence of hydrophobic PAN and copolymer PVDF in heterogeneous bi-layer PVA/PAN and PVA/copolymer PVDF did not show similar results to Nylon 6/PAN and Nylon 6/copolymer PVDF. The droplet was found to spread over PVA surfaces, which resulted in water contact angles lower than 90°. For heterogeneous bi-layer PAN/Nylon 6, copolymer PVDF/Nylon 6, PAN/PVA and copolymer PVDF/PVA, the membranes gave water contact angles more than 90°. This was attributed to the hydrophobicity of PAN and copolymer PVDF as top layers, which prevented the water droplet from directly penetrating through the membranes.

The tensile properties (such as tensile strength, strain and modulus) of homogenous and heterogeneous bi-layer membranes were also investigated in the study. The tensile stress of the homogeneous bi-layer membrane was affected by the membrane pore sizes and bonding between fibres in the membrane. It was found that membranes with smaller pore sizes and strong fibre-to-fibre bonding such as homogeneous bi-layer Nylon 6/Nylon 6 restricted the mobility of electrospun fibres in the membrane during the test. For membranes with poor fibre-to-fibre bonding, such as homogeneous bi-layer copolymer PVDF/PVDF, this bi-layer was found to exhibit lower tensile stress and modulus, but higher in tensile strains. The higher tensile strains were due to the alignment of electrospun

fibres in the loading direction. For heterogeneous bi-layer membranes, a combination of two different polymers enhanced the tensile properties of the membranes.

A new test method to measure the adhesion strength between two layer s of electrospun membranes has been developed in the study. The study developed a modified 180° peel test to evaluate adhesion strength between the top and bottom layers of bi-layer membranes. This method was found to give reproducible adhesion strength for the membrane. This adhesion test method would not only be of benefit to electrospun membranes but also to other thin porous materials or films. From the experiment, the homogenous bi-layer PVA/PVA exhibited the highest adhesion strengths compared to other bi-layer membranes.

The study also demonstrated the feasibility of using bi-layer electrospun membranes to remove suspended solids from textile effluents using a lab-scale filtration apparatus. The homogenous bi-layer Nylon 6/Nylon 6 membrane improved the effluent clarity by 99%. The heterogeneous bi-layer PAN/Nylon 6, Nylon 6/PAN, Nylon 6/copolymer PVDF and copolymer PVDF/Nylon 6 membranes also provided clear permeate with a 99% turbidity. The commercial membrane gave a much lower performance by improving the effluent turbidity by only 33 to 35%. For homogeneous bi-layer PAN/PAN and copolymer PVDF/PVDF, these bi-layers exhibited poor effluent turbidity at the range of 16 to 18%. Although the bi-layer Nylon 6/Nylon 6, PAN/Nylon 6, Nylon 6/PAN, Nylon 6/copolymer PVDF and copolymer PVDF/Nylon 6 showed excellent properties for the removal of textile effluent, these bi-layers were found to give the lowest flux as compared to commercial Nylon 6 other bi-layers. The reason of the low flux is due to the fact that the electrospun Nylon 6 has the smallest pore sizes compared to the other electrospun membranes. Due to its small pore sizes, some of the suspended solid formed a cake on the membrane surface. This resulted in membrane fouling for the bi-layer Nylon 6/Nylon 6, PAN/Nylon 6, Nylon 6/PAN, Nylon 6/copolymer PVDF and copolymer PVDF/Nylon 6. In most cases, fouling is always a problem with membrane filters.

CHAPTER 8 RECOMMENDATIONS FOR FUTURE RESEARCH

The study demonstrated the fabrication and characterization of homogeneous and heterogeneous bi-layer membranes, as well as the feasibility of using these membranes as filter media for removal of textile effluent. Based on the experience gained from this research, a number of recommendations for future work can be made. The proposed future works include:

1) *Improvement on fibre inter-bonding between electrospun fibres.* From the experimental results, it shows that the electrospun membranes have poor fibre-to-fibre bonding, which results in poor tensile strength of the membranes. Thus, it is proposed to improve fibre inter-bonding between the electrospun fibres using a number of methods such as the application of heat and adhesive.

2) *Aligned fibres for tensile tests.* The research study found that the interpretation of actual tensile properties for random oriented electrospun fibres was too complex. Hence, membrane with aligned fibres could exhibit the actual tensile properties of the membrane. For future research, it is suggested that to control the speed of a rotating collector in order to form aligned fibres.

3) *Improvement on membrane fouling for separation of solid from aqueous solutions.* The homogeneous bi-layer Nylon 6/Nylon 6, and heterogeneous bi-layers Nylon 6/PAN, PAN/Nylon 6, copolymer PVDF/Nylon 6 and Nylon 6/copolymer PVDF, exhibited excellent properties for removal of solids from liquid. However, fouling is one of the drawbacks using these membranes. An improvement of the membrane surfaces such as surface etching would help to prevent membrane fouling as well as to improve filtration efficiency (flux) of electrospun membranes.

REFERENCES

1. Grafe, T., and Graham, K. (2003) Polymeric nanofibers and nanofiber webs: a new class of nonwovens, *Nonwoven Technol Rev*, 51–55.
2. Ramakrishna, S., Fujihara, K., Teo, W., Lim, T., and Ma, Z. (2005) *An introduction to electrospinning and nanofibers*, World Scientific Singapore.
3. Sawicka, K., and Gouma, P. (2006) Electrospun composite nanofibers for functional applications, *Journal of Nanoparticle Research 8*, 769-781.
4. Graham, K., Gogins, M., and Schreuder-Gibson, H. (2003) Incorporation of electrospun nanofibers into functional structures, pp 15-18.
5. Nisbet, D., Rodda, A., Finkelstein, D., Horne, M., Forsythe, J., and Shen, W. (2009) Surface and bulk characterisation of electrospun membranes: Problems and improvements, *Colloids and Surfaces B: Biointerfaces*.
6. Ramakrishna, S., Fujihara, K., Teo, W., Yong, T., Ma, Z., and Ramaseshan, R. (2006) Electrospun nanofibers: solving global issues, *Materials today 9*, 40-50.
7. Feng, C., Khulbe, K., and Matsuura, T. (2010) Recent progress in the preparation, characterization, and applications of nanofibers and nanofiber membranes via electrospinning/interfacial polymerization, *Journal of Applied Polymer Science 115*, 756-776.
8. Greiner, A., and Wendorff, J. (2007) Electrospinning: a fascinating method for the preparation of ultrathin fibers, *Angewandte Chemie-International Edition 46*, 5670-5703.
9. Gopal, R., Kaur, S., Ma, Z., Chan, C., Ramakrishna, S., and Matsuura, T. (2006) Electrospun nanofibrous filtration membrane, *Journal of Membrane Science 281*, 581-586.
10. Deitzel, J., Kleinmeyer, J., Hirvonen, J., and Beck Tan, N. (2001) Controlled deposition of electrospun poly (ethylene oxide) fibers, *Polymer 42*, 8163-8170.
11. Grafe, T., and Graham, K. (2003) Nanofiber webs from electrospinning, In *Nonwovens in Filtration - Fifth International Conference*, pp 1–5.
12. Gibson, P., Schreuder-Gibson, H., and Rivin, D. (2001) Transport properties of porous membranes based on electrospun nanofibers, *Colloids and Surfaces A: Physicochemical and Engineering Aspects 187*, 469-481.
13. Schreuder-Gibson, H., Gibson, P., Senecal, K., and Tsai, P. (2000) Protective Materials Based on Electrospun Nanofibers, In *INDA international conference*, pp 1-5.
14. Lee, S., and Kay Obendorf, S. (2006) Developing protective textile materials as barriers to liquid penetration using melt-electrospinning, *Journal of Applied Polymer Science 102*, 3430-3437.
15. Schreuder-Gibson, H., Gibson, P., Senecal, K., SENNETT, M., WALKER, J., YEOMANS, W., ZIEGLER, D., and TSAI, P. (2002) Protective Textile Materials Based on Electrospun Nanofibers, *Journal of advanced materials 34*, 44-55.
16. Anonymous. (2006) Nanotechnology The Emerging Trends, *Textiles 33*, 21-24.
17. Subbiah, T., Bhat, G., Tock, R., Parameswaran, S., and Ramkumar, S. (2005) Electrospinning of nanofibers, *Journal of Applied Polymer Science 96*, 557-569.

18. Pattamaprom, C., Hongrojjanawiwat, W., Koombhongse, P., Supaphol, P., Jarusuwannapoo, T., and Rangkupan, R. (2006) The influence of solvent properties and functionality on the electrospinnability of polystyrene nanofibers, *Macromolecular Materials and Engineering 291*, 840-847.

19. Reneker, D., and Chun, I. (1996) Nanometre diameter fibres of polymer, produced by electrospinning, *Nanotechnology 7*, 216.

20. Formhals, A. (1934) PROCESS AND APPARATUS FOR PREPARING ARTIFICIAL THREADS, US Patents.

21. Yarin, A., and Zussman, E. (2004) Upward needleless electrospinning of multiple nanofibers, *Polymer 45*, 2977-2980.

22. Theron, S., Yarin, A., Zussman, E., and Kroll, E. (2005) Multiple jets in electrospinning: experiment and modeling, *Polymer 46*, 2889-2899.

23. Zhou, F., Gong, R., and Porat, I. (2009) Mass production of nanofibre assemblies by electrostatic spinning, *Polymer International 58*, 331-342.

24. Wang, X., Niu, H., and Lin, T. (2009) Needleless electrospinning of nanofibers with a conical wire coil, *Polymer Engineering and Science 49*, 1582-1586.

25. Liu, Y., and He, J. (2007) Bubble electrospinning for mass production of nanofibers, *International Journal of Nonlinear Sciences and Numerical Simulation 8*, 393.

26. Cengiz, F., and Jirsak, O. (2009) The effect of salt on the roller electrospinning of polyurethane nanofibers, *Fibers and Polymers 10*, 177-184.

27. Lin, T., and Wang, X. (2010) Recent developments in electrospinning of nanofibers and nanofiber yarns, In *International Conference on Advanced Textile Materials & Manufacturing Technology*, pp 560-563, Hangzhou, China.

28. Huang, C., Chen, S., Reneker, D., Lai, C., and Hou, H. (2006) High-strength mats from electrospun poly (p-phenylene biphenyltetracarboximide) nanofibers, *Advanced Materials 18*, 668-672.

29. Lyons, J., Li, C., and Ko, F. (2004) Melt-electrospinning part I: processing parameters and geometric properties, *Polymer 45*, 7597-7603.

30. Eda, G., Liu, J., and Shivkumar, S. (2007) Solvent effects on jet evolution during electrospinning of semi-dilute polystyrene solutions, *European Polymer Journal 43*, 1154-1167.

31. Geoff, H., Jeffry, M., Ralph, P., and William, H. (2006) *General chemistry, principles and modern application & basic media pack*.

32. Bower, D. (2002) *An introduction to polymer physics*, Cambridge Univ Pr.

33. Sperling, L. (2006) *Introduction to physical polymer science*, Wiley-Interscience.

34. Bahadur, P., and Sastry, N. (2005) *Principles of polymer science*, Alpha Science Intl Ltd.

35. Stevens, M. (1999) *Polymer Chemistry, An Introduction Third Edition*, Oxford University Press, New York.

36. Anonymous. (n.d) Chem Cool : Chemistry dictionary. http://www.chemcool.com/

37. Garbassi, F., Morra, M., and Occhiello, E. (1998) *Polymer surfaces: from physics to technology*, John Wiley & Sons Inc.

38. Kaplan, D. (1998) *Biopolymers from renewable resources*, Springer Verlag.

39. Heikkilä, P., and Harlin, A. (2008) Parameter study of electrospinning of polyamide-6, *European Polymer Journal 44*, 3067-3079.

40. Zhang, S., Shim, W., and Kim, J. (2009) Design of ultra-fine nonwovens via electrospinning of Nylon 6: Spinning parameters and filtration efficiency, *Materials and Design*.

41. Supaphol, P., Mit-Uppatham, C., and Nithitanakul, M. (2005) Ultrafine electrospun polyamide-6 fibers: Effect of emitting electrode polarity on morphology and average fiber diameter, *Journal of Polymer Science-B-Polymer Physics Edition 43*, 3699-3712.

42. Supaphol, P., Mit-uppatham, C., and Nithitanakul, M. (2005) Ultrafine electrospun polyamide-6 fibers: Effects of solvent system and emitting electrode polarity on morphology and average fiber diameter, *Macromolecular Materials and Engineering 290*, 933.

43. Stephens, J., Chase, D., and Rabolt, J. (2004) Effect of the electrospinning process on polymer crystallization chain conformation in nylon-6 and nylon-12, *Macromolecules 37*, 877-881.

44. Shan, G., Yang, W., Yang, M., Xie, B., Feng, J., and Fu, Q. (2007) Effect of temperature and strain rate on the tensile deformation of polyamide 6, *Polymer 48*, 2958-2968.

45. Ojha, S., Afshari, M., Kotek, R., and Gorga, R. (2008) Morphology of electrospun nylon-6 nanofibers as a function of molecular weight and processing parameters, *Journal of Applied Polymer Science 108*, 308-319.

46. Zhang, C., Yuan, X., Wu, L., Han, Y., and Sheng, J. (2005) Study on morphology of electrospun poly (vinyl alcohol) mats, *European Polymer Journal 41*, 423-432.

47. Yang, E., Qin, X., and Wang, S. (2008) Electrospun crosslinked polyvinyl alcohol membrane, *Materials Letters*.

48. Stanger, J., Tucker, N., Staiger, M., Kirwan, K., Coles, S., Jacobs, D., and Larsen, N. (2009) Effect of salts on the electrospinning of poly (vinyl alcohol), In *ADVANCED MATERIALS AND NANOTECHNOLOGY*, p 118.

49. Liu, Y., Bolger, B., Cahill, P., and McGuinness, G. (2009) Water resistance of photocrosslinked polyvinyl alcohol based fibers, *Materials Letters 63*, 419-421.

50. Lee, J., Choi, K., Ghim, H., Kim, S., Chun, D., Kim, H., and Lyoo, W. (2004) Role of molecular weight of atactic poly (vinyl alcohol)(PVA) in the structure and properties of PVA nanofabric prepared by electrospinning, *Journal of Applied Polymer Science 93*, 1638-1646.

51. Deitzel, J., Kleinmeyer, J., Harris, D., and Beck Tan, N. (2001) The effect of processing variables on the morphology of electrospun nanofibers and textiles, *Polymer 42*, 261-272.

52. Fong, H., Chun, I., and Reneker, D. (1999) Beaded nanofibers formed during electrospinning, *POLYMER-LONDON- 40*, 4585-4592.

53. Theron, S., Zussman, E., and Yarin, A. (2004) Experimental investigation of the governing parameters in the electrospinning of polymer solutions, *Polymer 45*, 2017-2030.

54. Tan, S., Inai, R., Kotaki, M., and Ramakrishna, S. (2005) Systematic parameter study for ultra-fine fiber fabrication via electrospinning process, *Polymer 46*, 6128-6134.

55. Buchko, C., Chen, L., Shen, Y., and Martin, D. (1999) Processing and microstructural characterization of porous biocompatible protein polymer thin films, *POLYMER-LONDON- 40*, 7397-7407.

56. Ding, B., Kim, J., Miyazaki, Y., and Shiratori, S. (2004) Electrospun nanofibrous membranes coated quartz crystal microbalance as gas sensor for NH3 detection, *Sensors and Actuators B: Chemical 101*, 373-380.

57. Ding, B., Yamazaki, M., and Shiratori, S. (2005) Electrospun fibrous polyacrylic acid membrane-based gas sensors, *Sensors & Actuators: B. Chemical 106*, 477-483.

58. Jalili, R., Hosseini, S., and Morshed, M. (2005) The Effects of Operating Parameters on the Morphology of Electrospun Polyacrilonitrile Nanofibres, *Iranian Polymer Journal 14*, 1074.

59. Jalili, R., Morshed, M., and Ravandi, S. (2006) Fundamental parameters affecting electrospinning of PAN nanofibers as uniaxially aligned fibers, *Journal of Applied Polymer Science 101*, 4350-4357.

60. Liu, H., and Hsieh, Y. (2006) Preparation of Water-Absorbing Polyacrylonitrile Nanofibrous Membrane, *Macromolecular rapid communications 27*, 142-145.

61. Qin, X., Yang, E., Li, N., and Wang, S. (2007) Effect of different salts on electrospinning of polyacrylonitrile (PAN) polymer solution, *Journal of Applied Polymer Science 103*, 3865-3870.

62. Fennessey, S., and Farris, R. (2004) Fabrication of aligned and molecularly oriented electrospun polyacrylonitrile nanofibers and the mechanical behavior of their twisted yarns, *Polymer 45*, 4217-4225.

63. Nasir, M., Matsumoto, H., Danno, T., Minagawa, M., Irisawa, T., Shioya, M., and Tanioka, A. (2006) Control of diameter, morphology, and structure of PVDF nanofiber fabricated by electrospray deposition, *Journal of Polymer Science-B-Polymer Physics Edition 44*, 779-786.

64. Choi, S., Lee, Y., Joo, C., Lee, S., Park, J., and Han, K. (2004) Electrospun PVDF nanofiber web as polymer electrolyte or separator, *Electrochimica Acta 50*, 339-343.

65. Gao, K., Hu, X., Dai, C., and Yi, T. (2006) Crystal structures of electrospun PVDF membranes and its separator application for rechargeable lithium metal cells, *Materials Science and Engineering: B 131*, 100-105.

66. Kim, J., Choi, S., Jo, S., Lee, W., and Kim, B. (2005) Characterization and properties of P (VdF-HFP)-based fibrous polymer electrolyte membrane prepared by electrospinning, *Journal of the Electrochemical Society 152*, A295.

67. Yao, C., Li, X., Neoh, K., Shi, Z., and Kang, E. (2009) Antibacterial activities of surface modified electrospun poly (vinylidene fluoride-co-hexafluoropropylene)(PVDF-HFP) fibrous membranes, *Applied Surface Science 255*, 3854-3858.

68. Singh, A., Steely, L., and Allcock, H. (2005) Poly [bis (2, 2, 2-trifluoroethoxy) phosphazene] superhydrophobic nanofibers, *Langmuir: the ACS journal of surfaces and colloids 21*, 11604.

69. Ma, M., Hill, R., Lowery, J., Fridrikh, S., and Rutledge, G. (2005) Electrospun poly (styrene-block-dimethylsiloxane) block copolymer fibers exhibiting superhydrophobicity, *Langmuir 21*, 5549-5554.

70. Kim, C., Frey, M., Marquez, M., and Joo, Y. (2005) Preparation of submicron-scale, electrospun cellulose fibers via direct dissolution, *Journal of Polymer Science Part B: Polymer Physics 43*, 1673-1683.

71. Liu, H., and Hsieh, Y. (2002) Ultrafine fibrous cellulose membranes from electrospinning of cellulose acetate, *Journal of Polymer Science Part B: Polymer Physics 40*, 2119-2129.

72. Kim, C., Kim, D., Kang, S., Marquez, M., and Joo, Y. (2006) Structural studies of electrospun cellulose nanofibers, *Polymer 47*, 5097-5107.

73. Zhang, Y., Ouyang, H., Lim, C., Ramakrishna, S., and Huang, Z. (2005) Electrospinning of gelatin fibers and gelatin/PCL composite fibrous scaffolds, *Journal of Biomedical Materials Research Part B: Applied Biomaterials 72*, 156-165.

74. Huang, Z., Zhang, Y., Ramakrishna, S., and Lim, C. (2004) Electrospinning and mechanical characterization of gelatin nanofibers, *Polymer 45*, 5361-5368.

75. Li, M., Guo, Y., Wei, Y., MacDiarmid, A., and Lelkes, P. (2006) Electrospinning polyaniline-contained gelatin nanofibers for tissue engineering applications, *Biomaterials 27*, 2705-2715.

76. Matthews, J., Wnek, G., Simpson, D., and Bowlin, G. (2002) Electrospinning of collagen nanofibers, *Biomacromolecules 3*, 232-238.

77. Matthews, J., Boland, E., Wnek, G., Simpson, D., and Bowlin, G. (2003) Electrospinning of collagen type II: a feasibility study, *Journal of bioactive and compatible polymers 18*, 125.

78. Buttafoco, L., Kolkman, N., Engbers-Buijtenhuijs, P., Poot, A., Dijkstra, P., Vermes, I., and Feijen, J. (2006) Electrospinning of collagen and elastin for tissue engineering applications, *Biomaterials 27*, 724-734.

79. Wnek, G., Carr, M., Simpson, D., and Bowlin, G. (2003) Electrospinning of nanofiber fibrinogen structures, *Nano letters 3*, 213-216.

80. McManus, M., Boland, E., Simpson, D., Barnes, C., and Bowlin, G. (2007) Electrospun fibrinogen: feasibility as a tissue engineering scaffold in a rat cell culture model, *J. Biomed. Mater. Res. Part A 81*, 299-309.

81. Geng, X., Kwon, O., and Jang, J. (2005) Electrospinning of chitosan dissolved in concentrated acetic acid solution, *Biomaterials 26*, 5427-5432.

82. Ohkawa, K., Cha, D., Kim, H., Nishida, A., and Yamamoto, H. (2004) Electrospinning of chitosan, *Macromolecular rapid communications 25*, 1600-1605.

83. Son, W., Youk, J., Lee, T., and Park, W. (2004) Preparation of antimicrobial ultrafine cellulose acetate fibers with silver nanoparticles, *Macromolecular rapid communications 25*, 1632-1637.

84. Ge, J., Hou, H., Li, Q., Graham, M., Greiner, A., Reneker, D., Harris, F., and Cheng, S. (2004) Assembly of well-aligned multiwalled carbon nanotubes in confined polyacrylonitrile environments: electrospun composite nanofiber sheets, *J. Am. Chem. Soc 126*, 15754-15761.

85. Sen, R., Zhao, B., Perea, D., Itkis, M., Hu, H., Love, J., Bekyarova, E., and Haddon, R. (2004) Preparation of single-walled carbon nanotube reinforced polystyrene and polyurethane nanofibers and membranes by electrospinning, *Nano letters 4*, 459-464.

86. Ye, H., Lam, H., Titchenal, N., Gogotsi, Y., and Ko, F. (2004) Reinforcement and rupture behavior of carbon nanotubes–polymer nanofibers, *Applied Physics Letters 85*, 1775.

87. Dror, Y., Salalha, W., Khalfin, R., Cohen, Y., Yarin, A., and Zussman, E. (2003) Carbon nanotubes embedded in oriented polymer nanofibers by electrospinning, *Langmuir 19*, 7012-7020.

88. Shin, M., Kim, Y., Kim, S., Kim, S., Lee, H., Spinks, G., and Kim, S. (2008) Enhanced conductivity of aligned PANi/PEO/MWNT nanofibers by electrospinning, *Sensors and Actuators B: Chemical 134*, 122-126.

89. Li, D., McCann, J., Xia, Y., and Marquez, M. (2006) Electrospinning: a simple and versatile technique for producing ceramic nanofibers and nanotubes, *Journal of the American Ceramic Society 89*, 1861-1869.

90. Gu, Y., Chen, D., and Jiao, X. (2005) Synthesis and electrochemical properties of nanostructured LiCoO2 fibers as cathode materials for lithium-ion batteries, *J. Phys. Chem. B 109*, 17901-17906.

91. Song, M., Kim, D., Ihn, K., Jo, S., and Kim, D. (2004) Electrospun TiO2 electrodes for dye-sensitized solar cells, *Nanotechnology 15*, 1861.

92. Zhang, Y., He, X., Li, J., Miao, Z., and Huang, F. (2008) Fabrication and ethanol-sensing properties of micro gas sensor based on electrospun SnO2 nanofibers, *Sensors and Actuators B: Chemical 132*, 67-73.

93. Zhu, R., Jiang, C., Liu, X., Liu, B., Kumar, A., and Ramakrishna, S. (2008) Improved adhesion of interconnected TiO nanofiber network on conductive substrate and its application in polymer photovoltaic devices, *Applied Physics Letters 93*, 013102.

94. Huang, C., Chen, S., Lai, C., Reneker, D., Qiu, H., Ye, Y., and Hou, H. (2006) Electrospun polymer nanofibres with small diameters, *Nanotechnology 17*, 1558.

95. Li, D., and Xia, Y. (2004) Electrospinning of nanofibers: Reinventing the wheel?, *Advanced Materials 16*, 1151-1170.

96. Jia, Y., Gong, J., Gu, X., Kim, H., Dong, J., and Shen, X. (2007) Fabrication and characterization of poly (vinyl alcohol)/chitosan blend nanofibers produced by electrospinning method, *Carbohydrate Polymers 67*, 403-409.

97. Doshi, J., and Reneker, D. (1995) Electrospinning process and applications of electrospun fibers, *Journal of Electrostatics 35*, 151-160.

98. Huang, Z., Zhang, Y., Kotaki, M., and Ramakrishna, S. (2003) A review on polymer nanofibers by electrospinning and their applications in nanocomposites, *Composites Science and Technology 63*, 2223-2253.

99. Mit-uppatham, C., Nithitanakul, M., and Supaphol, P. (2004) Ultrafine electrospun polyamide-6 fibers: effect of solution conditions on morphology and average fiber diameter, *Macromolecular Chemistry and Physics 205*, 2327-2338.

100. Shen, L., Xu, Z., Liu, Z., and Xu, Y. (2003) Ultrafiltration hollow fiber membranes of sulfonated polyetherimide/polyetherimide blends: preparation, morphologies and anti-fouling properties, *Journal of Membrane Science 218*, 279-293.

101. Shenoy, S., Bates, W., Frisch, H., and Wnek, G. (2005) Role of chain entanglements on fiber formation during electrospinning of polymer solutions: good solvent, non-specific polymer–polymer interaction limit, *Polymer 46*, 3372-3384.

102. Koski, A., Yim, K., and Shivkumar, S. (2004) Effect of molecular weight on fibrous PVA produced by electrospinning, *Materials Letters 58*, 493-497.

103. Ryu, Y., Kim, H., Lee, K., Park, H., and Lee, D. (2003) Transport properties of electrospun nylon 6 nonwoven mats, *European Polymer Journal 39*, 1883-1889.

104. Megelski, S., Stephens, J., Chase, D., and Rabolt, J. (2002) Micro-and nanostructured surface morphology on electrospun polymer fibers, *Macromolecules 35*, 8456-8466.

105. Baumgarten, P. (1971) Electrostatic spinning of acrylic microfibers, *J. Colloid Interface Sci 36*.

106. Pornsopone, V., Supaphol, P., Rangkupan, R., and Tantayanon, S. (2005) Electrospinning of methacrylate-based copolymers: Effects of solution concentration and applied electrical potential on morphological appearance of as-spun fibers, *Polymer Engineering and Science 45*, 1073-1080.

107. Morota, K., Matsumoto, H., Mizukoshi, T., Konosu, Y., Minagawa, M., Tanioka, A., Yamagata, Y., and Inoue, K. (2004) Poly (ethylene oxide) thin films produced by electrospray deposition: morphology control and additive effects of alcohols on nanostructure, *Journal of colloid and interface science 279*, 484-492.

108. Zhao, S., Wu, X., Wang, L., and Huang, Y. (2004) Electrospinning of ethyl-cyanoethyl cellulose/tetrahydrofuran solutions, *Journal of Applied Polymer Science 91*, 242-246.

109. Zong, X., Kim, K., Fang, D., Ran, S., Hsiao, B., and Chu, B. (2002) Structure and process relationship of electrospun bioabsorbable nanofiber membranes, *Polymer 43*, 4403-4412.

110. Mo, X., Xu, C., Kotaki, M., and Ramakrishna, S. (2004) Electrospun P (LLA-CL) nanofiber: a biomimetic extracellular matrix for smooth muscle cell and endothelial cell proliferation, *Biomaterials 25*, 1883-1890.

111. Demir, M., Yilgor, I., Yilgor, E., and Erman, B. (2002) Electrospinning of polyurethane fibers, *Polymer 43*, 3303-3309.

112. Andrady, A. (2008) Science and Technology of Polymer Nanofibers, John Wiley & Sons, New Jersey.

113. Kidoaki, S., Kwon, I., and Matsuda, T. (2006) Structural features and mechanical properties of in situ-bonded meshes of segmented polyurethane electrospun from mixed solvents, *Journal of Biomedical Materials Research Part B: Applied Biomaterials 76*, 219-229.

114. Tripatanasuwan, S., Zhong, Z., and Reneker, D. (2007) Effect of evaporation and solidification of the charged jet in electrospinning of poly (ethylene oxide) aqueous solution, *Polymer 48*, 5742-5746.

115. Casper, C., Stephens, J., Tassi, N., Chase, D., and Rabolt, J. (2004) Controlling surface morphology of electrospun polystyrene fibers: effect of humidity and molecular weight in the electrospinning process, *Macromolecules 37*, 573-578.

116. Macossay, J., Marruffo, A., Rincon, R., Eubanks, T., and Kuang, A. (2007) Effect of needle diameter on nanofiber diameter and thermal properties of electrospun poly (methyl methacrylate), *Polymers for Advanced Technologies 18*, 180-183.

117. Nair, L., Bhattacharyya, S., Bender, J., Greish, Y., Brown, P., Allcock, H., and Laurencin, C. (2004) Fabrication and optimization of methylphenoxy substituted polyphosphazene nanofibers for biomedical applications, *Biomacromolecules 5*, 2212-2220.

118. Kong, C., Lee, S., Lee, S., Lee, K., Jo, N., and Kim, H. (2009) Multi-jet ejection and fluctuation in electrospinning of polyvinyl alcohol with various nozzle diameters, *Polymer Engineering & Science 49*.

119. Taylor, G. (1964) Disintegration of water drops in an electric field, *Proceedings of the Royal Society of London. Series A, Mathematical and Physical Sciences 280*, 383-397.

120. Rangkupan, R., and Reneker, D. (2003) Electrospinning Process of Molten Polypropylene in Vacuum, *Journal of Metals, Materials and Minerals 12*, 81-87.

121. Reneker, D., Yarin, A., Fong, H., and Koombhongse, S. (2000) Bending instability of electrically charged liquid jets of polymer solutions in electrospinning, *Journal of Applied Physics 87*, 4531.

122. Cui, W., Li, X., Zhou, S., and Weng, J. (2008) Degradation patterns and surface wettability of electrospun fibrous mats, *Polymer Degradation and Stability*.

123. Ma, M., Mao, Y., Gupta, M., Gleason, K., and Rutledge, G. (2005) Superhydrophobic fabrics produced by electrospinning and chemical vapor deposition, *Macromolecules 38*, 9742-9748.

124. Barakat, N. A. M., Kanjwal, M. A., Sheikh, F. A., and Kim, H. Y. (2009) Spider-net within the N6, PVA and PU electrospun nanofiber mats using salt addition: Novel strategy in the electrospinning process, *Polymer 50*, 4389-4396.

125. Menini, R., and Farzaneh, M. (2008) Production of superhydrophobic polymer fibers with embedded particles using the electrospinning technique, *Polymer International 57*, 77-84.

126. Chen, F., Lee, C., and Teoh, S. (2007) Nanofibrous modification on ultra-thin poly (e-caprolactone) membrane via electrospinning, *Materials Science & Engineering C 27*, 325-332.

127. Hutten, I. (2007) *Handbook of nonwoven filter media*, Elsevier.

128. Li, W., Laurencin, C., Caterson, E., Tuan, R., and Ko, F. (2002) Electrospun nanofibrous structure: a novel scaffold for tissue engineering, *Journal of biomedical materials research 60*, 613-621.

129. Li, D., Frey, M., and Joo, Y. (2006) Characterization of nanofibrous membranes with capillary flow porometry, *Journal of Membrane Science 286*, 104-114.

130. Barhate, R., Loong, C., and Ramakrishna, S. (2006) Preparation and characterization of nanofibrous filtering media, *Journal of Membrane Science 283*, 209-218.

131. Gopal, R., Kaur, S., Feng, C., Chan, C., Ramakrishna, S., Tabe, S., and Matsuura, T. (2007) Electrospun nanofibrous polysulfone membranes as pre-filters: Particulate removal, *Journal of Membrane Science 289*, 210-219.

132. Aussawasathien, D., Teerawattananon, C., and Vongachariya, A. (2008) Separation of micron to sub-micron particles from water: Electrospun nylon-6 nanofibrous membranes as pre-filters, *Journal of Membrane Science 315*, 11-19.

133. McKee, M., Park, T., Unal, S., Yilgor, I., and Long, T. (2005) Electrospinning of linear and highly branched segmented poly (urethane urea) s, *Polymer 46*, 2011-2015.

134. Li, Y., Huang, Z., and L , Y. (2006) Electrospinning of nylon-6, 66, 1010 terpolymer, *European Polymer Journal 42*, 1696-1704.
135. Zhang, L., and Hsieh, Y. (2006) Nanoporous ultrahigh specific surface polyacrylonitrile fibres, *Nanotechnology 17*, 4416-4423.
136. Gu, S., Ren, J., and Vancso, G. (2005) Process optimization and empirical modeling for electrospun polyacrylonitrile (PAN) nanofiber precursor of carbon nanofibers, *European Polymer Journal 41*, 2559-2568.
137. Liu, Y., Cui, L., Guan, F., Gao, Y., Hedin, N., Zhu, L., and Fong, H. (2007) Crystalline Morphology and Polymorphic Phase Transitions in Electrospun Nylon 6 Nanofibers, *Macromolecules 40*, 6283.
138. Zheng, J., He, A., Li, J., and Han, C. (2007) Polymorphism Control of Poly (vinylidene fluoride) through Electrospinning, *Macromolecular rapid communications 28*, 2159-2162.
139. Na, H., Zhao, Y., Zhao, C., and Yuan, X. (2008) Effect of hot-press on electrospun poly (vinylidene fluoride) membranes, *Polymer Engineering and Science 48*, 934-940.
140. Bhattarai, N., Cha, D., Bhattarai, S., Khil, M., and Kim, H. (2003) Biodegradable electrospun mat: Novel block copolymer of poly (p-dioxanone-co-L-lactide)-block-poly (ethylene glycol), *Journal of Polymer Science-B-Polymer Physics Edition 41*, 1955.
141. Inai, R., Kotaki, M., and Ramakrishna, S. (2005) Structure and properties of electrospun PLLA single nanofibres, *Nanotechnology 16*, 208-213.
142. Peng, P., Chen, Y., Gao, Y., Yu, J., and Guo, Z. (2009) Phase morphology and mechanical properties of the electrospun polyoxymethylene/polyurethane blend fiber mats, *Journal of Polymer Science Part B: Polymer Physics 47*.
143. Inai, R., Kotaki, M., and Ramakrishna, S. (2005) Deformation behavior of electrospun poly (L-lactide-co-ϵ-caprolactone) nonwoven membranes under uniaxial tensile loading, *Journal of Polymer Science Part B: Polymer Physics 43*, 3205-3212.
144. Wong, S., Baji, A., and Leng, S. (2008) Effect of fiber diameter on tensile properties of electrospun poly (-caprolactone), *Polymer 49*, 4713-4722.
145. Kinloch, A. (1987) *Adhesion and adhesives*, Chapman and Hall London.
146. Chen, Z., Cotterell, B., and Chen, W. (1999) Characterizing the interfacial fracture toughness for microelectronic packaging, *Surface and Interface Analysis 28*, 146-149.
147. Gauthier, R., Joly, C., Coupas, A., Gauthier, H., and Escoubes, M. (1998) Interfaces in polyolefin/cellulosic fiber composites: Chemical coupling, morphology, correlation with adhesion and aging in moisture, *Polymer Composites 19*, 287-300.
148. Jang, B. (1992) Control of interfacial adhesion in continuous carbon and Kevlar fiber reinforced polymer composites, *Composites Science and Technology 44*, 333-349.
149. Joseph, K., Varghese, S., Kalaprasad, G., Thomas, S., Prasannakumari, L., Koshy, P., and Pavithran, C. (1996) Influence of interfacial adhesion on the mechanical properties and fracture behaviour of short sisal fibre reinforced polymer composites, *European Polymer Journal 32*, 1243-1250.
150. Kreckel, K., Hager, P., and Rickert, J. (2003) Removable adhesive tape, Google Patents.

151. Creton, C., and Fabre, P. (2002) Adhesion Science and Engineering: The Mechanics of Adhesion, Elsevier, New York.

152. Bundy, K., Schlegel, U., Rahn, B., Geret, V., and Perren, S. (2000) An improved peel test method for measurement of adhesion to biomaterials, *Journal of Materials Science: Materials in Medicine 11*, 517-521.

153. McCabe, J., Carrick, T., and Kamohara, H. (2002) Adhesive bond strength and compliance for denture soft lining materials, *Biomaterials 23*, 1347-1352.

154. Kim, I., Hong, J., Lee, B., Kim, D., Jeon, E., Choi, D., and Yang, D. (2007) Dye-sensitized solar cells using network structure of electrospun ZnO nanofiber mats, *Applied Physics Letters 91*, 163109.

155. Barhate, R., and Ramakrishna, S. (2007) Nanofibrous filtering media: filtration problems and solutions from tiny materials, *Journal of Membrane Science 296*, 1-8.

156. Homaeigohar, S., Buhr, K., and Ebert, K. (2010) Polyethersulfone electrospun nanofibrous composite membrane for liquid filtration, *Journal of Membrane Science*.

157. Truong, Y., Kyratzis, I., and Shen, W. (2009) Fabrication and characterization of electrospun PVDF-aliquat 336 fibre membrane for removal of cadmium from hydrochloric acid solutions, *Journal of Materials Science 44*, 1101-1106.

158. Heikkila, P., Taipale, A., Lehtimaki, M., and Harlin, A. (2008) Electrospinning of polyamides with different chain compositions for filtration application, *Polymer Engineering and Science 48*, 1168-1176.

159. Casarano, R., Bentini, R., Bueno, V. B., Iacovella, T., Monteiro, F. B. F., Iha, F. A. S., Campa, A., Petri, D. F. S., Jaffe, M., and Catalani, L. H. (2009) Enhanced fibroblast adhesion and proliferation on electrospun fibers obtained from poly(isosorbide succinate-b-L-lactide) block copolymers, *Polymer 50*, 6218-6227.

160. Yang, L., Kandel, R. A., Chang, G., and Santerre, J. P. (2009) Polar surface chemistry of nanofibrous polyurethane scaffold affects annulus fibrosus cell attachment and early matrix accumulation, *J. Biomed. Mater. Res. Part A 91A*, 1089-1099.

161. Pham, Q., Sharma, U., and Mikos, A. (2006) Electrospinning of polymeric nanofibers for tissue engineering applications: a review, *Tissue engineering 12*, 1197-1211.

162. Chiu, C., Lee, J., Chu, C., Chang, Y., and Wang, Y. (2008) Development of two alginate-based wound dressings, *Journal of Materials Science: Materials in Medicine 19*, 2503-2513.

163. Khil, M., Cha, D., Kim, H., Kim, I., and Bhattarai, N. (2003) Electrospun nanofibrous polyurethane membrane as wound dressing, *Journal of biomedical materials research 67*, 675-679.

164. Gu, S., Wang, Z., Ren, J., and Zhang, C. (2004) Fabrication and Characterization of Electrospun Poly (L-lactic acid) and Poly (L-lactide-co-glycolide) Mats as Wound Dressings, *Adv Mater 16*, 1164.

165. Ruiz-Cardona, L., Sanzgiri, Y., Benedetti, L., Stella, V., and Topp, E. (1996) Application of benzyl hyaluronate membranes as potential wound dressings: evaluation of water vapour and gas permeabilities, *Biomaterials 17*, 1639-1643.

166. Chen, J., Chang, G., and Chen, J. (2008) Electrospun collagen/chitosan nanofibrous membrane as wound dressing, *Colloids and Surfaces A: Physicochemical and Engineering Aspects 313*, 183-188.

167. Choi, S., Fu, Y., Ahn, Y., Jo, S., and Manthiram, A. (2008) Nafion-impregnated electrospun polyvinylidene fluoride composite membranes for direct methanol fuel cells, *Journal of Power Sources 180*, 167-171.

168. All you wanted to know about electron microscopy, (Company, F., Ed.).

169. Affandi, N., Truong, Y., Kyratzis, I., Padhye, R., and Arnold, L. (2010) A non-destructive method for thickness measurement of thin electrospun membranes using white light profilometry, *Journal of Materials Science 45*, 1411-1418.

170. Wenzel, R. (1936) Resistance of solid surfaces to wetting by water, *Industrial & Engineering Chemistry 28*, 988-994.

171. Cassie, A., and Baxter, S. (1944) Wettability of porous surfaces, *Transactions of the Faraday Society 40*, 546-551.

172. Quéré, D., and Reyssat, M. (2008) Non-adhesive lotus and other hydrophobic materials, *Philosophical Transactions A 366*, 1539.

173. Hernández, A., Calvo, J., Prádanos, P., and Tejerina, F. (1996) Pore size distributions in microporous membranes. A critical analysis of the bubble point extended method, *Journal of Membrane Science 112*, 1-12.

174. Jena, A., and Gupta, K. (2005) Pore volume of nanofiber nonwovens, *Int Nonwovens J 14*, 25-30.

175. Mulder, M. (1996) *Basic principles of membrane technology*, Springer.

176. Jena, A., and Gupta, K. (2002) Characterization of pore structure of filtration media, *Fluid particle Separation Journal 14*, 227-241.

177. Xuemei, D. (2003) Microstructure and water vapor transport properties of temperature sensitive polyurethanes, In *Institute of Textiles and Clothing*, pp 1-254, Hong Kong Polytechnic University, Hong Kong.

178. Pavia, D., Lampman, G., and Kriz, G. (2009) *Introduction to spectroscopy*, Brooks/Cole Pub Co.

179. Shackelford, J. (2004) *Introduction to materials science for engineers*, Prentice Hall.

180. Morton, W., and Hearle, J. Physical properties of textile fibres, *New York, 1993*.

181. Hazer, B. (1989) Handbook of Polymer Science and Technology.

182. Wong, S., Baji, A., and Gent, A. (2008) Effect of specimen thickness on fracture toughness and adhesive properties of hydroxyapatite-filled polycaprolactone, *Composites Part A 39*, 579-587.

183. Ronesi, V., Cheung, Y., Hiltner, A., and Baer, E. (2003) Adhesion of ethylene-styrene copolymers to polyethylene in microlayers, *Journal of Applied Polymer Science 89*, 153-162.

184. Ebeling, T., Hiltner, A., and Baer, E. (1998) Delamination failure mechanisms in microlayers of polycarbonate and poly (styrene-co-acrylonitrile), *Journal of Applied Polymer Science 68*, 793-805.

185. Boiko, Y., and Lyngaae-Jørgensen, J. (2005) Fracture energy–fracture stress relationship for weak polymer–polymer interfaces, *Polymer 46*, 6016-6024.

186. Boiko, Y., Bach, A., and Lyngaae-Jorgensen, J. (2004) Self-bonding in an amorphous polymer below the glass transition: A T-peel test investigation, *Journal of Polymer Science-B-Polymer Physics Edition 42*, 1861-1867.

187. Cheremisinoff, N. (1998) *Liquid filtration*, Butterworth-Heinemann.
188. Russell, S. (2007) *Handbook of nonwovens*, by Woodhead Publishing Limited in association with the textile institute"--TP verso Includes bibliographical references and index.
189. Wakeman, R., and Tarleton, E. (1999) *Filtration: equipment selection, modelling and process simulation*, Elsevier Science Ltd.
190. Purchas, D., and Sutherland, K. (2002) *Handbook of filter media*, Elsevier Science Ltd.
191. Singh, R. (2006) Hybrid membrane systems for water purification, *Eisevier Ltd., Kidlington*.
192. Porter, M. (1990) *Handbook of industrial membrane technology*, William Andrew Publishing.
193. Judd, S., and Jefferson, B. (2003) *Membranes for industrial wastewater recovery and re-use*, Elsevier Science & Technology.
194. Li, H., Cao, Y., Qin, J., Jie, X., Wang, T., Liu, J., and Yuan, Q. (2006) Development and characterization of anti-fouling cellulose hollow fiber UF membranes for oil–water separation, *Journal of Membrane Science 279*, 328-335.
195. Maximous, N., Nakhla, G., and Wan, W. (2009) Comparative assessment of hydrophobic and hydrophilic membrane fouling in wastewater applications, *Journal of Membrane Science 339*, 93-99.
196. Ying, L., Zhai, G., Winata, A., Kang, E., and Neoh, K. (2003) pH effect of coagulation bath on the characteristics of poly (acrylic acid)-grafted and poly (4-vinylpyridine)-grafted poly (vinylidene fluoride) microfiltration membranes, *Journal of colloid and interface science 265*, 396-403.
197. Pieracci, J., Crivello, J., and Belfort, G. (2002) Increasing membrane permeability of UV-modified poly (ether sulfone) ultrafiltration membranes, *Journal of Membrane Science 202*, 1-16.
198. Howell, J., Sanchez, V., and Field, R. (1993) *Membranes in bioprocessing: theory and applications*, Chapman & Hall, London.
199. Jönsson, C., and Jönsson, A. (1995) Influence of the membrane material on the adsorptive fouling of ultrafiltration membranes, *Journal of Membrane Science 108*, 79-87.
200. Cornelissen, E., van den Boomgaard, T., and Strathmann, H. (1998) Physicochemical aspects of polymer selection for ultrafiltration and microfiltration membranes, *Colloids and Surfaces A: Physicochemical and Engineering Aspects 138*, 283-289.
201. Ochoa, N., Masuelli, M., and Marchese, J. (2003) Effect of hydrophilicity on fouling of an emulsified oil wastewater with PVDF/PMMA membranes, *Journal of Membrane Science 226*, 203-211.
202. Marchese, J., Ponce, M., Ochoa, N., Prádanos, P., Palacio, L., and Hernández, A. (2003) Fouling behaviour of polyethersulfone UF membranes made with different PVP, *Journal of Membrane Science 211*, 1-11.
203. Nomura, T., Fujii, T., and Suzuki, M. (1997) Application of the ceramic membrane with hydrophobic skin layer to separation of activated sludge, *Water Science and Technology 35*, 137-144.
204. Choo, K., and Lee, C. (2000) Understanding membrane fouling in terms of surface free energy changes, *Journal of colloid and interface science 226*, 367-370.

205. Koros, W., Ma, Y., and Shimidzu, T. (1996) Terminology for membranes and membrane processes (IUPAC Recommendations 1996), *Journal of Membrane Science 120*, 149-159.

206. Li, J., Xu, Z., Yang, H., Yu, L., and Liu, M. (2009) Effect of TiO2 nanoparticles on the surface morphology and performance of microporous PES membrane, *Applied Surface Science 255*, 4725-4732.

207. Rouse Jr, P. (1953) A theory of the linear viscoelastic properties of dilute solutions of coiling polymers, *The Journal of Chemical Physics 21*, 1272.

208. Koombhongse, S., Liu, W., and Reneker, D. (2001) Flat polymer ribbons and other shapes by electrospinning, *Journal of Polymer Science Part B Polymer Physics 39*, 2598-2606.

209. Son, W., Youk, J., Lee, T., and Park, W. (2004) The effects of solution properties and polyelectrolyte on electrospinning of ultrafine poly (ethylene oxide) fibers, *Polymer 45*, 2959-2966.

210. Leader, G., and Gormley, J. (1951) The dielectric constant of N-methylamides, *Journal of the American Chemical Society 73*, 5731-5733.

211. Pai, C., Boyce, M., and Rutledge, G. (2009) Morphology of Porous and Wrinkled Fibers of Polystyrene Electrospun from Dimethylformamide, *Macromolecules 42*, 2102-2114.

212. Wang, L., Pai, C., Boyce, M., and Rutledge, G. (2009) Wrinkled surface topographies of electrospun polymer fibers, *Applied Physics Letters 94*, 151916.

213. Rotter, G., and Ishida, H. (1992) FTIR separation of nylon-6 chain conformations: Clarification of the mesomorphous and -crystalline phases, *Journal of Polymer Science Part B: Polymer Physics 30*, 489-495.

214. Raghavendra R. Hegde, M. G. K., Atul Dahiya. (N.d) Polymer Crystallinity.

215. Yee, W. A., Kotaki, M., Liu, Y., and Lu, X. (2007) Morphology, polymorphism behavior and molecular orientation of electrospun poly(vinylidene fluoride) fibers, *Polymer 48*, 512-521.

216. Bormashenko, Y., Pogreb, R., Stanevsky, O., and Bormashenko, E. (2004) Vibrational spectrum of PVDF and its interpretation, *Polymer Testing 23*, 791-796.

217. Gregorio Jr, R., and Cestari, M. (1994) Effect of crystallization temperature on the crystalline phase content and morphology of poly (vinylidene fluoride), *Journal of Polymer Science Part B: Polymer Physics 32*, 859-870.

218. Ramesh, C., and Gowd, E. (2001) High-Temperature X-ray Diffraction Studies on the Crystalline Transitions in the [alpha]-and [gamma]-Forms of Nylon-6, *Macromolecules 34*, 3308-3313.

219. Shao, C., Kim, H.-Y., Gong, J., Ding, B., Lee, D.-R., and Park, S.-J. (2003) Fiber mats of poly(vinyl alcohol)/silica composite via electrospinning, *Materials Letters 57*, 1579-1584.

220. Constantino, A. E. J., R.D. Simoes, J.A. Giacometti, V. Zucolotto, O.N. Oliveira Jr., G. Gozzi, D.L. Chinaglia. (2005) The Investigation of alpha to beta Phase Transition in Poly(Vinylidene Fluoride) (PVDF), In *Electrets, 2005. ISE-12. 2005 12th International Symposium* pp 178-181, Brazil

221. Kinloch, A., and Yuen, M. (1989) The Mechanical Behaviour of Polyimide/Copper Laminates Part 2: Peel Energy Measurements, *The Journal of Adhesion 30*, 151-170.

222. Kinloch, A., Lau, C., and Williams, J. (1994) The peeling of flexible laminates, *International Journal of Fracture 66*, 45-70.
223. Shashoua, V. (1958) Static electricity in polymers. I. Theory and measurement, *Journal of Polymer Science 33*, 65-85.

PUBLICATIONS

1. NDN. Affandi, YB. Truong, IL.Kyratzis, R.Padhye, L.Arnold, A non-destructive method for thickness measurement of thin electrospun membranes using white light profilometry, *Journal of Materials Science*, vol. 45, pp.1411-1418, (2010). Accepted
2. NDN. Affandi, YB. Truong, IL.Kyratzis, R.Padhye, L.Arnold, Fabrication and characterisation of hydrophobic and hydrophilic nanofibrous membranes, *Proceedings of International Conference on Scientific and Social Research, IEEE* (2010). Accepted.
3. NDN. Affandi, YB. Truong, IL.Kyratzis, R.Padhye, L.Arnold, A non-destructive method for thickness measurement of electrospun membrane, *Proceedings of International Conference on Nanoscience and Nanotechnology* (2010). Accepted
4. NDN. Affandi, YB. Truong, IL.Kyratzis, R.Padhye, L.Arnold, A study on the adhesion strength between electospun bi-layer membranes as measured by peel test, *International Conference on Electrospinning (Electrospin)* (2010). Accepted.
5. NDN. Affandi, YB. Truong, IL.Kyratzis, R.Padhye, L.Arnold, Adhesion strength of bi-layer membranes,*CSIRO Advanced Materials Conference* (2009). Accepted.
6. NDN. Affandi, YB. Truong, IL.Kyratzis, R.Padhye, L.Arnold, Effect of spinneret diameter on electrospun fibre morphology, *CSIRO Materials Science and Engineering* (2008). Accepted
7. NDN. Affandi, YB. Truong, IL.Kyratzis, R.Padhye, L.Arnold, Effect of spinnerets diameter on fibre morphology of electrospun membranes, *Conference Booklet of ARNAM 2008, Deakin University* (2008). Accepted.

LETTER

A non-destructive method for thickness measurement of thin electrospun membranes using white light profilometry

Nor Dalila Nor Affandi · Yen Bach Truong ·
Ilias Louis Kyratzis · Rajiv Padhye ·
Lyndon Arnold

Introduction

In recent years, the electrospun nanofibre membranes have gained a great deal of attention due to their unique contribution of properties such as small pore size, fine fibre diameter, light weight and larger surface-to-volume ratio compared to bulk fibres and film [1–3]. Such membranes fabricated by spinning fibres in the presence of an electric field, known as electrospinning. A charged jet of polymer solution is accelerated across a distance and is deposited onto the grounded collector as nanofibres.

Membrane thickness is one of the crucial properties for electrospun membrane. In air filtration, the membrane thickness has significantly influenced the membrane permeability [4, 5]. A number of studies have been carried out on filtration properties of electrospun membrane [4–10]. Barhate and Ramakrishna [7] reported that one of the characteristics of nanofibrous filter media is the membrane thickness. Two common methods for thickness measurement of electrospun membranes are, (1) scanning electron microscopy (SEM) [5] and (2) digital micrometer [8, 11, 12]. SEM has been used widely to measure thicknesses of materials because of its measurement accuracy and the ability to gain detailed information of sample surfaces. For an electrospun membrane, the membrane thickness is usually determined by measuring the membrane cross section. As reported by Barhate et al. [5], the thicknesses of their electrospun polyacrylonitrile are relatively easy to measure using SEM in a range of 100–240 μm. However, several problems were encountered mainly in SEM sample preparation. SEM requires cutting the membranes, which could distort the membrane structures. In addition, the SEM method is time consuming and relatively complex as instrumentation. A micrometer is fast and easy technique to measure thicknesses of any materials. It requires direct contact with the sample which involves applied force to determine the thickness. This is particularly a problem for electrospun membranes which may result in sample compression. The compression of electrospun membrane has been reported by Nisbet et al. [13]. Given its highly porous structures, the electrospun membranes are likely to be compressed and distorted during testing [13]. Another drawback of micrometer is the limitation of the micrometer measurement at such thicknesses.

A white light profilometry would be an ideal instrument to determine material thicknesses particularly for porous and fibrous material. It is equipped with a non-contact sensor device, which is more suitable for compressible membranes with open pore structures. Figure 1 illustrates the basic principle of white light profilometry which uses the reflection of white light to determine the sample height above a reference surface. The scanned surfaces form an image of 3-dimensional surface topography from which the sample thicknesses can be determined. This method has been reported by Menzies et al. [14] to determine thin film thickness of approximately 9 ± 1 μm. Apart from image analysis (3-dimensional surface topography), step height measurement is another potential method to determine sample thickness using white light profilometry.

N. D. N. Affandi · R. Padhye · L. Arnold
School of Fashion and Textiles, RMIT University, 25 Dawson Street, Brunswick, VIC 3056, Australia

N. D. N. Affandi · Y. B. Truong (✉) · I. L. Kyratzis
Division of Materials Science and Engineering, CSIRO, Private Bag 10, Clayton South MDC, VIC 3169, Australia
e-mail: yen.truong@csiro.au

Fig. 1 Schematic diagram of white light system
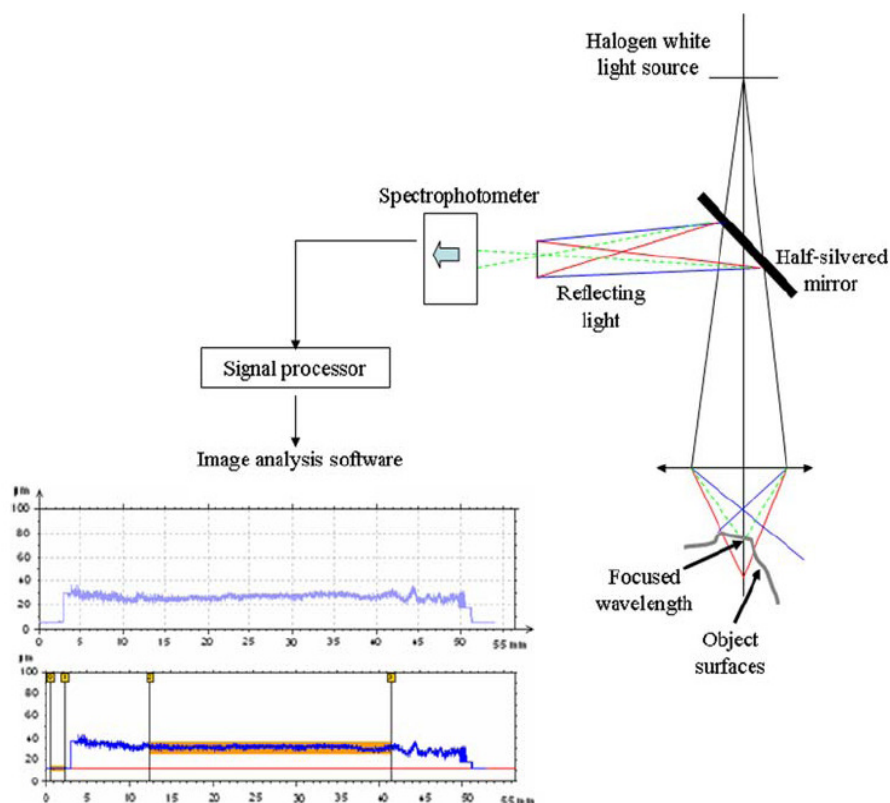
The step height measurement has been recognized as a method to measure the thickness of thin film [15, 16]. With the aid of surface analysis devices such as white light interferometry [15–18] and atomic force microscopy (AFM) [19], the thickness of film can be determined by scanning across two different film surfaces, reference surfaces (reference plane) and film surfaces. A large step from the reference surfaces (reference plane) to film surfaces gives sufficient information on the film thickness [18].

To date, there have been no reports of using white light profilometry to measure the thickness of electrospun membrane. The paper reports on the suitability of white light profilometry for thickness measurements of electrospun PAN and Nylon 6 membranes. The polymers PAN and Nylon 6 were selected because of the resultant fibre diameters and pore sizes for both polymeric membranes were significantly different. In addition, a comparative study was made using a micrometer.

Principle of white light profilometry

The basic principles of the white light profilometry are illustrated in Fig. 1. It consists of a white light source (quartz–halogen), lens, spectrophotometer, a signal processing system

and image analysis software. The white light focuses through a lens that imparts a high level of axial chromatic aberration onto the sample surfaces. As the white light is scanned across the sample, the light is reflected from the sample surface to a spectrophotometer. The software selects the wavelength that is focused on the surface point. The relative height of the surface points forms the step height graphs. Details about the white light profilometry can be found elsewhere [20].

Experimental method

Solution preparation

Two polymers were selected for the study, polyacrylonitrile (PAN) and Nylon 6. The PAN solution was prepared at 10% concentration w/w by dissolving the PAN (Sigma–Aldrich, Mw 150,000) in dimethyl formamide (DMF) at 50 °C for 4–5 h with stirring. The Nylon 6 (Ultramide BS700, BASF) was dissolved in formic acid at 16% concentration w/w and shaken at room temperature for 2–3 days. The solvents DMF and formic acid were analytical grade and obtained from Merck and BDH laboratory supply, respectively.

214

Electrospinning

Figure 2 illustrates the schematic diagram of the electrospinning system used in this study. The electrospinning conditions were a single nozzle spinneret consisting of 23G (Ø0.65 mm) needle, 0.2 mL/h flow rate, 20 cm distance-to-collector and 40–60% relative humidity at room temperature. The electrospinning voltages were at 9.2 and 32 kV for PAN and Nylon 6, respectively. The sample was prepared with two different surfaces, smooth glass surfaces (A and C) and electrospun membrane surfaces (B) (shown in Fig. 3a). The glass surfaces (A and C) were prepared by covering the glass edges with aluminium foils in order to prevent membrane formation (Fig. 2 inset). The uncovered glass slide forms the membrane surfaces (B). Both polymeric electrospun membranes (PAN and Nylon 6) were collected at five different collection times of 5, 10, 15, 30 and 60 min. The thicknesses of the membranes were measured using a non-contact white light profilometry and micrometer.

Step height measurement by white light profilometry

A white light profilometry (Cotec Altisurf 500 white light) was scanned across the electrospun glass slide from A to B to C (shown in Fig. 3a) with approximately 1000 data points/mm. The accuracy of the white light profilometry is approximately 0.05 µm. A lower probe sensor (which is in a range of 9.2–300 µm) was selected in the study in order to prevent the white light from passing through the glass. Ten separate line measurements were performed across the sample.

Digital micrometer measurement

The same sample used in step height measurement was also measured using a simple electronic digital micrometer (Kincrome with the lower limit of approximately 4 µm). Ten sets of measurements were taken at different places at random along the sample and the thicknesses were determined by Eq. 1.

$$h = h_1 - h_2 \tag{1}$$

where h, the thickness of electrospun membrane (µm), h_1 is the total thickness consisting of electrospun membrane and glass slide (µm) and h_2 is the thickness of glass slide (µm)

Characterization

Electrospun membranes were characterized using a Philips XL30 Field Emission Scanning Electron Microscope (FESEM). The membranes were coated with iridium for approximately 5 min. Digital images of sample were taken using a digital camera (Canon Power Shot G6). The pore size of electrospun PAN and Nylon 6 membranes were measured using the capillary flow porometer (Porous Media Inc.).

Fig. 2 Schematic diagram of electrospinning system used in this study. The inset provides details on how the electrospun membrane was collected on the collector electrode
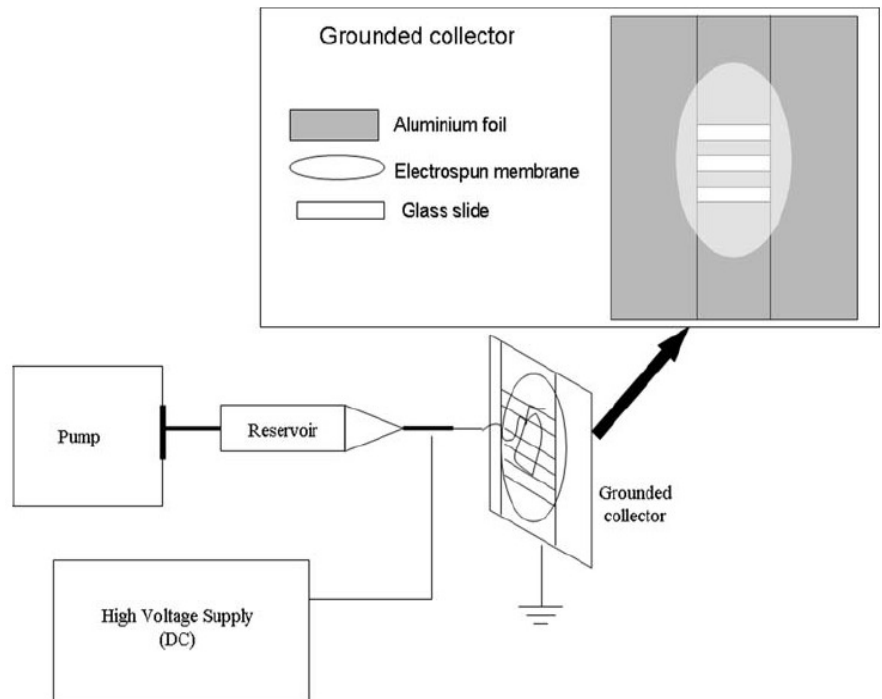
215

Fig. 3 a Photograph of a
typical electrospun membrane
deposited on a glass slide. The
green regions (labelled A and
C) and *white* region (labelled B)
correspond to the glass and
electrospun membrane,
respectively. **b** A typical graph
of single line measurement
taken from A to C

(a) A typical electrospun membrane on glass slide.

(b) A typical graph of single line measurement on plane A, B and C.
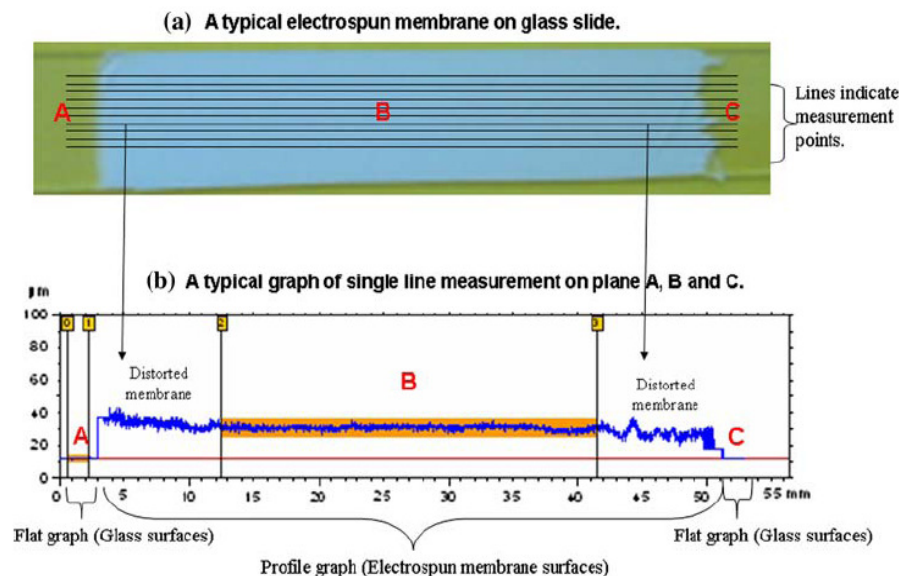
Result and discussion

A typical step height result of a single line measurement is
presented in Fig. 3b. The flat regions at either end represent
the glass surface (A and C), while the profile graph in the
middle represents the electrospun membrane surface (B).
The average height of the electrospun surface above the
glass determines the membrane thickness. The edges of the
electrospun membrane were not used because the mem-
brane structure was stretched and distorted while the
sample was transferred from the aluminium foil.

Comparison of electrospun membrane thicknesses
as measured by white light profilometry and a digital
micrometer

The thickness of electrospun PAN and Nylon 6 as mea-
sured by white light profilometry and digital micrometer is
shown in Table 1. The micrometer gave lower values for
PAN and Nylon 6 membranes as compared to the step
height measurement (white light profilometry). The results

indicate that the membranes are compressed by the
micrometer. This is confirmed by the white light profilom-
etry profiles shown in Figs. 4, 5, 6 and 7, which were taken
after measurement with a micrometer. An indentation is
clearly observed where the micrometer measurement was
taken. Furthermore, the indentation depth corresponds
closely to the difference between the micrometer measure-
ment and white light profilometry. In Table 1, the difference
in measurement between white light profilometry and
micrometer for electrospun PAN-(30 min) is 11 μm, which
is closely corresponded to the same indentation in Fig. 4b.
For electrospun PAN-(60 min), Nylon6-(30 min) and
Nylon 6-(60 min), the indentation depths are approximately
15, 4 and 10 μm, respectively (Figs. 5, 6, 7). Compression
of the samples is understandable given the highly pore
structures of these membranes. In Fig. 8, a membrane made
of small fibre diameters and smaller pore sizes such as
Nylon 6 produces more compact structures that does not
compress as much as structures made of larger fibre diam-
eter such as PAN. More work is required to confirm this
general phenomenon.

Table 1 The thickness of
electrospun PAN and Nylon 6
as measured by white light
profilometry and a digital
micrometer

Electrospun membrane	Collection time (min)	Thickness (μm)	
		White light profilometry (step height)	Digital micrometer
PAN-(30 min)	30	21 ± 1.1	10 ± 0.7
PAN-(60 min)	60	46 ± 0.8	30 ± 0.1
Nylon 6-(30 min)	30	10 ± 0.3	7 ± 0.6
Nylon 6-(60 min)	60	16 ± 0.1	6 ± 0.1
Glass slide[a]	–	1100 ± 0.1	1100 ± 0.1

[a] Control

216

Fig. 4 Profile obtained from white light profilometry for electrospun PAN-(30 min) of the B region. **a** Before measurement with a micrometer and **b** After measurement with a micrometer. The deformation caused by the micrometer can be clearly seen corresponding to a compression of 10 μm
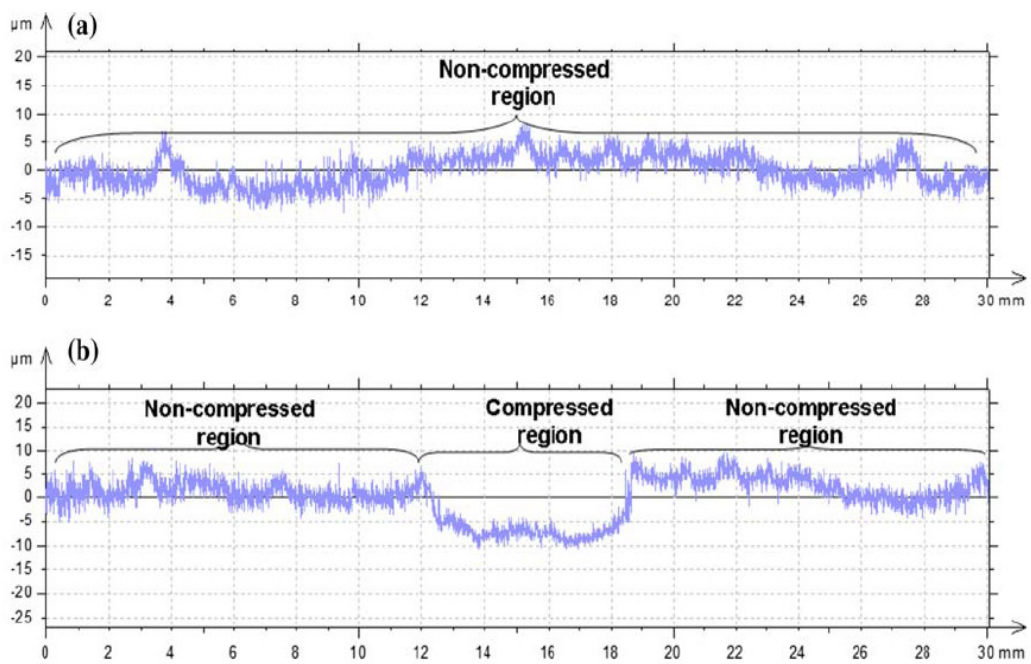
Fig. 5 Profile obtained from white light profilometry for electrospun PAN-(60 min) of the B region. **a** Before measurement with a micrometer and **b** After measurement with a micrometer. The deformation caused by the micrometer can be clearly seen corresponding to a compression of 15 μm

217
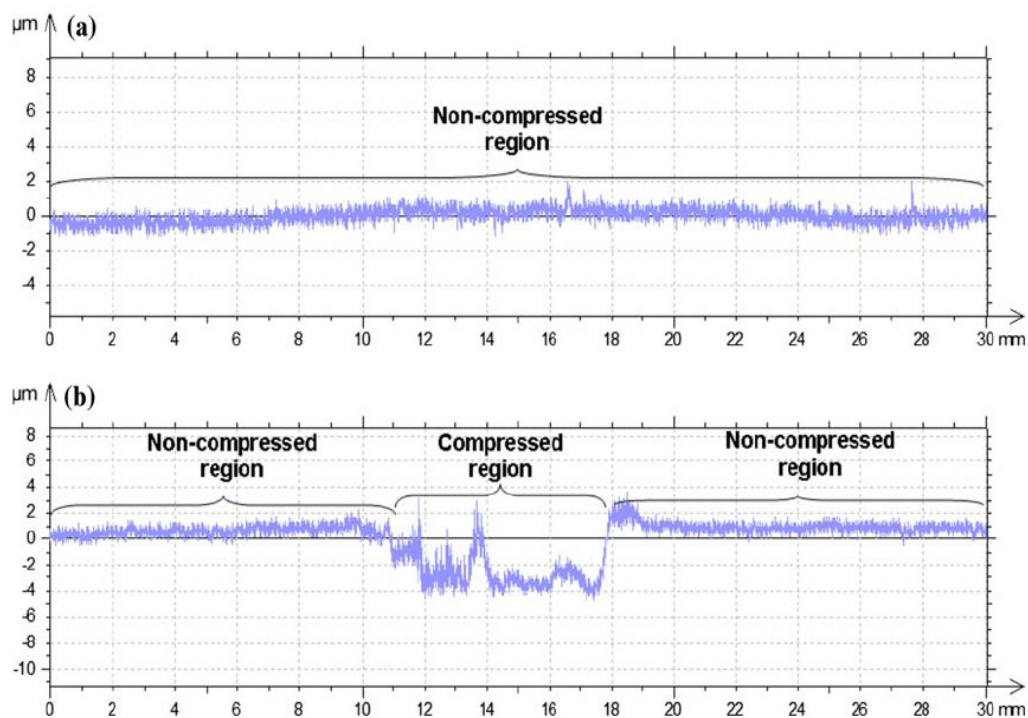
Fig. 6 Profile obtained from white light profilometry for electrospun Nylon 6-(30 min) of the B region. **a** Before measurement with a micrometer and **b** After measurement with a micrometer. The deformation caused by the micrometer can be clearly seen corresponding to a compression of 4 µm
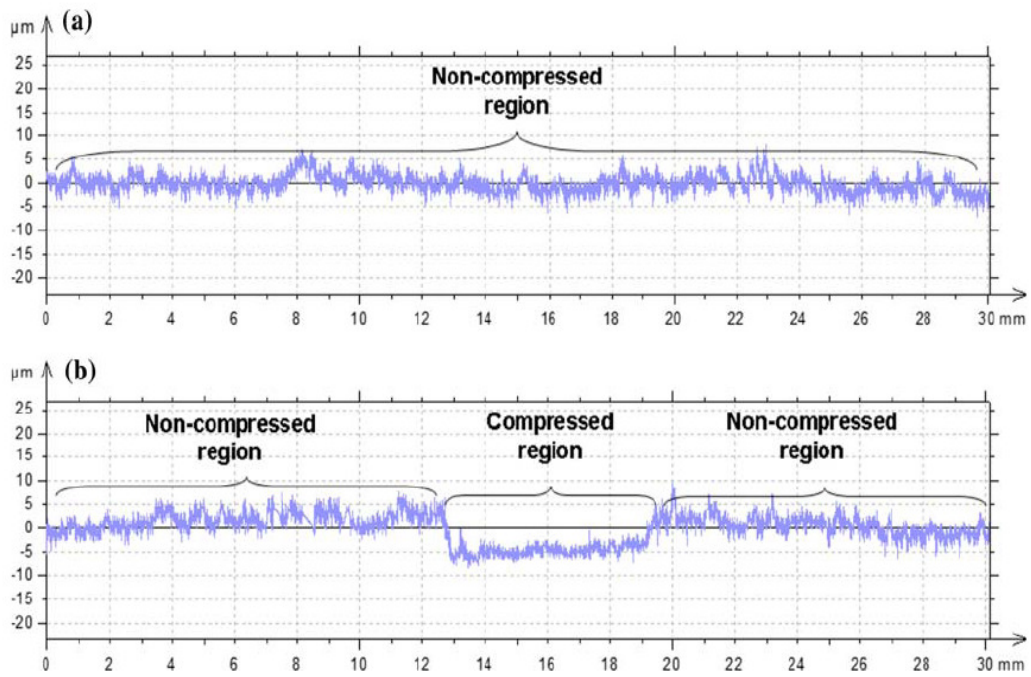

Fig. 7 Profile obtained from white light profilometry for electrospun Nylon 6-(60 min) of the B region. **a** Before measurement with a micrometer and **b** After measurement with a micrometer. The deformation caused by the micrometer can be clearly seen corresponding to a compression of 10 µm
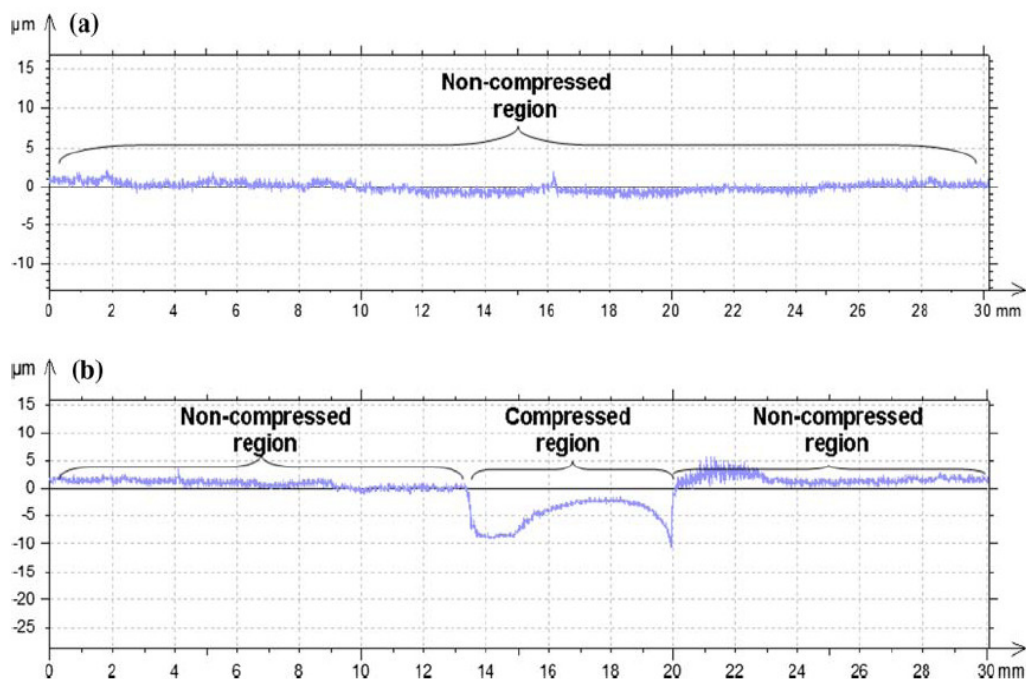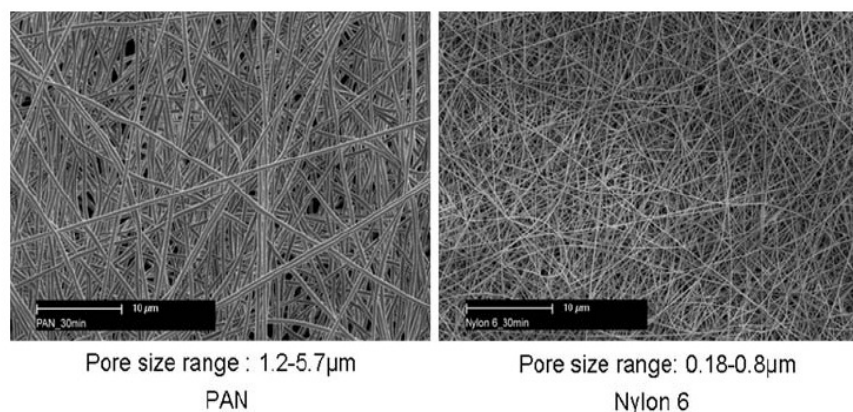
Fig. 8 SEM images of electrospun PAN and Nylon 6 membrane collected for 30 min

Pore size range : 1.2-5.7μm

PAN

Pore size range: 0.18-0.8μm

Nylon 6

Membrane thicknesses at different collection time

Figure 9 represents the thickness of PAN and Nylon 6 collected for 5, 10, 15, 30 and 60 min as measured by white light profilometry. It was found that the thicknesses of PAN and Nylon 6 were linearly proportional to the electrospinning collection time. The membrane thickness increases with deposition time. At 5 min collection time, the thickness of PAN and Nylon 6 were 2 ± 0.1 and 0.8 ± 0.1 μm, respectively. The results indicate only a few fibres were deposited in the first 5 min. As the collection time was increased, an opaque membrane was formed for both polymeric electrospun membranes.

The electrospun PAN has greater thickness than that of the electrospun Nylon 6 because the PAN fibres having large fibre diameter as compared to the Nylon 6 membrane (shown in Fig. 8). The stacking of larger fibre diameters on top of each other produces thicker membrane.

In addition, the large pore sizes of PAN (shown in Fig. 8) form spongy and open pore structures of PAN membrane. For Nylon 6, the fine pore sizes form a compact and therefore thinner structure membrane.

Conclusion

The experimental results have shown a correlation between the membrane thickness and the collection period. Results from this method were compared to those using a micrometer. The thicknesses found using the micrometer gave lower thickness values for the same sample due to sample compressions. The advantages of using step height measurements are:

1. The use of white light to scan the sample will not damage the sample. The scanned sample is reusable for other testing.
2. The step height technique using white light profilometry does not compress a sample and therefore it is more suitable for spongy membranes with open pore structures.
3. The step height method can measure the electrospun thickness in the nanometer range, which is beyond the limit of a micrometer. The minimum measurement of micrometer is approximately 4 μm.
4. The technique is able to measure the thickness across a large region. In the SEM, only the cross section can determine the electrospun thickness.
5. It is a faster method to measure the thickness of electrospun membrane compared to SEM. Ten measurements can be done over a 30 min period (depending on the sample length).
6. Minimal sample preparation (no freeze-sectioning and coating) is required for this method.

This study has shown that white light profilometry can successfully employed to measure the thickness of thin electrospun membranes onto glass slide.

Fig. 9 A plot of membrane thickness versus collection period for the electrospun PAN and Nylon 6 membranes as measured by white light profilometry. Values represent the average of 10 measurements at different places

References

1. Graham K, Schreuder-Gibson H, Gogins M (2003) Presented at INTC 2003, sponsored by INDA, Association of the Nonwoven Fabrics Industry and TAPPI, Technical Association of the Pulp & Paper Industry, Baltimore, MD, 15–18 September 2003. http://

219

www.asia.donaldson.com/en/filtermedia/support/datalibrary/050
271.pdf

2. Ramakrishna S, Fujihara K, Wee-Eong T, Thomas Y, Ma Z, Ramakrishna R (2006) Mater Today 9:40
3. Huang Z-M, Zhang Y-Z, Kotaki M, Ramakrishna S (2003) Compos Sci Technol 63:2223
4. Zhang S, Shim WS, Kim J (2009) Mater Des 30:3659
5. Barhate RS, Loong CK, Ramakrishna S (2006) J Membr Sci 283:209
6. Shin C, Chase GG, Reneker DH (2005) Colloids Surf A 262:211
7. Barhate RS, Ramakrishna S (2007) J Membr Sci 296:1
8. Gopal R, Kaur S, Feng CY, Chan C, Ramakrishna S, Tabe S, Matsuura T (2007) J Membr Sci 289:210
9. Heikkilä P, Taipale A, Lehtimäki M, Harlin A (2008) Polym Eng Sci 48:1168
10. Gopal R, Kaur S, Ma Z, Chan C, Ramakrishna S, Matsuura T (2006) J Membr Sci 281:581
11. Gao K, Hu X, Dai C, Yi T (2006) Mater Sci Eng B 131:100
12. Aussawasathien D, Teerawattananon C, Vongachariya A (2008) J Membr Sci 315:11
13. Nisbet DR, Rodda AE, Finkelstein DI, Horne MK, Forsythe JS, Shen W (2009) Collods Surf B Biointerfaces 71:1
14. Menzies DB, Bourgeois LY, Cheng-B Y, Simon GP, Brack N, Spiccia LJ (2005) Surf Coat Technol 198:118
15. Dai H, Shen Y, Zhou H, Cai X (2008) Thin Solid Films 516:1796
16. Flournoy PA, McClure RW, Wyntjes GJ (1972) Appl Opt 11:1907
17. Kim SW, Kim GH (1999) J Appl Opt 38:5968
18. Shabana HM (2004) Polym Test 23:695
19. Lui PK-M, Chen Y-L, Chen C-J, Peng G-S, Lin VT-Y (2002) Proceedings of the second international symposium on instrumentation science and technology, Jinan, China, 18–22 August 2002, vol 2. Harbin Institute of Technology Press, Harbin, p 29
20. Strater HD, Carouge DG, Jauch KM (1992) US Patent 5,165,063

Appendix I Fibre morphologies for electrospun Nylon 6 at different concentrations, applied voltage and distance

Concentration (%wt)	Distance (cm)	Voltage (kV)				
		15	20	25	30	35
5	5	Droplets	Droplets	Droplets	Droplets	Droplets
	10	Droplets	Droplets	Droplets	Droplets	Droplets
	15	Droplets	Droplets	Droplets	Droplets	Droplets
	20	Droplets	Droplets	Droplets	Droplets	Droplets
12	5	Cylindrical fibres	Cylindrical fibres	Cylindrical fibres	Cylindrical fibres	Cylindrical fibres
	10	Cylindrical fibres	Cylindrical fibres	Cylindrical fibres	Cylindrical fibres	Cylindrical fibres
	15	Cylindrical fibres	Cylindrical fibres	Cylindrical fibres	Cylindrical fibres	Cylindrical fibres
	20	Cylindrical fibres	Cylindrical fibres	Cylindrical fibres	Cylindrical fibres	Cylindrical fibres
14	5	Cylindrical fibres	Cylindrical fibres	Cylindrical fibres	Cylindrical fibres	Cylindrical fibres
	10	Cylindrical fibres	Cylindrical fibres	Cylindrical fibres	Cylindrical fibres	Cylindrical fibres
	15	Cylindrical fibres	Cylindrical fibres	Cylindrical fibres	Cylindrical fibres	Cylindrical fibres
	20	Cylindrical fibres	Cylindrical fibres	Cylindrical fibres	Cylindrical fibres	Cylindrical fibres
16	5	Cylindrical fibres	Cylindrical fibres	Cylindrical fibres	Cylindrical fibres	Cylindrical fibres-**clogging**
	10	Cylindrical fibres	Cylindrical fibres	Cylindrical fibres	Cylindrical fibres	Cylindrical fibres-**clogging**
	15	Cylindrical fibres	Cylindrical fibres	Cylindrical fibres	Cylindrical fibres	Cylindrical fibres-**clogging**
	20	Cylindrical fibres	Cylindrical fibres	Cylindrical fibres	Cylindrical fibres	Cylindrical fibres-**clogging**
18	5	Cylindrical fibres + flat ribbon fibres	Cylindrical fibres + flat ribbon fibres	Cylindrical fibres + flat ribbon fibres	Cylindrical fibres + flat ribbon fibres	Cylindrical fibres + flat ribbon fibres
	10	Cylindrical fibres + flat ribbon fibres	Cylindrical fibres + flat ribbon fibres	Cylindrical fibres + flat ribbon fibres	Cylindrical fibres + flat ribbon fibres	Cylindrical fibres + flat ribbon fibres
	15	Cylindrical fibres + flat ribbon fibres	Cylindrical fibres + flat ribbon fibres	Cylindrical fibres + flat ribbon fibres	Cylindrical fibres + flat ribbon fibres	Cylindrical fibres + flat ribbon fibres
	20	Cylindrical fibres + flat ribbon	Cylindrical fibres + flat ribbon	Cylindrical fibres + flat ribbon	Cylindrical fibres + flat ribbon	Cylindrical fibres + flat ribbon

		fibres	fibres	fibres	fibres	fibres
20	5	Cylindrical fibres + flat ribbon fibres	Cylindrical fibres + flat ribbon fibres	Cylindrical fibres + flat ribbon fibres	Cylindrical fibres + flat ribbon fibres	Cylindrical fibres + flat ribbon fibres
	10	Cylindrical fibres + flat ribbon fibres	Cylindrical fibres + flat ribbon fibres	Cylindrical fibres + flat ribbon fibres	Cylindrical fibres + flat ribbon fibres	Cylindrical fibres + flat ribbon fibres
	15	Cylindrical fibres + flat ribbon fibres	Cylindrical fibres + flat ribbon fibres	Cylindrical fibres + flat ribbon fibres	Cylindrical fibres + flat ribbon fibres	Cylindrical fibres + flat ribbon fibres
	20	Cylindrical fibres + flat ribbon fibres	Cylindrical fibres + flat ribbon fibres	Cylindrical fibres + flat ribbon fibres	Cylindrical fibres + flat ribbon fibres	Cylindrical fibres + flat ribbon fibres
25	5	Flat ribbon fibres	Flat ribbon fibres	Flat ribbon fibres	Flat ribbon fibres	Flat ribbon fibres
	10	Flat ribbon fibres	Flat ribbon fibres	Flat ribbon fibres	Flat ribbon fibres	Flat ribbon fibres
	15	Flat ribbon fibres	Flat ribbon fibres	Flat ribbon fibres	Flat ribbon fibres	Flat ribbon fibres
	20	Flat ribbon fibres	Flat ribbon fibres	Flat ribbon fibres	Flat ribbon fibres	Flat ribbon fibres

Further experiments on applied voltage for Nylon 6 solutions

Concentration (%wt)	Distance (cm)	Voltage (kV)			
		31	32	33	34
16	5	Cylindrical fibres	Cylindrical fibres	Cylindrical fibres-**clogging**	Cylindrical fibres-**clogging**
	10	Cylindrical fibres	Cylindrical fibres	Cylindrical fibres-**clogging**	Cylindrical fibres-**clogging**
	15	Cylindrical fibres	Cylindrical fibres	Cylindrical fibres-**clogging**	Cylindrical fibres-**clogging**
	20	Cylindrical fibres	Cylindrical fibres	Cylindrical fibres-**clogging**	Cylindrical fibres-**clogging**
	5	Cylindrical fibres	Cylindrical fibres	Cylindrical fibres-**clogging**	Cylindrical fibres-**clogging**

Appendix I Fibre morphologies for electrospun PVA at different concentrations, applied voltage and distance

Concentration (%wt)	Distance (cm)	Voltage (kV)				
		15	20	25	30	35
4	5	Beaded fibres	Beaded fibres	Beaded fibres	Beaded fibres	Beaded fibres
	10	Beaded fibres	Beaded fibres	Beaded fibres	Beaded fibres	Beaded fibres
	15	Beaded fibres	Beaded fibres	Beaded fibres	Beaded fibres	Beaded fibres
	20	Beaded fibres	Beaded fibres	Beaded fibres	Beaded fibres	Beaded fibres
6	5	Beaded fibres	Beaded fibres	Beaded fibres	Beaded fibres	Beaded fibres
	10	Beaded fibres	Beaded fibres	Beaded fibres	Beaded fibres	Beaded fibres
	15	Beaded fibres	Beaded fibres	Beaded fibres	Beaded fibres	Beaded fibres
	20	Beaded fibres	Beaded fibres	Beaded fibres	Beaded fibres	Beaded fibres
8	5	Beaded fibres	Beaded fibres	Beaded fibres	Beaded fibres	Beaded fibres
	10	Beaded fibres	Beaded fibres	Beaded fibres	Beaded fibres	Beaded fibres
	15	Beaded fibres	Beaded fibres	Beaded fibres	Beaded fibres	Beaded fibres
	20	Beaded fibres	Beaded fibres	Beaded fibres	Beaded fibres	Beaded fibres
10	5	Cylindrical fibres	Cylindrical fibres	Cylindrical fibres	Cylindrical fibres	Cylindrical fibres
	10	Cylindrical fibres	Cylindrical fibres	Cylindrical fibres	Cylindrical fibres	Cylindrical fibres
	15	Cylindrical fibres	Cylindrical fibres	Cylindrical fibres	Cylindrical fibres	Cylindrical fibres
	20	Cylindrical fibres	Cylindrical fibres	Cylindrical fibres	Cylindrical fibres	Cylindrical fibres
12	5	Cylindrical fibres	Cylindrical fibres	Cylindrical fibres	Cylindrical fibres	Cylindrical fibres
	10	Cylindrical fibres	Cylindrical fibres	Cylindrical fibres	Cylindrical fibres	Cylindrical fibres
	15	Cylindrical fibres	Cylindrical fibres	Cylindrical fibres	Cylindrical fibres	Cylindrical fibres
	20	Cylindrical fibres	Cylindrical fibres	Cylindrical fibres	Cylindrical fibres	Cylindrical fibres

**Appendix I Fibre morphologies for electrospun PAN at different concentrations, applied voltage and distance**

Concentration (%wt)	Distance (cm)	Voltage (kV)				
		15	20	25	30	35
5	5	Beaded fibres	Beaded fibres	Beaded fibres	Beaded fibres	Beaded fibres
	10	Beaded fibres	Beaded fibres	Beaded fibres	Beaded fibres	Beaded fibres
	15	Beaded fibres	Beaded fibres	Beaded fibres	Beaded fibres	Beaded fibres
	20	Beaded fibres	Beaded fibres	Beaded fibres	Beaded fibres	Beaded fibres
9	5	Beaded fibres	Beaded fibres	Beaded fibres	Beaded fibres	Beaded fibres
	10	Beaded fibres	Beaded fibres	Beaded fibres	Beaded fibres	Beaded fibres
	15	Beaded fibres	Beaded fibres	Beaded fibres	Beaded fibres	Beaded fibres
	20	Beaded fibres	Beaded fibres	Beaded fibres	Beaded fibres	Beaded fibres
10	5	Cylindrical fibres	Cylindrical fibres	Cylindrical fibres	Cylindrical fibres	Cylindrical fibres
	10	Cylindrical fibres	Cylindrical fibres	Cylindrical fibres	Cylindrical fibres	Cylindrical fibres
	15	Cylindrical fibres	Cylindrical fibres	Cylindrical fibres	Cylindrical fibres	Cylindrical fibres
	20	Cylindrical fibres	Cylindrical fibres	Cylindrical fibres	Cylindrical fibres	Cylindrical fibres
11	5	Blobs + fibres	Blobs + fibres	Blobs + fibres	Blobs + fibres	Blobs + fibres
	10	Blobs + fibres	Blobs + fibres	Blobs + fibres	Blobs + fibres	Blobs + fibres
	15	Blobs + fibres	Blobs + fibres	Blobs + fibres	Blobs + fibres	Blobs + fibres
	20	Blobs + fibres	Blobs + fibres	Blobs + fibres	Blobs + fibres	Blobs + fibres
13	5	Blobs + fibres	Blobs + fibres	Blobs + fibres	Blobs + fibres	Blobs + fibres
	10	Blobs + fibres	Blobs + fibres	Blobs + fibres	Blobs + fibres	Blobs + fibres
	15	Blobs + fibres	Blobs + fibres	Blobs + fibres	Blobs + fibres	Blobs + fibres
	20	Blobs + fibres	Blobs + fibres	Blobs + fibres	Blobs + fibres	Blobs + fibres

Appendix I Fibre morphologies for electrospun copolymer PVDF at different concentrations, applied voltage and distance

Concentration (%wt)	Distance (cm)	Voltage (kV)				
		15	20	25	30	35
5	5	Droplets	Droplets	Droplets	Droplets	Droplets
	10	Droplets	Droplets	Droplets	Droplets	Droplets
	15	Droplets	Droplets	Droplets	Droplets	Droplets
	20	Droplets	Droplets	Droplets	Droplets	Droplets
10	5	Droplets + fibres	Droplets + fibres	Droplets + fibres	Droplets + fibres	Droplets + fibres
	10	Droplets + fibres	Droplets + fibres	Droplets + fibres	Droplets + fibres	Droplets + fibres
	15	Droplets + fibres	Droplets + fibres	Droplets + fibres	Droplets + fibres	Droplets + fibres
	20	Droplets + fibres	Droplets + fibres	Droplets + fibres	Droplets + fibres	Droplets + fibres
15	5	Beaded fibres	Beaded fibres	Beaded fibres	Beaded fibres	Beaded fibres
	10	Beaded fibres	Beaded fibres	Beaded fibres	Beaded fibres	Beaded fibres
	15	Beaded fibres	Beaded fibres	Beaded fibres	Beaded fibres	Beaded fibres
	20	Beaded fibres	Beaded fibres	Beaded fibres	Beaded fibres	Beaded fibres
20	5	Cylindrical fibres	Cylindrical fibres	Cylindrical fibres	Cylindrical fibres	Cylindrical fibres
	10	Cylindrical fibres	Cylindrical fibres	Cylindrical fibres	Cylindrical fibres	Cylindrical fibres
	15	Cylindrical fibres	Cylindrical fibres	Cylindrical fibres	Cylindrical fibres	Cylindrical fibres
	20	Cylindrical fibres	Cylindrical fibres	Cylindrical fibres	Cylindrical fibres	Cylindrical fibres
25	5	Coalesced fibres	Coalesced fibres	Coalesced fibres	Coalesced fibres	Coalesced fibres
	10	Coalesced fibres	Coalesced fibres	Coalesced fibres	Coalesced fibres	Coalesced fibres
	15	Coalesced fibres	Coalesced fibres	Coalesced fibres	Coalesced fibres	Coalesced fibres
	20	Coalesced fibres	Coalesced fibres	Coalesced fibres	Coalesced fibres	Coalesced fibres

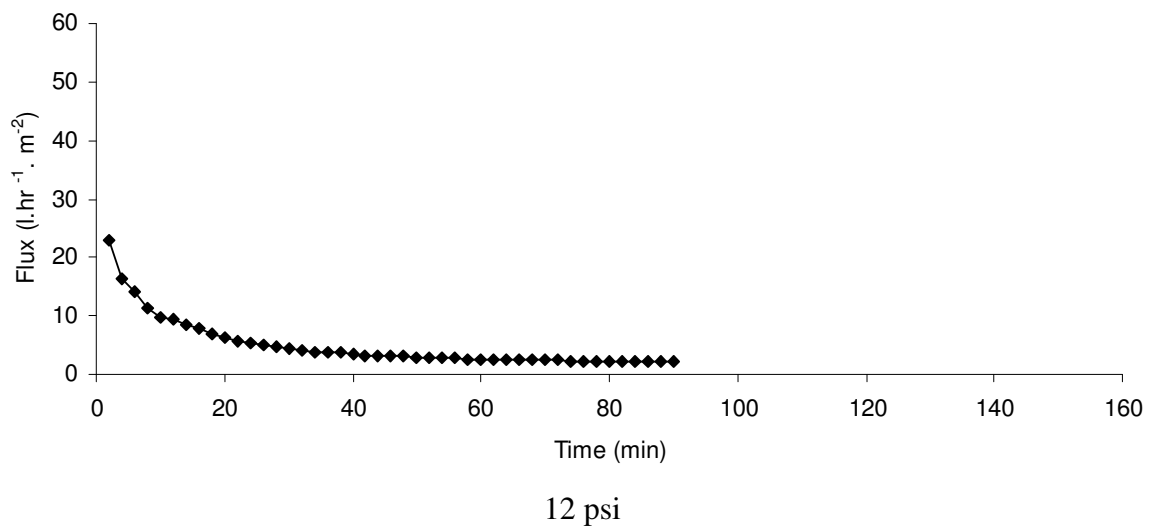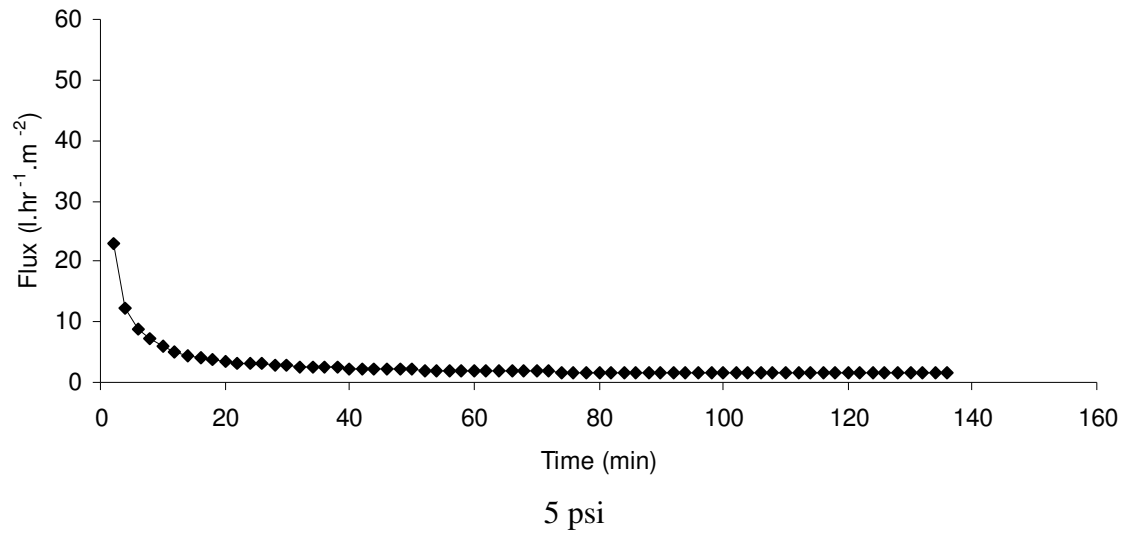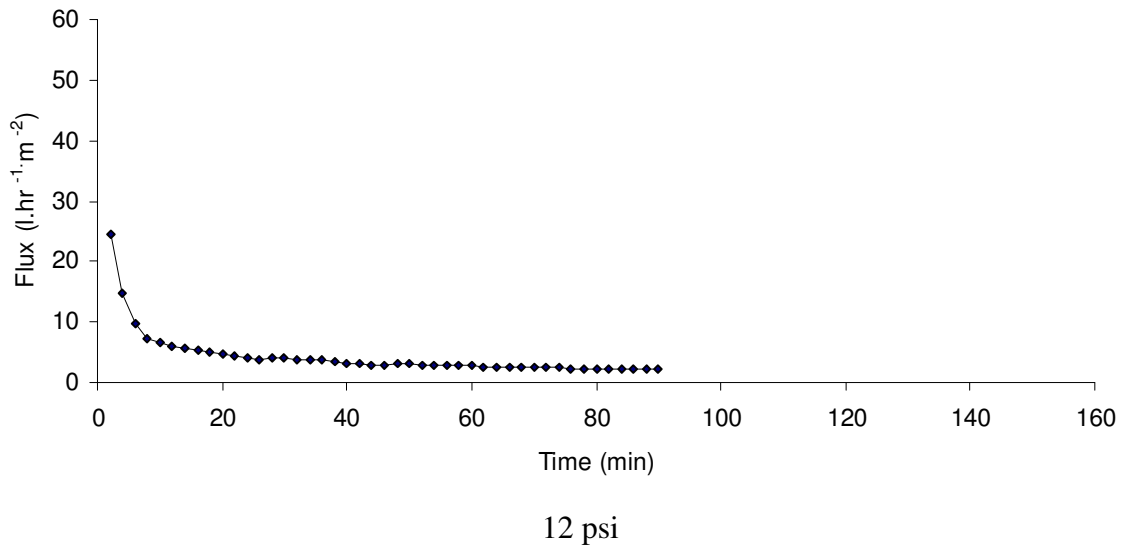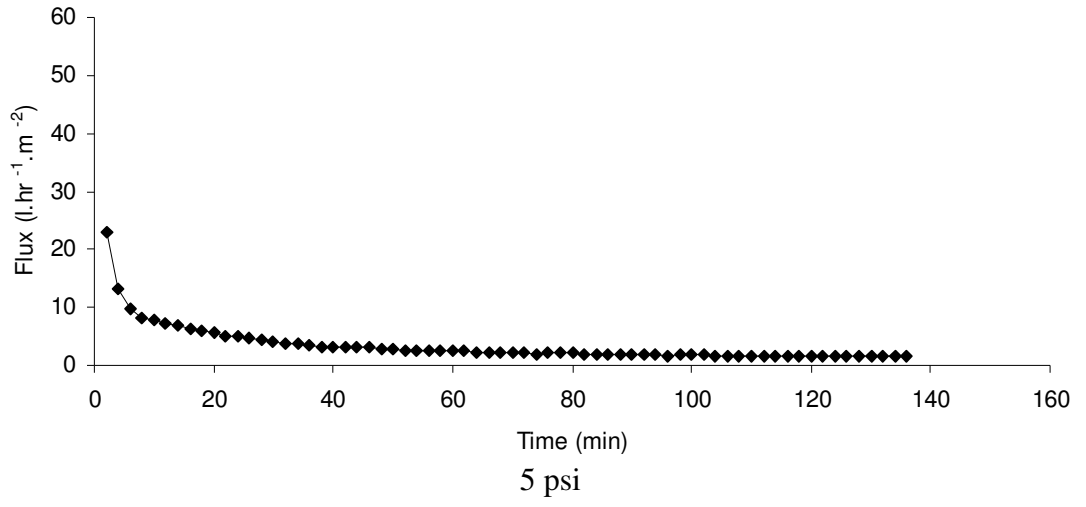**Appendix II Typical fluxes of membranes**

1. Commercial membrane
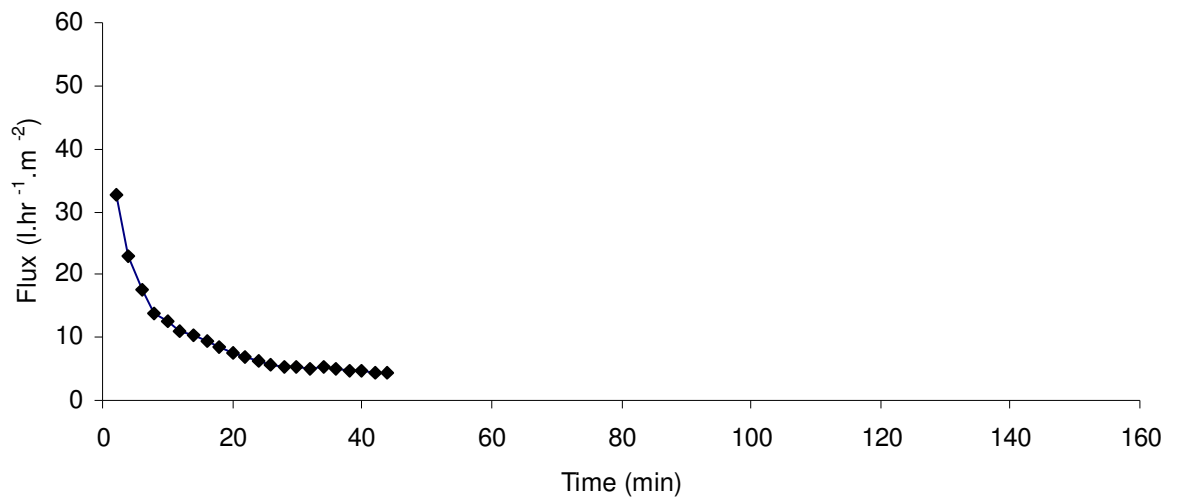
5 psi
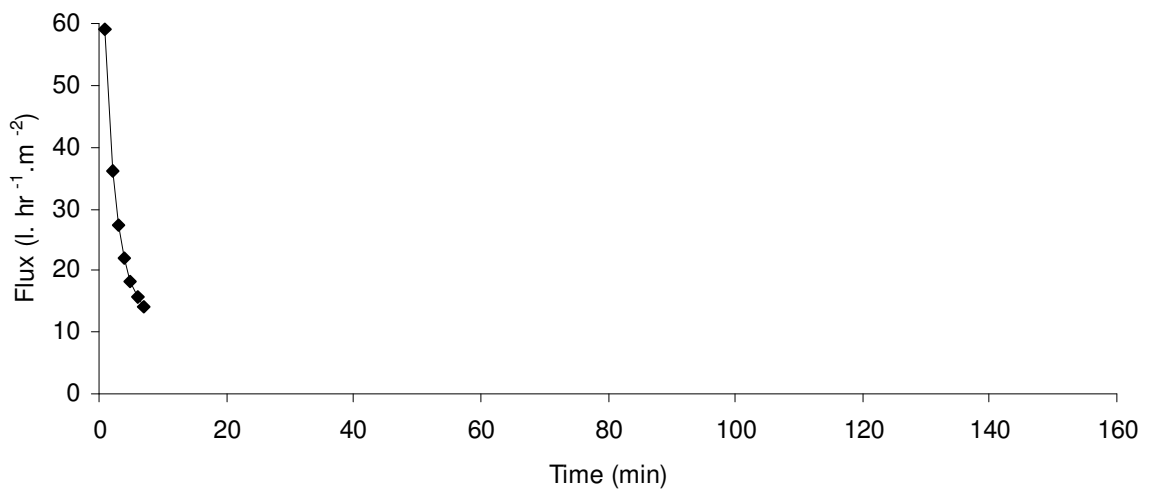
12 psi

2. Homogeneous bi-layer Nylon 6/Nylon 6

5 psi

12 psi

3) Heterogeneous bi-layer Nylon 6/PAN

5 psi

12 psi

4) Heterogeneous bi-layer PAN/Nylon 6

5 psi

12 psi